INFORMATION TO USERS

76-16,234

SCHUSTER, William John, 1948-
  THIRTEEN-COLOR PHOTOMETRY OF SUBDWARFS.

The University of Arizona, Ph.D., 1976
Physics, astronomy & astrophysics

THIRTEEN-COLOR PHOTOMETRY OF SUBDWARFS

by

William John Schuster

_____

A Dissertation Submitted to the Faculty of the

DEPARTMENT OF ASTRONOMY

In Partial Fulfillment of the Requirements
For the Degree of

DOCTOR OF PHILOSOPHY

In the Graduate College

THE UNIVERSITY OF ARIZONA

1 9 7 6

THE UNIVERSITY OF ARIZONA

GRADUATE COLLEGE

I hereby recommend that this dissertation prepared under my

direction by _____ William John Schuster _____

entitled _____ Thirteen-Color Photometry of Subdwarfs _____

_____

be accepted as fulfilling the dissertation requirement of the

degree of _____ Doctor of Philosophy _____

Harold L. Johnson
Dissertation Director

Dec 5, 1975
Date

After inspection of the final copy of the dissertation, the

following members of the Final Examination Committee concur in

its approval and recommend its acceptance:*

Stephen E. Strom   12-14-75

Rodger I. Thompson   12-15-75

Walter S. Fitch   12/18/75

_____   _____

_____   _____

*This approval and acceptance is contingent on the candidate's
adequate performance and defense of this dissertation at the
final oral examination. The inclusion of this sheet bound into
the library copy of the dissertation is evidence of satisfactory
performance at the final examination.

STATEMENT BY AUTHOR

This dissertation has been submitted in partial fulfillment of requirements for an advanced degree at The University of Arizona and is deposited in the University Library to be made available to borrowers under rules of the Library.

Brief quotations from this dissertation are allowable without special permission, provided that accurate acknowledgment of source is made. Requests for permission for extended quotation from or reproduction of this manuscript in whole or in part may be granted by the head of the major department or the Dean of the Graduate College when in his judgment the proposed use of the material is in the interests of scholarship. In all other instances, however, permission must be obtained from the author.

SIGNED: _William J. Schuster_

ACKNOWLEDGMENTS

TABLE OF CONTENTS

TABLE OF CONTENTS--<u>Continued</u>

LIST OF ILLUSTRATIONS

LIST OF ILLUSTRATIONS--<u>Continued</u>

LIST OF ILLUSTRATIONS--<u>Continued</u>

LIST OF TABLES

LIST OF TABLES--<u>Continued</u>

ABSTRACT

Thirteen-color narrow- and intermediate-band photometry for 119 subdwarfs and for over 50 Hyades dwarfs has been obtained at the Mexican National Observatory in Baja California. The metal-poor subdwarfs have been compared to the Hyades dwarfs at constant effective temperature to obtain blanketing curves for studying the metallicity sensitivity of the 13-color indices. Field giants have been compared to the Hyades dwarfs to obtain luminosity-difference curves which have shown us the surface gravity sensitivity of the indices. These studies have shown that 37-45 is a good metallicity index, G [(35-52)-(37-45)] is a good gravity index, and 45-63 and 58-99 good temperature indices. We have then calibrated these indices for measuring their respective stellar atmospheric parameters. Model atmospheres have been used for the surface gravities, for blanketing corrections to the temperature indices, and for a theoretical temperature calibration. Stars with measured angular diameters have been used to obtain an additional, strictly observational temperature calibration. High dispersion spectroscopic studies of solar-like dwarfs and subdwarfs have been the basis of the metallicity versus ultraviolet excess correlation. With these results we can obtain temperatures accurate to $\pm 100^{\circ}$, [Fe/H] values accurate to ± 0.1, and log g's with errors of 0.1 or 0.2. We have also derived bolometric corrections and absolute blanketing changes for the 13-color magnitudes.

Using these calibrations we have then obtained the effective temperatures and metal contents for most of the subdwarfs. The positions of the subdwarfs in the (M_{bol}, T_e) and (G, 45-63) diagrams have been studied as a function of metal content. These results show that in the (M_{bol}, T_e) plane the extreme subdwarfs are indeed fainter (at constant temperature) than the Hyades main sequence for effective temperatures less than about 5700°. However, the mild subdwarfs show little separation from the Hyades dwarfs perhaps indicating greater evolution at the lower temperatures than for the extreme subdwarfs. These comparisons have also shown us that the helium abundances of the extreme subdwarfs are not much different from the Hyades values.

The (G, 45-63) diagram has given us an even clearer picture of the extreme subdwarfs' evolution. We find that an approximate "zero-age" line is apparent for effective temperatures less than about 6000°, that all extreme subdwarfs hotter than about 6000° are significantly evolved, and that a subdwarf turnoff is well defined at about 6400°. We see that several of the hottest subdwarfs should be called metal-poor subgiants, that -9^o5491 and $+ 41^o3735$ are in fact metal-poor giants, and that in the (G, 45-63) diagram a subgiant-giant branch for extreme Population II objects is easily noted. In addition we find a considerable number of cool, evolved subdwarfs, some nearly as cool as 5000°, which are between the "zero-age" line and the subgiant-giant branch. These cool, evolved metal-poor stars, when fit by globular cluster isochrones, imply ages of 20×10^9 years or more and suggest that the extreme Population II stars were formed over a time span of at least 4×10^9 years. Also, the

position of the subdwarfs' "zero-age" line indicates that unevolved sub-
dwarfs have log g's 0.2 to 0.3 greater than the Hyades values (for equal
temperatures).

Finally, the (M_{bol}, T_e) and (G, 45-63) diagrams have been used
together to estimate subdwarf masses as a ratio to Hyades masses at
constant temperature. The average mass ratio for seven extreme subdwarfs
lies in the range 0.5 to 0.75.

CHAPTER 1

INTRODUCTION

The first hints pointing to the possible existence of the sub-
dwarfs came in a series of papers by W. S. Adams and his coworkers
(Adams 1915, Adams and Joy 1922, Adams et al. 1935). These papers, which
were concerned with spectroscopic absolute magnitudes, noted a small
group of stars with peculiar spectra; the hydrogen lines appeared narrow
and sharp, and the lines of the metals were very weak. These investi-
gators concluded that these stars "are of comparatively low luminosity"
(Adams 1915, p. 187) and "seem to form a group midway between the faint
'white dwarfs,' such as the companion to Sirius, and the stars of early
type belonging to the main sequence" (Adams et al. 1935, p. 191). In a
series of short papers on the spectral types of stars with large proper
motions Kuiper and Seyfert (1938) and Kuiper (1938, 1939) also discovered
a number of stars with brightnesses intermediate between main sequence
stars and white dwarfs. At first the term "intermediate white dwarf"
was used for these stars, but Kuiper (1939) soon recognized that these
stars are more similar to main sequence dwarfs than to white dwarfs and
so coined the term "subdwarf."

Since the emergence of subdwarfs as a separate class of stars,
they have been extensively studied (for example, see the review articles
of Andersen 1971 and Buscombe 1959). The importance of studying these

1

stars lies in their extreme ages and their similarities to globular-cluster stars. Their extreme metal deficiencies and extreme kinematic properties have led to a number of interesting but difficult problems for the spectroscopist, the photometrist, and the theoretician. In this introduction we will outline several of these problems, especially those that have not been adequately solved to date, and show how the following analyses will give new and hopefully more complete answers to these problems.

The basis of the present study is the development of a new photometric system by Johnson, Mitchell and Latham (1967) and by Mitchell and Johnson (1969). This 13-color narrow- and intermediate-band system was originally set up to study O and B stars together with satellite based ultraviolet photometry. However, papers by Johnson, MacArthur, and Mitchell (1968) and by Johnson and Mitchell (1968) showed the applicability of such multi-band photometric systems to the study of sub-dwarfs. So, the present investigation was undertaken. But since this photometric system is relatively new, little has been done concerning the sensitivity and calibration of the 13-color indices for determining effective temperatures (T_e's), compositions, and surface gravities of stars. Hence, a significant part of this thesis will be directed toward an understanding of these sensitivities of the 13-color indices and toward their calibration.

Problems of Subdwarf Interpretations

The main inadequately solved problems for the subdwarfs are the following: (a) determining their chemical compositions as compared to

more normal Population I stars (by chemical composition we mean helium content as well as metallicity); (b) determining accurate effective temperatures; (c) obtaining accurate blanketing corrections in order to understand the subdwarf positions in the various color-color and color-magnitude diagrams; (d) finding out the evolutionary status of the subdwarfs as a function of composition, temperature, and kinematic properties; (e) understanding the positions of the subdwarfs in the (M_{bol}, T_e) diagram in terms of helium abundances, metallicities, evolution, blanketing corrections, effective temperatures, bolometric corrections, parallax errors, and so forth; and (f) getting some estimate of the subdwarf masses compared to the Sun or to the Hyades main sequence. (Most of the literature references relating to these problems are not given here but in Chapters 5, 6 and 7.)

For the question of the metallicities of the subdwarfs the main difficulty seems to be the accuracy of the spectroscopic abundance studies which are used to analyze individual subdwarfs and to calibrate the photometric indices. The problems seem to arise more from the techniques and models used to interpret the spectra than from the data itself. A good example of these problems can be seen by comparing the abundances determined for HD140283 and HD19445 by Aller and Greenstein (1960) and by Cohen and Strom (1968) using exactly the same data; the only differences were the techniques of analysis.

For the helium abundances the problem is even more acute since helium lines are not observed in the spectra of F, G and K stars. The helium abundances must be inferred indirectly using interior models of

metal-poor stars and the positions of the subdwarfs in the (M_{bol}, T_e) diagram. However, even these rather crude comparisons lead to some puzzling conclusions when both mild and extreme subdwarfs are included in the analysis (Eggen 1973, 1974). These problems will be outlined in Chapter 7.

For determining effective temperatures of the subdwarfs we must worry most about blanketing corrections, convection efficiencies, and surface-gravity differences. Since the subdwarfs have extremely low metal contents, determination of their temperatures using unblanketed model atmospheres will probably not lead to any serious errors. However, we wish to compare the subdwarfs to the Hyades main sequence, and the blanketing corrections for these Population I stars may be quite large depending on the wavelength interval with which we are working. Concerning convection, various investigations (Cohen and Strom 1968, Travis and Matsushima 1973, and others) have shown that convection is more important in metal-poor stars than in metal-rich ones, and so an adequate treatment of convection is very important when determining T_e's of the subdwarfs. Yet, the theory of convection used in model atmospheres is still rather crude (Kurucz 1970). Part of this problem can be circumvented by calibrating for T_e's using field stars with measured angular diameters. However, most such stars are fairly metal-rich, and so we must still apply blanketing corrections from the models when applying such observational calibrations to our subdwarfs. And finally, when applying the theoretical T_e calibrations we might assume that log g = 4.5 is a good approximation for the subdwarfs. However, the results of Chapter 7

show that many of the subdwarfs are significantly evolved; log g = 4.0 or 3.5 might be more appropriate. It seems then that we may also have to worry about surface-gravity corrections when determining T_e's.

Blanketing corrections for UBV photometry have been determined by Wildey et al. (1962) and have been used extensively in the literature (for example, see Eggen and Sandage 1962, Sandage 1964, Johnson et al. 1968, Dixon 1965, and many others). These blanketing corrections and the corresponding blanketing vectors in color-color diagrams seem to be entirely adequate for the analyses of the hotter metal-poor stars (in the temperature range of F and early-G dwarfs). But for the cooler stars (temperatures of late-G and K dwarfs) these blanketing corrections may need revision (see Cayrel 1968). The corrections for other photometric systems have been studied somewhat (Fischel 1964, Sandage and Smith 1963, Cayrel 1968) but have found considerably less use than those for UBV. A preliminary study of the blanketing in the 13-color indices was made by Johnson and Mitchell (1968).

The evolutionary status of the subdwarfs has received some attention in recent years (for example, see Eggen 1973, Sears and Whitford 1969, Cayrel 1968, Dixon 1965, Sandage 1964) with all of these studies making use of the subdwarfs' positions in the (M_{bol}, T_e) diagram (or some equivalent color-magnitude diagram) or using the apparent blue cutoff in B-V of the observed subdwarfs. These investigators argue that the turn-up of the subdwarfs in the (M_{bol}, T_e) plane and the cutoff in B-V are equivalent to the turnoff points observed for the main sequences of globular clusters. These arguments seem plausible but have not been

tested by studying the subdwarfs' surface gravities as a function of temperature. Such evolutionary effects are extremely important to consider if one wishes to understand the subdwarfs' positions in the (M_{bol}, T_e) plane (for example, see the series of papers by Sandage and Eggen 1959, Eggen and Sandage 1962, and Eggen 1973), and if one wishes to use the subdwarfs' luminosities, as compared to Hyades stars, for studying helium abundances (see Strom and Strom 1967).

As can be seen from the above discussions, the focus of the above problems comes to rest in the (M_{bol}, T_e) diagram. If we can determine accurate blanketing and bolometric corrections for the subdwarfs and Hyades stars, if we can measure good parallaxes, and if we can accurately take into account convective and surface-gravity differences when determining the T_e's, then we can accurately plot the subdwarfs and Hyades dwarfs in this diagram. We can next use static and evolving interior models, plus a little good judgment, to try to understand the relative positions of the subdwarfs and Hyades stars in terms of differing metallicities, differing helium abundances, and differing evolution. The problem is certainly not an easy one, but the results can give us important information concerning the subdwarfs and in turn important information concerning globular clusters and the early epochs of the Galaxy.

Finally, not much is known about the masses of the extreme Population II objects. Very few are found in binary systems, and these few are not well studied. Only 85 Peg (BS 9088), which is a mild subdwarf, has a fairly well determined orbit, and yet Eggen (1963) gives a mass of

0.59 the solar mass and Harris, Strand and Worley (1963) give a mass of 0.81. Considering these uncertainties and lack of data, any sort of mass determination for extreme Population II dwarfs, whether direct or indirect determinations, will provide valuable information.

Photometric Sensitivity and the Calibration of Photometric Indices

In Chapter 5 of this thesis we will discuss the sensitivities of the 13-color indices to the basic stellar atmospheric parameters, and in Chapter 6 will be given the calibration of these indices, but in this introduction we wish to outline briefly the thinking and ideas which have motivated the direction of this investigation.

The main factors determining the spectral distribution of a star's energy output are the effective temperature, the surface gravity, and the metallicity. Other factors (such as the atmospheric helium content or microturbulence) are either relatively insignificant or are functions of the temperature, gravity, and metallicity. Hence our first task will be to study the sensitivity of the 13-color indices to these three main parameters, and to select those indices which are most sensitive and which give the clearest separation between changes in temperature, gravity, and metallicity. Ideally we would like to find an index which is highly sensitive to only effective temperature, another index which is highly sensitive to only surface gravity, and a third which is highly sensitive to only metallicity.

Using a strictly observational approach it is extremely difficult, perhaps impossible, to obtain a complete separation of the index

sensitivities. If we do 13-color photometry in clusters and if we assume that chemical composition is constant in a given cluster, we are left with only the effective temperature and surface gravity effects to disentangle. If we obtain 13-color photometry of subdwarfs and of Hyades dwarfs and if we assume these stars have equal surface gravities, we are left with only temperature and composition differences to sort out. Finally, using 13-color photometry of stars with observed angular diameters and restricting our attention to normal field stars of constant MK luminosity classifications, we can isolate the effective temperature sensitivity of the 13-color indices. However, all of these techniques involve assumptions which are only approximately correct. Stars in a given cluster may have some small range in compositions, subdwarfs do not have exactly the same surface gravities as Hyades dwarfs (at constant T_e), and the field stars with measured angular diameters certainly do not have identical compositions. In the final analysis, if we wish a completely unambiguous picture of the 13-color sensitivities, we will probably have to rely somewhat on the results of model atmospheres.

Once we know which indices are sensitive to which atmospheric parameters, we can proceed with the calibrations. In this thesis the calibration for effective temperature will be obtained from model atmospheres and from stars with measured angular diameters. In this way we will have two independent calibrations, one observational and one theoretical, for comparing and checking systematic effects. However, all of the necessary blanketing corrections will come from the models. The metallicity calibration will be based primarily upon high dispersion,

spectroscopic studies of dwarfs and subdwarfs; the models will be used
only to extend the temperature range of this calibration. We realize
that these spectroscopic studies may contain significant errors, but
they represent the best available means of calibration at the moment.
For the hotter subdwarfs ($T_e \gtrsim 6000^{\circ}$) the surface gravities will be de-
termined by fitting the observed 13-color energy distributions to
theoretical distributions. In the cooler temperature ranges the surface-
gravity calibrations will be based upon stars whose gravities (or
equivalently masses and radii) have been well determined previously and
given in the literature. Finally, one other calibration needs mention-
ing. To place stars in the (M_{bol}, T_e) plane we need to know bolometric
corrections for some 13-color magnitude. For this calibration we will
use 13-color and UBV photometry for Hyades dwarfs plus the bolometric
correction versus spectral type relation of Johnson (1966). The above
calibration schemes are certainly not perfect but are the best possible
with the available data.

What is to be Learned About Subdwarfs

Once we have understood the 13-color photometry for F, G, and K
stars and once we have obtained the various calibrations, we can attack
the remaining problems for the subdwarfs. The subdwarf metallicities
and effective temperatures will come directly from the calibrations.
The blanketing curves, which were used previously in studying the sensi-
tivity of the photometric indices, will be used to examine the relative
importance of metallicity and surface gravity (evolution) upon the ultra-
violet excesses of the subdwarfs and to give us an idea of the surface

gravities of unevolved subdwarfs. These blanketing curves will also help us understand the positions of subdwarfs in color-color and color-magnitude diagrams. In our study of photometric sensitivity we will find one index sensitive to gravity but nearly independent of metallicity and temperature and another index sensitive to temperature but insensitive to gravity and metallicity. A color-color plot of these two indices will give us a very clear picture of the evolutionary status of most of the subdwarfs. Our calibrations will also be used to place the subdwarfs and Hyades dwarfs in the (M_{bol}, T_e) plane. These results agree well with previous studies lending support to these investigations and giving us confidence in our techniques of calibration. The luminosities and surface gravities of the subdwarfs, as compared to Hyades dwarfs, will be used to calculate masses of the subdwarfs as a ratio to Hyades masses at constant T_e. The luminosities of the subdwarfs will also be used to gain some idea of their helium abundances, but the interpretations of these results are not unambiguous. And finally, the problems and implications resulting from several seemingly evolved, cool subdwarfs will be discussed and used to argue about the early conditions in the Galaxy.

So we see that the analyses of this thesis will contribute significant information in most of the problem areas related to the subdwarfs. The only points which will not be completely resolved concern the subdwarf helium abundances and the seeming evolution of several cool subdwarfs.

CHAPTER 2

INSTRUMENTATION AND PHOTOMETRIC TECHNIQUES

Instrumentation

The observational equipment used for this thesis can be described in three categories--telescopes, photometers, and electronics. In the first category only two telescopes, the 60" and the 32" of the San Pedro Martir Observatory, were used to take data for this thesis. (The 21" on The University of Arizona campus was used for gaining experience with the 8C photometer, but was never used to take data for the thesis.) The 60" telescope was used for the bulk of the observing; only a small number of nights were obtained on the 32".

The 60" telescope was designed to be, and is used only as, a photometric telescope, a "light bucket." As Table 1 shows its aluminum mirror produces a rather sizable image. To the eye the image of a bright star appears to be about 1 and 1/2 to 2 mm in size (13 to 17.5 arc seconds), and as Table 1 shows a 2 mm diaphragm includes only 67% of the light and a 3 mm diaphragm 95%. Previous observers suggested that a 3 mm diaphragm would probably be adequate for the photometry, but that a 4 mm diaphragm would certainly not hurt. Upon seeing the image (with its several rays and fish tails) I decided to use a 4 mm diaphragm. Since then the image shape and size has been greatly improved by removing the mirror supports, which the observing assistants had added to the 60"

Table 1. Image characteristics of the 60" telescope.

Diaphragm (6RC photometer)	Diameter (mm)	% Light
E	9	99.9
F	7	100.0
G	4	95.4
H	3	94.6
A	2	67.1
B	1	55.2
C	1/2	23.3
D	1/4	7.2

mirror, and by recollimating the 60". However, a 4 mm diaphragm has been used for all the observing in this thesis. Good photometry for other observing projects has been obtained with the 3 mm diaphragm.

It may seem strange that good photometry can be done with only 95% of the light. However, the remaining 5% lies in a rather broad, flat halo surrounding the stellar images. To check that the omitted 5% of the light produces negligible errors in the photometry a simple experiment was performed. A bright star was centered in the 4 mm diaphragm and then the light was passed to the photomultiplier. With the DC amplifier an adequate deflection was obtained on the chart recorder or on the telescope's ammeter. The value of this deflection was carefully noted. Next, using the telescope's slow motion controls the image was moved back and forth, up and down, while the deflection value was closely watched. It was found that the image could be moved about considerably without the deflection value changing in the slightest. This indicates several things. First, the omitted 5% of the light does indeed lie in a rather broad, flat halo (scattered light within the telescope) and will produce negligible effects on the photometric accuracy. An equivalent 5% of the light will be excluded for all stars as long as they are fairly near being centered in the photometer. (The 60" mirror has since been cleaned and re-aluminized. Although no further tests have been made, it is quite obvious to the eye alone that the light in the outer halo has been considerably reduced, to probably one or two percent of the light. It seems then that the outer halo was caused almost entirely by the dirtiness of the mirror.) Second, the above check

shows that the chosen diaphragm size is adequate, or even perhaps more than adequate. And third, the check shows that the field lenses of the photometers are doing a good job. The above testing was done on a number of different occasions with both photometers.

The 32" is quite a different story. When first used to obtain observations for this thesis, its mirror suffered from rather severe turned-down edge in the outer 1 and 1/2 inches. This turned-down edge produced a rather large halo about each image. However, when stopped down to 29", this telescope produced near-perfect images. Two of the 8C nights of photometry were obtained in this stopped-down configuration. Since that time the 32" mirror has been refigured by Norman Cole of the Kitt Peak optical shop and now has a near perfect image for a full 32" aperature. This refigured 32" mirror was used to obtain part of the Hyades photometry, the photometry of YY Gem, and some of the last 6RC photometry of the subdwarfs.

Two photometers were used for the observing in this thesis--the 8C photometer as described by Johnson, Mitchell, and Latham (1967) and the 6RC photometer as described by Mitchell and Johnson (1969). All of the 13-color photometry of this thesis has been taken with the original photometers (photomultipliers, filters, and so forth) that were used to define the 13-color system. The eight colors of the 8C system, whose effective wavelengths range from $3370\overset{o}{A}$ to $6350\overset{o}{A}$, are combined with the six colors of the 6RC system, whose effective wavelengths range from $5830\overset{o}{A}$ to $11,080\overset{o}{A}$, to form a 13-color narrow and intermediate band system. (The $5830\overset{o}{A}$ filter is common to the 8C and 6RC systems; this is why eight

colors plus six colors give only 13. With this overlap the two systems
can be tied together using only colors, not magnitudes.) The approximate
half-intensity widths vary from 90Å for the three ultraviolet filters to
645Å for the 1.1μ filter. The names of the filters are obtained from
their effective wavelengths; for example, the filter band with an approx-
imate effective wavelength of 0.33μ produces the 33 magnitude, and so
forth. The 8C photometer uses the S-4 photosensitive surface of an RCA
1P21, and the 6RC photometer uses the S-1 surface of an RCA 7102, the
same two photomultipliers of UBVRI photometry. An absolute calibration
for the entire 13-color system was obtained by Mitchell and Johnson (1969).
However, this initial calibration was revised when Oke and Schild's
(1970) absolute calibration of α Lyrae appeared in the literature; this
revised calibration has been published by Johnson and Mitchell (1975).
In Table 2 are listed the characteristics of the entire 13-color system.

The construction of the two photometers is basically that of the
Cassegrain-focus photometer described by Johnson (1962), except that
neither has the second eyepiece for viewing the focal-plane diaphragm.
Each has only a single wide-field eyepiece. The 60" was originally con-
structed with the JHKL photometer, which has its diaphragm a great
distance behind the front surface of the photometer, in mind. Also, the
secondary of the 60" is greatly aspherical. These two facts necessitate
the use of a spacer when mounting the 8C and 6RC photometers on the 60"
in order to obtain the best focus at the diaphragm.

Only DC techniques have been used in obtaining the data of this
thesis. Throughout the entire observing time only two different DC

Table 2. Characteristics of the 13-color photometric system.

Filter Band	λ_{eff} (μ)	Approx. Half-intensity Width (Å)	Effective Rectangular Bandpass (%)	Relative Energy of Mean AOV (Mag.)	Mean Extinctions at San Pedro Martir	Mean Extinctions at Catalina
33	.337	92	3.3	+0.263	0.664	0.692
35	.353	93	3.6	+0.302	0.540	0.570
37	.375	87	3.4	+0.005	0.443	0.459
40	.402	209	5.6	-0.640	0.335	0.352
45	.459	230	6.1	-0.381	0.222	0.237
52	.518	233	5.0	0.000	0.164	0.180
58	.583	197,220	3.8	+0.363	0.147/ 0.145	0.164/ 0.158
63	.635	263	5.1	+0.670	0.109	0.122
72	.724	620	8.1	+1.087	0.078	0.096
80	.800	450	5.4	+1.436	0.064	0.077
86	.858	510	5.6	+1.652	0.051	0.061
99	.985	610	5.9	+1.973	0.057	0.05
110	1.108	645	7.4	+2.384	0.050	0.05

amplifiers were used, numbers 1 and 4 of the San Pedro Martir Observatory. Amplifier 4 was used for only a short time during the fall of 1973 and was calibrated only once. Amplifier 1 was used a little at the end of 1973 and then throughout all of 1974; this amplifier has been calibrated three times. All of these calibrations were carried out using the AC/DC calibrator built and described by Ortega M. (1971). This calibrator produces an extremely constant current signal, the magnitude of which is controlled by a very accurate, calibrated potentiometer (accuracy 0.01%). Hence two means of calibration are available. In the first method the calibrator signal is left constant while the gain of the DC amp is varied. The ratios of the output signals from the DC amp then give its calibration. In the second method the calibration signal is varied using the very accurate, calibrated potentiometer so that the output signal of the DC amp remains constant as its gain is varied. Then ratios of the readings of the calibrated potentiometer give the amplifier calibration. The first technique is simpler, but the second is more accurate in that it eliminates any nonlinearities of the recording equipment (v-to-f converters, counters, chart recorders, and so forth). The simple technique was used for the calibration of amp #4 and for the first calibration of amp #1. The more accurate technique has been used in the later calibrations of amp #1. In making the calibrations, great care was taken to obtain stability and equilibrium of the electronics and to subtract out any zero point drifting of the DC amp by making multiple measures with the calibrator signal on, then off, then on, and so forth. Considering the stability of the calibrator signal,

the techniques of measurement, and the repeatability of the measures, I would estimate the individual calibrations to be accurate to two or three thousandths of a magnitude. Three calibrations of amp #1 were made covering a time span of more than a year and a half and including the full temperature range of the seasons. The three calibrations agree to better than one percent (0.007 magnitude or better) indicating that amp #1 has good temperature and temporal stability.

For recording the data two systems were used. For the first few observing runs the electronics rack of the automated data-collection system (Johnson and Mitchell 1962) was used. However, various parts of the automatic system had been disconnected and so the signal from the rack was merely fed to a digital voltmeter and all data was recorded by hand. This system proved unsatisfactory because of the hand recording of data and because of various intermittent problems with the rack and digital voltmeter. Most of the data for this thesis was taken with a second system made up of a voltage-to-frequency converter, counter, digital clock, and automatic printer for recording the time and deflections. The star names, filter numbers, and gain settings were still recorded by hand. A chart recorder was usually used as a back-up system.

A number of times during the course of the observations the linearity and consistency of these recording devices were checked. Three separate measures are available for this testing--the measures of the v-to-f plus counter system, measures of the chart recorder, and measures of an ammeter taking its signal directly from the back of the DC amp. The linearity of the v-to-f converter and of the chart recorder

could be checked by plotting their readings versus those of the ammeter (assuming of course that the ammeter is linear). A further, more accurate check of the v-to-f converter was obtained by plotting its reading versus those of the chart recorder. The entire system is entirely consistent and linear to within the accuracy of my ability to read the chart paper or make eye measurements of the ammeter (better than 1% for the chart recorder and a few percent for the ammeter).

Techniques of Photometry

In doing the 13-color photometry of this thesis a number of rules of thumb were followed as closely as practically possible while observing. First, all standard stars used were primary standards from Table 7 of Mitchell and Johnson (1969). Primary standards are those stars observed ten or more times previously in the 8C and/or 6RC. Thirty such primary standards exist of which 23 were used for my 8C photometry and 28 for the 6RC photometry. (Only when observing in the Hyades were secondary standards used. Four Hyades stars which had been observed previously four or more times were observed repeatedly and reduced as standard stars.) During each and every full observing night eight or more standards were observed--usually ten standards per night was the goal. That is, 20% or more of each night was set aside for standards. Of each night's standards some were chosen to be very red, some very blue, and some of intermediate color (of F and G spectral types if possible). This wide range in color allows a good solution for the color term of the transformation to the standard color system. Also, every night approximately four standard star observations were made at

small air mass (~1.0-1.3), 2 to 4 standard star observations at inter-
mediate air mass (~1.3-2.0), and 2 to 4 observations at large air mass
($\gtrsim$ 2.0). With this range of air mass a good solution for the atmos-
pheric extinction coefficients could be made. In general slightly more
stars were observed at small and intermediate air mass than at large
air mass in order that the zero point term and color coefficient of the
transformation could be well determined. It has been found that the
average air mass of the standard star observations is about 1.5. And
finally, standard stars were observed throughout the night, not all at
one time. Usually three were observed at a night's beginning, two or
three at the end, and the rest scattered throughout the middle of the
night. With the standard stars thus spaced throughout a night it is
possible to check the stability and performance of the equipment for the
entire night and to see whether the atmospheric extinction has perhaps
changed during the night.

For the standard stars and brighter subdwarfs three ten-second
integrations were usually made per filter--one star integration, then a
sky integration, and finally another star measurement. Sometimes for
standard stars measured at large air mass five or more integrations were
made per filter, especially for the ultraviolet filters--the number of
integrations depending mainly upon the steadiness (constancy) of the
atmosphere. For the fainter subdwarfs five or more integrations per
filter was the rule--the number of integrations depending upon the
largeness of the signal, the conditions of the atmosphere, and the
stability of the electronics. All program stars (subdwarfs, Hyades, and

so forth) were observed as near the meridian as possible to minimize
the air mass and thereby minimize the atmospheric effects upon the
observations and decrease the probable errors of observation.

After every star observation the standard lamp of the photometer
was observed as quickly as possible in order to measure the fatigue of
the phototube (only important for very bright stars) and to calibrate
out any drifting of the electronics such as, for example, drifting of
the high voltage supply. These standard lamp observations are used for
reducing only the magnitudes and have no part in the color reductions.
Hence the order of observing the filters was arranged so that the
standard lamp was observed as soon as convenient after the filter which
is to be reduced as a magnitude. For example, in 6RC photometry the
standard lamp is observed immediately after the 58 filter which is to
be reduced as a magnitude. In 8C photometry the standard lamp is ob-
served with only two filters (58 and 63) intervening between it and the
52 filter, which is to be reduced as a magnitude. For a few nights of
8C observing the standard lamp did not work well due perhaps to low line
voltage, and so these nights were reduced without the lamp relying upon
the inherent stability of the electronics for calculating the magnitudes.
In general these nights without the standard lamp reduced as well as
nights with the lamp.

On many occasions the centering of the photometer crosshairs
with respect to the diaphragm center was checked. This was carried out
by centering a bright star on the crosshairs, passing the light to the
phototube, and then watching the signal as the star was moved east and

west, north and south with the slow motion controls. It was found that the crosshairs of the 8C photometer are well centered in the 60" telescope and only slightly off center in the 32". For the 6RC photometer the reverse is true--well centered in the 32" but slightly off center in the 60". However, the lack of centering of the photometers, when observing near the meridian, was so small as to be negligible, and so no attempt to correct the centering was made. But, on the 60" it was noted that the displacement of the crosshairs from the diaphragm center did increase somewhat when the telescope was more than three hours from the meridian. This was taken into account, by displacing the stars from the center of the crosshairs, when observing standard stars at large air mass.

Finally, throughout the night the observing assistant and myself would keep close watch on the repeatability of the star integrations using both the numbers of the counter and the deflections of the chart recorder as checks. If the integrations varied by one or two percent, things were fine. Variations of three or four percent would cause concern, especially if observing in the blue or yellow (filters 40 to 58) and at small air mass, and would lead to five or more integrations per filter in order to examine the trend of the variations and perhaps average then out. Variations of more than four percent at small air mass and for a continued length of time would certainly lead to the termination of a night's observing. Such continued monitoring of the data is necessary for obtaining quality photometry.

Specific Problems

During the course of the observations and reductions a number of
problems were confronted and solved. The knowledge and procedures
learned from this experience will be presented briefly in this section.

In columns 6 and 7 of Table 2 are listed the mean atmospheric
extinction coefficients (in magnitudes/air mass) for the 13-color
photometry at San Pedro Martir (S.P.M.) and at the Catalina observatory
(Johnson et al. 1967, Mitchell and Johnson 1969). The S.P.M. values have
been obtained from 26 nights of 8C observing and 30 nights of 6RC ob-
serving. The point to note here is the large extinction of the ultra-
violet filters. These large extinctions often caused problems when
trying to observe standard stars at large air mass. Also, for this
reason a conscious effort was made to observe all program stars as close
to the meridian as possible.

Dr. Johnson (1975) pointed out that the RCA 7102 phototube of
the 6RC photometer becomes nonlinear for large output currents. Hence,
all 6RC photometry was carried out at gains 4+1 to 6+6 in order to main-
tain linearity. For some bright, red stars the high voltage had to be
reduced in order to stay in this range of gains. Also, it was found by
experience that a high voltage of 900 to 920 volts is optimum for the
6RC photometry. This high voltage maintains good sensitivity without
leading to instabilities or drifting of the output current. For my first
two observing runs 1000 volts were used on the 6RC photometer (since
1000 volts is used for the RCA 7102 of the UBVRI photometer of San Pedro
Martir), but this voltage was found to produce at high gains (6+3 to 6+6)

much noise, rapid drifting, and at times extremely erratic changes in the output signal. All 6RC photometry for stars fainter than about 9th magnitude from these first observing runs was thrown out.

It was also discovered during the course of the observing that in the 6RC photometer the brightness of the standard lamp as measured by the phototube varies strongly with declination. This variation, which amounts to about 0.2 magnitude in going from declination -30 to +60°, is caused by some sort of flexure in the photometer. However, the effect does not show up in the reduced photometry, and so evidently the flexure affects the star measurements as much as the standard lamp measures. Hence, as long as the lamp is working well there are no problems. But, on one night the standard lamp of the 6RC photometer was erratic, probably due to low line voltage. For this night (October 25-26, 1973) it was necessary to substitute averaged standard lamp measures derived from the standard-lamp-brightness versus declination curves of previous nights. In reality all of this is unimportant since the 58 magnitudes of 6RC photometry are never used in the final results of this thesis. The final 13-color photometry of the subdwarfs and Hyades stars makes use of only the 6RC colors, and the measurement of colors, which indicate ratios of stellar intensity, would not be affected by flexure in the photometer.

In carrying out the large amount of observing which has gone into this thesis, a good idea of the limiting magnitudes observable with the 13-color system was obtained. Working on the 60", wanting probable errors of a single observation of one to three hundredths, and desiring to use ten or fewer integrations per filter, one could work

previously to 12th magnitude with the 8C photometer, to 7th or 8th magnitude with the 110 filter (1.1μ) of the 6RC photometry, and to 10th or 11th magnitude with the other 6RC filters. Fainter magnitudes were of course available with more integrations and work. Since the time of the thesis observing, the 60" has been re-aluminized and now has close to two magnitudes greater sensitivity.

In reducing the 8C photometry it became obvious that red leak corrections were necessary for some of the redder subdwarfs and Hyades stars, of spectral types K and M. But this presented a problem since the 13-color red leak corrections of Johnson, Mitchell and Latham (1967) were calibrated in terms of the color index U-R of broad-band photometry. This causes no problems for bright stars since nearly all stars in the LPL catalogues (Johnson et al. 1967, Mitchell and Johnson 1969) have UBVRI photometry (Johnson et al. 1966). However, some of the subdwarfs have no U photometry and many no R photometry. It was found that for bright field stars (mostly dwarfs and giants) a good mean relation be- tween the 37-72 index of 13-color photometry and U-R could be derived. This relation could be defined to an accuracy of much better than 0.1 magnitude. A similar relation between 35-63 and U-R with only slightly larger scatter was also found. So, for subdwarfs with complete 13-color photometry the 35-72 index gives U-R, using the mean relation of the field stars, which in turn gives the red leak corrections. For subdwarfs with only 8C photometry (some of the fainter ones) 35-63 gives U-R and so forth. If this process seems somewhat crude, it should be noted that for all subdwarfs of spectral type F and G (the majority of

subdwarfs) the red leak corrections are less than one thousandth of a magnitude and have been neglected. Only at spectral type K5 does the red leak correction become as large as two or three thousandths of a magnitude (for the 33 filter); corrections of this size have been applied to the included photometry. The reddest subdwarf observed, G102-22, has a spectral type of sdM4 and has red leak corrections of 0.040 for the 33-52 index, 0.009 for 35-52, and 0.001 for 37-52.

In addition to the subdwarf and Hyades observations, the star YY Gem was also observed, and its photometry is used in deriving the observational effective temperature calibration. This star is also component C of the α Geminorum (Castor) multiple star system, and is about one minute of arc from Castor. It has a V magnitude of about 9.1 while components A and B of Castor have a combined V magnitude of 1.59. At first it was attempted to observe YY Gem with the 60", but tests showed that significant amounts of scattered light from Castor were passing through the diaphragm. Only one 6RC observation of YY Gem was made with the 60". Fortunately the 32" was not being used at this time, and so the observations were continued on this telescope. With the 32" tests showed that negligible scattered light from Castor was passing through the diaphragm when YY Gem was centered for observation. Comparisons between the one 60" observation and the 32" observations have shown that errors as large as 0.2 magnitude could have resulted had the observations of YY Gem been made on the 60". This attests to the large halo of scattered light mentioned earlier for the 60" before its mirror was cleaned and realuminized.

CHAPTER 3

REDUCTION OF THE PHOTOMETRY

The Computer Program

The computer program used to reduce the 13-color photometry pre-
sented herein is basically the same program written and used by Richard
I. Mitchell to obtain the bright star 13-color photometry which essen-
tially defines this photometric system (see Johnson and Mitchell 1962;
Johnson, Mitchell and Latham 1967; Mitchell and Johnson 1969). This
computer program has been changed only enough to make it compatible with
the Nova mini-computer system which is available in Ensenada. The main
change has been to run the program in two large parts using disk files
for the storage and transference of the data rather than having CALL LINK
statements and COMMON blocks to tie together eight small sections as
originally. The first part of the present program is concerned primarily
with raw data reduction while the second part contains the least-square
analysis and the final data output. The input for this program is also
divided into two parts. The first input tape (inputting is by means of
paper tapes) is referred to as the "instrument tape" and contains all of
the data which will not change from night to night, such as the amplifier
calibration and the colors of the standard stars. The second part of the
input (the "data tape") contains all of the observations for a given
night. To combine these two blocks of data, to correct punching errors,

27

and to facilitate the analysis of the photometry, the program has been arranged to make considerable use of the disk files and TEXT EDITOR facilities of the Nova system. Such an arrangement leads to great versatility when the photometry of a given night seems particularly interesting or problematic.

What the Program Does

The computer program is set up to reduce only narrow-band photometry--no second order color term is included for the extinction. Using the standard star observations the program solves by least squares for three quantities for each color or magnitude. These are the following: (a) a correction to the mean extinction, which is part of the input, (b) the zero point term of the transformation to the standard system, and (c) the coefficient of the color dependent term of the transformation. Once these three quantities are known the program then determines standard magnitudes and colors for all stars observed. The program can handle up to ten different filters; the output is presented as two magnitudes and eight colors.

It is somewhat convenient that the program runs in two halves because the first half does only the raw data reduction, and so it can be used to produce raw, instrumental magnitudes for any type of photometry--narrow-band, broad-band, red leak measures, etc. First of all the first half outputs general information from the instrument and data tapes such as the name of the observatory, size of the telescope, number of the D.C. amplifier, color system code, filter names, filter number codes, error tolerances, color and air mass ranges needed for a

least squares solution, and the mean extinction coefficients. Next a list of all stars observed is output along with their positions and times of observation. Finally the raw instrumental magnitudes and colors, their weights, and the hour angles, air masses, and Julian Dates of the observations are printed. The raw magnitudes and colors are calculated by converting the star-minus-sky differences to magnitudes and then adding on the correct number of magnitudes corresponding to the gain setting. (An arbitrary zero point is included for the straight magnitudes.) A mean extinction correction is also included in these raw magnitudes; this correction is $-kX$, where k is the mean extinction for a given magnitude and X is the exact air mass for the given filter observation.

The second half of the program starts by searching through the list of stars observed comparing each with the list of standard stars input on the instrument tape. In this way the standard stars observed in a given night are selected out for the least squares solution. The program now outputs a list of the standard stars observed, including the name of the standard, the air mass of the observation, the observed colors, the standard colors, and a crude zero point obtained by subtracting the observed color from the standard color. These crude zero points are averaged, and any standard whose color deviates by more than the weighted error tolerance from the average is rejected and not used in the least squares. The weighted error tolerance is the error tolerance input on the instrument tape times the air mass of the observation. For example, in most of the reductions for this thesis the error tolerance

was 0.15, and so the weighted error tolerance is 0.15 at one air mass, 0.30 at two air masses, etc. The program outputs a list of all standards so rejected.

Next comes the least-squares solution for the zero point and color term of the transformation and for the correction to the mean extinction coefficient. The program computes the air mass range for the standard stars of the night, and if this range is greater than the air mass criterion of the instrument tape, then a correction to the mean extinction coefficients is included as part of the least-squares solution. If not, the default differential extinction corrections from the instrument tape are used, and this part of the least-squares is dropped. In all the present work the air mass range needed for a solution was 0.80, and the default corrections were all 0.00. The program also computes the color range for the standards of the night, and if this range exceeds the color range criterion of the instrument tape, the least-squares calculates the coefficient of the color term of the transformation. If not, the default color coefficients from the instrument tape are used, and this part of the least-squares is dropped. In all the present work the color range needed for a solution has been 0.50, and the default color terms have been 0.000 for the magnitudes and 1.000 for the colors. If only one or zero standards were observed in a night, the program does no least-squares and only uses the default values of the instrument tape including default zero points. In the present work the default zero points have never been used. If they had been needed, their values could have been the averages of the zero points from preceding and following nights.

The mean extinction coefficients needed as part of the input have caused some problems since San Pedro Martir is a new observing site for 13-color photometry. So, no mean extinction coefficients were known when this work began. For some of the first trials on the computer mean extinctions from Kitt Peak were used. Later, when serious reductions began, "mean" extinctions from one or two nights, that had been reduced by hand, were used. As the work progressed the mean extinctions were continually improved as more and more nights were reduced and averaged in. It has been found that the extinction coefficients can change rather drastically from night to night (more than 0.10 magnitude/air mass), and these changes often do not show any systematic trend. Hence, for nights where the air mass range is not sufficient for a good extinction solution, the total mean extinction coefficients have been used rather than a mean of only those nights of the same observing period.

Once the least-squares solution is completed, the computer outputs the calculated zero point, color coefficient, and correction to the mean extinction coefficient. Next it gives a list of the standard stars, the air masses of their observation, their standard colors, their observed colors, the calculated colors using the results of the least-squares, and finally the residuals between the standard colors and the calculated colors. Such a list is output for each of the magnitudes and colors reduced. The residuals give a fairly good indication as to whether or not the night was really good for photometry. For example, a good night will give residuals of one or two hundredths of a magnitude

for most colors when eight to ten standards have been observed. Larger residuals can be expected for the ultraviolet filters, for the individual magnitudes, and for the colors involving the 1 micron filter.

Finally, the program lists the final standard magnitudes and colors for all stars observed during the night. With this list is included the weights of the observations, the hour angles, the air masses, the Julian dates, and a number code which indicates what type of least-squares solution was obtained (for example, a zero indicates no standards and hence no solution; a one indicates only the zero point term was calculated; and so forth).

CHAPTER 4

THE OBSERVATIONS

In this chapter the observations of the subdwarfs, of the Hyades stars, of YY Gem, and of BS5270 will be presented. The quality of these observations will be discussed in terms of the probable errors of observation and in terms of any systematic differences from the previous Catalina 13-color photometry. The results indicate that the present observations are of high quality.

The Subdwarfs

The stars observed in this thesis were selected from a large number of lists of subdwarfs, extreme Population II objects, stars with large ultraviolet excesses, stars lying significantly (> 1/4 magnitude) below the main sequence in the (M_{bol}, T_e) diagram, and so forth. In general most of the stars were selected because they have been classified subdwarfs spectroscopically or because they lie below the main sequence (but not so far below as to be degenerate objects). Only a few were selected for their ultraviolet excess or because of Population II characteristics and large trigonometric parallaxes. The starting point for the search for observable subdwarfs was Eggen's (1964) list of high velocity objects. Other subdwarfs were then added from the work of Sandage and Eggen (1959), Strom and Strom (1967), Roman (1955), Sandage

and Smith (1963), Eggen (1969a), Eggen and Sandage (1959), Johnson et al. (1968), Eggen and Sandage (1962), and Gliese (1969). A final list of 149 subdwarfs was derived, and finding charts were made for all.

Of the 149 subdwarfs 119 were observed at least once--all 119 were observed with the 8C photometer and 114 with the 6RC photometer. An attempt was made to observe each subdwarf four times with each photometer. The observing was carried out at San Pedro Martir during the fall of 1973 and throughout most of 1974, and in total the subdwarfs were observed on 57 different nights--25 nights for the 8C photometry and 32 nights for the 6RC photometry.

In Table 3 is listed the complete, reduced 13-color photometry of the 119 observed subdwarfs transformed onto the standard 13-color system of Mitchell and Johnson (1969). No problems were encountered with the transformations since the original 13-color filters and photo-multipliers, which were used to define the system, have been used for the present observations. Also, the same standard stars have been used, and for these reasons one should not expect any systematic differences between the San Pedro Martir observations and Catalina observations. For a few subdwarfs the previous 13-color observations of Johnson and Mitchell (1968) have been averaged in with the San Pedro Martir observations. In Table 3, column 1 gives the subdwarf name (in general the name reflects the source of the finding chart), column 2 gives the 52 magnitude, columns 3 to 14 the other 12 filters reduced as colors with respect to the 52 filter, and column 15 the number of blue (8C) and red (6RC) observations, NB and NR respectively. A "D" following the star

Table 3. 13-color photometry of subdwarfs.

Name	52	33-52	35-52	37-52	40-52	45-52	52-58	52-63	52-72	52-80	52-86	52-99	52-110	NB/NR
+54°223	5.362	0.484	0.351	0.615	0.788	0.314	0.368	0.606	0.803	1.000	1.051	1.188	1.291	4/4 (4)
-9°256	9.069	0.340	0.232	0.454	0.664	0.294	0.291	0.492	0.714	0.865	0.925	0.989	1.143	4/4 (2)
+19°279	5.464	0.966	0.862	1.122	1.022	0.332	0.459	0.710	0.945	1.141	1.221	1.337	1.452	9/8 (7)
-16°295	3.690	0.652	0.501	0.753	0.845	0.328	0.380	0.630	0.845	1.026	1.104	1.209	1.342	8/8 (8)
-26°828	6.532	0.595	0.482	0.752	0.836	0.331	0.383	0.621	0.833	1.017	1.081	1.186	1.325	6/7 (7)
-17°484	10.610	-0.023	-0.062	0.097	0.442	0.266	0.239	0.416	0.580	0.729	0.785	0.805	--	4/3 (0)
-13°482	9.902	-0.014	-0.047	0.084	0.422	0.232	0.263	0.398	0.638	0.760	0.821	0.862	--	3/3 (0)
-26°957	8.896	0.350	0.243	0.400	0.646	0.286	0.289	0.488	0.750	0.858	0.927	0.979	1.112	3/4 (4)
G4-37	11.543	0.010	-0.101	0.153	0.467	0.258	0.244	0.441	0.645	0.838	0.902	0.934	--	4/3 (0)
+33°529	10.082	1.976	1.662	1.857	1.618	0.456	0.828	1.271	1.684	2.051	2.197	2.406	2.604	5/3 (3)
-13°544	6.277	1.106	0.957	1.189	1.067	0.341	0.492	0.766	0.982	1.181	1.269	1.386	1.593	4/4 (3)
+25°495	8.185	-0.061	-0.156	0.131	0.477	0.278	0.262	0.455	0.647	0.789	0.852	0.888	1.017	4/4 (3)
G78-26D	11.038	1.577	1.504	1.835	1.495	0.405	0.777	1.215	1.489	1.808	1.960	2.137	--	3/3 (0)
+11°468	10.890	0.092	-0.004	0.248	0.599	0.311	0.290	0.494	0.781	0.918	0.922	1.001	--	4/2 (0)
G5-36	10.908	0.210	0.058	0.261	0.566	0.297	0.264	0.477	0.679	0.829	0.925	0.923	--	4/3 (0)
G38-1	11.588	1.846	1.717	1.919	1.739	0.491	0.834	1.248	1.756	2.085	2.236	2.466	--	3/4 (0)
-7°603	8.389	0.360	0.248	0.487	0.688	0.309	0.331	0.551	0.766	0.928	1.022	1.040	1.219	3/3 (2)
-3°592	6.849	0.231	0.094	0.303	0.601	0.280	0.282	0.488	0.675	0.829	0.882	0.954	0.986	4/4 (2)
+34°796	8.769	1.177	0.674	0.996	1.057	0.421	0.478	0.770	1.066	1.283	1.372	1.501	1.669	4/4 (4)
+21°607	9.329	0.000	-0.095	0.149	0.446	0.249	0.220	0.425	0.594	0.740	0.760	0.777	--	3/4 (0)
G175-39	8.583	1.257	1.115	1.357	1.094	0.334	0.529	0.784	0.981	1.205	1.292	1.419	--	4/4 (0)
+45°992	7.091	0.327	0.197	0.418	0.648	0.290	0.326	0.532	0.729	0.883	0.978	1.023	1.376	4/3 (3)
G102-22	11.820	2.546	2.404	2.085	1.987	0.834	0.577	1.293	2.501	3.259	3.576	4.064	4.384	4/2 (2)
G99-31D	11.543	0.256	0.151	0.450	0.700	0.298	0.328	0.530	0.826	0.907	1.051	1.117	--	2/2 (0)
+37°1312	7.554	1.008	0.864	1.113	1.008	0.321	0.460	0.727	0.913	1.154	1.195	1.348	1.385	4/4 (4)
+19°1185A	9.450	0.246	0.154	0.422	0.680	0.300	0.353	0.578	0.838	1.059	1.149	1.204	1.255?	4/4 (2)
-0°1520	9.111	0.277	0.191	0.399	0.647	0.285	0.279	0.490	0.699	0.854	0.909	0.993	1.072?	4/4 (4)
+47°1419	5.699	0.325	0.211	0.438	0.651	0.283	0.298	0.502	0.662	0.815	0.870	0.943	1.138	4/4 (4)
-33°4113	5.425	0.218	0.126	0.372	0.670	0.315	0.263	0.464	0.655	0.814	0.922	0.986	1.034	2/4 (4)

Table 3. 13-color photometry of subdwarfs. -- __continued__.

Name	52	33-52	35-52	37-52	40-52	45-52	52-58	52-63	52-72	52-80	52-86	52-99	52-110	NB/NR
+31°1684	8.413	0.219	0.049	0.375	0.684	0.330	0.320	0.565	0.809	0.936	1.006	1.108	1.195	4/4 (3)
-34°4036	5.068	0.126	0.071	0.271	0.490	0.243	0.264	0.403	0.548	0.705	0.811	0.780	0.823?	1/1 (1)
-1°1883	7.606	0.543	0.404	0.696	0.827	0.332	0.381	0.635	0.827	1.052	1.175	1.275	1.433	4/4 (3)
+29°1664	7.170	0.618	0.468	0.723	0.838	0.327	0.398	0.635	0.857	1.052	1.116	1.224	1.351	4/4 (4)
G194-22	9.889	-0.017	-0.101	0.168	0.484	0.270	0.256	0.440	0.659	0.814	0.869	0.891	0.951	4/3 (2)
-3°2333	5.714	0.168	0.086	0.281	0.527	0.252	0.245	0.417	0.569	0.706	0.751	0.799	0.872	4/4 (4)
HD74000	9.772	-0.059	-0.131	0.098	0.440	0.241	0.217	0.407	0.599	0.709	0.818	0.867	--	4/3 (0)
G115-22	11.121	0.183	0.039	0.355	0.636	0.321	0.309	0.504	0.758	0.933	0.991	1.086	--	4/2 (0)
+25°1981	9.404	-0.004	-0.072	0.115	0.336	0.192	0.170	0.310	0.481	0.591	0.641	0.664	0.971	4/4 (3)
+42°1922	8.874	1.212	1.116	1.385	1.136	0.308	0.609	0.898	1.186	1.427	1.542	1.677	1.904	4/4 (4)
-12°2669D	10.336	-0.069	-0.089	0.084	0.323	0.182	0.156	0.297	0.358	0.468	0.523	0.529	--	4/6 (0)
G46-5	11.477	0.575	0.404	0.735	0.878	0.363	0.386	0.624	0.890	1.058	1.140	1.304	--	4/4 (0)
G114-26	9.765	-0.007	-0.056	0.185	0.508	0.288	0.266	0.459	0.605	0.792	0.863	0.893	1.094?	4/4 (2)
G115-49	11.793	0.000	-0.133	0.163	0.516	0.280	0.266	0.482	0.513	0.733	0.813	0.880	--	4/3 (0)
+9°2190	11.307	-0.035	-0.106	0.098	0.397	0.230	0.183	0.393	0.511	0.651	0.735	0.824	--	4/4 (0)
G48-29	10.627	-0.050	-0.122	0.074	0.382	0.231	0.188	0.362	0.551	0.712	0.696	0.820	--	4/3 (0)
HD84937	8.449	-0.040	-0.109	0.098	0.403	0.228	0.211	0.389	0.570	0.705	0.752	0.791	1.065?	4/4 (2)
+44°1910	11.105	0.044	-0.004	0.141	0.457	0.280	0.212	0.408	0.600	0.676	0.826	0.815	--	4/3 (0)
+23°2207	5.981	0.197	0.115	0.326	0.566	0.264	0.259	0.420	0.611	0.748	0.804	0.848	0.931	4/4 (4)
G119-32	10.406	-0.019	-0.097	0.184	0.536	0.266	0.254	0.458	0.697	0.861	0.897	0.974	0.892	4/4 (3)
G196-47	12.794	0.173	0.050	0.351	0.626	0.321	0.344	0.541	--	--	--	--	--	5/0 (0)
+21°2247	8.441	-0.037	-0.082	0.168	0.484	0.259	0.260	0.445	0.682	0.829	0.884	0.930	1.176	5/4 (4)
G10-4	11.577	0.364	0.211	0.464	0.803	0.398	0.366	0.642	--	--	--	--	--	4/0 (0)
+36°2165	9.957	0.013	-0.044	0.148	0.444	0.250	0.230	0.376	0.593	0.715	0.794	0.875	1.040?	4/4 (2)
+26°2251	10.535	0.072	0.022	0.242	0.541	0.269	0.258	0.442	0.505	0.680	0.724	0.776	--	4/3 (0)
+51°1696	10.063	0.163	0.060	0.302	0.646	0.330	0.286	0.510	0.690	0.895	0.911	0.978	0.792	2/4 (3)
BS4550	6.626	0.556	0.419	0.738	0.873	0.348	0.390	0.655	0.894	1.099	1.183	1.300	1.430	55/48(48)
G13-9	10.115	-0.030	-0.065	0.096	0.402	0.223	0.223	0.374	0.624	0.738	0.819	0.836	-0.038?	4/4 (3)
G11-44	11.157	-0.005	-0.081	0.164	0.466	0.280	0.214	0.426	0.664	0.812	1.042	0.875	--	4/3 (0)
HD106038	10.285	0.026	-0.043	0.189	0.502	0.267	0.242	0.455	0.616	0.768	0.793	0.879	--	4/4 (0)

Table 3. 13-color photometry of subdwarfs. -- <u>continued</u>.

Name	52	33-52	35-52	37-52	40-52	45-52	52-58	52-63	52-72	52-80	52-86	52-99	52-110	NB/NR
HD108177	9.811	-0.058	-0.123	0.140	0.460	0.261	0.241	0.437	0.583	0.777	0.804	0.799	1.330?	4/4 (3)
+40°2570	6.129	0.223	0.128	0.388	0.620	0.268	0.282	0.481	0.684	0.847	0.896	0.981	1.062	4/4 (3)
G60-48	11.403	0.009	-0.053	0.170	0.547	0.308	0.235	0.430	0.740	0.815	0.914	0.984	--	4/4 (0)
-9°3595	7.776	0.809	0.628	0.937	0.934	0.345	0.420.	0.683	0.910	1.117	1.196	1.324	1.463	4/4 (4)
+10°2519	8.918	0.389	0.256	0.488	0.692	0.311	0.330	0.556	0.743	0.900	0.968	1.065	1.000	4/4 (4)
G14-45D	11.192	1.417	1.147	1.415	1.230	0.323	0.664	0.951	1.305	1.591	1.702	1.868	2.152?	4/3 (1)
+34°2476	10.188	-0.025	-0.084	0.108	0.414	0.243	0.210	0.393	0.587	0.720	0.769	0.817	1.208?	4/5 (3)
G65-22	11.786	0.529	0.403	0.657	0.797	0.354	0.307	0.604	--	--	--	--	--	4/0 (0)
G64-37	11.201	-0.010	-0.082	0.154	0.422	0.264	0.143	0.334	--	--	--	--	--	3/0 (0)
-13°3834	10.810	0.215	0.093	0.357	0.664	0.343	0.282	0.514	0.655	0.867	0.919	1.056	--	3/3 (0)
+1°2920	6.414	0.384	0.293	0.551	0.722	0.305	0.320	0.536	0.733	0.907	0.965	1.046	1.183	5/4 (4)
+30°2536	4.579	0.053	0.010	0.182	0.391	0.192	0.200	0.345	0.437	0.564	0.602	0.613	0.653	5/4 (4)
G66-22	10.611	0.456	0.399	0.680	0.828	0.351	0.375	0.623	0.867	1.062	1.107	1.275	--	4/3 (0)
+26°2606	9.827	-0.055	-0.124	0.139	0.457	0.275	0.224	0.412	0.561	0.718	0.771	0.807	--	4/5 (0)
-8°3858	9.698	0.587	0.465	0.693	0.818	0.326	0.372	0.624	0.816	1.016	1.078	1.192	--	4/4 (0)
-21°4009	8.655	0.208	0.078	0.274	0.599	0.312	0.281	0.497	0.721	0.878	0.957	1.055	1.078	2/4 (4)
+25°2873	5.012	0.159	0.106	0.287	0.491	0.221	0.236	0.397	0.538	0.657	0.692	0.731	0.759	4/4 (4)
-15°4041	9.669	0.845	0.735	1.023	1.009	0.375	0.459	0.757	1.051	1.261	1.352	1.510	1.849	4/5 (4)
-15°4042	9.292	0.600	0.462	0.782	0.893	0.365	0.401	0.672	0.967	1.172	1.261	1.370	1.489	4/4 (3)
G15-24	11.611	0.248	0.088	0.368	0.637	0.335	0.308	0.514	0.782	0.896	0.910	1.069	--	4/2 (0)
-10°4149	7.322	0.078	-0.006	0.181	0.517	0.315	0.255	0.478	0.662	0.821	0.907	0.995	1.077	4/4 (4)
+42°2667	10.007	0.034	-0.040	0.208	0.498	0.272	0.240	0.453	0.666	0.782	0.856	0.903	--	4/4 (0)
+39°2947	6.871	0.620	0.490	0.759	0.857	0.336	0.388	0.646	0.872	1.052	1.131	1.231	1.382	4/4 (4)
+39°2950	8.951	1.250	1.181	1.446	1.181	0.319	0.590	0.905	1.212	1.440	1.524	1.674	1.920	4/4 (4)
G168-42	11.701	0.497	0.345	0.629	0.801	0.374	0.371	0.636	--	--	--	--	--	4/0 (0)
G180-58	11.571	0.354	0.198	0.460	0.766	0.386	0.335	0.643	0.903	1.129	1.218	1.331	--	4/5 (0)
-3°3968	9.796	0.545	0.371	0.697	0.842	0.347	0.394	0.671	0.926	1.129	1.220	1.355	1.439	4/4 (2)
+37°2804	8.671	0.891	0.824	1.075	0.990	0.337	0.447	0.697	0.942	1.150	1.207	1.303	1.530	5/4 (3)
+43°2659	6.971	0.442	0.330	0.530	0.694	0.301	0.321	0.552	0.741	0.898	0.958	1.037	1.082	4/4 (4)
+17°3154	9.288	0.400	0.298	0.527	0.681	0.299	0.312	0.548	0.711	0.871	0.893	1.002	1.387?	4/4 (3)

Table 3. 13-color photometry of subdwarfs. -- <u>continued</u>.

Name	52	33-52	35-52	37-52	40-52	45-52	52-58	52-63	52-72	52-80	52-86	52-99	52-110	NB/NR
+1°3421	7.073	0.289	0.194	0.401	0.625	0.285	0.312	0.520	0.710	0.850	0.918	0.985	1.064	4/4 (4)
G170-56	9.894	0.086	0.017	0.231	0.502	0.274	0.248	0.445	0.581	0.747	0.817	0.869	0.859?	4/4 (2)
+2°3375	10.042	-0.052	-0.111	0.155	0.459	0.275	0.254	0.444	0.638	0.802	0.851	0.930	--	4/4 (0)
+37°2926	8.534	0.261	0.170	0.404	0.618	0.292	0.290	0.496	0.719	0.883	0.903	0.977	1.106?	4/4 (4)
+25°3344	7.036	0.408	0.347	0.087	0.144	0.095	0.104	0.198	0.286	0.338	0.378	0.424	0.449	4/4 (4)
C20-15	10.724	0.240	0.128	0.374	0.625	0.344	0.306	0.581	0.751	0.965	1.055	1.225	--	4/4 (0)
G183-11D	9.848	-0.028	-0.110	0.140	0.438	0.253	0.235	0.401	0.586	0.725	0.796	0.807	0.941	4/4 (2)
G154-36	9.747	0.215	0.157	0.438	0.675	0.337	0.305	0.567	0.728	0.918	0.984	1.111	1.282?	2/4 (1)
+13°3683	10.740	0.299	0.199	0.384	0.675	0.386	0.354	0.632	0.900	1.104	1.210	1.345	--	4/4 (0)
G206-34D	11.499	-0.075	-0.220	0.144	0.436	0.271	0.228	0.416	0.582	0.776	0.773	0.866	--	4/3 (0)
+20°3926	4.310	0.237	0.154	0.317	0.514	0.236	0.238	0.407	0.525	0.636	0.679	0.711	0.846	4/4 (3)
AC+20°1463-148	11.236	2.252	2.301	2.393	2.006	0.680	0.819	1.394	2.252	2.835	3.055	3.357	3.690	3/4 (3)
AC+20°1463-154	11.247	2.401	2.159	2.260	1.992	0.669	0.818	1.433	2.233	2.850	3.060	3.395	3.602	3/4 (3)
+41°3306	9.107	0.838	0.671	0.944	0.918	0.326	0.437	0.733	0.934	1.163	1.238	1.383	1.483	4/4 (3)
+11°3833	5.342	0.849	0.777	0.964	0.919	0.334	0.392	0.626	0.792	0.952	1.003	1.116	1.198	3/4 (4)
+10°4091	8.964	0.136	0.055	0.351	0.649	0.319	0.310	0.555	0.729	0.932	0.962	1.060	1.130	3/4 (4)
+5°4481	10.306	0.332	0.190	0.401	0.647	0.301	0.296	0.509	0.735	0.896	0.959	1.104	--	4/5 (0)
-21°5703	8.747	0.098	0.031	0.259	0.562	0.314	0.276	0.494	0.735	0.850	0.945	0.995	1.163	3/5 (4)
+41°3735	9.182	0.615	0.444	0.481	0.712	0.362	0.306	0.533	0.811	0.983	1.073	1.187	1.321	4/6 (5)
+9°4529	8.457	0.056	0.004	0.202	0.513	0.264	0.247	0.416	0.612	0.799	0.848	0.889	1.142?	4/5 (5)
-9°5491	9.716	0.448	0.313	0.326	0.622	0.349	0.317	0.582	0.832	1.044	1.131	1.248	1.451	4/4 (4)
+17°4519	7.534	0.075	-0.004	0.235	0.541	0.270	0.265	0.458	0.650	0.814	0.845	0.906	0.992	4/4 (4)
G188-30	11.211	0.330	0.214	0.441	0.748	0.362	0.328	0.602	0.881	1.032	1.149	1.219	--	5/3 (0)
G126-62	9.589	0.032	-0.043	0.188	0.485	0.269	0.224	0.422	0.565	0.728	0.779	0.906	1.717?	4/5 (3)
G18-39	10.502	0.086	-0.054	0.182	0.505	0.267	0.210	0.406	0.576	0.728	0.808	0.876	--	3/4 (0)
-8°5980	8.189	0.448	0.334	0.573	0.735	0.306	0.338	0.545	0.768	0.946	0.990	1.084	1.173	4/5 (5)
G28-43	10.121	0.402	0.285	0.552	0.784	0.326	0.380	0.639	0.894	1.094	1.171	1.289	1.586?	4/4 (1)
G190-15	11.236	0.188	0.083	0.378	0.708	0.384	0.346	0.593	0.856	1.053	1.151	1.277	--	4/3 (0)
-14°6437	8.297	0.019	-0.071	0.187	0.512	0.277	0.261	0.456	0.663	0.817	0.862	0.925	1.038	4/5 (5)
+26°4734	5.932	0.414	0.295	0.552	0.748	0.312	0.375	0.610	0.851	1.049	1.122	1.231	1.404	5/7 (6)

name in column 1 indicates that the photometry was contaminated by a
fainter nearby star which may contribute one percent or more of the light
measured. At the 110 filter the RCA 7102 phototube is about three magni-
tudes less sensitive than for the other 6RC filters, and for this reason
many of the subdwarfs were not measured at 1.1µ. And, for many of the
subdwarfs that were observed through this 110 filter problems were en-
countered. In column 14, for the 52-110 color, a question mark follow-
ing the color indicates one of the three following things: (a) the
probable error of the mean of the 52-110 color is greater than 0.07
magnitude, (b) only one 1.1µ measurement was made, or (c) somewhat arbi-
trary editing of the 1.1µ data was made keeping in mind what real stars
tend to look like. In column 15 the number in parenthesis following NR
gives the number of observations through the 110 filter; this number is
always equal to or less than the number of observations through the other
6RC filters.

In Table 4 are listed the bright star numbers (Hoffleit 1964) of
six additional stars with moderately large ultraviolet excesses. These
stars, which are not included in the original list of 149 subdwarfs, are
taken from the subdwarf list of Johnson et al. (1968), and their 13-color
photometry has been obtained from Mitchell and Johnson (1969) and from
Johnson and Mitchell (1975). These six stars were not observed at San
Pedro Martir, but their photometry is included in the analyses of this
thesis.

Table 4. Mild subdwarfs whose 13-color photometry was not taken at
          San Pedro Martir.

Name	45-63	Sp
BS 77	0.806	G2V
BS 219D	0.795	G0V
BS 1008	0.945	G5V
BS 6752D	1.102	K0V
BS 6927	0.714	F7V
BS 8181	0.721	F8V

Hyades, G Stars, YY Gem, and BS5270

For comparison with the subdwarf photometry 13-color photometry
of the Hyades cluster was obtained. This Hyades photometry comes from
eight nights of observing on San Pedro Martir during November of 1974,
from Johnson and Mitchell (1968) and from Mitchell and Johnson (1969).
In total 50 Hyades stars have been observed with the 8C photometer and
56 Hyades stars with the 6RC photometer. Of the 8C Hyades photometry
approximately 40% was obtained on San Pedro Martir and of the 6RC
photometry about 60%. In Table 5 is given the Hyades 13-color photometry
reduced to the standard photometric system of Mitchell and Johnson
(1969). In column 1 is given the number of the star taken from van
Bueren (1952), in column 2 is the 52 magnitude, in columns 3 to 9 the
other 8C colors with respect to the 52 filter, in columns 10 to 14 the

Table 5. 13-color photometry of Hyades stars.

Name	52	33-52	35-52	37-52	40-52	45-52	52-58	52-63	58-72	58-80	58-86	58-99	58-110	NB/NR
H6	6.062	0.179	0.119	0.242	0.393	0.171	0.177	0.300	0.242	0.340	0.354	0.371	0.411	1/2
7	9.266	1.172	1.084	1.278	1.121	0.337	0.504	0.769	0.509	0.712	0.767	0.907	1.053	2/3
9									0.452	0.623	0.669	0.781	0.868	0/2
20	6.422	0.206	0.130	0.278	0.452	0.180	0.224	0.362	0.264	0.349	0.396	0.440	0.540	2/3
22	8.534	0.743	0.654	0.890	0.912	0.318	0.420	0.650	0.466	0.672	0.744	0.853	1.018	2/2
25	9.917	1.350	1.274	1.505	1.214	0.315	0.583	0.889						
26									0.454	0.619	0.692	0.779	0.939	0/2
27	8.64	0.74	0.63	0.85	0.88	0.32	0.38	0.59	0.437	0.609	0.649	0.765	0.842	2/2
28	3.868	1.531	1.371	1.445	1.292	0.453	0.460	0.743	0.521	0.740	0.830	0.976	1.141	2/3
29	7.002	0.338	0.262	0.471	0.645	0.260	0.292	0.475	0.366	0.506	0.550	0.604	0.727	2/2
30	5.655	0.302	0.211	0.254	0.339	0.129	0.155	0.258	0.197	0.271	0.277	0.305	0.369	2/8
33	5.338	0.254	0.193	0.230	0.269	0.100	0.139	0.215	0.144	0.195	0.206	0.228	0.274	2/2
34	6.269	0.217	0.141	0.335	0.520	0.219	0.231	0.390	0.306	0.428	0.450	0.485	0.547	1/2
35	6.92	0.18	0.13	0.30	0.49	0.20	0.22	0.38	0.308	0.415	0.446	0.476	0.572	1/2
36	6.921	0.186	0.118	0.304	0.496	0.213	0.222	0.380	0.301	0.420	0.442	0.476	0.562	1/2
40									0.396	0.537	0.581	0.646	0.741	0/2
41	3.997	1.584	1.422	1.488	1.308	0.456	0.472	0.749	0.508	0.718	0.806	0.949	1.108	2/2
43	9.634	1.115	1.039	1.269	1.122	0.344	0.494	0.772	0.581	0.800	0.905	1.039	1.276	2/3
45	5.742	0.322	0.250	0.314	0.380	0.126	0.166	0.256	0.163	0.233	0.252	0.276	0.259	2/2
46	9.386	1.017	0.936	1.178	1.064	0.348	0.468	0.705	0.507	0.697	0.777	0.886	1.007	2/3
47	4.861	0.265	0.220	0.221	0.205	0.077	0.109	0.156	0.118	0.160	0.155	0.202	0.232	2/2
48									0.334	0.487	0.520	0.564	0.668	0/2
50	7.75	0.43	0.32	0.56	0.70	0.28	0.31	0.51	0.423	0.591	0.639	0.673	0.851	2/2
51									0.318	0.422	0.454	0.490	0.575	0/2
52									0.405	0.560	0.591	0.675	0.828	0/1
53	6.089	0.250	0.178	0.290	0.427	0.188	0.206	0.337	0.257	0.353	0.373	0.464	0.497	1/2
54	4.288	0.281	0.229	0.202	0.172	0.054	0.105	0.152	0.078	0.128	0.131	0.156	0.197	2/2
56	4.320	0.101	0.074	0.085	0.069	0.014	0.048	0.061	0.024	0.044	0.030	0.055	0.077	2/8
57	6.599	0.250	0.167	0.369	0.553	0.236	0.271	0.449	0.320	0.446	0.471	0.516	0.622	1/2
58	7.711	0.589	0.514	0.739	0.808	0.299	0.363	0.579	0.442	0.593	0.650	0.727	0.855	1/2
59									0.379	0.522	0.553	0.609	0.721	0/2

Table 5. -- <u>continued</u>.

Name	52	33-52	35-52	37-52	40-52	45-52	52-58	52-63	58-72	58-80	58-86	58-99	58-110	NB/NR
H60	4.384	0.408	0.307	0.237	0.292	0.126	0.179	0.276	0.189	0.255	0.286	0.330	0.420	2/2
64	8.255	0.536	0.469	0.693	0.782	0.292	0.332	0.543	0.415	0.582	0.616	0.710	0.840	1/2
65									0.369	0.504	0.539	0.589	0.710	0/2
68	5.966	0.254	0.183	0.275	0.384	0.154	0.168	0.286	0.235	0.325	0.315	0.384	0.489	1/3
69	8.806	0.749	0.636	0.866	0.880	0.309	0.384	0.612	0.437	0.609	0.656	0.777	0.946	2/2
70	3.781	1.698	1.520	1.576	1.384	0.467	0.484	0.754	0.510	0.726	0.845	0.977	1.163	2/2
71	4.090	1.476	1.306	1.407	1.266	0.439	0.462	0.727	0.503	0.711	0.806	0.951	1.122	11/4
72	3.475	0.313	0.252	0.205	0.209	0.060	0.094	0.173	0.135	0.177	0.175	0.223	0.256	13/3
73	8.009	0.447	0.340	0.568	0.705	0.279	0.319	0.514	0.434	0.578	0.626	0.692	0.780	1/2
77	7.152	0.245	0.164	0.373	0.554	0.239	0.272	0.447	0.346	0.488	0.537	0.581	0.640	1/2
79	9.162	0.915	0.864	1.094	1.018	0.324	0.434	0.680	0.489	0.660	0.725	0.832	0.891	2/1
82	4.840	0.275	0.216	0.218	0.193	0.069	0.109	0.146	0.082	0.135	0.135	0.175	0.167	2/2
85	6.607	0.214	0.137	0.320	0.506	0.222	0.228	0.394	0.303	0.401	0.447	0.494	0.534	1/2
87	8.806	0.754	0.643	0.914	0.893	0.327	0.406	0.629	0.451	0.608	0.668	0.785	0.972	1/2
91									0.561	0.779	0.859	0.986	1.176	0/2
92									0.479	0.620	0.672	0.787	0.930	0/2
94	6.706	0.195	0.119	0.295	0.493	0.216	0.224	0.382						1/0
95	4.765	0.265	0.200	0.230	0.271	0.096	0.113	0.190	0.140	0.199	0.220	0.234	0.291	2/2
97	8.10	0.46	0.39	0.61	0.74	0.27	0.31	0.49						2/0
104	4.329	0.257	0.204	0.190	0.159	0.048	0.082	0.109	0.065	0.100	0.108	0.137	0.176	2/2
108	4.721	0.274	0.225	0.218	0.190	0.062	0.087	0.111	0.107	0.166	0.169	0.206	0.235	2/2
117	9.974	1.403	1.330	1.555	1.307	0.369	0.627	0.953	0.640	0.887	1.018	1.205	1.408	1/2
123	5.153	0.294	0.227	0.242	0.261	0.103	0.121	0.181	0.118	0.183	0.197	0.235	0.388	3/2
129	4.670	0.318	0.27	0.224	0.197	0.076	0.097	0.137						1/0
141	4.565	0.356	0.265	0.239	0.274	0.119	0.162	0.251	0.154	0.241	0.266	0.310	0.360	2/2
169	4.159	0.265	0.225	0.206	0.209	0.062	0.086	0.146	0.125	0.202	0.210	0.261	0.336	3/1
175	10.580	1.392	1.392	1.588	1.304	0.350	0.623	0.950	0.605	0.834	0.932	1.078	1.056	1/3
176	9.311	1.167	1.060	1.302	1.136	0.319	0.565	0.850	0.556	0.765	0.859	0.987	1.165	3/4
181	10.768	1.798	1.728	1.919	1.515	0.307	0.791	1.111	0.693	0.965	1.056	1.269	1.369	2/3

6RC colors with respect to the 58 filter, and in column 15 the number of 8C and 6RC observations, NB and NR respectively. Since on the average the Hyades stars are considerably brighter than many of the subdwarfs, the 110 filter in all cases was observed as many times as the other 6RC filters.

The finding charts for the Hyades observations were prepared from the Bonner Durchmusterung using the BD numbers from the lists of van Bueren (1952). The Hyades were observed and reduced in exactly the same manner as the subdwarfs except for the fact that secondary standards were used. The Hyades stars #71 and #72 were observed and reduced as 8C standards; #71 had six previous 8C observations (Mitchell and Johnson 1969) and #72 seven. The Hyades stars #30 and #56 were observed and reduced as 6RC standards; each of these stars had four previous 6RC observations.

Throughout 1974 as part of the bright star 13-color program which is underway at the San Pedro Martir observatory 81 solar-type stars of spectral types F9 to G5 and of luminosity classes dwarf and subgiant were observed. These stars from the Bright Star Catalogue (Hoffleit 1964) were observed and reduced in exactly the same manner as the subdwarfs. This photometry is not tabulated here but has been published by Schuster (1976). The 13-color photometry of these solar-type stars is plotted in many of the color-color plots to follow and is used in the ultraviolet excess versus chemical composition calibration of Chapter 6.

In Chapter 6 of this thesis an observational calibration of 13-color indices versus effective temperature is carried out in the manner

of Johnson (1966) and Mendoza (1969). Twenty-seven stars whose angular

diameters have been well measured are available for this calibration.

Thirteen-color photometry for 26 of these stars was available from

previous sources (Mitchell and Johnson 1969, Johnson and Mitchell 1975),

but YY Gem had not been observed previously. This star was observed

five times with the 33" telescope of San Pedro Martir during November

1974; two 8C observations were made and three 6RC observations. The

techniques used for these observations were described briefly in

Chapter 2, and the final photometry, reduced in exactly the same manner

as for the subdwarfs, is given in Table 6.

The star BS5270 was originally included on our subdwarf lists

since Roman (1955), Hoffleit (1964) and others give its spectral type as

G0VI. It was observed three times with 8C photometry and five times with

6RC; its photometry is also given in Table 6. However, later investi-

gators such as Wallerstein et al. (1963) have shown that BS5270

(HD122563) is really a metal-poor red giant.

Quality of the Observations

To examine the quality of the observations presented in this

thesis two approaches were made. First, the probable errors of the

standard star and subdwarf observations were calculated and compared with

the errors of the Catalina observations (Johnson et al. 1967, Mitchell

and Johnson 1969). Second, observations of stars observed at both San

Pedro Martir (S.P.M.) and the LPL Catalina observatory were compared to

determine if the observations of this thesis deviate systematically in

Table 6. 13-color photometry of YY Gem and of BS5270.

Name	52	33-52	35-52	37-52	40-52	45-52	52-58	52-63	52-72	52-80	52-86	52-99	52-110
YY Gem	9.446	1.208	1.141	1.289	1.223	0.391	0.833	1.298	1.906	2.368	2.539	2.824	3.087
BS5270	6.392	1.292	0.916	0.880	1.052	0.510	0.430	0.760	1.086	1.331	1.453	1.613	1.774

any way from the Catalina observations which define the 13-color system.
In general these checks show that the S.P.M. observations are of a
quality similar to the Catalina ones.

In Table 7 are found the estimated probable errors of a single
observation for the S.P.M. standard star observations. These probable
errors are compared to those of the Catalina observations. The S.P.M.
probable errors are estimated using the residuals of the standard stars
from 15 nights of 8C photometry and 23 nights of 6RC photometry--nights
when nine or more standard stars were observed. These standard star
residuals are the differences between the calculated colors and the
standard colors from Table 7 of Mitchell and Johnson (1969). When cal-
culating the probable errors, these residuals for a given night and
filter were squared, summed, and divided by n-3, where n is number of
standards. Then the square root was taken and multiplied by 0.6745.
n-3 was used as the divisor to account for the fact that these same
standard stars have been used to solve for the extinction and transforma-
tion coefficients in each of the nights (i.e., the number of degrees of
freedom has been reduced by two from that of a simple average). The
probable errors from the different nights were then averaged and correct-
ed to an air mass of 1.25--approximately the average air mass of the
Catalina observations--to obtain the results of Table 7.

In Table 8 are listed the probable errors of a single observa-
tion for the subdwarfs grouped according to brightness. The headings of
the columns give the range of magnitudes--52 magnitudes for 8C photometry
and 58 magnitudes for 6RC photometry--for the subdwarfs whose probable

Table 7. Probable errors of a single observation for the standard stars.

Color	Probable Errors San Pedro Martir	Probable Errors Catalina
52	0.024	0.017
33-52	0.018	0.014
35-52	0.017	0.012
37-52	0.016	0.011
40-52	0.012	0.011
45-52	0.008	0.009
52-58	0.013	0.011
52-63	0.015	0.013
58	0.022	--
58'	0.019	0.025
58-72	0.015	0.021
58-80	0.014	0.019
58-86	0.015	0.021
58-99	0.017	0.023
58-110	0.028	0.033

Table 8. Probable errors of a single observation for the subdwarfs.

Color	≤ 6.999	7.000-7.999	8.000-8.999	9.000-9.999	10.000-10.999	≥ 11.000
52	0.030	0.028	0.026	0.022	0.034	0.028
33-52	0.018	0.019	0.022	0.028	0.031	0.039
35-52	0.013	0.014	0.021	0.020	0.024	0.033
37-52	0.013	0.013	0.017	0.018	0.020	0.027
40-52	0.009	0.012	0.014	0.014	0.015	0.016
45-52	0.009	0.013	0.011	0.012	0.012	0.014
52-58	0.012	0.012	0.011	0.013	0.017	0.018
52-63	0.018	0.013	0.013	0.017	0.020	0.027
58	0.027	0.028	0.026	0.025	0.031	0.027
58'	0.022	0.021	0.029	0.037	0.035	0.044
58-72	0.017	0.024	0.028	0.033	0.033	0.050
58-80	0.017	0.021	0.027	0.031	0.029	0.046
58-86	0.019	0.015	0.030	0.030	0.033	0.045
58-99	0.022	0.020	0.029	0.033	0.036	0.057
58-110	0.045	0.053	0.088	0.098	--	--

errors are used in each group. There are from 8 to 25 stars in each group. All subdwarfs have been included in these averaged probable errors except for two very southern subdwarfs (declinations of -26° and -33°) which have been dropped from the brightest group (52 or 58 ≤ 6.999) and six very red subdwarfs which have been dropped from the faintest group of the 8C probable errors. These stars were dropped so that the resulting probable errors are more nearly representative of the observations of the great majority of F and G subdwarfs. ·The probable errors of each subdwarf have been calculated individually, and then these individual values have been merely averaged to give the numbers of Table 8.

An examination of Tables 7 and 8 (primarily the bright star group of Table 8) reveals several interesting facts. First, for the 6RC photometry the S.P.M. probable errors are generally smaller than the Catalina values and together with the smaller extinction values of S.P.M. (see Table 2 of Chapter 2) indicates that this site is good for red and infrared photometry. For 8C photometry the story is different. For most of the 8C filters the S.P.M. probable errors are very nearly the same as the Catalina values. The only clear differences occur for the 52 magnitude and for the 33-52 color in which the S.P.M. errors are larger than the Catalina ones. Perhaps the largeness of the S.P.M. 33-52 probable errors indicates that the site is not as good for ultraviolet observations near the atmospheric cutoff, but this conclusion is not very certain. For the 52 magnitude all observations, of both the standard stars and of the subdwarfs, show errors significantly larger than the

Catalina value. In contrast it should be noted that the S.P.M. probable error for the 58 magnitude is smaller than the Catalina value. These results strongly suggest that the standard lamp of the 8C photometer, whose observations are used when reducing the 52 magnitude, is not as stable as it once was.

In checking for systematic differences between S.P.M. and Catalina photometry there are overlapping observations for 24 subdwarfs and Hyades stars in 8C photometry and seven subdwarfs in 6RC photometry. (The standard stars, most of which have of course been observed many times at both observatories, cannot be used in this analysis since the least squares solution of the photometric reduction program automatically forces the average of their residuals to be zero.) Two of the subdwarfs which were observed five or six times with both photometers at S.P.M. have been given double weight in the following analysis while all other stars have only one or two S.P.M. observations and so have been given unit weight. Residuals of the form (S.P.M. color) - (Catalina color) have been calculated for every filter of every comparison star. In Table 9 are given the averages of these residuals. For 6RC photometry none of the average residuals are significant--the largest, +0.012, for the 58-99 color is ignorable considering the small number of comparison stars.

For 8C photometry the number of comparison stars is large enough to try a more detailed analysis. First of all, looking at Table 9 and remembering that 24 comparison stars are involved, we see that only the average residuals of the 52 and 58 magnitudes and of the 52-63 color are

Table 9. Average residuals between San Pedro Martir and Catalina photometry.

8C Color	Average Residual (24 stars)	6RC Color	Average Residual (7 stars)
52	+0.016	58	+0.006
33-52	-0.000	58-72	+0.009
35-52	-0.007	58-80	+0.007
37-52	+0.003	58-86	-0.006
40-52	+0.000	58-99	+0.012
45-52	-0.004	58-110	-0.004
52-58	+0.008		
52-63	+0.015		
58	+0.012		

significant. Nevertheless the individual residuals of the 24 comparison stars have been plotted versus declination and versus color for all of the filters. For the 52 magnitude and for the 52-63 color the residuals have also been plotted versus the magnitude of the star, versus the 37-45 ultraviolet excess (see Chapter 5), and versus the hour angle of the observation. Of all of these graphs none seem to contain any significant correlations. Perhaps the residuals of the 52 (and 58) magnitude depend slightly upon declination, and maybe the residuals of the 52-63 color depend slightly upon color. As a final check the reductions of the nights during which the comparison stars were observed were analyzed more carefully. It was found that most of the comparison stars contributing larger than average positive residuals for 52, 58, and 52-63 were observed near the end of six nights in February and April, 1974. In fact, nearly all of these troublesome comparison-star observations were made shortly before or after the last standard star observations, and on four of these nights the least-square residuals of these last standard stars are positive. Hence the conclusion seems obvious that none of the 8C residuals of Table 9 would indicate any systematic difference between S.P.M. and Catalina photometry; the larger residuals of 52, 58, and 52-63 are merely due to extinction changes near the ends of six nights when unfortunately many of the comparison stars were observed.

So, we may conclude that, except for the 52 magnitude and the 33-52 color, the probable errors of the S.P.M. 13-color photometry are of the same size or smaller than Catalina probable errors. Also, to a significance level of 0.01 magnitude or smaller, the available

observations indicate no systematic deviations of the S.P.M. 13-color

photometry from the standard 13-color system of Mitchell and Johnson

(1969).

CHAPTER 5

THE SENSITIVITY OF 13-COLOR INDICES TO
BASIC STELLAR ATMOSPHERIC PARAMETERS

The use of 13-color photometry to study the subdwarfs can be
divided into the following three stages: (a) understanding the sensitivi-
ty of the 13-color indices to composition, surface gravity, and effec-
tive temperature, and selecting those indices which are most sensitive,
(b) calibrating the 13-color indices to give quantitative measures of
the atmospheric parameters, and (c) using the calibration to analyze the
subdwarfs. In this chapter the first of these three stages will be
described. The technique used will be essentially a modification and
extension of that used by Johnson and Mitchell (1968). In their analysis
Johnson and Mitchell (p. 216) used R-I, which "is practically independent
of the stellar atmospheric content . . ." to obtain blanketing correc-
tions for the 52-63 13-color index. (For the remainder of this thesis the
term "blanketing" will refer, unless otherwise indicated, to the combined
effect of line blocking of radiation plus backwarming.) Then 52-63 is
used to match a subdwarf's 13-color photometry to mean Hyades colors at
constant effective temperature. The difference between the Hyades'
colors and a subdwarf's colors at constant T_e gives color excesses which
are plotted versus the effective wavelengths of the filters to give a
"blanketing curve" such as is plotted in Figure 2 of Johnson and Mitchell

(1968). To a first approximation such blanketing curves show which 13-color indices are sensitive to metallicity. In the present analysis 45-63 rather than 52-63 is used for matching the Hyades and the sub-dwarfs at constant T_e, and model atmospheres are used to obtain the blanketing corrections for 45-63. This method is also extended to obtain "luminosity-difference curves" which show to a first approximation which 13-color indices are sensitive to surface gravity. These curves are obtained by matching giants or subgiants to the Hyades main sequence at constant T_e using 45-63 plus surface-gravity corrections from the model atmospheres. Hence of fundamental importance to this technique is the derivation of good mean Hyades colors and the use of theoretical 13-color photometry from blanketed model atmospheres. These two sets of information will be described in the next two sections.

Derivation of Mean Hyades Colors

Using the Hyades photometry of Chapter 4 mean Hyades colors as a function of spectral type and as a function of 45-63 index have been obtained. Of the 60 Hyades stars in Table 5 excellent spectral types are available for 51 from the work of Morgan and Hiltner (1965). This set of spectral types represents as uniform and accurate a classification of Hyades stars onto the Yerkes two-dimensional system as has ever been made; only these spectral types of Morgan and Hiltner have been used in deriving the mean colors. The Hyades stars used in determining the mean colors (versus spectral type) range from A3V to K4V, and only main sequence stars (class V) have been used; all evolved stars (giants and

subgiants) and all Am stars have been excluded. The mean colors have been derived by merely hand drawing lines of best fit through 12 different spectrum-color diagrams. For this 36 stars were available in 8C photometry and 42 in 6RC photometry.

To make maximum use of the available data, since some of the stars have 8C photometry but do not have an accurate spectral type, the mean colors were also derived as a function of 45-63. This will also simplify matters later since 45-63 will be used both as an effective temperature indicator and for matching subdwarf colors to the mean Hyades colors at constant T_e. Twelve color-color plots (13-color index versus 45-63) were made using 43 stars for the 8C plots and 39 stars for the 6RC ones. Again the mean relations were obtained by merely hand fitting curves to the plotted data.

The two sets of mean colors were tied together using a 45-63 versus spectral type diagram. In Table 10 are given the combined Hyades mean colors as a function of both spectral type and 45-63. In Table 10 all colors are given with respect to the 52 filter; however, in the original derivation of the mean colors the 6RC ones were always derived with respect to 58. In comparing the two independently derived sets of mean colors and in examining the various color-color and spectrum-color plots it has been possible to get a good idea of the accuracy of the mean colors of Table 10. For spectral types A4 to K0 and for colors 35-52 to 52-99 the probable errors are equal to or less than 0.01 magnitude. Colors 33-52 and 52-110 have probable errors somewhat larger, in the range 0.01 to 0.02. For spectral types K2 and K4 the probable errors may be twice those quoted above.

Table 10. Mean Hyades colors.

Sp	45-63	33-52	35-52	37-52	40-52	45-52	52-58	52-63	52-72	52-80	52-86	52-99	52-110
A4	0.108	0.178	0.150	0.140	0.102	0.026	0.062	0.074	0.104	0.130	0.128	0.154	0.180
A6	0.200	0.272	0.221	0.208	0.184	0.062	0.095	0.131	0.185	0.226	0.231	0.260	0.292
A8	0.291	0.283	0.216	0.232	0.258	0.098	0.125	0.192	0.264	0.319	0.330	0.360	0.403
F0	0.382	0.274	0.188	0.251	0.330	0.132	0.156	0.256	0.346	0.415	0.430	0.462	0.516
F2	0.464	0.228	0.154	0.262	0.391	0.164	0.183	0.309	0.419	0.500	0.522	0.556	0.619
F4	0.548	0.196	0.127	0.288	0.454	0.194	0.211	0.360	0.487	0.585	0.615	0.654	0.726
F6	0.634	0.203	0.134	0.334	0.524	0.224	0.245	0.409	0.563	0.675	0.718	0.761	0.846
F8	0.719	0.310	0.217	0.445	0.614	0.250	0.280	0.461	0.640	0.778	0.821	0.877	0.971
G0	0.766	0.406	0.306	0.532	0.680	0.269	0.304	0.492	0.696	0.845	0.883	0.951	1.066
G2	0.802	0.474	0.370	0.610	0.722	0.283	0.324	0.519	0.730	0.886	0.924	1.000	1.124
G4	0.835	0.529	0.434	0.676	0.761	0.295	0.342	0.543	0.758	0.918	0.959	1.043	1.168
G6	0.875	0.605	0.512	0.750	0.810	0.306	0.364	0.574	0.793	0.959	1.005	1.094	1.221
G8	0.934	0.742	0.640	0.873	0.889	0.318	0.394	0.618	0.846	1.018	1.072	1.174	1.306
K0	1.012	0.909	0.820	1.056	0.991	0.328	0.442	0.680	0.937	1.117	1.193	1.300	1.450
K2	1.132	1.135	1.068	1.303	1.128	0.334	0.518	0.782	1.070	1.281	1.375	1.501	1.692:
K4	1.315	1.472	1.460	1.658	1.327	0.337	0.663	1.032	1.289	1.552	1.645	1.809	1.963:

Blanketed Model Atmospheres

The theoretical 13-color photometry used throughout this thesis to obtain blanketing corrections, effective temperatures and surface gravities of the subdwarfs, theoretical banketing and luminosity-difference curves and so forth has been provided by Kurucz (1975). The model atmospheres which give the necessary stellar flux distributions were calculated using the ATLAS computer code as given and described by Kurucz (1970). These model atmospheres are blanketed, flux constant, plane-parallel, and homogeneous (except in the radial direction) and make use of convective as well as radiative energy transport; assumptions of steady-state, hydrostatic equilibrium, and chemical uniformity are also made. Some of the available models (see Kurucz 1974) have been calculated with a solar abundance and a microturbulent velocity of 2 km/sec covering effective temperatures from 5500° to 10000° in steps of 500° and surface gravitites with logarithms of 4.5 and less in steps of 0.5. Other models with 0.1 and 0.01 of the solar abundance and a micro-turbulent velocity of 2 km/sec have T_e from 5500° to 8000° and also 10000° and log g's of 4.5 and less. A few models with solar abundances and a microturbulence of 4 km/sec were also provided. (From now on the notation (T_e, log g, composition, microturbulent velocity) will be used for the models; for example, (6000, 4.5, 1X, 2) designates the model with $T_e = 6000^{o}$, log g = 4.5, solar abundance, and a microturbulence of 2 km/sec.) Models with the parameters (5700, 4.44, 1X, 2) and (9400, 3.95, 1X, 2) were also included as representative of the Sun and Vega respectively.

The theoretical magnitudes were calculated according to the formula $-2.5\log(\int S_\lambda H_\lambda d\lambda / \int S_\lambda d\lambda)$, where H_λ is the emergent flux per wavelength interval from the models, and S_λ is the filter-detector response function of the particular 13-color filter (Johnson et al. 1967, Mitchell and Johnson 1969). The theoretical colors were then normalized to the standard 13-color system by fitting the (9400, 3.95, 1X, 2) model to the 13-color observations of Vega (with 4 8C observations and 36 6RC observations). This choice of parameters for Vega was based in part upon fits of Kurucz's models to Hayes and Latham's (1975) observed energy distribution for Vega.

The great importance and usefulness of Kurucz's models to the present study of subdwarfs lies in the fact that they are blanketed models of F and G stars. Earlier models included blanketing for F and G stars in a strictly empirical manner, added after the models were calculated, or by some artificial theoretical means such as the "picket fence" model. A complete theoretical treatment of the many thousands of atomic lines is prohibited by the need for huge amounts of computer time to iterate for flux constancy and so forth. But these recent models of Kurucz overcome these difficulties by means of a statistical representation of the line opacities as described by Strom and Kurucz (1966), and by Kurucz (1970, 1974). Under this technique the spectrum is broken up into a number of segments, and for each segment the line opacity (l_ν) versus frequency (ν) curve is converted into a probability (f) versus l_ν distribution, where the range of l_ν is from $l_{\nu max}$ to $l_{\nu min}$, the maximum and minimum values in the original segment of the spectrum.

The probability, f, ranging in value from 0 to 1, essentially tells how important the corresponding l_ν is in that part of the spectrum, how often a particular l_ν occurs with respect to the other l_ν's. This f versus l_ν curve is next integrated to give a distribution function (f') which shows how many l_ν's in that segment of the spectrum are equal to or smaller than a given l_ν. This monotonically increasing function can be inverted to give an l_ν versus f' curve which is similar to a line profile and can be tabulated as function of T_e, electron number, abundance, and microturbulence. These distribution functions, l_ν versus f', are represented by step functions in the computer solutions. The heights of the steps, $l_{\nu i}$'s, are used to solve for opacity increments, $\tau_{\nu i}$'s, source function increments, $S_{\nu i}$'s, mean intensity increments, $J_{\nu i}$'s, and so forth. The widths of the steps, $W_{\nu i}$'s, are weights used in summations for determining the monochromatic radiation parameters for that portion of the spectrum; for example, $J = \Sigma W_{\nu i} J_{\nu i}$ gives the monochromatic mean intensity. The following two assumptions are inherent in the above approach: (a) the distribution function, l_ν versus f', does not change with height in the atmosphere (for all heights where the line opacities are important), and (b) the solution for a given spectral segment does not depend strongly on the position (frequency) of the various spectral features in that segment. As Kurucz points out (1970) the first assumption needs to be checked using detailed calculations with the exact l_ν versus ν curves, and the second assumption is valid as long as the frequency width of a spectral segment is sufficiently small.

Throughout the course of the present study these models have been checked repeatedly against the various observations and observational calibrations. In general the agreement has been excellent, except in one particular area. The ultraviolet filters 33 and 35 show rather significant discrepancies in three independent checks for the coolest model, T_e = 5500° (and to a lesser extent for the 6000° model). This is somewhat unfortunate since the ultraviolet filters are most sensitive to metallicity and surface gravity, and so any irregularities in the ultraviolet make the models considerably less useful. These discrepancies are mentioned now since their existence determines in part how the models are used in the analyses. The three comparisons which show the discrepancies are the following: (a) the theoretical blanketing curves for the 5500° models (obtained by subtracting the colors of a 0.01X model from the colors of a 1X model at constant T_e and constant surface gravity) are quite different in the ultraviolet from the observed blanketing curves; the theoretical curves show less blanketing in the 35 filter and much less in the 33 filter (relative to the 37 blanketing) than do the observational curves; (this discrepancy also shows up, but to a much lesser extent, for the 6000° models); (b) the 33-52 and 35-52 colors of the (5770, 4.44, 1X, 2) model, which supposedly represents the Sun, do not agree with derived 13-color solar photometry of R. Mitchell (1975; also Schuster 1976); the theoretical 33-52 is 0.126 magnitude too blue and the theoretical 35-52 is 0.056 magnitude too blue; and (c) a color-color plot of 33-35 versus 45-63 was made including the theoretical points, the Hyades mean colors, and the subdwarf observations;

33-35 measures the slope of the continuum below the Balmer discontinuity and 45-63 is primarily a temperature index; in this diagram the 0.01X models fit very well the subdwarf observations for all temperatures while the 0.1X and especially the 1X models deviate significantly (> 0.1 magnitude) from the mean Hyades colors at 5500° (and to a lesser extent at 6000°). All of these checks agree as to the sense of the discrepancy --the 35 filter and especially the 33 filter of the (5500, --, 1X, 2) models do not have enough blanketing. Figure 20 of Kurucz (1974) which shows a comparison between the (5770, 4.44, 1X, 2) model and Labs and Neckel's (1968, 1970) measured solar central intensities has exactly the same type of discrepancy (the blanketed models are too bright in the ultraviolet) as indicated by the above analysis. Kurucz (1974, 1975) suggests the problem results because molecular opacities have been omitted from the models.

Blanketing and Luminosity-
difference Curves

In attempting to derive difference curves (such as blanketing or luminosity-difference curves) in the manner of Johnson and Mitchell (1968) it is necessary to select some photometric index which is a good measure of only effective temperature in order to match the subdwarfs to the Hyades mean colors at truly constant effective temperature. If this could be done perfectly, effective temperature effects would completely subtract out, and we would be left only the blanketing and surface gravity effects to disentangle. Unfortunately all indices which we might select, B-V, R-I, b-y, 45-63, 58-99 and so forth, are dependent to

some degree on metallicity (blanketing including backwarming effects) and/or on luminosity (surface gravity). With subdwarfs the problem of differing metallicities is particularly acute since the chemical composition of their atmospheres is very different from the Hyades'. And perhaps, if the hotter subdwarfs are evolving as suggested by Eggen (1973) and confirmed later in this thesis, we may also need to worry about surface gravity effects in selecting our effective temperature index. The best we can really hope to do at this point is to select an index that our observational and theoretical checks show to be sensitive to effective temperature and as insensitive to composition and luminosity as possible. Then use the model atmospheres to correct for the residual composition and luminosity effects ("blanketing corrections" and "luminosity corrections"). Of course, if we have great confidence in our model atmospheres, we could study the sensitivity of the 13-color indices using only the theoretical photometry. This approach would make it extremely simple to separate the effects of effective temperature, composition and surface gravity. However I do not feel that the present models are good enough to warrant this completely theoretical approach. I prefer to use the models only for the small blanketing corrections and as a comparison with the observational results.

According to the observational results of Johnson and Mitchell (1968) the 45-63 index should be fairly independent of metallicity, changing by about -0.03 magnitude going from the Hyades main sequence to extreme subdwarfs at constant T_e. This result depends upon the assumption that the broad-band index R-I is independent of the composition of

a stellar atmosphere. This assumption has been documented and used in a number of recent investigations (see Johnson et al. 1968, Johnson and Mitchell 1968, Eggen 1973, Eggen 1974). In Figure 1 a direct observational check of the blanketing of 45-63 has been made by plotting the color-color diagram, 45-63 versus R-I, using mean Hyades colors, five extreme subdwarfs ([Fe/H] $\leq$ -1.0), and 12 mild subdwarfs (-0.25 $\geq$ [Fe/H] > -1.0). The mean Hyades colors come from Table 10 of this chapter for 45-63 and from Table 2 of Johnson et al. (1968) for R-I. (The R-I values of the subdwarfs also come from this last source.) For the compositions used here and from now on in the thesis, I have had to get somewhat ahead of myself in the analysis. These come from the calibration of Chapter 6 where the composition, given as the logarithmic iron to hydrogen ratio relative to the Sun, [Fe/H], is determined from a star's position in the 37-45 versus 45-63 diagram. Figure 1 shows that removal of the blanketing changes 45-63 by about -0.04 magnitude if R-I remains constant or R-I by about +0.02 magnitude if 45-63 remains constant. Kurucz's models suggest that 45-63 changes by about -0.02 magnitude going from solar abundance to 0.01 solar abundance at constant T_e; this holds over a rather wide temperature range ($5500^\circ \leq T_e \leq 7000^\circ$). Hence, a possible compromise in Figure 1 would be that 45-63 changes by -0.02 and R-I by +0.01. In any case to a significance level of one or two hundredths of a magnitude Figure 1 does not indicate any discrepancy between the blanketing corrections of Kurucz's models and the assumption that R-I is invariable with metallicity. In Figure 2 are plotted 45-63 versus T_e curves from the models; one curve is for solar abundance
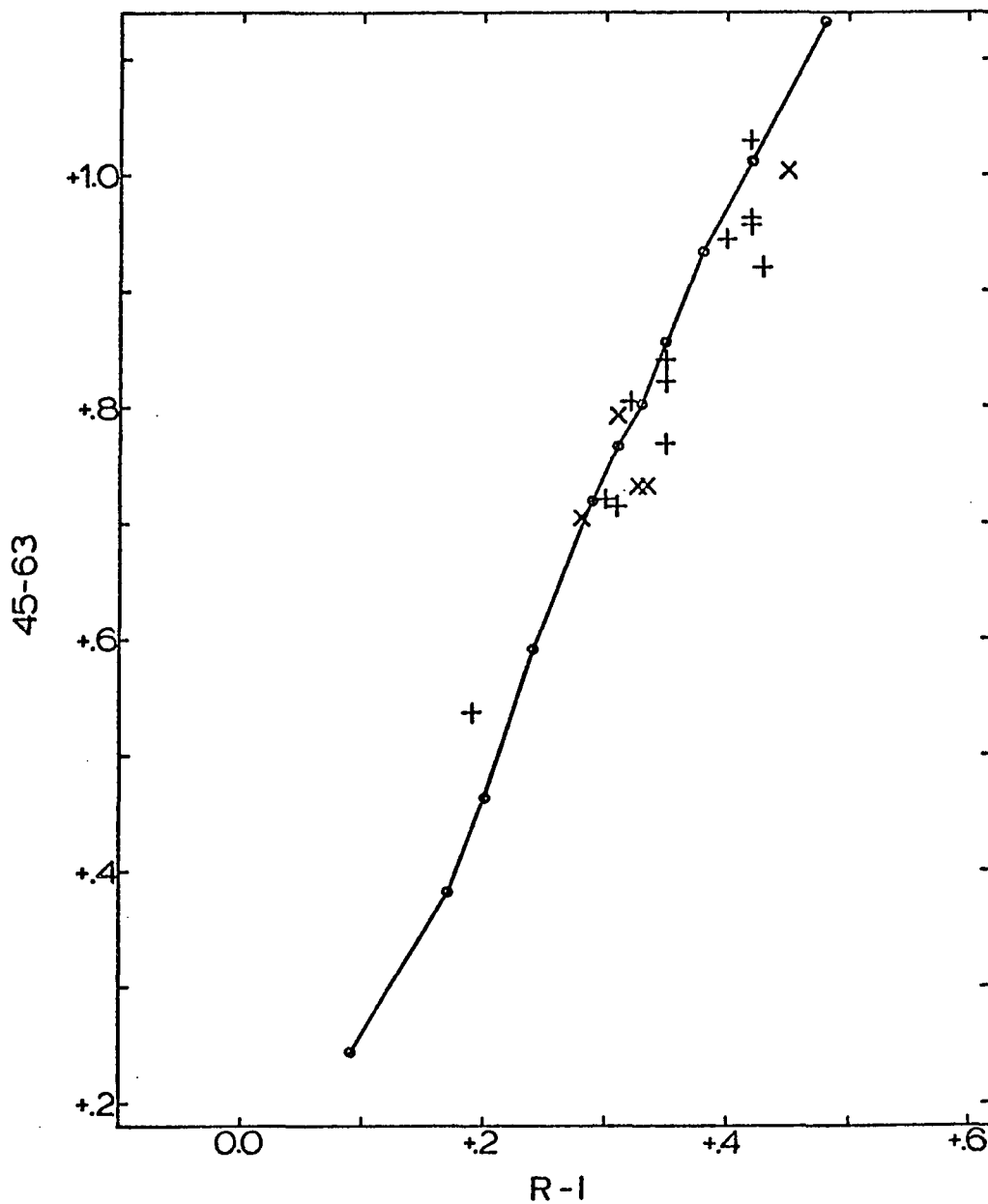
Figure 1, 45-63 versus R-I, -- The circles and solid line represent the mean Hyades colors, the plus signs mild subdwarfs, and the X's extreme subdwarfs.
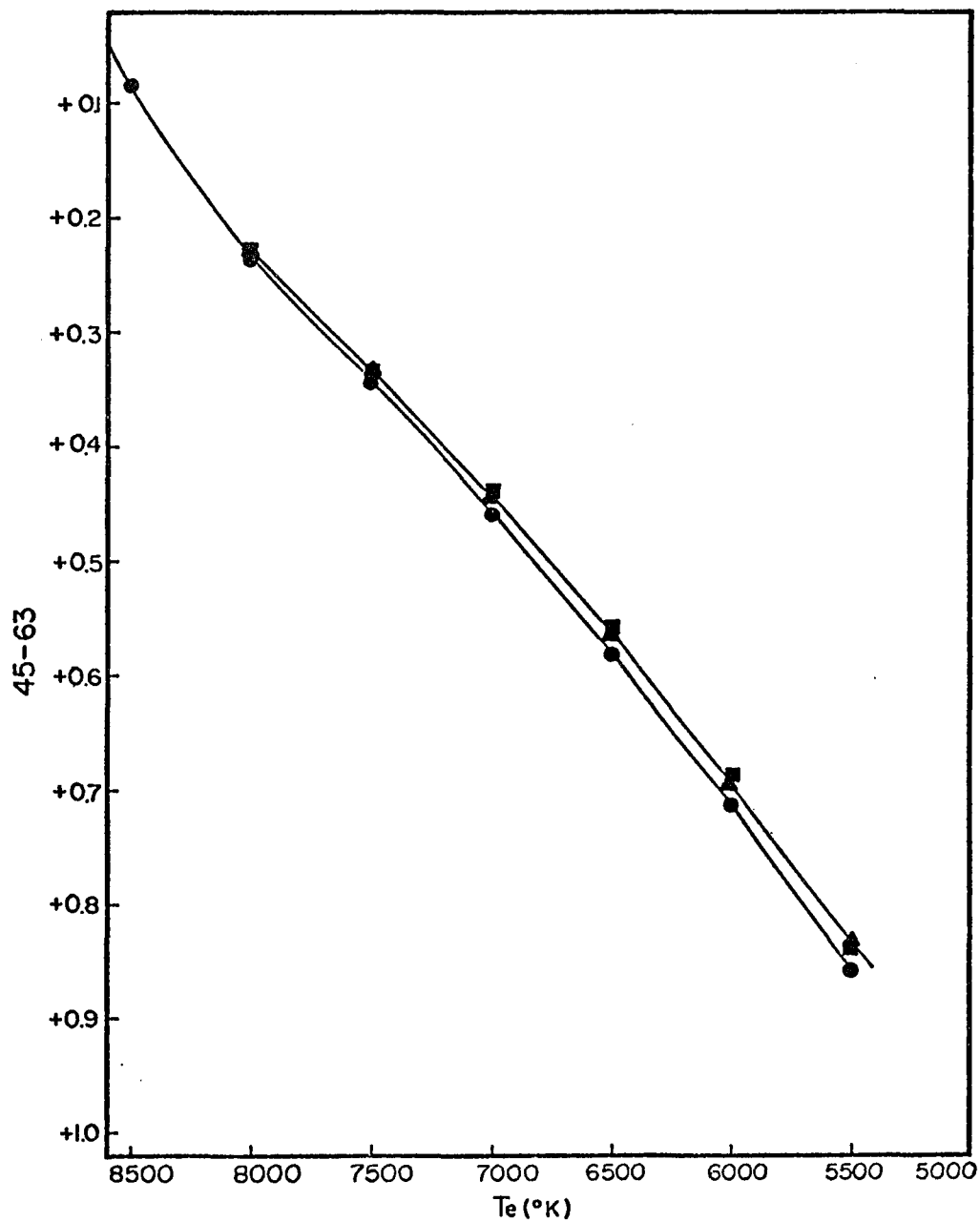
Figure 2. Theoretical 45-63 versus T_e curves. -- Filled circles are for solar abundance, triangles for 0.1 solar abundance, and squares 0.01. Log g = 4.0.

(1X), one for 0.1X and one for 0.01X; the surface gravity is kept constant at $\log g = 4.0$. These curves reinforce the above arguments that 45-63 requires only very small blanketing corrections. Other similar theoretical curves have been plotted keeping the composition constant but varying the surface gravity; these show that 45-63 needs very small luminosity corrections. For these reasons the 45-63 index is used throughout the remainder of this chapter for matching subdwarfs, subgiants, giants and so forth to the mean Hyades colors at constant T_e.

Some basic observed quantities, part of which will be used to derive the blanketing curves of the subdwarfs, are given in Table 11; these are obtained from the photometry of Table 3. The method for calculating a blanketing curve is simply this. The star's photometry is plotted in a 37-45 versus 45-63 diagram and the star's ultraviolet excess, $\delta(37-45)$, plus the observed 45-63 give the star's composition, [Fe/H], according to the calibration of the next chapter. Then with the composition and observed 45-63 one enters the graph of Figure 2 to obtain 45-63 corrected to the solar abundance, $(45-63)_s$. In Table 11 column 4 gives the observed 45-63 and column 6, $(45-63)_s$. Now, the assumption is made that since the solar abundances and Hyades abundances are not very different and since the blanketing corrections of 45-63 are small even for large composition differences, the 45-63 of solar abundance is the same as the 45-63 of Hyades abundance (at constant T_e). This assumption, I feel, is not in error by more than a few thousandths of a magnitude. Next $(45-63)_s$ is used to interpolate in Table 10 for the Hyades mean colors with the same T_e as the subdwarf. The differences between these Hyades mean colors and the

Table 11. Observed quantities for subdwarfs. -- In the second "Name" column no letter indicates an HD number, "Y" designates a number from the Yale parallax catalogue, "W" a number from Wilson's (1953) radial velocity catalogue, and "LTT" a number from Luyten's (1961) proper motion catalogue.

Name	Name	37-45	45-63	$\delta(37\text{-}45)$	$(45\text{-}63)_s$	58-99	$(58\text{-}99)_s$	G	Sp
$+54^\circ223$	6582	0.301	0.920	+0.228	0.928	0.820	0.814	+0.050	G5VI
$-9^\circ256$	7983	0.160	0.786	+0.138	0.790	0.698	0.693	+0.072	G2V
$+19^\circ279$	10476	0.790	1.042	+0.000	1.036	0.878	0.883	+0.072	K1V
$-16^\circ295$	10700	0.425	0.958	+0.182	0.963	0.829	0.825	+0.076	G8Vp
$-26^\circ828$	14412	0.421	0.952	+0.174	0.956	0.803	0.800	+0.061	G5V
$-17^\circ484$	Y 509	-0.169	0.682	+0.324	0.706	0.566	0.528	+0.107	F0VI
$-13^\circ482$	16031	-0.148	0.630	+0.258	0.652	0.599	0.566	+0.101	sdF4
$-26^\circ957$	16623	0.114	0.774	+0.163	0.781	0.690	0.683	+0.129	G2VI
G4-37	--	-0.105	0.699	+0.279	0.721	0.690	0.663	+0.004	sdF8
$+33^\circ529$	--	1.401	1.727	--	1.727?	1.578	1.578?	+0.261	sdK6
$-13^\circ544$	17925	0.848	1.107	+0.067	1.107	0.894	0.894	+0.109	dK0
$+25^\circ495$	19445	-0.147	0.733	+0.360	0.755	0.626	0.589	-0.009	sdF7
G78-26D	Y 674	1.430	1.620	--	1.620?	1.360	1.360?	+0.074	sdK5
$+11^\circ468$	--	-0.063	0.805	+0.396	0.826	0.711	0.681	+0.059	sdG5
G5-36	Y 715	-0.036	0.774	+0.318	0.796	0.659	0.632	+0.094	sdG5
G38-1	Y 721	1.428	1.739	--	1.739?	1.632	1.632?	+0.289	sdK5
$-7^\circ603$	21543	0.178	0.860	+0.241	0.874	0.709	0.698	+0.070	G2V-VI
$-3^\circ592$	22879	0.023	0.768	+0.243	0.785	0.672	0.654	+0.071	F9V
$+34^\circ796$	25329	0.575	1.191	+0.510	1.211	1.023	0.999	+0.099	K1V
$+21^\circ607$	Y 934	-0.100	0.674	+0.246	0.693	0.557	0.528	+0.005	sdG0
G175-39	Y 1002	1.023	1.118	-0.087	1.112	0.890	0.895	+0.092	K2V
$+45^\circ992$	30649	0.128	0.822	+0.230	0.837	0.697	0.684	+0.069	G1V-VI
G102-22	Y 1305	1.251	2.127	--	2.127?	3.487	3.487?	+1.153	sdM4
G99-31D	Y 1315	0.152	0.828	+0.219	0.840	0.789	0.780	-0.001	sdF7
$+37^\circ1312$	38230	0.792	1.048	+0.011	1.042	0.888	0.893	+0.072	dK2

Table 11. Observed quantities for subdwarfs. -- <u>continued</u>.

Name	Name	37-45	45-63	δ(37-45)	(45-63)$_s$	58-99	(58-99)$_s$	G	Sp
+19°1185	250792	0.122	0.878	+0.325	0.898	0.851	0.833	+0.032	sdG8
-0°1520	51754	0.114	0.775	+0.165	0.783	0.714	0.708	+0.077	sdG2
+47°1419	55575	0.155	0.785	+0.142	0.789	0.645	0.638	+0.056	G0V
-33°4113	63077	0.057	0.779	+0.229	0.794	0.723	0.709	+0.069	G0V
+31°1684	64090	0.045	0.895	+0.435	0.915	0.788	0.760	+0.004	G2VI
-34°4036	64379	0.028	0.646	+0.093	0.648	0.516	0.512	+0.043	F5V
-1°1883	64606	0.364	0.967	+0.265	0.983	0.894	0.880	+0.040	G8V
+29°1664	65583	0.396	0.962	+0.222	0.972	0.826	0.818	+0.072	G8V
G194-22	Y 1969	-0.102	0.710	+0.286	0.732	0.635	0.606	+0.001	sdG5
-3°2333	70958	0.029	0.669	+0.112	0.673	0.554	0.548	+0.057	dF2
HD74000	Y 2074	-0.143	0.648	+0.265	0.671	0.650	0.617	+0.012	sdF7
G115-22	W5757	0.034	0.825	+0.328	0.848	0.777	0.758	+0.005	sdF8
+25°1981	--	-0.077	0.502	+0.171	0.521	0.494	0.461	+0.005	sdF2
+42°1922	74377	1.077	1.206	+0.035	1.206	1.068	1.068	+0.039	dK5
-12°2669D	Y 2099	-0.098	0.479	+0.195	0.500	0.373	0.335	+0.009	sdF
G46-5	Y 2107	0.372	0.987	+0.300	1.007	0.918	0.898	+0.032	sdG6
G114-26	Y 2151	-0.103	0.747	+0.339	0.768	0.627	0.594	+0.047	sdG3
G115-49	W5951	-0.117	0.762	+0.376	0.785	0.614	0.578	-0.016	sdF5
+9°2190	LTT12503	-0.132	0.623	+0.238	0.645	0.641	0.611	+0.026	sdF?
G48-29	W6236	-0.157	0.593	+0.256	0.616	0.632	0.596	+0.035	sdA7p
HD84937	Y 2323	-0.130	0.617	+0.233	0.638	0.580	0.549	+0.021	sdF5
+44°1910	W6296	-0.139	0.688	+0.301	0.709	0.603	0.569	+0.135	sdF
+23°2207	89125	0.062	0.684	+0.096	0.686	0.589	0.587	+0.053	dF3
G119-32	Y 2513	-0.082	0.724	+0.283	0.744	0.720	0.695	-0.015	sdG5
G196-47	Y 2518	0.030	0.862	+0.392	0.885	--	--	+0.020	sdG0
+21°2247	94028	-0.091	0.704	+0.269	0.725	0.670	0.644	+0.009	sdF8/GSIV
G10-4	Y 2601	0.066	1.040	+0.721	1.060	--	--	+0.145	sdG5
+36°2165	W6880	-0.102	0.626	+0.209	0.645	0.645	0.619	+0.058	sdG0
+26°2251	W7117	-0.027	0.711	+0.212	0.726	0.518	0.497	+0.049	sdG0

Table 11. Observed quantities for subdwarfs. -- <u>continued</u>.

Name	Name	37-45	45-63	δ(37-45)	(45-63)$_s$	58-99	(58-99)$_s$	G	SP
+51°1696	Y 2723	-0.028	0.840	+0.416	0.860	0.692	0.660	+0.088	sdG0
BS4550	103095	0.390	1.003	+0.319	1.023	0.910	0.887	+0.029	G8VI
G13-9	W7266	-0.127	0.597	+0.227	0.619	0.613	0.580	+0.062	sdG0
G11-44	Y 2805	-0.116	0.706	+0.296	0.727	0.661	0.630	+0.035	sdF2
HD106038	Y 2810	-0.078	0.722	+0.277	0.741	0.637	0.609	+0.035	F6V-VI
HD108177	Y 2863	-0.121	0.698	+0.294	0.720	0.558	0.527	-0.002	sdG0
+40°2570	110897	0.120	0.749	+0.115	0.751	0.699	0.697	+0.008	G0V
G60-48	W7729	-0.138	0.738	+0.358	0.760	0.749	0.717	+0.085	sdF4
-9°3595	112758	0.592	1.028	+0.170	1.037	0.904	0.896	+0.036	dK1
+10°2519	114606	0.177	0.867	+0.252	0.882	0.735	0.723	+0.079	G3V
G14-45D	Y 3044	1.092	1.274	+0.151	1.274?	1.204	1.204?	+0.055	sdK5
+34°2476	Y 3189	-0.135	0.636	+0.247	0.657	0.607	0.574	+0.051	sdG2
G65-22	Y 3197	0.303	0.958	+0.307	0.978	--	--	+0.100	sdG3
G64-37	W8248	-0.110	0.598	+0.210	0.617	--	--	+0.028	sdF
-13°3834	Y 3219	0.014	0.857	+0.401	0.877	0.774	0.749	+0.084	sdG5
+1°2920	126053	0.246	0.841	+0.145	0.843	0.726	0.723	+0.047	dG3
+30°2536	128167	-0.010	0.537	+0.104	0.546	0.413	0.400	+0.020	F2V
G66-22	Y 3327	0.329	0.974	+0.315	0.994	0.900	0.880	+0.070	sdG2
+26°2606	W8603	-0.136	0.687	+0.297	0.709	0.583	0.550	+0.012	sdG1
-8°3858	--	0.367	0.950	+0.224	0.960	0.820	0.812	+0.098	sdG
-21°4009	132475	-0.038	0.809	+0.378	0.831	0.774	0.749	+0.116	sdG4
+25°2873	134083	0.066	0.618	+0.037	0.615	0.495	0.498	+0.040	F5V
-15°4041	134440	0.648	1.132	+0.321	1.152	1.051	1.019	+0.087	K2VI
-15°4042	134439	0.417	1.037	+0.363	1.057	0.969	0.937	+0.045	sdK1
G15-24	LTT14607	0.033	0.849	+0.372	0.871	0.761	0.736	+0.055	sdG
-10°4149	140283	-0.134	0.793	+0.446	0.814	0.740	0.702	+0.128	sdG2
+42°2667	Y 3642	-0.064	0.725	+0.265	0.744	0.663	0.638	+0.024	sdG1
+39°2947	144579	0.423	0.982	+0.238	0.996	0.843	0.830	+0.067	dG8
+39°2950	144872	1.127	1.224	+0.018	1.220	1.084	1.088	+0.054	K3V
G168-42	Y 3710	0.255	1.010	+0.469	1.030	--	--	+0.090	sdG2
G180-58	Y 3750	0.074	1.029	+0.691	1.049	0.996	0.960	+0.124	sdG1
-3°3968	149414	0.350	1.018	+0.390	1.038	0.961	0.927	+0.021	sdG
+37°2804	151877	0.738	1.034	+0.035	1.030	0.856	0.860	+0.086	K7V
+43°2659	152792	0.229	0.853	+0.178	0.860	0.716	0.709	+0.101	G0V
+17°3154	154276	0.228	0.847	+0.170	0.853	0.690	0.684	+0.070	G2V
+1°3421	157089	0.116	0.805	+0.217	0.817	0.673	0.660	+0.078	G0V
G170-56	Y 4012	-0.043	0.719	+0.238	0.739	0.621	0.598	+0.060	sdG3

Table 11. Observed quantities for subdwarfs. -- <u>continued</u>.

Name	Name	37-45	45-63	δ(37-45)	(45-63)$_s$	58-99	(58-99)$_s$	G	Sp
+2°3375	--	-0.120	0.719	+0.315	0.740	0.676	0.645	+0.009	sdG0
+37°2926	160693	0.112	0.788	+0.191	0.799	0.687	0.678	+0.058	G0V
+25°3344	161817	-0.008	0.293	+0.142	∼0.300	0.320	∼0.282	+0.355	sdA2
G20-15	Y 4059	0.030	0.925	+0.507	0.945	0.919	0.883	+0.098	sdF8
G183-11D	LTT15298	-0.113	0.654	+0.241	0.674	0.572	0.542	+0.003	sdG1
G154-36	163810	0.101	0.904	+0.396	0.924	0.806	0.782	+0.056	sdF8
+13°3683	Y 4269	-0.002	1.018	+0.742	1.038	0.991	0.955	+0.201	sdG5
G206-34D	W11060	-0.127	0.687	+0.288	0.709	0.638	0.606	-0.093	sdG0
+20°3926	173667	0.081	0.643	+0.037	0.640	0.473	0.476	+0.073	F6V
AC+20°1463-148	--	1.713	2.074	--	2.074?	2.538	2.538?	+0.588	sdM2
AC+20o1463-154	--	1.591	2.102	--	2.102?	2.577	2.577?	+0.568	sdM2
+41°3306	Y 4524	0.618	1.059	+0.205	1.075	0.946	0.932	+0.053	K1
+11°3833	182572	0.630	0.960	-0.016	0.954	0.724	0.729	+0.147	G8IVp
+10°4091	188510	0.032	0.874	+0.409	0.894	0.750	0.722	+0.023	sdG7
+5°4481	G24-13	0.100	0.810	+0.239	0.825	0.808	0.799	+0.090	G4V-VI
-21°5703	193901	-0.055	0.808	+0.391	0.830	0.719	0.690	+0.086	sdG3
+41°3735	LTT15972	0.119	0.895	+0.361	0.915	0.881	0.859	+0.325	sdG0
+9°4529	194598	-0.062	0.680	+0.216	0.698	0.642	0.619	+0.066	sdG2
-9°5491	195636	-0.023	0.931	+0.572	0.951	0.931	0.895	+0.336	sdG6
+17°4519	201891	-0.035	0.728	+0.241	0.747	0.641	0.619	+0.031	F9VI
G188-30	Y 5296	0.079	0.964	+0.543	0.984	0.891	0.855	+0.135	dG2
G126-62	Y 5368	-0.081	0.691	+0.246	0.709	0.682	0.659	+0.038	sdG0
G18-39	Wolf1032	-0.085	0.673	+0.229	0.691	0.666	0.640	+0.031	sdG0
-8°5980	216777	0.267	0.851	+0.139	0.853	0.746	0.744	+0.067	G6V
G28-43	W14539	0.226	0.965	+0.398	0.985	0.909	0.880	+0.059	sdG2
G190-15	Y 5617	-0.006	0.977	+0.655	0.997	0.931	0.895	+0.089	sdG8
-14°6437	219617	-0.090	0.733	+0.303	0.755	0.664	0.635	+0.019	sdG2
+26°4734	224930	0.240	0.922	+0.292	0.938	0.856	0.842	+0.055	G2V
BS77	1581	0.147	0.806	+0.186	0.809	0.728	0.725	+0.092	G2V
BS219D	4614	0.153	0.795	+0.161	0.800	0.694	0.689	+0.047	G0V
BS1008	20794	0.391	0.945	+0.189	0.951	0.761	0.755	+0.087	G5V
BS6752D	165341	0.793	1.102	+0.113	1.102	0.950	0.950	+0.104	K0V
BS6927	170153	0.039	0.714	+0.149	0.722	0.632	0.622	+0.044	F7V
BS8181	203608	-0.003	0.721	+0.200	0.735	0.591	0.574	0.000	F8V

subdwarf's observed colors are calculated and plotted versus the effective wavelengths of the filters to give a blanketing curve. (In all of the following analyses no reddening corrections have been applied to the subdwarf photometry. Most subdwarfs lie within 100 parsecs and so require no reddening corrections. A few may be as far away as 250 parsecs, but since only statistical corrections exist, as shown by Sandage's (1964) discussion of the use of Parenago's (1940) reddening equation, no reddening corrections have been attempted for the individual stars.)

According to the graph of Figure 2 stars with metallicities of one-tenth the solar abundance or less have blanketing corrections of about +0.02 regardless of the exact composition; the 0.1X and 0.01X curves lie nearly on top of one another. For metallicities in the range $0.0 \geq [Fe/H] \geq -1.0$ the blanketing corrections have been linearly interpolated (proportional to $[Fe/H]$) between the values of 0.00 and approximately +0.02. However, the models give these corrections down to an effective temperature of only 5500° (45-63 = +0.86). Figure 1 shows that the blanketing corrections do not change much to at least 45-63 = +1.00 which corresponds to $T_e = 5250^{\circ}$, and so the blanketing corrections of the models have been extrapolated with good confidence to $T_e = 5250^{\circ}$. This includes about 75% of the subdwarfs. The blanketing corrections have also been applied to 17 other subdwarfs in the range $5250^{\circ} > T_e > 4690^{\circ}$, but with much less confidence. Figures 1 and 2 show that the blanketing corrections are small and are changing very slowly with temperature for $T_e \geq 5250^{\circ}$. These facts argue that perhaps the blanketing corrections are good for $T_e < 5250^{\circ}$, but the appearance of

molecules could alter this drastically. It should be kept in mind then that the blanketing corrections applied to the 45-63 indices of 17 stars with $T_e < 5250^o$ are very uncertain. For three other cool stars no corrections have been applied since they seem to have approximately solar abundances, and for the seven coolest stars no corrections have been applied since they are beyond the cool end of the chemical composition calibration; for these seven stars their $(45-63)_s$'s of Table 11 are followed by question marks.

In Figures 3 to 9 are plotted the observational blanketing curves of seven groups of subdwarfs, and in Table 12 are given the mean characteristics of these groups, where column one gives the group number, column two the number of stars in the group, column three the average effective temperature, column four the average composition and column five the average blanketing for the 37-52 color. (At this point are plotted only average blanketing curves since the aim is to study the sensitivity of the 13-color indices and not the peculiarities of individual stars. Later the individual curves of some interesting subdwarfs will be given.) In these graphs the straight horizontal line represents the energy distribution of a Hyades main sequence star while the plotted points represent the relative distribution of the subdwarfs. The curves which pass through the points are drawn only to help the eye detect relationships and do not represent interpolations of the data. To a good first approximation we can assume that these observational blanketing curves show only effects of metallicity since the subdwarfs have compositions drastically different from the Hyades, but small surface gravity
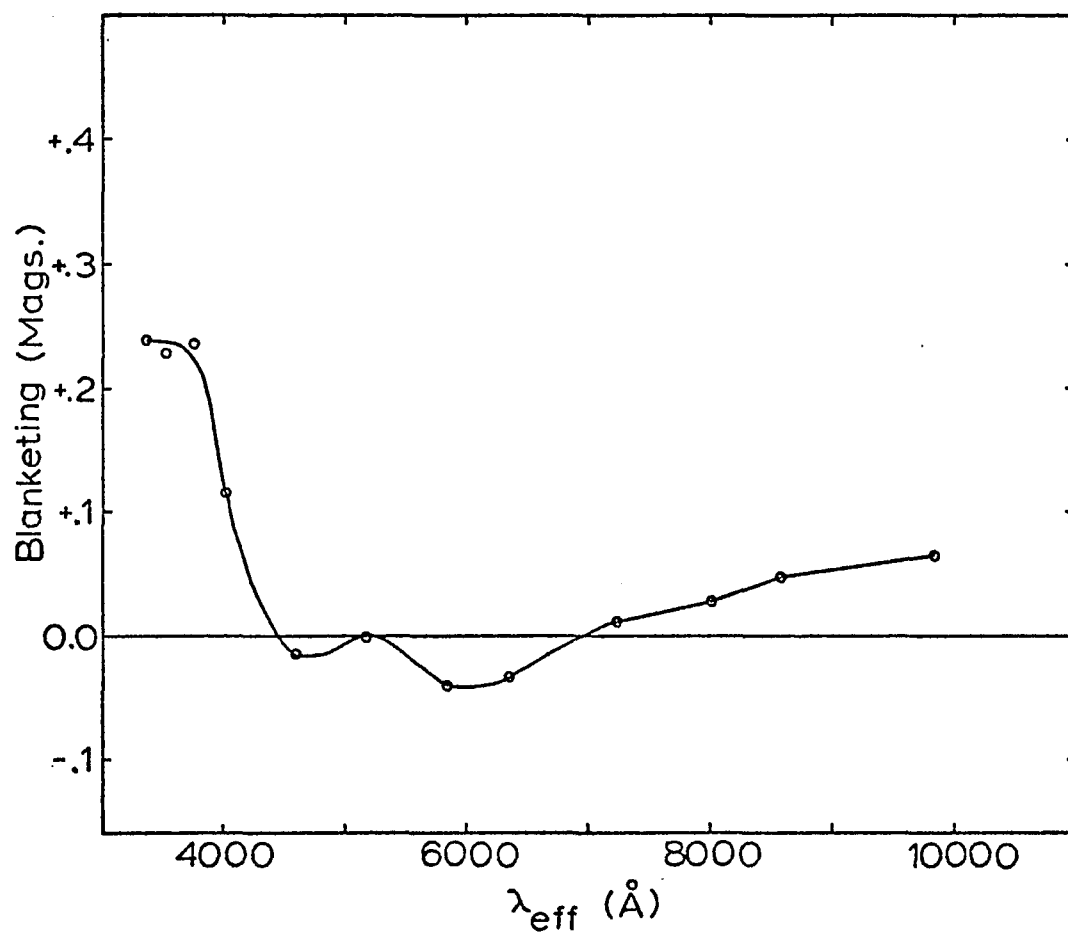
Figure 3. The average observational blanketing curve for the subdwarfs of group 1.
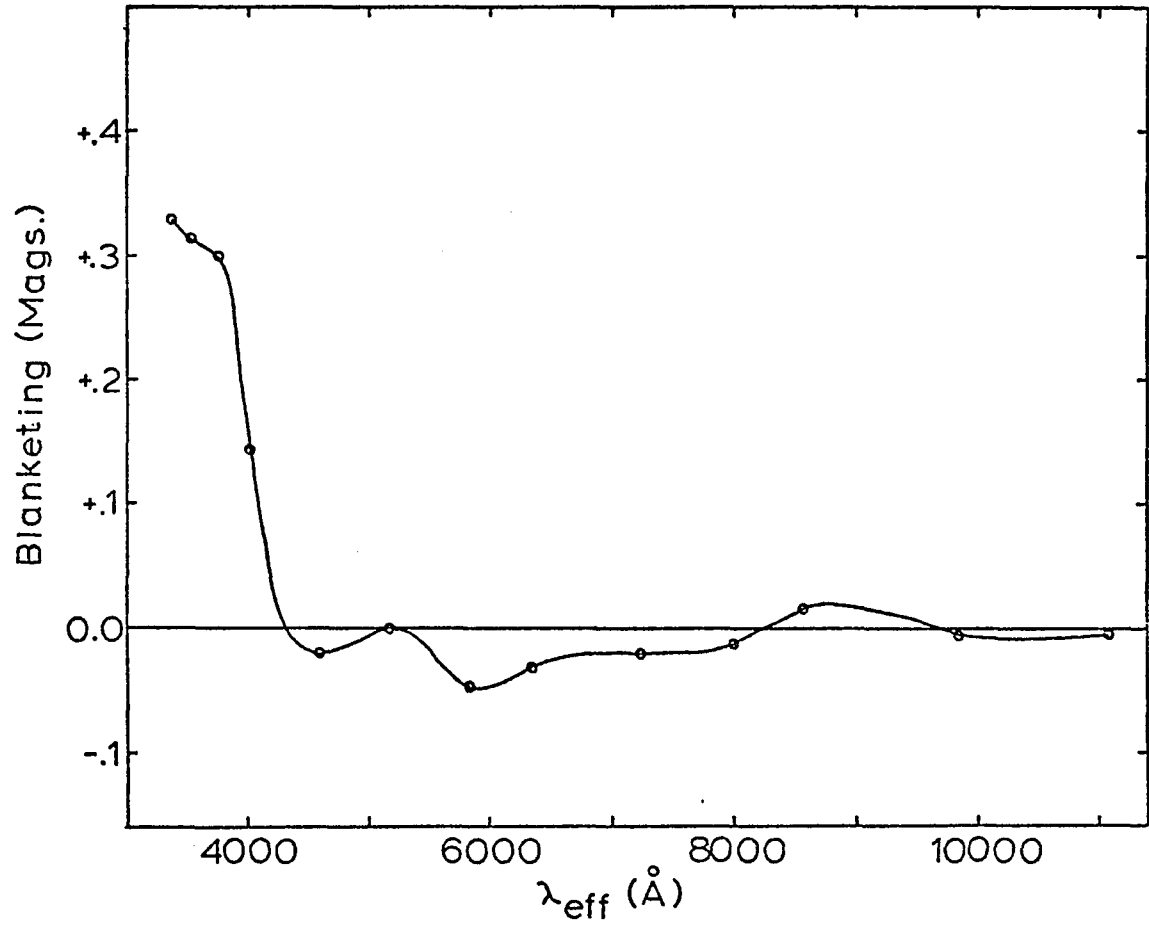
Figure 4. The average observational blanketing curve for the subdwarfs of group 2.
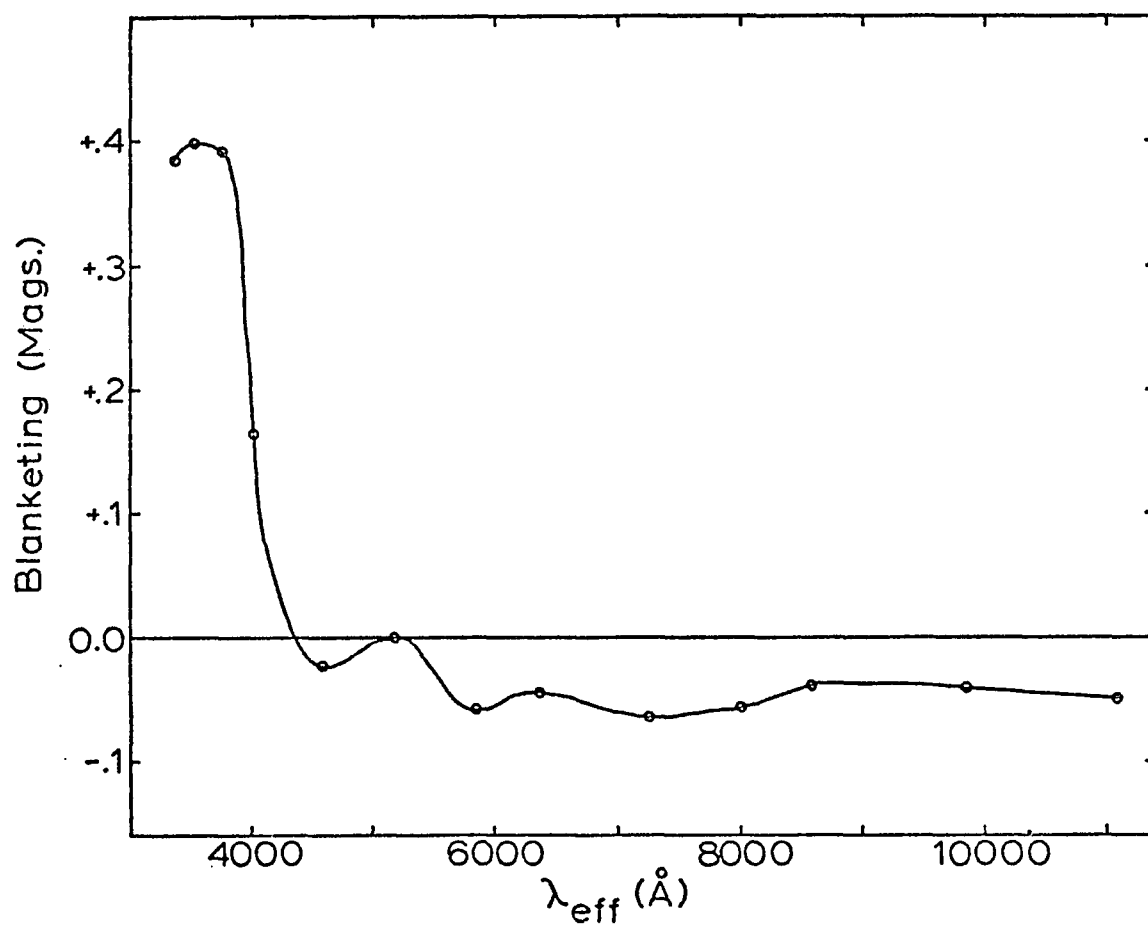
Figure 5. The average observational blanketing curve for the subdwarfs of group 3.
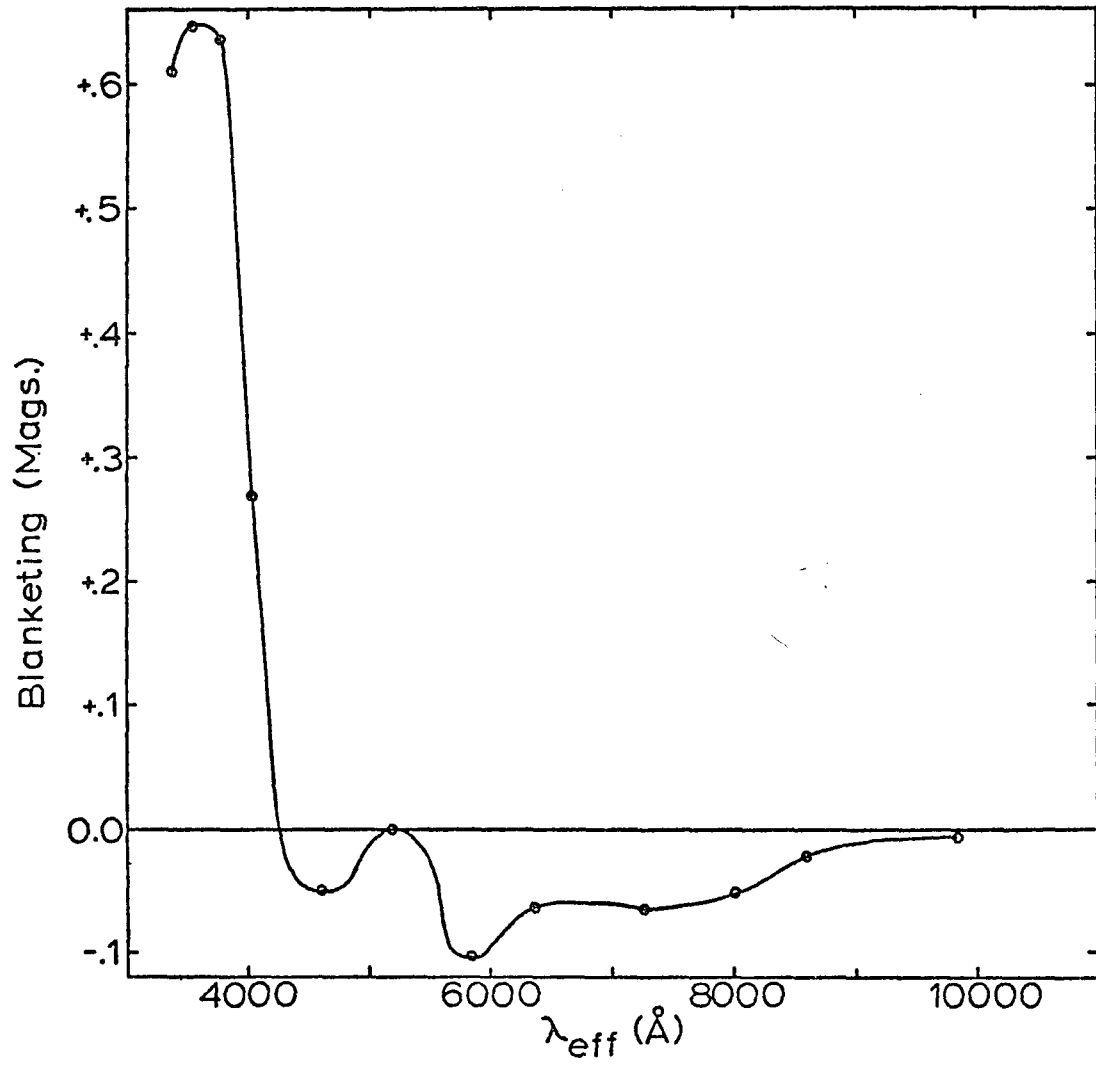
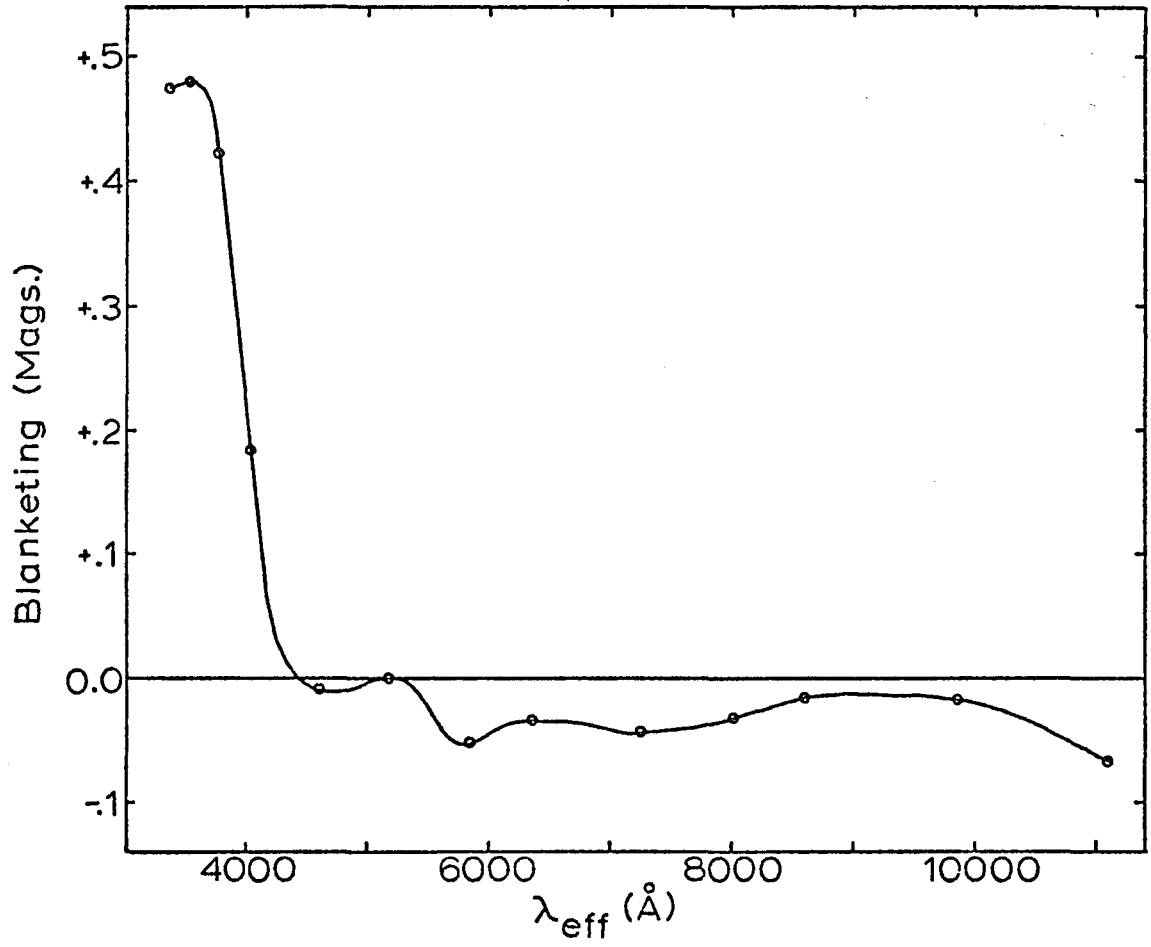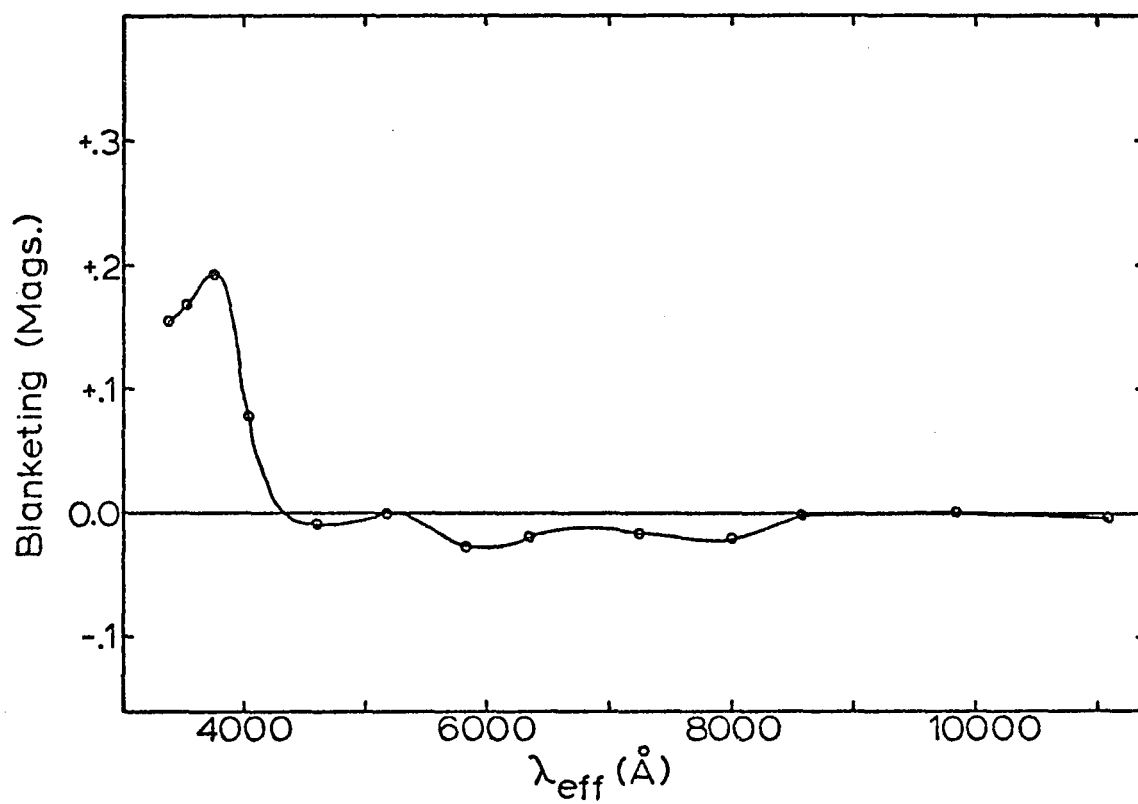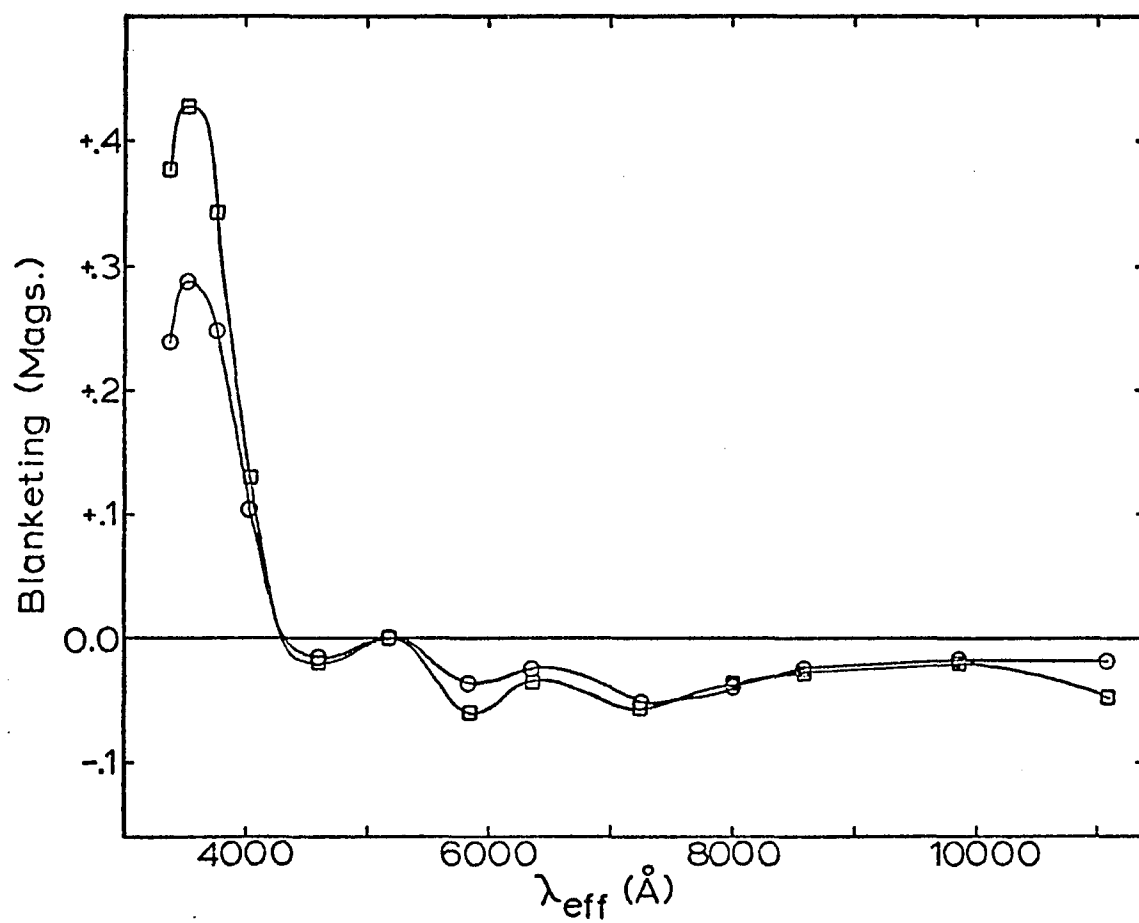Figure 6. The average observational blanketing curve for the subdwarfs of group 4.

Figure 7. The average observational blanketing curve for the subdwarfs of group 5.

Figure 8. The average observational blanketing curve for the subdwarfs of group 6.

Figure 9. The average observational blanketing curve for the subdwarfs of group 7 (circles) plus the blanketing curve for BS 4550 (squares).

Table 12. The groups of subdwarfs in Figures 3 to 9.

Group No.	No. of Stars	$(T_e)_{Ave}$	$[Fe/H]_{Ave}$	$\Delta(37-52)_{Ave}$
1	9	6210	-1.43	0.235
2	18	6000	-1.38	0.299
3	11	5730	-1.48	0.391
4	6	5170	<-2.0	0.635
5	5	5510	-1.38	0.422
6	9	5750	-0.37	0.193
7	9	5320	-0.63	0.247
BS4550	1	5180	-1.30	0.342

effects are also included as will be shown shortly. In Figures 10, 11 and 12 are plotted theoretical blanketing curves; these are obtained by subtracting the 0.1X and 0.01X colors from the 1X colors at constant T_e and constant log g. These theoretical curves show only effects of composition.

A comparison of the observational curves shows the following: (a) the degree of blanketing increases with effective temperature in the range $6500^o \geq T_e \geq 5500^o$; examining groups 1, 2, 3, and 5, all of which have nearly the same average composition, we see that the blanketing increases nearly linearly with T_e from 6200° to 5700° and then starts leveling off at $T_e = 5500^o$. This agrees with the results of Eggen (1968, 1969a) who shows that in broad-band photometry the blanketing, as measured by $\delta(U-B)$, increases to a maximum ($\simeq +0.30$) at an observed B-V of about +0.5. Using Wildey et al. (1962) with $\delta(U-B) = +0.3$ and $(B-V)_{obs} = +0.5$ gives $(B-V)_{corr} = +0.71$ which corresponds to $T_e \simeq 5500^o$ (Johnson 1966). In contrast Sandage (1969a) finds that the maximum blanketing occurs at $(B-V)_{obs} = +0.6$ and with $\delta(U-B) = +0.31$ which implies $(B-V)_{corr} = +0.82$ and $T_e \simeq 5240^o$. (b) It is difficult to extend the above analysis to $T_e < 5500^o$ since the chemical composition calibration is not well defined in this range (see the next chapter). However, the star BS 4550 has $T_e = 5180^o$, is very well observed in the 13-colors (55 8C observations and 48 6RC), and has a recent spectroscopic composition determination of [Fe/H] = -1.30 (Tomkin and Bell 1973). This star, which is also part of group 7, has been listed separately in Table 12. In Figure 13 we plot the blanketing of the 37-52 color ($\Delta(37-52)$) versus the effective
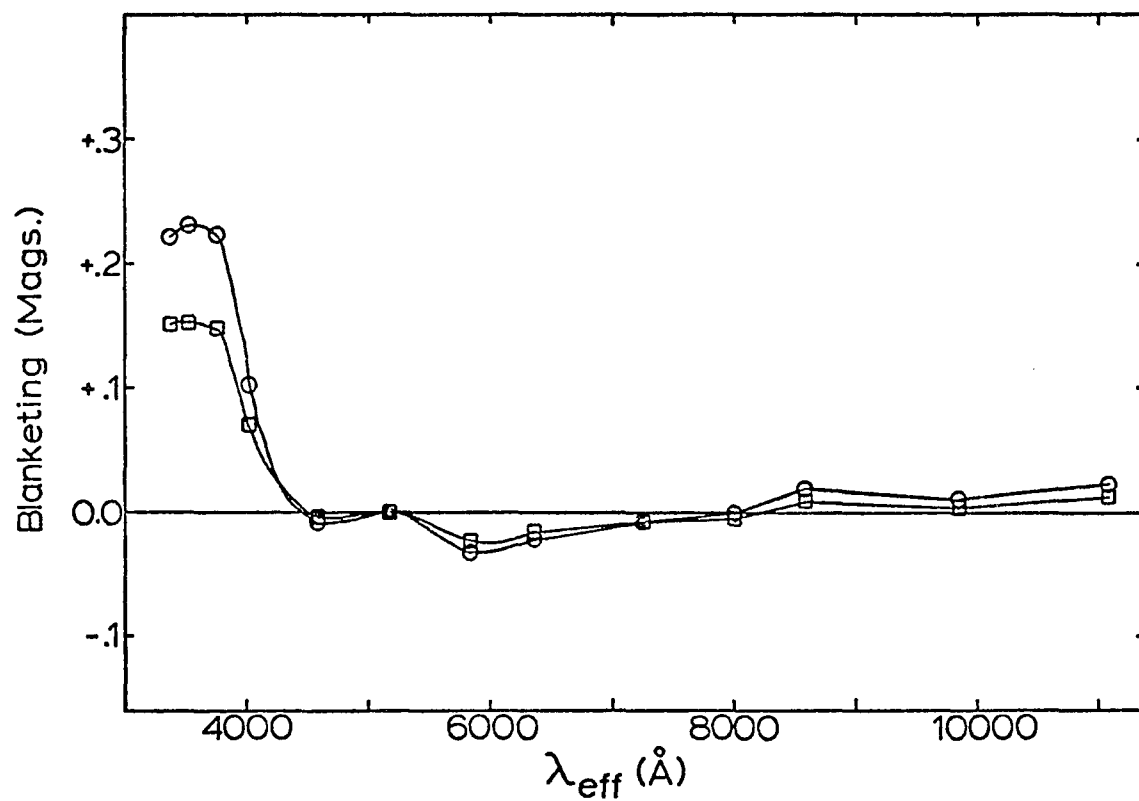
Figure 10. Theoretical blanketing curves for T_e = 6500° and log g = 4.5.
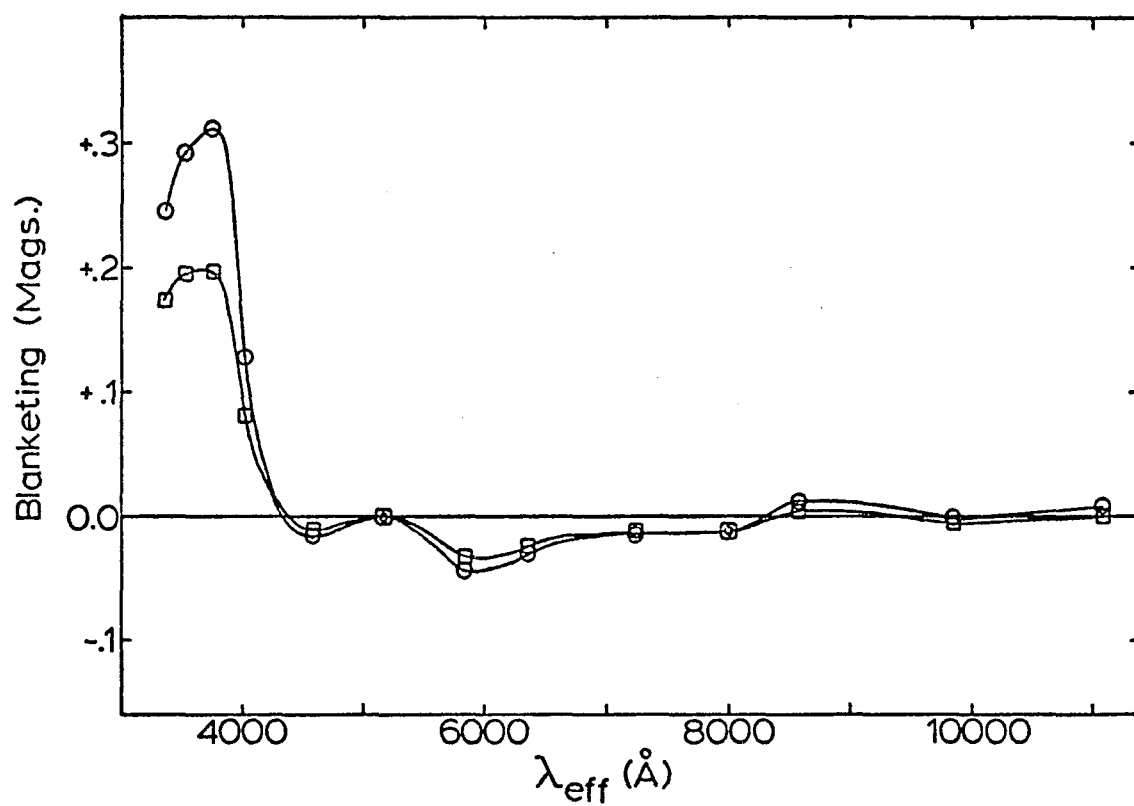-- Squares are for 0.1 solar abundance and circles 0.01.

Figure 11. Theoretical blanketing curves for $T_e = 6000^{\circ}$ and log g = 4.5. -- Squares are for 0.1 solar abundance and circles 0.01.
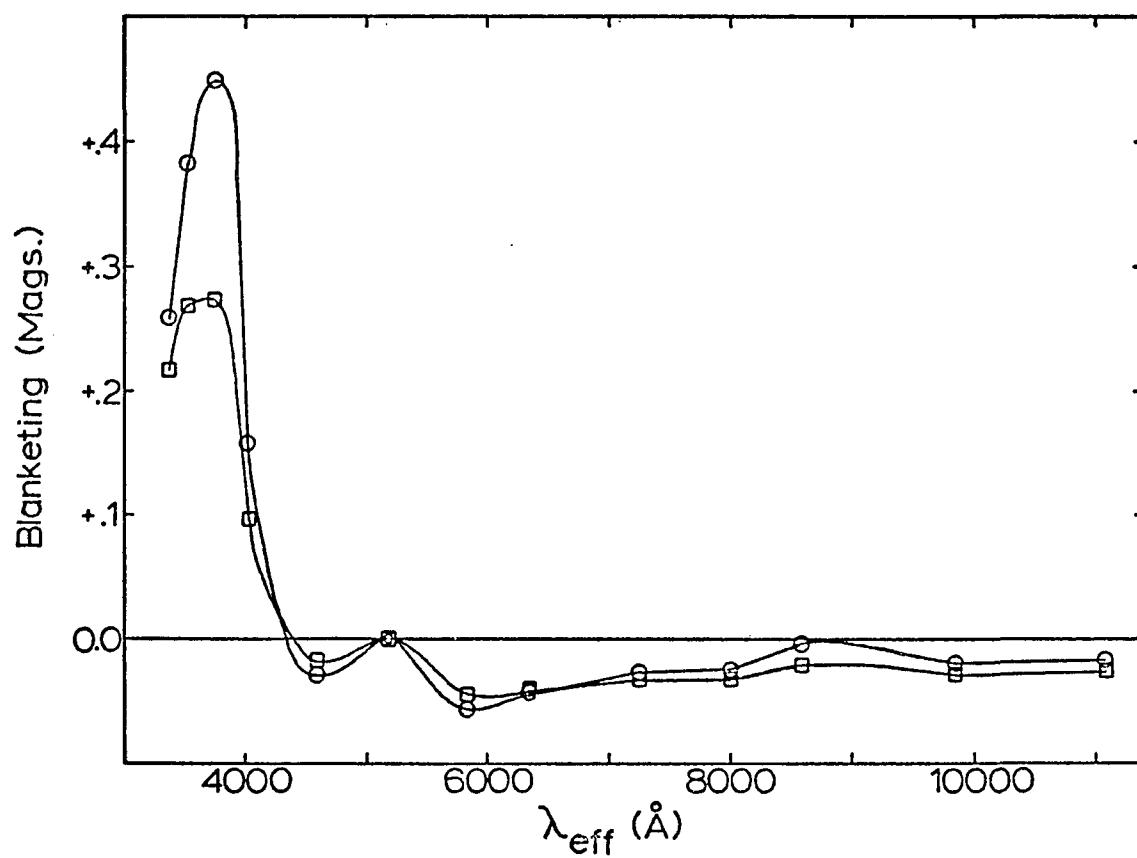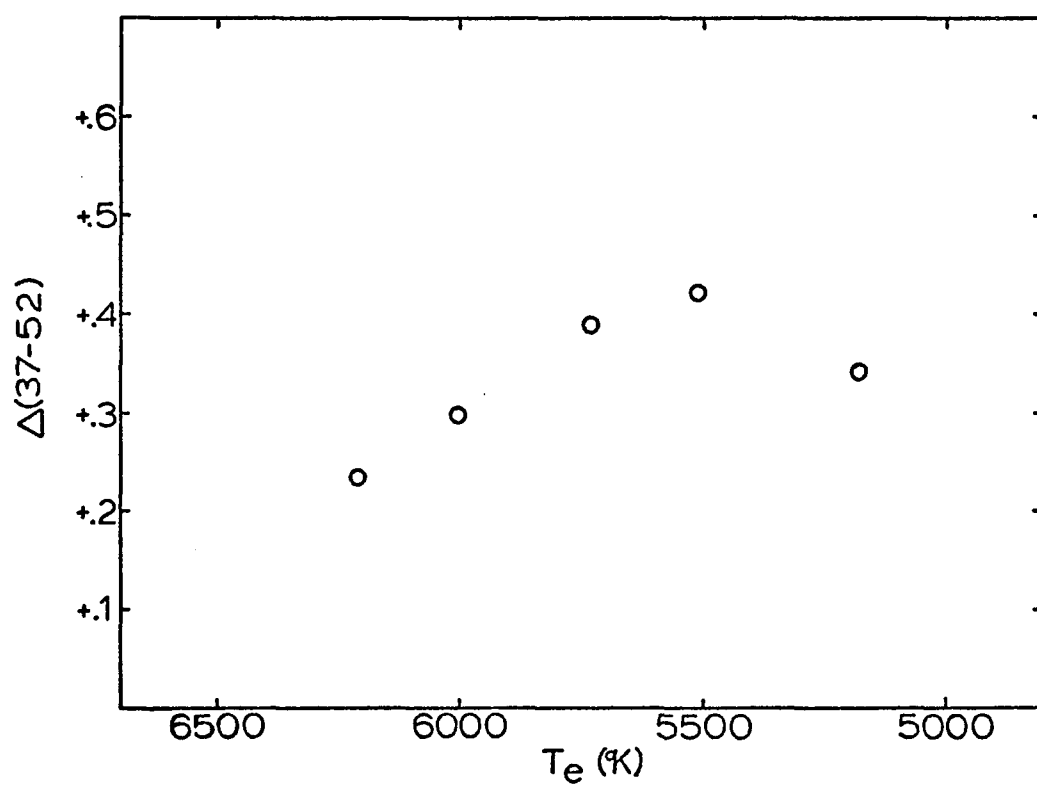
Figure 12. Theoretical blanketing curves for T_e = 5500° and log = 4.5.
-- Squares are for 0.1 solar abundance and circles 0.01.

86

Figure 13. Δ(**37**-52) versus $(T_e)_{ave}$ for groups 1, 2, 3 and 5 and for BS 4550.

temperature for groups 1, 2, 3, and 5 and for BS4550, all of which have similar compositions. We see that for a given composition, blanketing produces its maximum effect at an effective temperature of 5500° or 5400°. (c) The shapes of the blanketing curves remain remarkably similar over the range of T_e's and compositions represented by the seven groups. The blanketings of filters 33, 35, and 37 are always nearly equal and are large and positive with respect to filter 52. The blanketing of filter 40 is always about half that of filters 33, 35, and 37. Filter 45 always has negative blanketing with respect to 52, a small peak always occurs at filter 52 (which has been arbitrarily set to zero blanketing at this point), and filter 58 nearly always has the most negative blanketing. In the red and infrared the curves are generally level or sloping slightly upward going to longer wavelengths. The constancy of these curves' shapes shows that a single 13-color metallicity index will be sufficient over the full temperature range of the subdwarfs.

(d) As suggested by Johnson and Mitchell (1968) the 37-45 index seems to be excellent for measuring metallicity since it contains nearly the full sensitivity to composition changes. Other indices such as 35-58 or 37-58 have slightly greater sensitivities but have other disadvantages. Filter 35 is below the Balmer discontinuity, and so we would expect that for F stars it will also be sensitive to surface gravity. The color 37-58 should have slightly larger accidental errors of observation than 37-45 since 37 and 45 are always observed much closer together in time than 37 and 58. For these reasons the 37-45 index has been used exclusively in determining metallicities.

As mentioned earlier the theoretical blanketing curves agree very well with the observational ones except for the 33 and 35 filters at the coolest temperatures. We can see this clearly comparing Figures 5 and 12. This discrepancy of the theoretical curves can be removed by playing with the surface gravities. For example, subtracting the colors of a (5500, 4.5, 0.01, 2) model from those of a (5500, 3.5, 1X, 2) model gives a curve very similar to the observational curves of Figures 5 and 7. However, if we try changing gravities to obtain agreement in the 33-35 versus 45-63 diagram, mentioned earlier, we obtain log g = 3.0-3.5 for the Hyades main sequence; this is clearly not correct. Also, we cannot justifiably change the surface gravity of the solar model to obtain agreement with the derived solar colors. Indeed, the models do seem to have problems in the ultraviolet at $T_e = 5500^o$.

In Figures 14, 15, and 16 are plotted observational luminosity-difference curves and in Figures 17, 18, and 19 theoretical curves. The observational curves have been obtained in the same manner as the blanketing curves except that giant stars, not subdwarfs, have been compared to the Hyades main sequence at constant T_e, and 45-63 has been corrected for luminosity differences using the models instead of for composition differences. The surface gravities needed for interpolating the corrections have been estimated from Allen (1973); this rather crude method should not lead to any significant errors since the 45-63 corrections are all small (≤ 0.03 magnitude). At $T_e = 5500^o$ the correction is zero, and so for all stars with $T_e \leq 5500^o$ no luminosity correction has been applied; again since the 45-63 corrections are small and change slowly
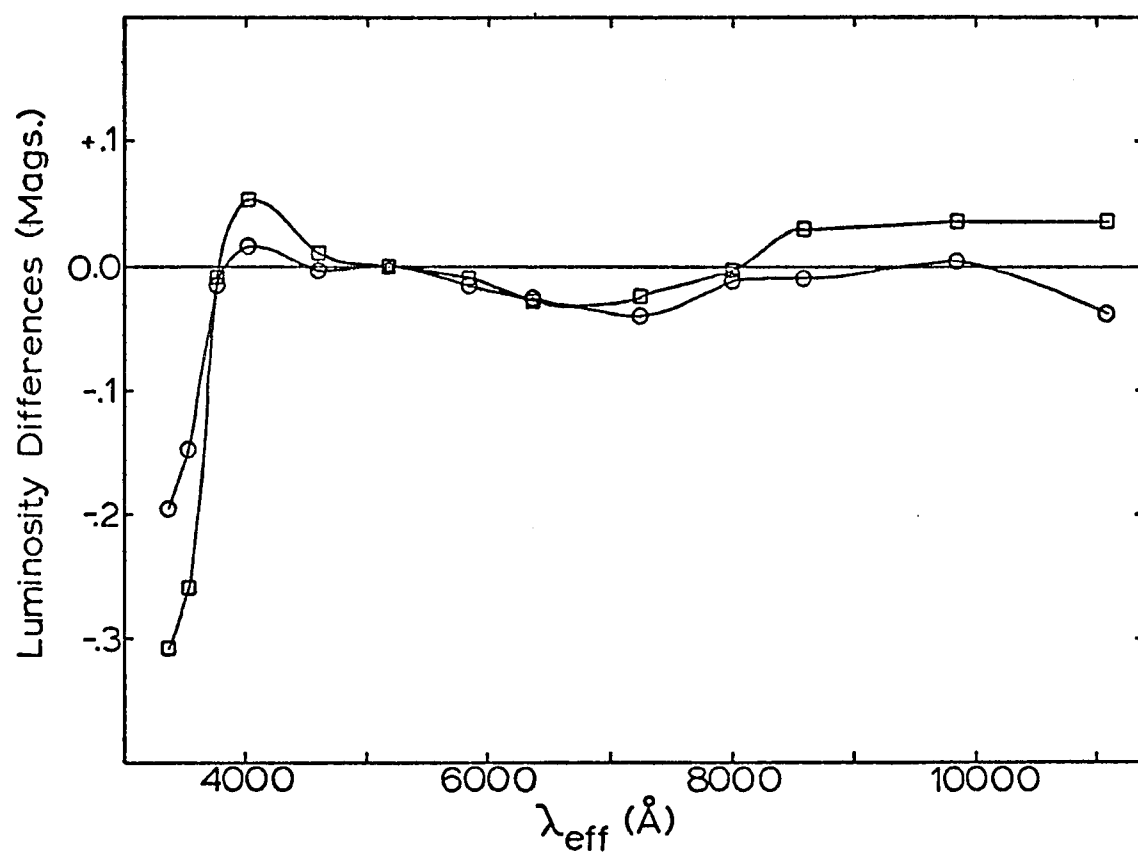
Figure 14. Observational luminosity-difference curves for two F
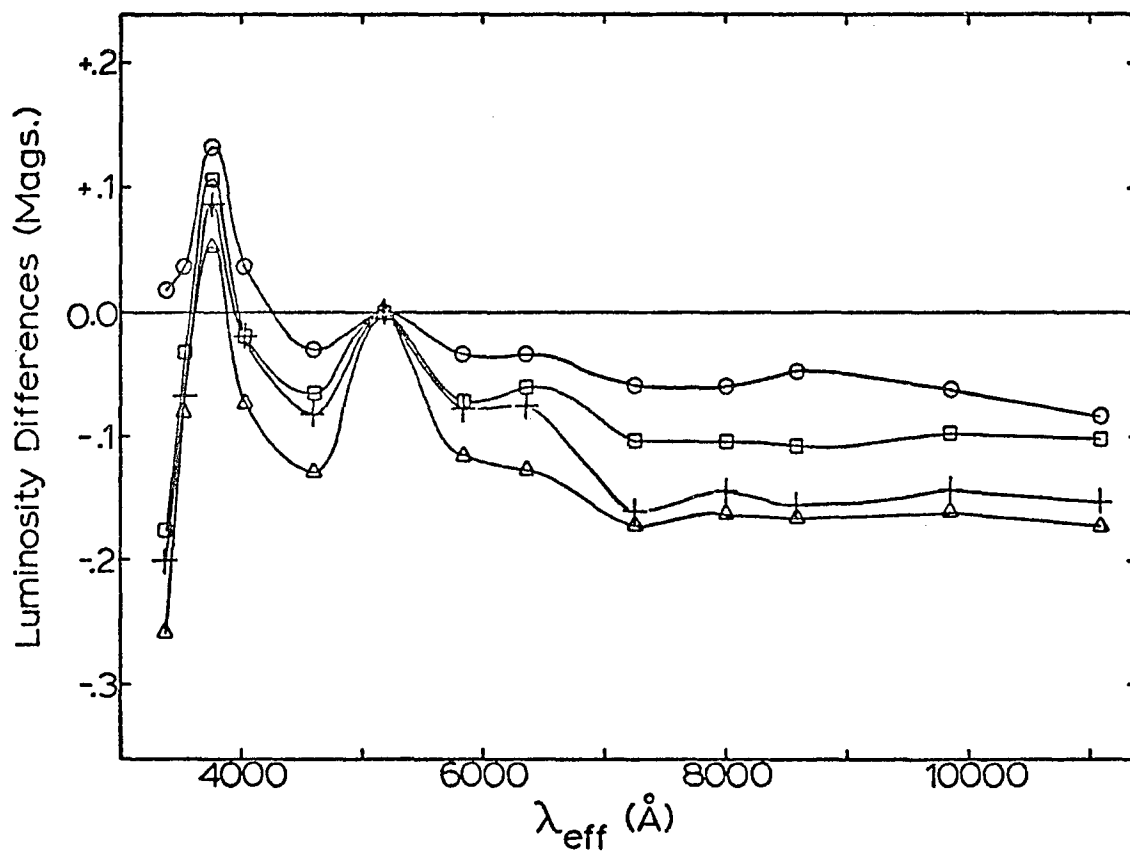giants. -- Squares represent BS 4031 (FOIII) and circles
BS 2930 (F3III).

Figure 15. Observational luminosity-difference curves for G giants. --
Circles represent BS 5409 (G2III), squares BS 1829 (G5III),
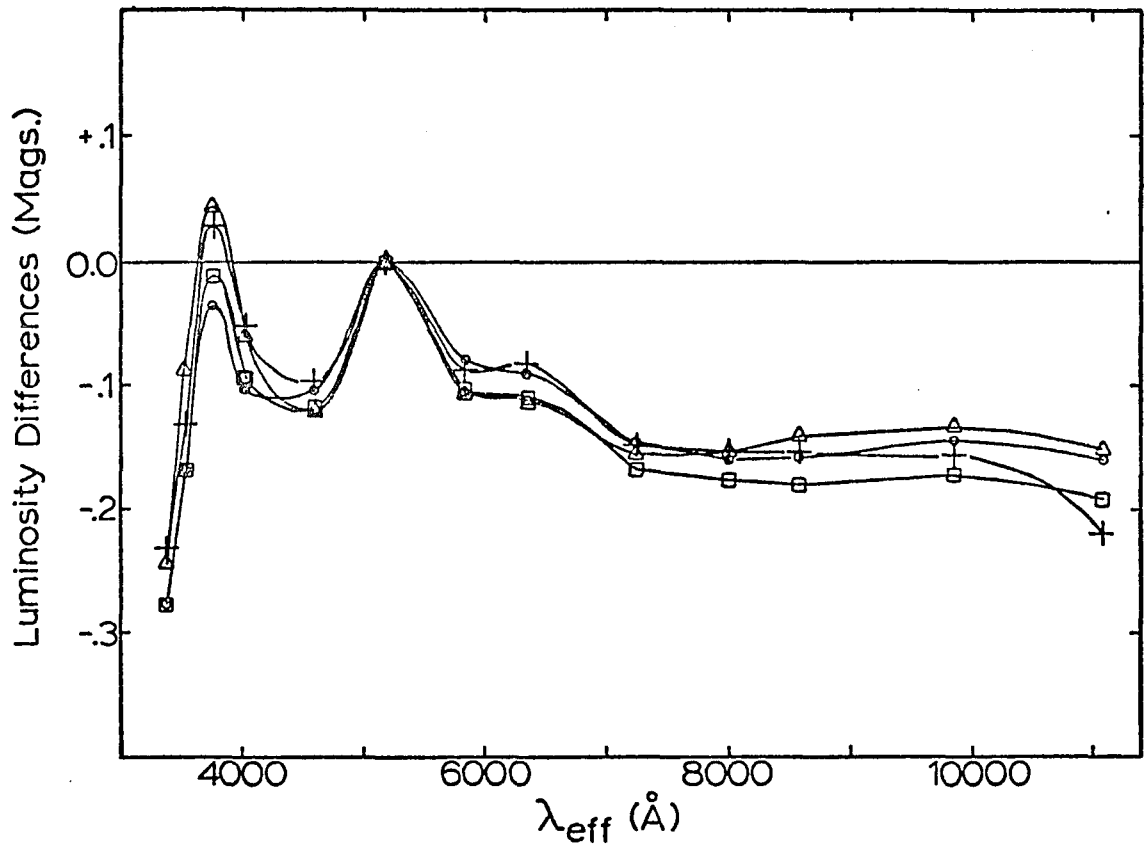triangles BS 442 (G8III), and pluses BS 5997 (gG2).

Figure 16. Observational luminosity-difference curves for late-G and
early-K giants. -- Circles represent the Hyades giant, H71
(G9III), squares the Hyades giant, H28 (KOIII), triangles
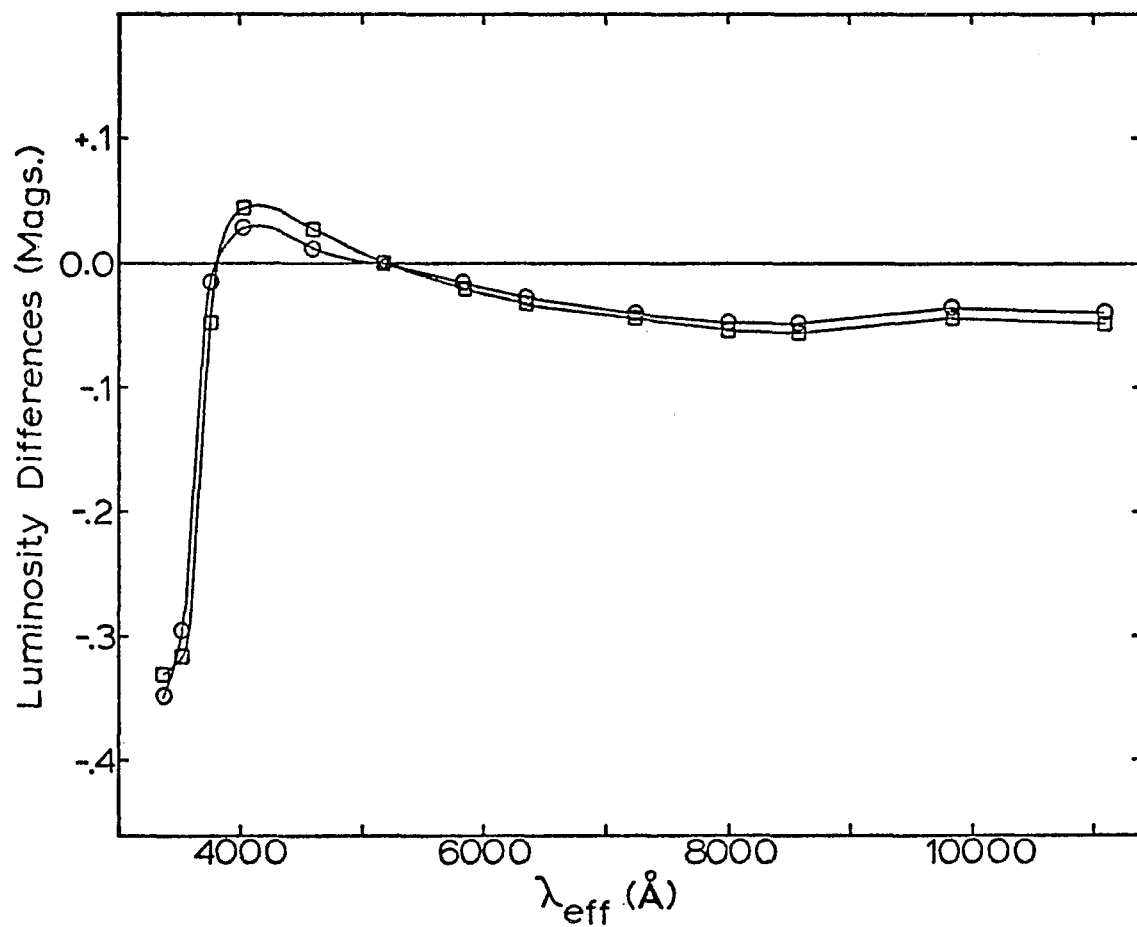BS 6075 (G9III), and pluses BS 6703 (G9III).

Figure 17. Theoretical luminosity-difference curves for $T_e = 6500°$. --
Log g = 3.0 photometry is compared to log g = 4.5. Circles
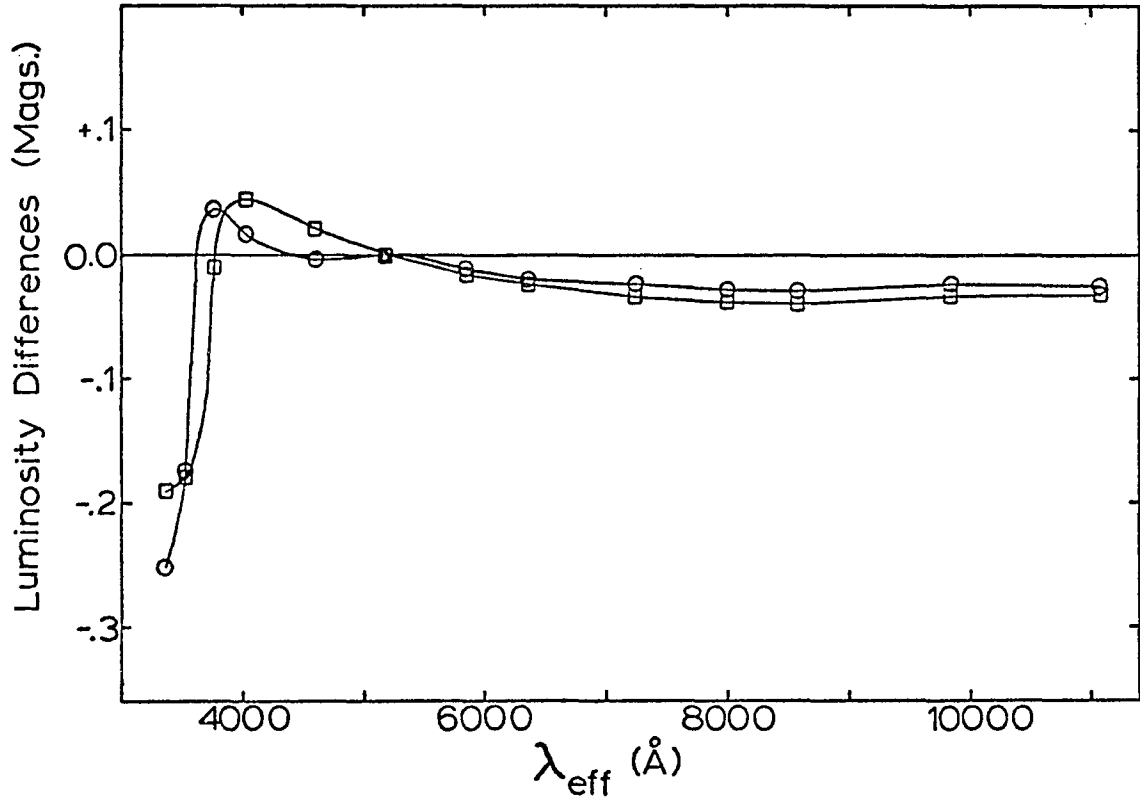are for solar abundance and squares 0.01 solar abundance.

Figure 18. Theoretical luminosity-difference curves for $T_e = 6000^o$. --
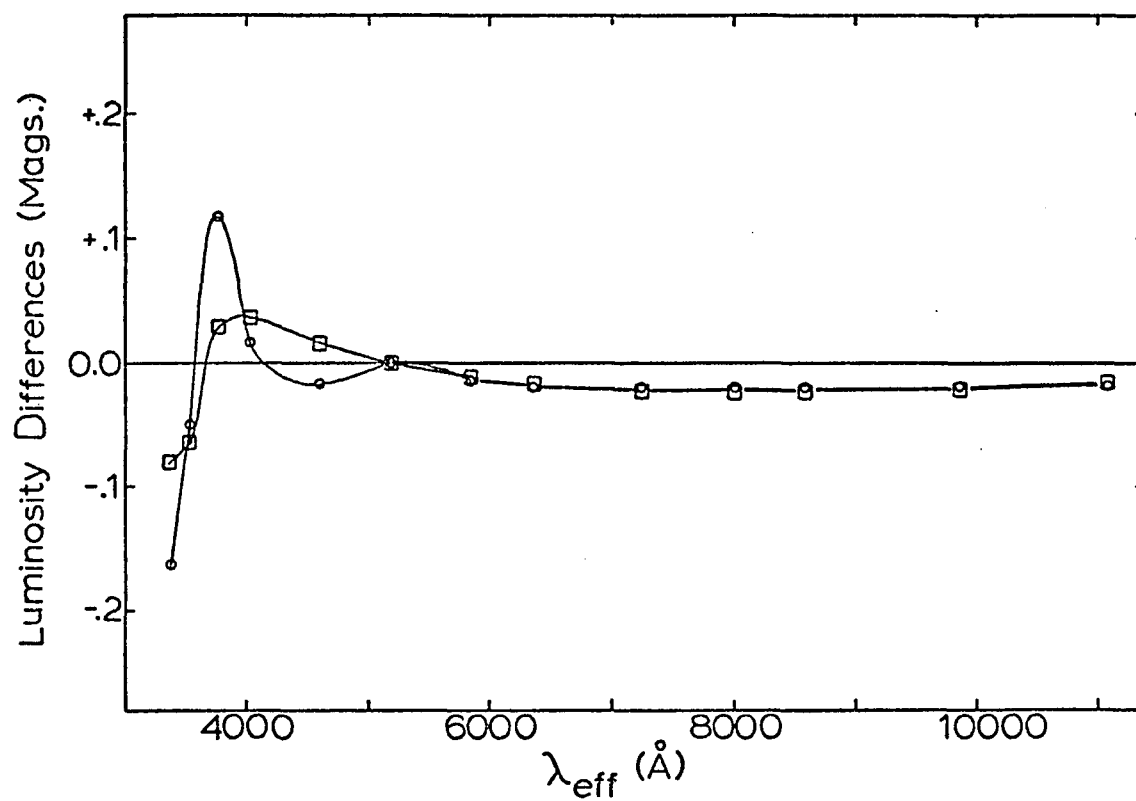Circles are for solar abundance and squares 0.01 solar
abundance.

Figure 19. Theoretical luminosity-difference curves for $T_e = 5500^o$. -- Circles are for solar abundance and squares 0.01 solar abundance.

with temperature, this approximation should not lead to any problems as long as molecules are not important for the 45-63 index. The differences plotted in Figures 14 through 19 are calculated in the sense: color of the large-surface-gravity star minus the color of the small-surface-gravity star. For the theoretical curves the log g = 4.5 models are compared to the log g = 3.0 ones. By comparing the curves of Figures 14 through 19 we can conclude the following: (a) The important thing to note is the behavior of filters 33, 35, and 37. Decreasing the surface gravity always moves the positions of filters 33 and 35 downward with respect to filter 37. For the F stars this occurs because the filters 33 and 35 are below the Balmer discontinuity while filter 37 is above, and in this hotter temperature range the Balmer jump is sensitive to surface gravity. For the cooler stars the shapes of the luminosity-difference curves depend more upon the surface gravity sensitivities of the thousands of atomic absorption lines which fall in filters 33, 35, 37, and 52. This behavior of filters 33 and 35 with respect to 37 appears in all six figures and so must hold over a rather wide tempera-ture range--at least from the T_e of FOIII stars to the T_e of KOIII. All subgiants in this temperature range as well as the giants plotted here show a similar depression of 33 and 35 with respect to 37. The exact shapes of the curves may change significantly, as seen comparing Figures 14 and 16, but this ultraviolet depression is always present. (b) The observational luminosity-difference curves show primarily surface gravity effects, but small blanketing effects are also present. This is demonstrated clearly in Figure 16 where two field giants (both G9III)

and two Hyades giants (G9III and KOIII) have been compared to the Hyades

main sequence. The Hyades giants probably have greater metallicities

than the field giants since the Hyades main sequence has a metallicity

greater than most field dwarfs. Indeed, in Figure 16 the field giants

show excesses with respect to the Hyades giants for filters 33, 35, 37,

and 40. (c) A comparison of the theoretical and observational curves

shows no significant discrepancies. (d) An examination of the curves

shows several indices which are luminosity sensitive. For the early F

stars the 33 or 35 filter when compared to any one of the other 11

filters provides a good luminosity index. For the late G stars the 37

filter when compared to any other filter, except perhaps 52, gives a good

luminosity index. A good compromise seems to be the index (35-52)-(37-45)

which has several advantages. First, it retains its luminosity sensi-

tivity over a wider temperature range than a simple two filter index;

(35-52) is sensitive for the hotter stars while (37-45) is not, but for

cooler stars (35-52) is less sensitive and (37-45) starts becoming

sensitive. Second, the blanketing of this index is nearly zero since

the blanketing of (35-52) nearly cancels that of (37-45); this remains

true over a fairly wide temperature range as shown by the unchanging

shapes of the blanketing curves. Third, for a given luminosity class

the value of (35-52)-(37-45) remains nearly constant with changing T_e for

the F and G stars; that is, in a (35-52)-(37-45) versus 45-63 diagram

lines of constant luminosity are nearly horizontal. Hence to determine

a star's luminosity class it is not important to measure very accurately

its temperature. This compensates in part for the larger accidental

errors of the four-color (35-52)-(37-45) index. From now on the index

(35-52)-(37-45) will be designated by the letter "G." For the sub-

dwarfs the G values are given in column 9 of Table 11.

In Figures 20 and 21 are shown observational blanketing curves

for giants; that is, the effects caused by changing the metallicity of

a giant while keeping the surface gravity (and T_e) approximately constant.

Figure 20 is derived directly from Figure 16 by subtracting the average

colors of the two field giants from the average colors of the two Hyades

giants. Figure 21 has been obtained by comparing the colors of the metal

poor giant HD122563 (BS5270) (see Wallerstein et al. 1963) to the average

colors of various groups of field giants, bright giants, and supergiants

as explained in the caption. Matching has been done at approximately

constant 45-63. Various similarities and differences between these

curves and the subdwarf blanketing curves can be noted.

Two Important Color-color Diagrams

In Figures 22 and 23 are plotted 37-45 versus 45-63 diagrams

which the preceding analyses show should be composition sensitive; 37-45

is very sensitive to metallicity and 45-63 is not, being a good tempera-

ture indicator. In Figure 22 are plotted the subdwarfs, the Hyades mean

colors, and the solar-type stars (Schuster 1976). The dashed line repre-

sents the locus with an ultraviolet excess, $\delta(37-45)$, of +0.15 and the

dot-dash line is a reddening line —all reddening lines for the 8C

photometry have been obtained from the work of Borgman (1961). The

seven groups of subdwarfs of Figures 3 to 9 are outlined and numbered

in Figure 22. We see that indeed the subdwarfs are well separated from
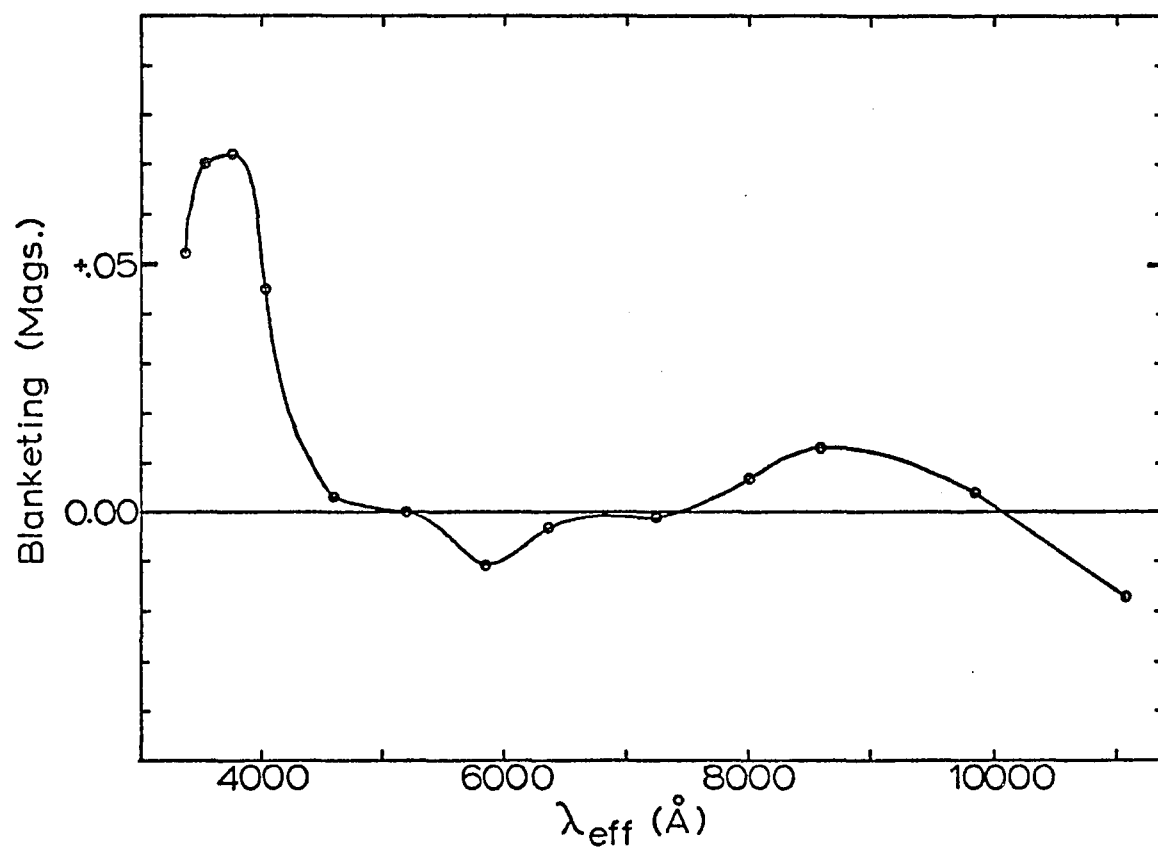
Figure 20. An observational blanketing curve for cool giants. -- H28 plus H71 are compared to BS 6075 plus BS 6703.
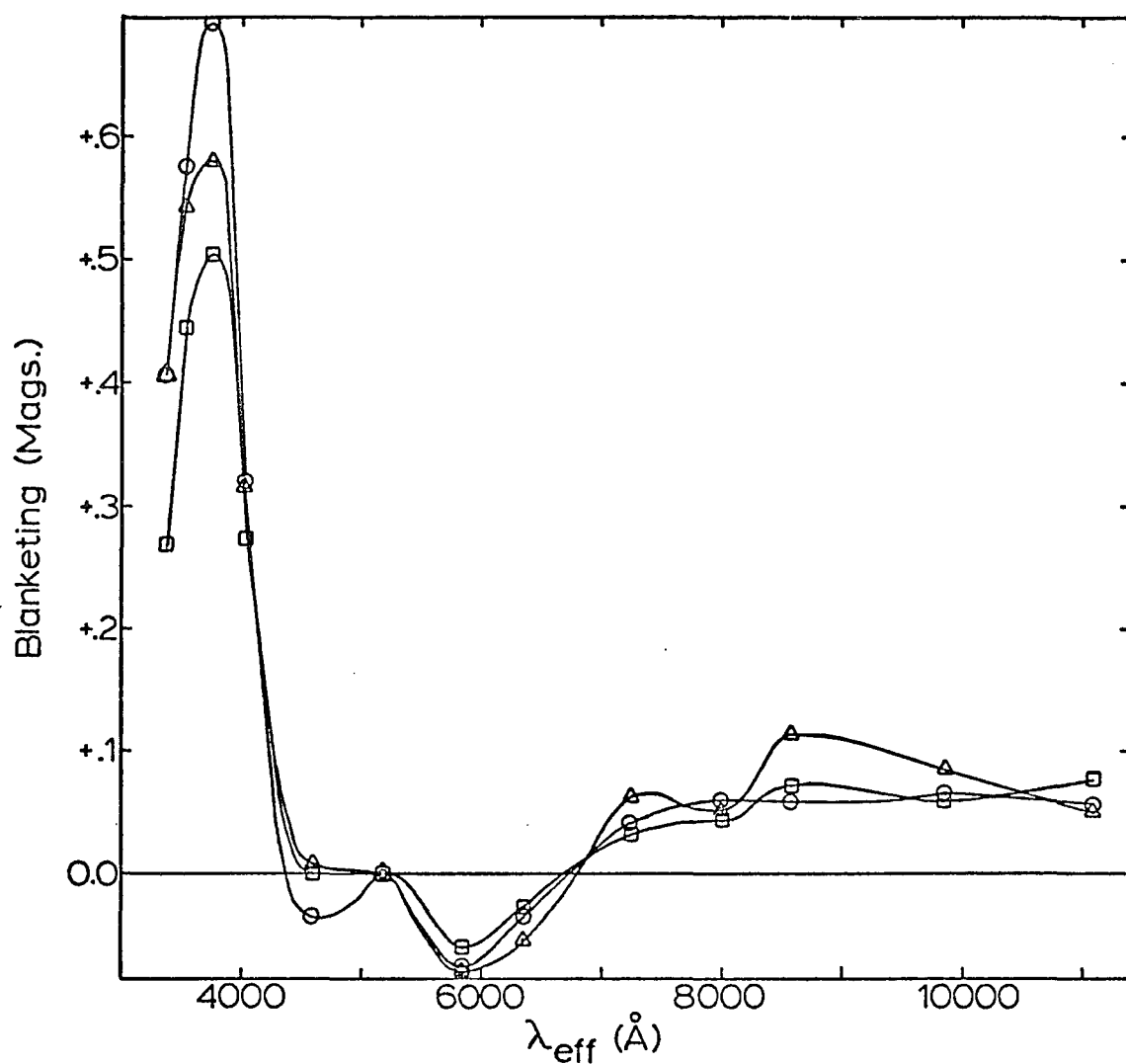
Figure 21. Observational blanketing curves for BS 5270. -- Circles
represent a comparison with the average colors of BS 3
(K1III), BS 188 (K1III), and BS 351 (G8III); squares a
comparison with BS 6536 (G2II) plus BS 7063 (G5II); and
triangles a comparison with BS 7747 (G3Ib).
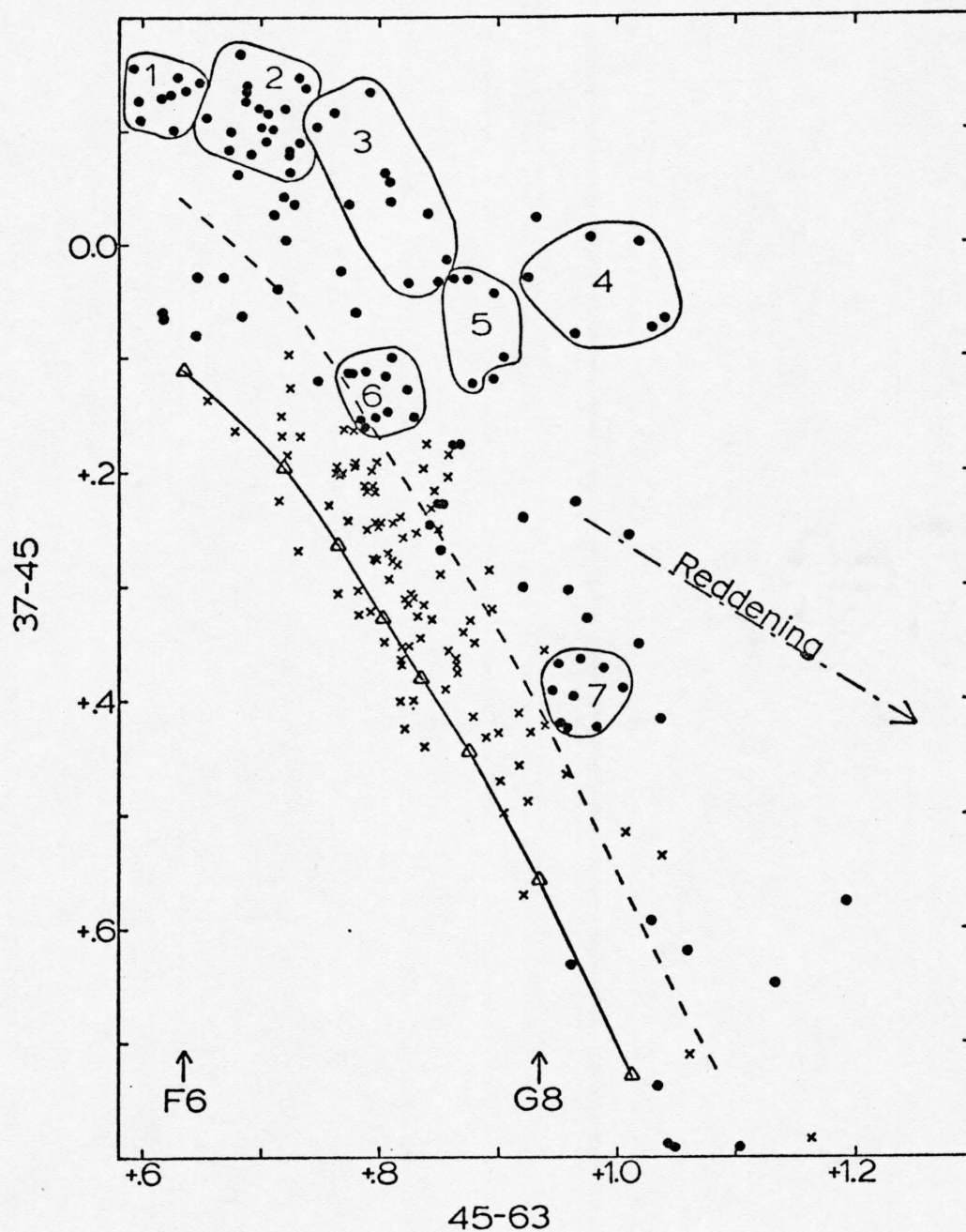
Figure 22. 37-45 versus 45-63. -- Filled circles are for subdwarfs, X's for solar-type stars, and the triangles and solid line for the Hyades mean colors. The other features are explained in the text.

Figure 23. 37-45 versus 45-63 for evolved stars. -- The triangles and
solid line represent the Hyades mean colors, the pluses
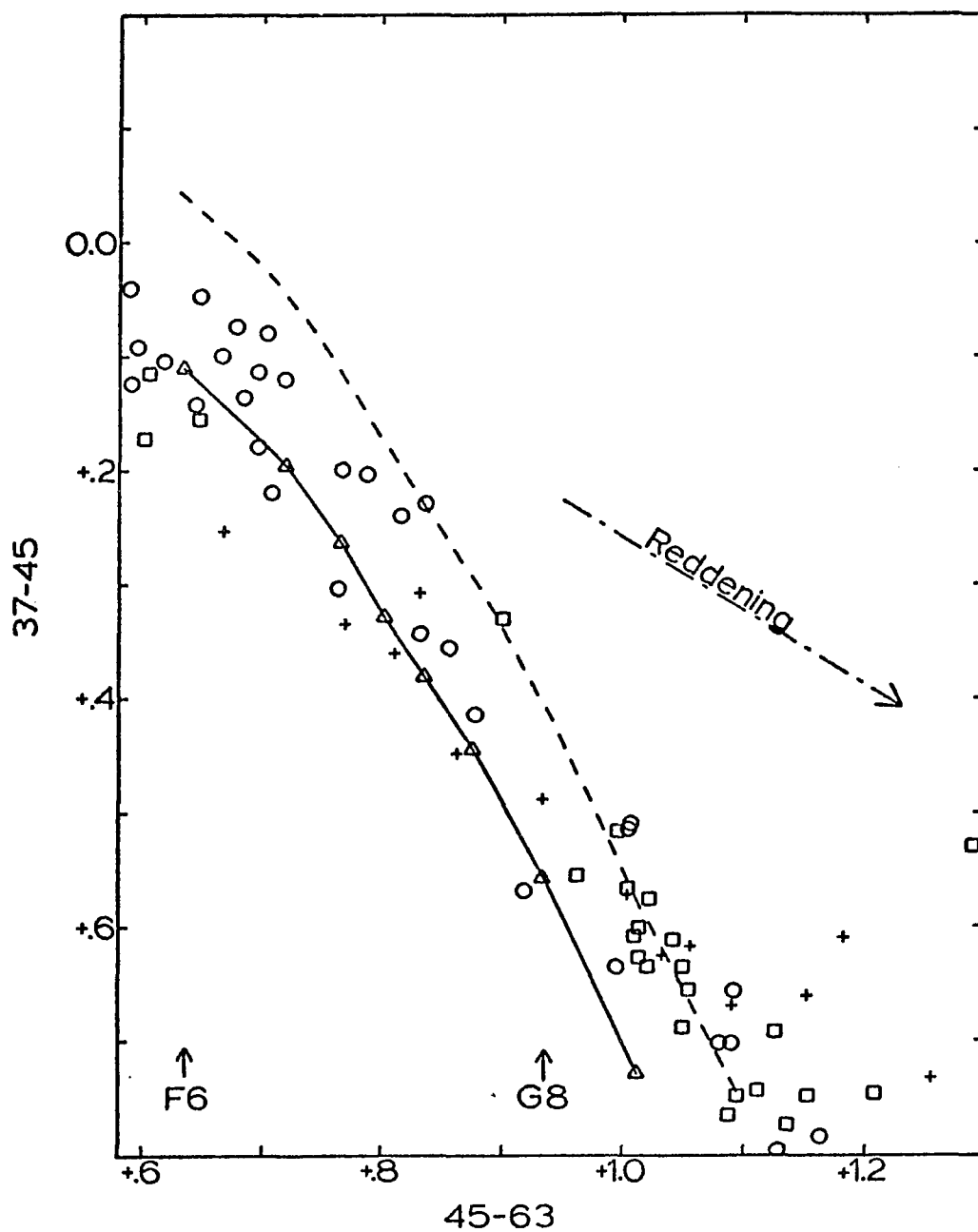supergiants (class I), the squares giants (II and III),
and the open circles subgiants (IV-V, IV, and III-IV).

the Hyades and solar-type field stars and that the dashed line repre-
sents a reasonable criterion for selecting metal-poor stars in this
temperature range ($0.60 \leq 45 - 63 \leq .04$) as suggested by Schuster (1976).
The only subdwarfs which lie below the dashed line, such as the group
of six at approximately $45-63 = 0.65$ and $37-45 = +0.05$, have been called
subdwarfs because their parallaxes place them below the main sequence in
a (M_{bol}, T_e) diagram and not because they have been classified subdwarfs
spectroscopically. Hence, stars lying above the dashed line in Figure 22
can be selected as good candidates for being metal poor. (We can only
say these are candidates because of the problem of microturbulence; see
Conti and Deutsch 1966, 1967 and Eggen 1973). Also, we see that the
solar-type stars have on the average a 37-45 excess ($\delta(37-45)$) of
+0.06 to +0.08 with respect to the Hyades main sequence; this excess
reaffirms the fact that the Hyades are metal rich when compared to
general field dwarfs and many other clusters (for example, see Alexander
1967 and Bell 1971).

In Figure 23 are plotted subgiants, giants, and supergiants
(whose photometry comes from Mitchell and Johnson 1969 and Johnson and
Mitchell 1975) and the same Hyades mean colors, ultraviolet excess line
($\delta(37-45) = +0.15$), and reddening line as Figure 22. If we assume that
these evolved field stars have approximately the same compositions as
the solar-type field stars (probably not too bad an assumption for the
subgiants and giants), then, if (37-45) and (45-63) are completely un-
affected by luminosity changes, these evolved stars should be distributed
in Figure 23 between the solid line of the Hyades mean colors and the

dashed line just as the solar-type stars are in Figure 22. (The colors of the supergiants probably include significant reddening effects, and no reddening corrections have been applied.) Any deviations from such a distribution will tell us how luminosity differences affect the position of a star in the 37-45 versus 45-63 diagram. We see that for the hottest stars (45-63 $\approx$ 0.62) increasing the luminosity tends to decrease slightly the 37-45 excess; the three giants in the range $0.60 \leq 45 - 63 \leq 0.65$ are all below the mean Hyades line. For the coolest stars (45-63 $\geq$ +1.00) the ultraviolet excess is increased by increasing luminosity; for 45-63 $\geq$ 1.08 most of the subgiants and giants lie above the dashed line. The cross-over, where the diagram is completely insensitive to luminosity, occurs somewhere in the range $+0.8 \leq 45\text{-}63 \leq +0.9$. Hence, Figures 22 and 23 together show that the 37-45 versus 45-63 diagram is very sensitive to composition but for the range $0.6 \leq 45\text{-}63 \leq 1.0$ is insensitive to luminosity. This confirms the results of the previous section.

In Figure 24 we have plotted a G versus 45-63 diagram including the subdwarfs, the Hyades mean colors, the solar-type field stars, a reddening line, and F-type dwarfs, subgiants, giants, bright giants and supergiants from the work of Mitchell and Johnson (1969) and Johnson and Mitchell (1975). The "calibration" of this diagram will be discussed in the next chapter. As suggested in the preceding section this diagram does indeed seem to be very luminosity sensitive. For 45-63 $\leq$ +0.58 and for 45-63 $\geq$ +1.00 there is a good separation between the Hyades main sequence, the subgiants, and the giants. In the range $+0.60 \leq 45\text{-}63 \leq 1.0$
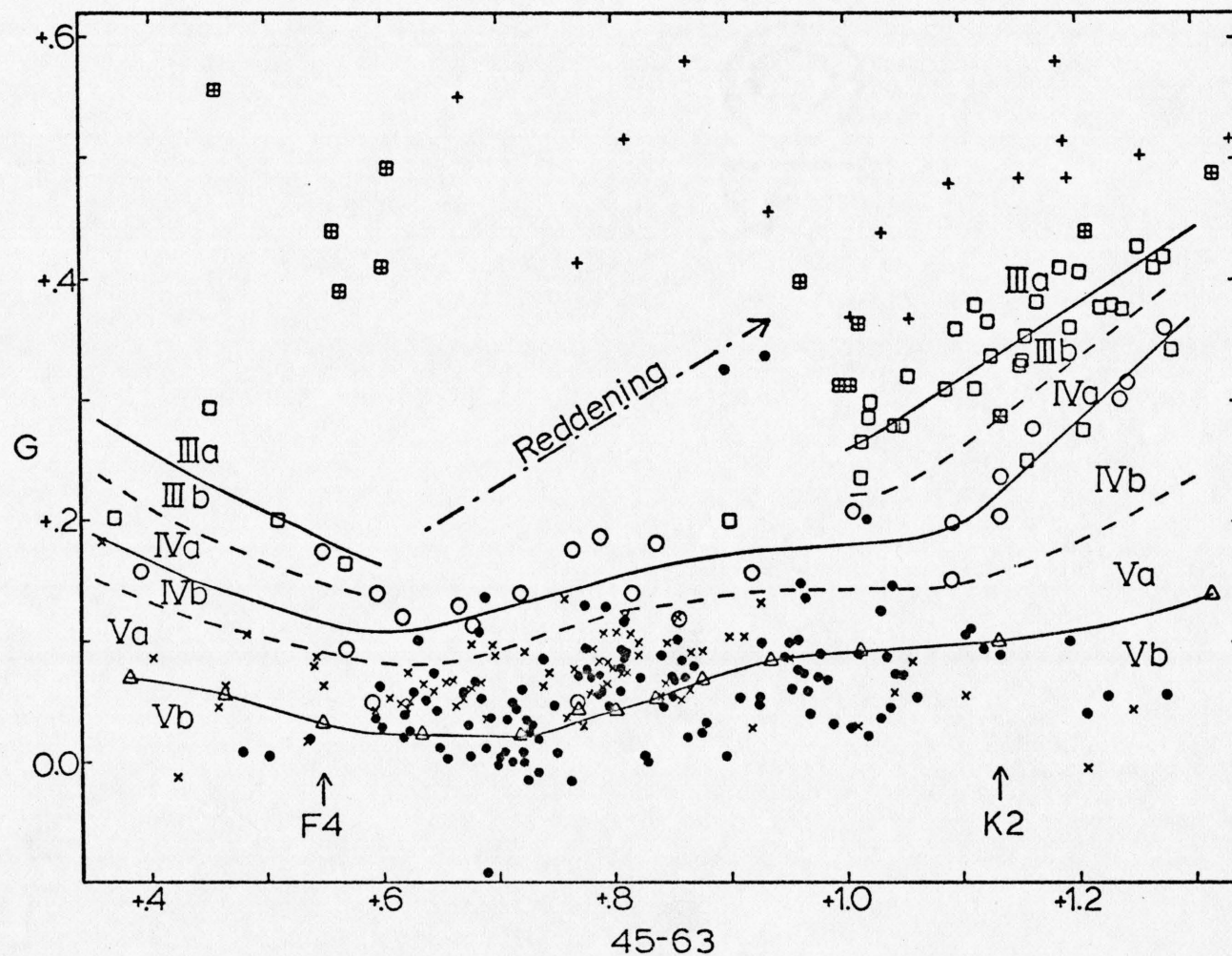
Figure 24. G versus 45-63. -- The triangles and lowest solid line represent the Hyades
mean colors, the pluses are for supergiants (class I), the crossed squares
bright giants (II), the squares giants (III), the open circles subgiants (IV),
the X's F and G dwarfs, and the filled circles subdwarfs.

there is only one giant available with 13-color photometry, and so little can be said for giants. But in this range there are a number of sub-giants, and these maintain a good separation from the Hyades. At 45-63 = 0.77 ($\sim$ G0) there is at least a 0.1 magnitude separation between the Hyades main sequence and the mean subgiant line. It should also be noted that most of the F and G field dwarfs lie above the line defined by the mean Hyades colors. This is not too surprising since the field stars in general belong to an older population with ages similar to the Sun's (4.5×10^9 years) than the Hyades with an age of about 5×10^8 years (Eggen 1974). Hence the field stars have been able to evolve further from the zero age main sequence. Finally, at this point we can only say that Figure 24 does not contradict the contention that the G index is nearly independent of blanketing--the subdwarfs are not much displaced from the Hyades and solar-type field stars. But we cannot argue this point convincingly from Figure 24 since we do not yet know how the subdwarfs' surface gravities compare to the Hyades'.

Some Preliminary Conclusions
About Subdwarfs

In Figure 24 one can see that there is a rather sudden cutoff of the subdwarfs at 45-63 = 0.59; only four subdwarfs have 45-63 < 0.59 and one of these ($+30^{\circ}2536$) is a mild subdwarf ([Fe/H] = -0.46), and another ($-25^{\circ}3344$) is probably a metal deficient horizontal branch star. Yet the subdwarfs just to the right of this cutoff (group 1 of Figure 22) have rather large ultraviolet excesses (see Figure 3) implying that subdwarfs just to the left should still have sizable ultraviolet excesses

(δ(37-45) > 0.2 magnitude) and be easily recognizable both photometri-cally and spectroscopically. Why then the cutoff? Sandage (1964) and Dixon (1963, 1965) have suggested that this cutoff, which is equally apparent using the B-V index, is analogous to the main sequence turnoff of globular clusters; that is, subdwarfs which originally had 45-63 < 0.59 have evolved to become metal deficient red giants. Sandage (1964) even goes so far as to suggest that the two stars BD+25°1981 and BD-12° 2669, which are bluer than the cutoff in B-V, are equivalent to the blue stragglers seen in some globular clusters (such as M3); that is, they are stars on an extension of the main sequence brighter than the turnoff point. These two stars are the other two subdwarfs plotted in Figure 24 with 45-63 < 0.59. Eggen (1973) also claims that the hotter subdwarfs are evolving and for this reason they correct onto the Hyades main se-quence in the (M_V, B-V) diagram when blanketing corrections (Wildey et al. 1962) are applied while the cooler subdwarfs are unevolved and still form a sequence separate from the Hyades main sequence. In support of this overall picture are the two "subdwarfs," -9°5491 and +41°3735, which are plotted at approximately 45-63 = +0.92 and G = +0.33 in Figure 24. These are obviously not subdwarfs but giants, and yet they show large 37-45 excesses in Figure 22. I suggest that these are metal-poor red giants which are evolving away from the turnoff at 45-63 = 0.59 along a line parallel to the giant branch sketched for the field giants. More will be said of these stars later.

If the above picture is true, the stars of group 1 of Figure 22 should contain significant evolutionary effects. Figure 1 of Eggen

(1973) shows that for the old disk main sequence stars just to the right (red) of the turnoff have evolved one to two magnitudes above the zero-age main sequence. The work of Blaauw (1963) suggests that at spectral types F5 and F6 (45-63 = 0.59 to 0.63) a change of 1.3 to 1.6 magnitudes will change a star from a main sequence luminosity classification (V) to a subgiant classification (IV). However, Figures 3 and 24 do not show any such obvious evolutionary effects for group 1. In Figure 3 the curve is not depressed at filters 33 and 35, relative to 37, as the previous discussions of this chapter indicate will happen for decreasing surface gravity. For comparison in Figure 25 we plot the average "blanketing" curve for seven F-type main sequence stars (class V) with about the same temperature range as group 1 and with small ultraviolet excesses $(0.05 \leq \delta(37\text{-}45) \leq 0.10)$. The curve of Figure 25 shows greater apparent evolutionary effects than the curve of Figure 3. In Figure 24 of the nine stars of group 1 five appear very close to the Hyades line, three are 0.03-0.04 magnitude above the Hyades line but still appear as main sequence stars, and only one star, BD-13°482, falls in the subgiant region. Why this apparent lack of evolutionary effects when we know the stars <u>are</u> evolving? Perhaps for extremely metal-poor objects the 13-color indices are less sensitive to changing surface gravity. The theoretical curves in Figure 19 (T_e = 5500°) indicate that this may be the case for cooler temperatures. However, group 1 has $(T_e)_{Ave}$ = 6210° and Figures 17 and 18 (for T_e = 6500° and 6000° respectively) show only a slight decrease of sensitivity with decreasing metal content. Besides, the stars -9°5491 and +41°3735 mentioned earlier, as well as HD122563
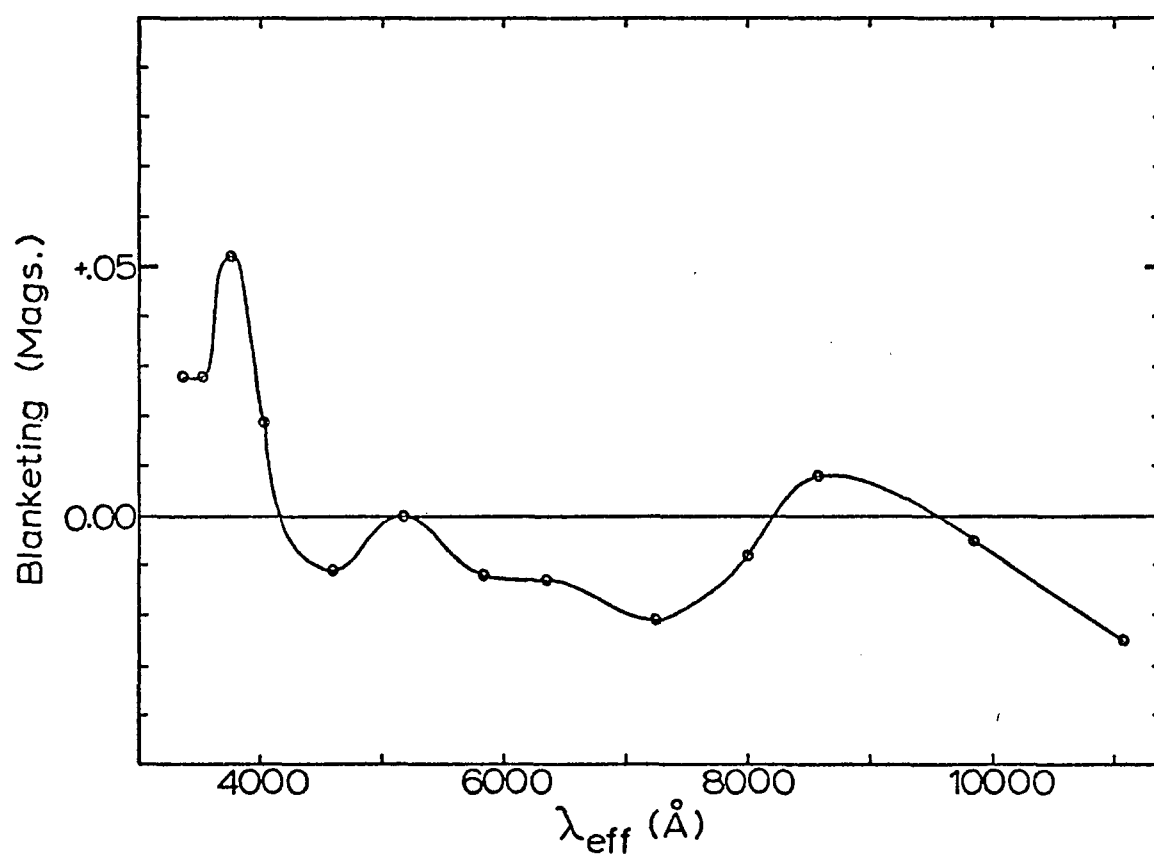
Figure 25. The average observational blanketing curve for seven F-type main sequence stars.

(BS5270) with 45-63 = 1.270 and G = +0.546, are all extremely metal
deficient red giants and indicate large sensitivities for the G index
even for the cooler temperature range.

The only other possible solution for the above puzzle is that in
the "blanketing" curves of zero-age subdwarfs the 33 and 35 filters are
elevated with respect to the 37 filter, and so subsequent evolution
(decreasing surface gravity) has served to make the "blanketing" equal
in the three ultraviolet filters as seen in Figure 3. Supporting evi-
dence for this is seen in Figure 7 for group 5. The stars of group 5
are on the average further below the Hyades line in Figure 24 than groups
1, 2, 3, or 4; that is, group 5 shows the smallest average evolutionary
effect, and so it probably comes closest to representing the zero-age
subdwarf sequence. And, indeed, in Figure 7 the 33 and 35 filters are
elevated with respect to 37. But why then are filters 33 and 35 elevated
in unevolved subdwarfs? There are the following three possibilities:
(a) the zero-age subdwarfs have the same surface gravities as Hyades
stars but there is intrinsically more blanketing (more metal lines) for
filters 33 and 35 than for 37, (b) filters 33 and 35 have the same (or
even less) blanketing than 37 but the unevolved subdwarfs have higher
surface gravities than the Hyades stars, or (c) some intermediate case
between (a) and (b). To separate these possibilities is almost impos-
sible observationally, and so we must resort to the models. Examining
Figures 10 and 11, which contain the blanketing curves for $T_e = 6500^o$
and 6000° (there is no reason to suspect the 6500° models and the 6000°
models show only small discrepancies in the ultraviolet as mentioned

earlier), we see that the blanketing of filters 33 and 35 at constant

gravity is equal to (or smaller than) the blanketing of filter 37.

Hence, possibility (b) seems most probable: The surface gravities of un-

evolved subdwarfs are larger than the surface gravities of unevolved

Hyades stars with equal T_e.

Examining the blanketing curves of Figures 3 through 9 as well

as Figures 22 and 24 we notice the following: (a) Group 2 shows less

evolutionary effects on the average than group 1. This is to be ex-

pected since group 2 contains cooler objects than group 1. However,

groups 3 and 4 show approximately the same average evolution as group 1;

all of the stars of group 4 are on or above the mean Hyades line in

Figure 24. The appearance of so many evolved subdwarfs cooler than the

turnoff at 45-63 $\approx$ 0.59 is somewhat surprising. This suggests that the

subdwarfs were formed over a rather significant time interval and not

all at one time. The evolving stars of group 4 represent the oldest

subdwarfs while the cutoff at 45-63 $\approx$ 0.59 and the stars of group 1

represent the most recently formed subdwarfs--formed a considerable time

after the subdwarfs of group 4, and (b) the stars of group 4 seem some-

what special and require further comment. In Figure 22 we see that

group 4 projects out from the envelope formed by groups 1, 2, 3, and 5

and by the other subdwarfs; perhaps this merely represents a cutoff

(like the one at 45-63 = 0.59) of a very old, extremely metal poor sub-

dwarf population, or maybe it arises from selection effects included when

I choose which subdwarfs to observe. (There also exists the possibility

that part of the 37-45 excess of group 4 is due to evolution; as shown

in the previous section 37-45 starts becoming sensitive to surface gravity for 45-63 $\gtrsim$ 0.90.) In Figure 6 the average blanketing in filters 33, 35, and 37 for group 4 is seen to be more than +0.6 magnitude. At first thought this seems to be too much--more than abundance effects could possibly cause. But this is not the case as the following analysis shows. As mentioned earlier Eggen (1968, 1969a) found the maximum abundance effect to occur at $(B-V)_{obs}$ = +0.5 with $\delta(U-B)$ = +0.30 which implies (Wildey et al. 1962, Johnson 1966) $(B-V)_{corr}$ = 0.71, T_e = 5500°, and $\Delta(U-B)$ = +0.536, where $\Delta(U-B)$ is the correction to be applied to obtain the U-B of a star at a Hyades composition. Sandage's (1969a) data showed that $(B-V)_{obs}$ = +0.6 and $\delta(U-B)$ = +0.31 for the maximum effect which implies $(B-V)_{corr}$ = 0.82, T_e = 5240°, and $\Delta(U-B)$ = 0.636. The stars of group 4 fall in the range 0.92 $\lesssim$ 45-63 $\lesssim$ 1.04 which implies 5100° $\lesssim$ T_e $\lesssim$ 5400° and $(T_e)_{ave}$ = 5170° (from Table 12). Hence the T_e of group 4 corresponds rather closely with the abundance-effect maximum of Sandage. Now if we remember that filters 33, 35, and 37 fall within the half-intensity width of the B filter, and if we re-examine Figure 6, we see that the derived blanketing of filters 33, 35, and 37 for group 4 is not really excessive considering Sandage's $\Delta(U-B)$ = 0.636 (or even Eggen's $\Delta(U-B)$ = 0.536). But now there arises another puzzle: as shown in section 3 of this chapter for a given composition, blanketing produces its maximum effect at T_e = 5500° or 5400° and yet the maximum 13-color excesses are observed in the range 5100° $\leq$ T_e $\leq$ 5400°. (It should also be mentioned that four of the stars of group 4 appear in Eggen's (1969a) list (Table 6) of accepted subdwarfs with the largest ultraviolet

excesses. Five other stars from this list are also plotted in Figure 22 but do not show the extreme positions of group 4.) The most reasonable explanation appears to be that although we can conceive that the total 37-45 excesses of group 4 are caused by only blanketing, probably a small part of these excesses is contributed by differences in surface gravity (evolution).

Many of the conclusions of this chapter depend rather strongly upon the accuracy of the chemical composition and effective temperature calibrations which are to be derived and discussed in the next chapter.

CHAPTER 6

CALIBRATION OF THE 13-COLOR INDICES

In this chapter the 13-color photometry will be calibrated for
F, G, and K stars to give chemical compositions, effective temperatures,
apparent bolometric magnitudes, and an idea of a star's surface gravity
(evolutionary status). These calibrations have already been used in the
previous chapter and will be used to much greater extent in the detailed
subdwarf analyses of Chapter 7.

Composition Calibration

The composition calibration has been obtained in a form very
similar to that of Wallerstein (1962) except that the temperature de-
pendence of the ultraviolet excess has been taken into account. The
logarithmic iron-to-hydrogen ratio relative to the Sun, [Fe/H], has been
found as a function of both the observed 45-63 index and the ultra-
violet excess, $\delta(37-45)$, where $\delta(37-45)$ is defined as the difference
between the Hyades mean 37-45 color and a star's 37-45 color for equal
45-63 colors. Not all blanketing of course is caused by iron, but
spectroscopic analyses (Wallerstein 1962) have shown that in most cases
the logarithmic ratios of other metals to iron, [other metal/Fe], do not
change from star to star by amounts great enough to invalidate an assump-
tion that [Fe/H] can be used to represent the total metallicity. Or,

113

when the ratios do change significantly, the changes are correlated with changes in [Fe/H]; that is, [other metal/Fe] is a function of [Fe/H] (for example, see Figures 10 and 14 of Wallerstein 1962). Such correlations will also not affect the assumption that [Fe/H] is a useful, though perhaps not simple, measure of the total metallicity nor will they cause scatter in a [Fe/H] versus ultraviolet excess plot (Alexander 1967).

The calibration has been carried out in two parts for two different temperature ranges. Using Kurucz's models and the results of detailed spectroscopic analyses of early G dwarfs an accurate calibration has been obtained for $T_e \gtrsim 5500°$. For temperatures in the range $5100° \lesssim T_e \lesssim 5500°$ a more approximate calibration has been determined using spectroscopic studies of HD103095 (BS4550) and of HD10700 (τ Cet) plus results from the G star studies. For subdwarfs with $T_e \lesssim 5100°$ either no composition determination has been made, or only a very rough approximation made. In any case, for $T_e \gtrsim 5100°$ the compositions are sufficiently well known for interpolating the blanketing corrections of the temperature indices.

The 13-color photometry for the calibration comes from Tables 3 and 5, from Schuster (1976), and from Mitchell and Johnson (1969). The compositions ([Fe/H]'s) for the first part of the calibration ($T_e \gtrsim 5500°$) come exclusively from three sources, Wallerstein (1962), Alexander (1967) and Aller and Greenstein (1960); in all three sources only stars with temperatures similar to the Sun's have been analyzed--late-F and early-G dwarfs and subdwarfs. A number of other sources (Cohen and Strom 1968; Helfer, Wallerstein, and Greenstein 1960, 1963; Wallerstein and Helfer

1959, 1961) have been checked for consistency and systematic effects.
For example, the extreme subdwarfs HD140283 and HD19445 have been
analyzed by both Aller and Greenstein (1960), using differential curve
of growth techniques, and by Cohen and Strom (1968) using model atmos-
pheres; the equivalent widths of Aller and Greenstein were used in both
studies. For HD140283 Aller and Greenstein obtained [Fe/H] = -2.00
while Cohen and Strom found [Fe/H] to be in the range -1.93 to -1.45.
For HD19445 Aller and Greenstein measured [Fe/H] = -1.75 and Cohen and
Strom -2.55. There certainly are significant differences, but they are
not systematic. Hence, the older set of data of Wallerstein and of
Aller and Greenstein has been used since it represents a rather uniform
treatment of a fairly large number of stars and since it leads to less
scatter in the [Fe/H] versus δ(37-45) diagram than the more recent
measurements. Alexander's (1967) values for the G-dwarf compositions
agree very well, except for two Hyades stars, with those of Wallerstein,
and so they have been simply averaged with Wallerstein's values. For
the one Hyades star used in the final calibration only Alexander's value
of [Fe/H] has been used for the reasons given in Alexander's paper. In
total the compositions of 34 G dwarfs and subdwarfs were available from
the cited sources. One Hyades dwarf was rejected due to the arguments
of Alexander, and one field dwarf could not be used since its 45-63
value placed it outside the range of the models (see below). Of the re-
maining 32 stars 13-color photometry exists for 25; these 25 are used to
define the calibration.

From previous observational and theoretical work it is known
that for a given composition the ultraviolet excess depends upon tempera-
ture. Kurucz's models and the blanketing curves of Chapter 5 clearly
show this. (In Chapter 5 we determined that blanketing has its maximum
effect at $T_e \approx 5400\text{-}5500^o$, but this result depends to a large extent on
the composition calibration which we are now deriving.) Hence before
obtaining the final [Fe/H] versus $\delta(37\text{-}45)$ curve all of the ultraviolet
excesses were corrected using the models to a 45-63 of 0.81. This was
done since the three extreme subdwarfs have (45-63)'s bluer than the
average 45-63 of the other G dwarfs. The corrections were obtained by
plotting a theoretical 37-45 versus 45-63 diagram and then by calculat-
ing ratios of the theoretical $\delta(37\text{-}45)$'s as a function of 45-63. Table
13 and Figure 26 give the final calibration of $\delta(37\text{-}45)$ versus [Fe/H]
for 45-63 = 0.81. In Table 13 the first column gives the star's HD
number, the second column the observed 45-63, the third column the ob-
served $\delta(37\text{-}45)$, the fourth column the $\delta(37\text{-}45)$ corrected to 45-63 =
0.81, and the fifth column the value of [Fe/H]. By examining Figure 26
we see the following: (a) the $\delta(37\text{-}45)$ versus [Fe/H] curve is similar in
shape to the $\delta(U\text{-}B)$ versus [Fe/H] curve of Wallerstein (1962, Figure 9),
but as expected $\delta(37\text{-}45)$ is much more sensitive to metallicity than
$\delta(U\text{-}B)$; $\delta(U\text{-}B)$ has a range of 0.32 magnitude while Figure 26 shows that
$\delta(37\text{-}45)$ varies by more than 0.5 magnitude for the same stars, (b) the
scatter of Figure 26 is similar to that of Figure 9 of Wallerstein
(1962); this together with the previous result indicates $\delta(37\text{-}45)$ is a
more accurate and useful metallicity parameter than $\delta(U\text{-}B)$, and

Table 13.   The chemical composition calibration.

Name	45-63	$\delta(37-45)_{obs}$	$\delta(37-45)_{corr}$	[Fe/H]
HD10307	0.811	0.098	0.098	+0.16
13974	0.856	0.231	0.194	-0.34
19373	0.789	0.058	0.062	+0.12
22879	0.768	0.250	0.279	-0.57
28344	0.793	0.023	0.024	+0.30
30649	0.822	0.232	0.224	-0.20
34411	0.814	0.070	0.069	+0.15
55575	0.785	0.143	0.153	-0.21
86728	0.820	-0.070	-0.068	+0.34
90508	0.789	0.091	0.097	-0.20
102870	0.743	0.013	0.015	+0.32
110897	0.703	0.041	0.054	-0.33
114710	0.764	0.066	0.075	+0.21
142267	0.838	0.210	0.191	-0.28
143761	0.845	0.181	0.160	-0.16
152792	0.853	0.184	0.156	-0.38
157089	0.805	0.218	0.221	-0.52
157214	0.842	0.160	0.144	-0.32
160693	0.788	0.191	0.204	-0.69
186408	0.875	0.117	0.089	+0.24
186427	0.865	0.054	0.043	+0.12
187923	0.820	0.045	0.044	0.00
19445	0.733	0.364	0.442	-1.75
140283	0.793	0.446	0.470	-2.00
219617	0.733	0.307	0.373	-1.40

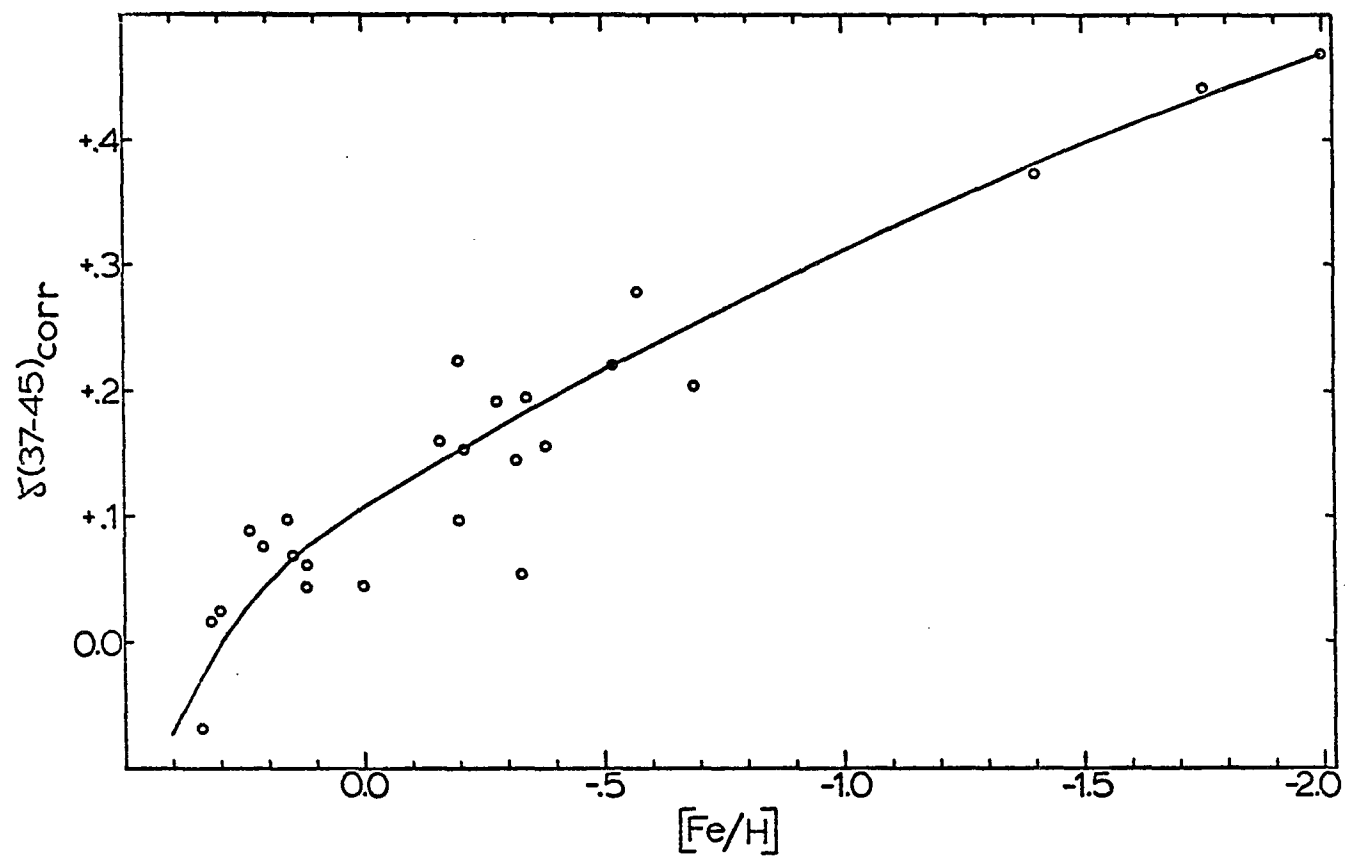Figure 26. $\delta(37\text{-}45)_{\text{corrected}}$ versus [Fe/H].

(c) Figure 26 implies that the composition of the Hyades (δ(37-45) = 0.00) is [Fe/H] $\approx$ +0.3; this value is large compared to the results of many investigators (for example, see Chaffee, Carbon, and Strom 1971) but does lie in the range given by Alexander (1967).

For stars (subdwarfs) with 45-63 not equal to 0.81 the models were once again used. The ratios of the theoretical δ(37-45)'s were used to construct a calibration of [Fe/H] versus both 45-63 and δ(37-45) for all (45-63)'s less than 0.87 ($T_e \approx 5500^o$). In the next paragraph it will be shown that this preliminary calibration is not very good for stars in the range 0.82 $\lesssim$ 45-63 $\lesssim$ 0.87 due to problems with the coolest model ($T_e = 5500^o$). Also, it should be pointed out that the models are not good enough by themselves, due to zero point problems, inaccuracies arising from approximations made in constructing them, and so forth, for determining compositions directly. For this reason the observational calibration of Table 13 and Figure 26 has been used to set the scale of the metallicity parameter, δ(37-45). However, ratios which come from the models, such as ratios of indices, ratios of blanketing, and so forth, will be more accurate since many of the errors will be in common to the two items being ratioed and so will cancel out to a large degree. The above combination of theory and observation seems the best for determining compositions of the hotter subdwarfs. In Table 14 are given derived quantities for the subdwarfs, where column one gives the subdwarf's name and column 2 gives the value of [Fe/H]. For stars with 45-63 $\leq$ 0.82 the values of [Fe/H] come directly from the calibration described above; for 45-63 > 0.82 the calibration is outlined below.

Table 14. Derived quantities for subdwarfs.

Name	[Fe/H]	T_e(models)	T_e(obs)	T_e(final)	Lum. Class
+54°223	(-0.4)	5415	5400	5405	Vb
-9°256	-0.17	5775	5780	5780	Va
+19°279	(~+0.3)	--	5170	5170	Vb
-16°295	-0.26*	5380	5340	5350	Vb
-26°828	(-0.2)	5460	5385	5410	Vb
-17°484	-1.82	6220	6160	6190	IVb
-13°482	-1.55	6250	6180	6215	IVb
-26°957	-0.32	5810	5805	5810	IVb
G4-37	-1.32	5940	5915	5930	Vb
+33°529	--	--	~3855	~3855	--
-13°544	(~solar)	--	5060	5060	Va
+25°495	-1.77	6020	5990	6005	Vb
G78-26D	--	--	~4070	~4070	--
+11°468	-1.54	5735	5750	5740	Va
G5-36	-1.22	5870	5865	5870	Va
G38-1	--	--	~3830	~3830	--
-7°603	(-0.5)	5620	5650	5635	Va
-3°592	-0.79	5850	5845	5850	Va
+34°796	-1.32*	--	4800	4800	Vb
+21°607	-1.19	6240	6180	6210	Vb
G175-39	(>+.3)	--	5050	5050	Vb
+45°992	(-0.6)	5710	5725	5720	Va
G102-22	--	--	~3180	~3180	--
G99-31D	(-0.5)	5550	5580	5565	Vb
+37°1312	(~+0.3)	--	5145	5145	Vb
+19°1185	(-1.0)	--	5420	5420	Vb
-0°1520	-0.33	5765	5750	5760	Va
+47°1419	-0.20	5870	5860	5865	Va
-33°4113	-0.67	5745	5735	5740	Va
+31°1684	(-1.6)	5595	5495	5530	Vb
-34°4036	-0.14	6360	6275	6320	Va
-9°3595	(-0.45)	--	5150	5150	Vb
+10°2519	(-0.6)	5570	5595	5580	Va
G14-45D	--	--	~4530	~4530	Vb
+34°2476	-1.41	6220	6155	6190	Va
G65-22	(-1.0)	--	5315	5315	Va
G64-37	-1.27	6370	6360	6365	Va
-13°3834	(-1.4)	5535	5570	5550	Va
+1°2920	(-0.1)	5640	5660	5650	Vb
+30°2536	-0.46	6790	6700	6745	Vb
G66-22	(-1.1)	--	5230	5230	Vb
+26°2606	-1.54	6170	6120	6145	Vb
-8°3858	(-0.5)	5420	5360	5380	Va
-21°4009	-1.39	5615	5640	5630	Va
+25°2873	+0.17	6450	6360	6405	Va
-15°4041	(-1.8)	--	4850	4850	Vb
-15°4042	(-1.8)	--	5075	5075	Vb
G15-24	(-1.3)	5565	5600	5580	Vb
-10°4149	-1.99	5720	5730	5725	IVb
+42°2667	-1.09	5945	5925	5935	Va
+39°2947	(-0.7)	--	5290	5290	Vb
+39°2950	(~+.2)	--	4690	4690	Vb
G168-42	(<-2.0)	--	5180	5180	Vb
G180-58	(<-2.0)	--	5055	5055	Va
-3°3968	(-1.9)	--	5110	5110	Vb
+37°2804	(+0.2)	--	5205	5205	Vb
+43°2659	(-0.3)	5630	5660	5645	Va
+17°3154	(-0.25)	5680	5700	5690	Va
+1°3421	-0.52	5785	5790	5790	Va
G170-56	-0.93	6030	6000	6015	Va
+2°3375	-1.50	5940	5920	5930	Vb
+37°2926	-0.44	5785	5795	5790	Va
-1°1883	(-0.8)	--	5240	5240	Vb
+29°1664	(-0.5)	5400	5340	5360	Vb
G194-22	-1.32	6025	6000	6010	Vb
-3°2333	-0.23	6240	6170	6205	Va
HD74000	-1.50	6120	6060	6090	Vb
G115-22	(-1.1)	5570	5600	5585	Vb
+25°1981	-1.37	6710	6590	6650	Vb
+42°1922	(~solar)	--	4730	4730	Vb
-12°2669D	-1.88	7030	6975	7000	Vb
G46-5	(-1.1)	--	5190	5190	Vb
G114-26	-1.51	5985	5965	5975	Va
G115-49	-1.70	5990	5970	5980	Vb
+9°2190	-1.40	6180	6115	6150	Va
G48-29	-1.81	6260	6190	6225	Va
HD84937	-1.38	6310	6230	6270	Vb
+44°1910	-1.57	6135	6090	6110	IVa
+23°2207	-0.10	6145	6090	6120	Va
G119-32	-1.23	5850	5840	5845	Vb
G196-47	(-1.4)	5410	5570	5490	Vb
+21°2247	-1.23	5970	5940	5955	Vb
G10-4	(<-2.0)	--	5105	5105	IVb-Va
+36°2165	-1.11	6160	6105	6130	Va
+26°2251	-0.79	6240	6190	6215	Va
+51°1696	(-1.6)	5710	5730	5720	Va
BS4550	-1.30*	--	5180	5180	Vb
G13-9	-1.44	6285	6210	6250	Va
G11-44	-1.42	5990	5960	5975	Va
HD106038	-1.19	6000	5980	5990	Va
HD108177	-1.45	6195	6140	6170	Vb
+40°2570	-0.12	5840	5830	5835	Vb
G60-48	-1.71	5790	5780	5785	Va
+25°3344	(<-2.0)?	~7590	~7600	~7595	III?
G20-15	(<-2.0)	--	5290	5290	Va
G183-11D	-1.25	6250	6180	6215	Vb
G154-36	(-1.4)	5520	5450	5470	Vb
+13°3683	(<-2.0)	--	5075	5075	IVa
C206-34D	-1.46	6065	6030	6050	Vb
+20°3926	+0.17	6450	6360	6405	Va
AC+20°1463-148	--	--	~3330	~3330	--
AC+20°1463-154	--	--	~3300	~3300	--
+41°3306	(~-0.8)	--	5060	5060	Vb
+11°3833	(>+.3)	5695	5490	5560	IVb
+10°4091	(-1.5)	5720	5580	5630	Vb
+5°4481	-0.62	5540	5580	5560	Va
-21°5703	-1.48	5710	5730	5720	Va
+41°3735	(-1.2)	--	5360	5360	II
+9°4529	-0.93	6060	6020	6040	Va
-9°5491	(<-2.0)	--	5270	5270	II
+17°4519	-0.92	5975	5955	5965	Va
G188-30	(<-2.0)	--	5270	5270	Va
G126-62	-1.10	5970	5940	5955	Va
G18-39	-1.06	6035	5990	6010	Va
-8°5980	(-0.1)	5580	5620	5600	Va
C28-43	(-1.6)	--	5240	5240	Vb
G190-15	(<-2.0)	--	5205	5205	Vab
-14°6437	-1.38	5930	5915	5920	Vb
+26°4734	(-0.8)	--	5350	5350	Vb
BS77	-0.16	5690	5705	5700	Va
BS219D	-0.27	5765	5770	5770	Va
BS1008	(-0.3)	5610	5455	5510	Vab
BS6752D	(~solar)	--	5000	5000	Va
BS6927	-0.37	6010	5980	5995	Va
BS8181	-0.68	6080	6045	6060	Vb

For the cooler stars the composition calibration depends upon the following three items: (a) the shape and scale of the calibration curve of Figure 26,   (b) the 13-color observations (55 8C observations and 48 6RC observations) and the chemical composition (Tomkin and Bell 1973) of HD103095 (BS4550, Groombridge 1830), and (c) the 13-color observations (8 8C and 8 6RC observations) and the chemical composition (Herbig 1965, Pagel 1963) of τ Cet (HD10700, BS509). The complete chemical composition calibration is given in Figure 27 where lines of constant [Fe/H] are plotted in a 37-45 versus 45-63 diagram. For 45-63 $\leq$ 0.82 the lines have been plotted as given by Figure 26 and the models. For 45-63 $\geq$ 0.82 the lines of constant composition have been drawn to satisfy the following criteria: (a) at 45-63 = 0.82 the lines should join smoothly with the curves for 45-63 < 0.82, (b) at 45-63 = 0.958 and at 45-63 = 1.003 the values of δ(37-45) and [Fe/H] should be consistent with the corresponding values of τ Cet and HD103095, respectively, and (c) for a constant value of 45-63 the shape of the δ(37-45) versus [Fe/H] curve should be the same as in Figure 26. This last criteria has been used for all of the interpolations and extrapolations needed to construct Figure 27. The calibration has been terminated at 45-63 = 1.04 since there is no justification for large extrapolations. For the range 0.81 $\lesssim$ 45-63 $\lesssim$ 0.87 we note in Figure 27 that two sets of curves are drawn. The upper curves come from the models and Figure 26 while the lower, smooth curves are derived from the observations of τ Cet and HD103095. Since the theoretical curves are turning upward sharply, especially for large metal deficiencies, we feel that they are
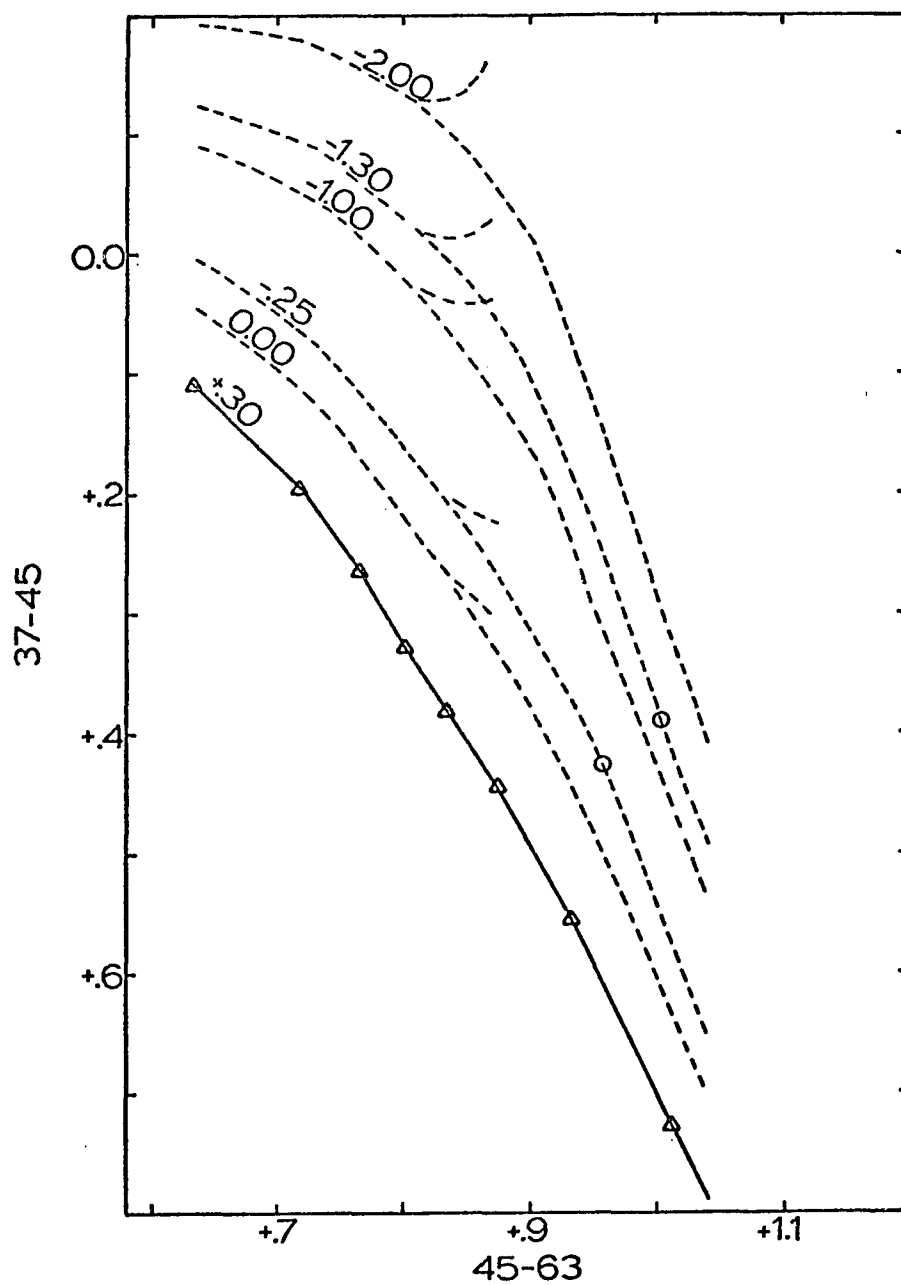
Figure 27. Lines of constant composition in the 37-45 versus 45-63
diagram. -- The triangles and solid line represent the
Hyades mean colors. The dashed lines represent different
compositions as labelled, and the two circles are for BS
4550 and BS 509.

not realistic and probably give further proof of the inadequacies of the 5500° models. In this range only the lower, strictly observational curves have been used to determine subdwarf compositions. It is admitted that the calibration for the cooler stars (45-63 $\gtrsim$ 0.82) is somewhat crude, but with the available models and spectroscopic observations it is the best possible. From Figure 26 it is estimated that for 45-63 $\lesssim$ 0.82 the calibration of Figure 27 gives [Fe/H] with a probable error of 0.1 or better. This is equal to or better than the accuracy obtainable with uvby photometry (for example, see Stromgren 1966, page 464). For the range 0.82 $\lesssim$ 45-63 $\leq$ 1.04, [Fe/H] is measurable with a probable error of about 0.2. These accuracies are sufficient to give useful data about individual subdwarfs, to permit statistical studies of the sub- dwarfs as a class, and to allow good interpolations for the small blanketing corrections needed in determining T_e's.

At this point it is instructive to analyze in further detail the errors of the composition determinations. The errors given in the pre- ceding paragraph were estimated exclusively from Figures 26 and 27 by considering the scatter of the observed spectroscopic abundances and by noting the scarcity of good compositions for cooler stars. It is also important to analyze these errors in terms of the observational photo- metric errors and in terms of inaccuracies of the temperature determina- tions. In Chapter 4 we saw that the probable error of a single observa- tion for 45-63 is about 0.02 magnitude. For 45-63 = 0.81 ($T_e \approx 5750^{\circ}$) this amounts to an error of about 0.03 magnitude for a derived 37-45 excess and an error of between 0.1 and 0.2 for [Fe/H]. For 45-63 = 1.04

$(T_e \approx 5150^o)$ the errors are about 0.04 magnitude for the ultraviolet excess and between 0.2 and 0.3 for [Fe/H]. Of course if a star has been observed four times (as for many of the subdwarfs), all of these errors are reduced by a factor of two.

It is also interesting to consider in a more physical sense how errors in the derived temperatures (resulting from photometric errors or from incorrect blanketing corrections) are related to errors in the derived blanketing values and to errors in the abundance determinations. For example, there are at least five major temperature-dependent atmospheric quantities which determine the observed values of ultraviolet indices such as 37-45 or 35-52. The quantities are the following: (a) the total emergent energy, (b) the strengths of the continuum opacity sources such as H^- or hydrogen bound-free transitions, (c) the ionization states of the line absorbers (metals), (d) the excitation states of the metals, and (e) the amount of backwarming in the atmosphere, which is directly related to the total strengths of the metal lines. To gain some idea of the significance of these effects we will analyze the 37-45 index in terms of temperature-related changes in the excitation states of the metals and in the continuum opacity sources. We will assume that all of the line absorption occurs in the 37 filter and none in the 45 filter. The tables, spectra, and spectrophotometry of Seitter (1970) show that the 37 filter contains at least 43 major lines which have an average intensity of about 690 (the equivalent width in m$\overset{o}{A}$) and an average excitation energy of about 3.7 electron volts. The 45 filter contains at least 54 lines most of which are very weak (average intensity

of about 135) and which have an average excitation energy of about 3 electron volts. We will assume that the line mass absorption coefficient, k_λ(lines), varies according to Boltzmann's equation, $\exp(-E/kT)$, where E is the excitation energy of a line and T is the temperature. The assumption will be made that H^- is the only continuum absorber and that its mass absorption coefficient, $k_\lambda(H^-)$, varies as $T^{-2.5}$ (Aller 1963). The strengths of the spectral lines will be taken as equal to the ratio of the line absorption coefficient to the continuum absorption coefficient, k_λ(lines)$/k_\lambda(H^-)$. And finally, considering the results of the next section we will assume that temperature errors of about $\pm 100^\circ$ will be made. Now, for example, if we have a subdwarf with a true temperature of 5150° but we assign it a T_e of 5250° and if a Hyades dwarf with $T_e = 5150^\circ$ has 30% of its ultraviolet energy removed by line absorption, we calculate that this subdwarf would be matched to a Hyades dwarf with about 37% of its ultraviolet energy removed by lines. This result agrees with Figure 13 of Chapter 5 which shows that the line blanketing increases with temperature for $T_e \lesssim 5500^\circ$. However, in this hypothetical case we would in fact underestimate the blanketing since we have not taken into account the change of a star's total energy distribution with temperature. In Chapter 5 we showed that in the 37-45 versus 45-63 diagram the 37-45 index is highly sensitive to composition but nearly independent of surface gravity. But, 37-45 is not independent of temperature-caused changes in a star's emergent energy distribution. That is, at $T_e = 5150^\circ$ for a fixed Hyades-like composition 37-45 is becoming bluer with increasing temperature in spite of what is happening

to the line strengths. Next, let us repeat this analysis for a hotter subdwarf. Assume that we have a subdwarf with a true temperature of 5750° but that we assign a T_e of 5850°, and assume that a Hyades dwarf with $T_e = 5750^O$ has 40% of its ultraviolet radiation absorbed by lines. We find that this hypothetical subdwarf would be matched to a Hyades dwarf with about 47% of its ultraviolet energy removed by lines. However, this result does not agree with Figure 13 of Chapter 5 which shows that the line blanketing is decreasing with temperature for $T_e \gtrsim 5500^O$. This discrepancy results because we have neglected ionization of the metals in our simple analysis. As one goes to higher and higher T_e's, for a given number of neutral (or singly ionized) metal atoms, one finds more and more atoms with electrons in the excited levels which cause the ultraviolet line absorptions. However, at high enough temperatures the total number of neutral (or singly ionized) metal atoms starts decreasing rapidly due to (further) ionization. These effects, when compared to the temperature dependencies of the continuum absorbers (H^- and hydrogen bound-free), explain why the blanketing maximizes at around $T_e = 5500^O$.

In Table 14 column 2 gives all the compositions ([Fe/H]'s) from the above calibration. For stars with 45-63 $\leq$ 0.82 the compositions have been given to the nearest 0.01 in [Fe/H]. For stars with 0.82 < 45-63 $\leq$ 1.04 the compositions have been given to the nearest 0.1, and the values placed in parentheses to denote less accuracy. For three stars the compositions are marked by asterisks; these three compositions come strictly from the literature. (The value for $+34^O796$ comes from

Heiser 1960 and Pagel and Powell 1966.) For 8 subdwarfs with 45-63 > 1.04 the given compositions are only very rough estimates, and for nine extreme subdwarfs the compositions are given as (< -2.0) since their 37-45 excesses place them above the [Fe/H] = -2.0 line of Figure 27. The composition of $-15^{\circ}4041$ (with 45-63 = 1.132) has been taken as equal to that of $-15^{\circ}4042$; these two stars have proper motions and parallaxes that are equal to within observational errors indicating that they are moving together in space and that they probably formed from the same interstellar material.

After the above calibration was completed the compositions of another three stars with 13-color photometry were found in the literature. These have been used to check the calibration. Danziger (1966) gives [Fe/H] = -0.67 for γ Pav (BS8181) (45-63 = 0.721) while the present calibration gives -0.68--very good conformation. For μ Cas (BS321) (45-63 = 0.920) Cohen (1968) gives [Fe/H] = -0.57 and Catchpole, Pagel and Powell (1967), -0.62 while the above calibration gives (-0.4). For HD224930 (45-63 = 0.922) Wallerstein (1962) gives -0.54 and the present calibration (-0.8). For these last two stars the agreement is not particularly good, and yet no systematic differences are indicated. For μ Cas the 13-color calibration gives a metal deficiency which is about 0.2 too small while for HD224930 the calibration gives a deficiency about 0.26 too large.

Effective Temperature Calibration

Once compositions are known, blanketing corrections can be obtained from the models and accurate effective temperatures calculated.

The following questions now arise: What parameters are best for measuring T_e and what are the most reliable means of calibration? In answer to the first question the ultimate T_e parameter from 13-color photometry would be the use of the energy distribution given by <u>all</u> filters for which the blanketing and surface gravity effects are small and/or canceling. For example, the shape of the energy distribution of filters 45 through 110, but excluding 52, defines such a parameter. (See the blanketing and luminosity-difference curves of Chapter 5.) Such a many-filter parameter has the advantage that (a) the derived T_e depends on measures made in eight different filters and so the accidental errors of observation tend to cancel out and (b) the derived energy distribution from the eight filters covers a significant fraction of the star's total energy output, and it is this total energy output (plus the star's radius or projected angular radius) that goes into defining T_e. However, are the blanketing corrections and energy distributions of the theoretical 13-color photometry accurate enough to warrant such a detailed, multifilter analysis? I suspect not. The following compromise has then been made: only the indices 45-63 and 58-99 have been used for determining T_e's. Both indices have small blanketing and gravity corrections, both have reasonably small probable errors of observation since 45-63 is strictly an 8C index and 58-99 strictly a 6RC index, and together the two indices span a significant portion of the total energy output of F and G stars. 45-63 measures the blue-to-red part of the energy spectrum and 58-99 the yellow-to-near-infrared portion.

For both indices two different calibrations have been obtained--
a theoretical one using Kurucz's models and an observational one using
stars with measured angular diameters. All subdwarfs with 13-color
photometry have had their T_e's measured using the two observational
calibrations and all subdwarfs with $T_e \gtrsim 5500^o$, using the two theoretical
calibrations. The blanketing corrections of the models have been extra-
polated to lower temperatures $(T_e \approx 4700^o)$, but the theoretical T_e cali-
brations themselves have not; they terminate where the models terminate,
$T_e = 5500^o$.

In Figures 1 and 2 of Chapter 5 the blanketing corrections and
theoretical T_e calibration for 45-63 were given and analyzed. In
Figures 28 and 29 are found the equivalent diagrams for 58-99. Figure 29
shows the theoretical T_e calibration for various compositions (1X, .1X,
and .01X), and Figure 28 gives a comparison between 58-99 and R-I to be
used in checking the blanketing changes of Figure 29. All data comes
from the same sources as Figures 1 and 2. Figure 28 seems to indicate
zero or very small negative changes in 58-99 as the blanketing is re-
moved, assuming R-I remains constant. Figure 29 indicates, however,
positive changes of 0.03 or 0.04 magnitude. A possible compromise would
be that in going from the Hyades composition to a subdwarf composition
of [Fe/H] $\approx$ -1.5, 58-99 changes by about +0.03 magnitude and R-I by +0.02
magnitude. It is interesting to note that both the analysis of Figures
1 and 2 and the present analysis suggest small positive changes in R-I
as the blanketing is removed. In any case, there does not seem to be
any evidence for large discrepancies in the theoretical blanketing
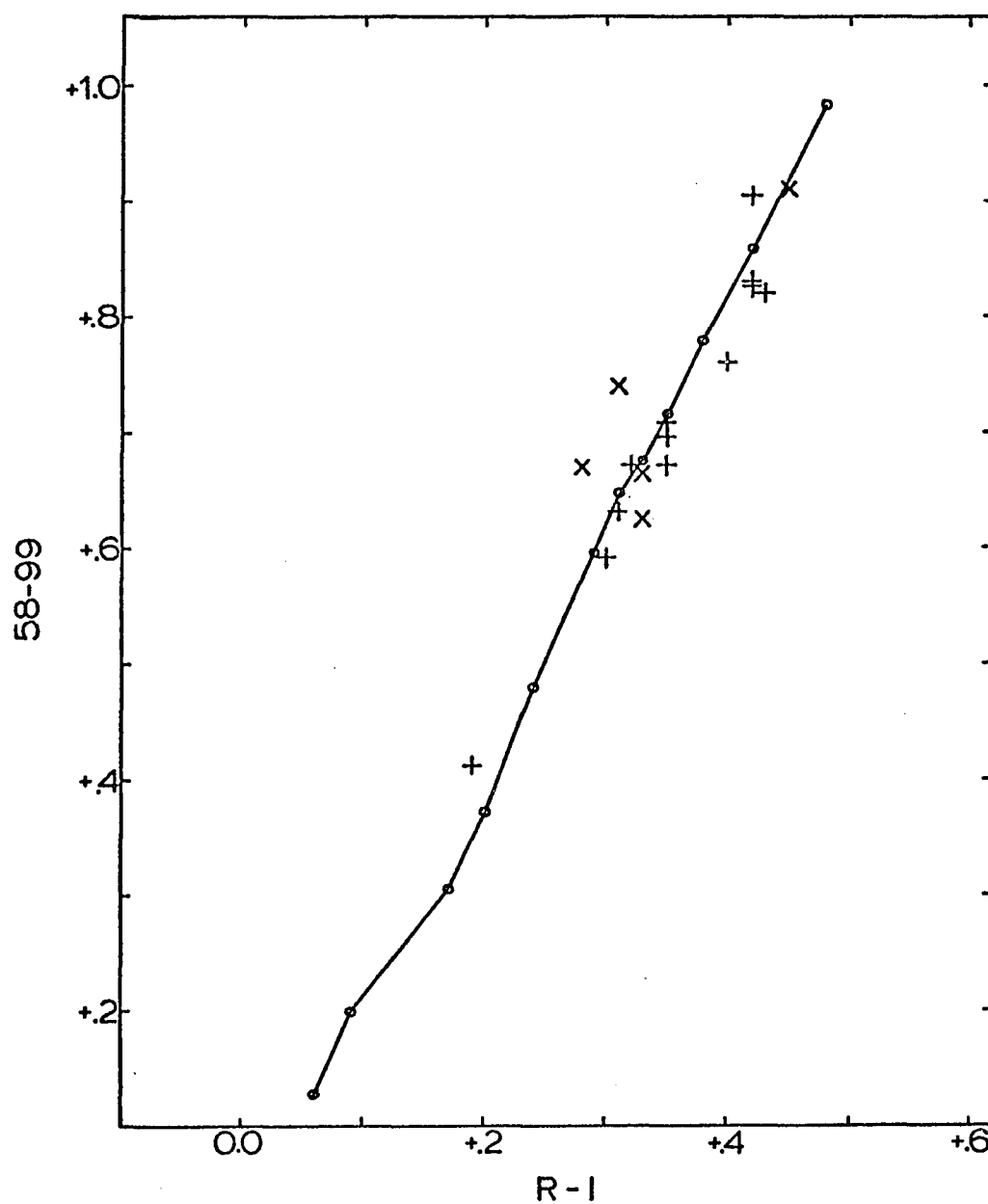
Figure 28. 58-99 versus R-I. -- The circles and solid line represent the mean Hyades colors, the plus signs mild subdwarfs, and the X's extreme subdwarfs.
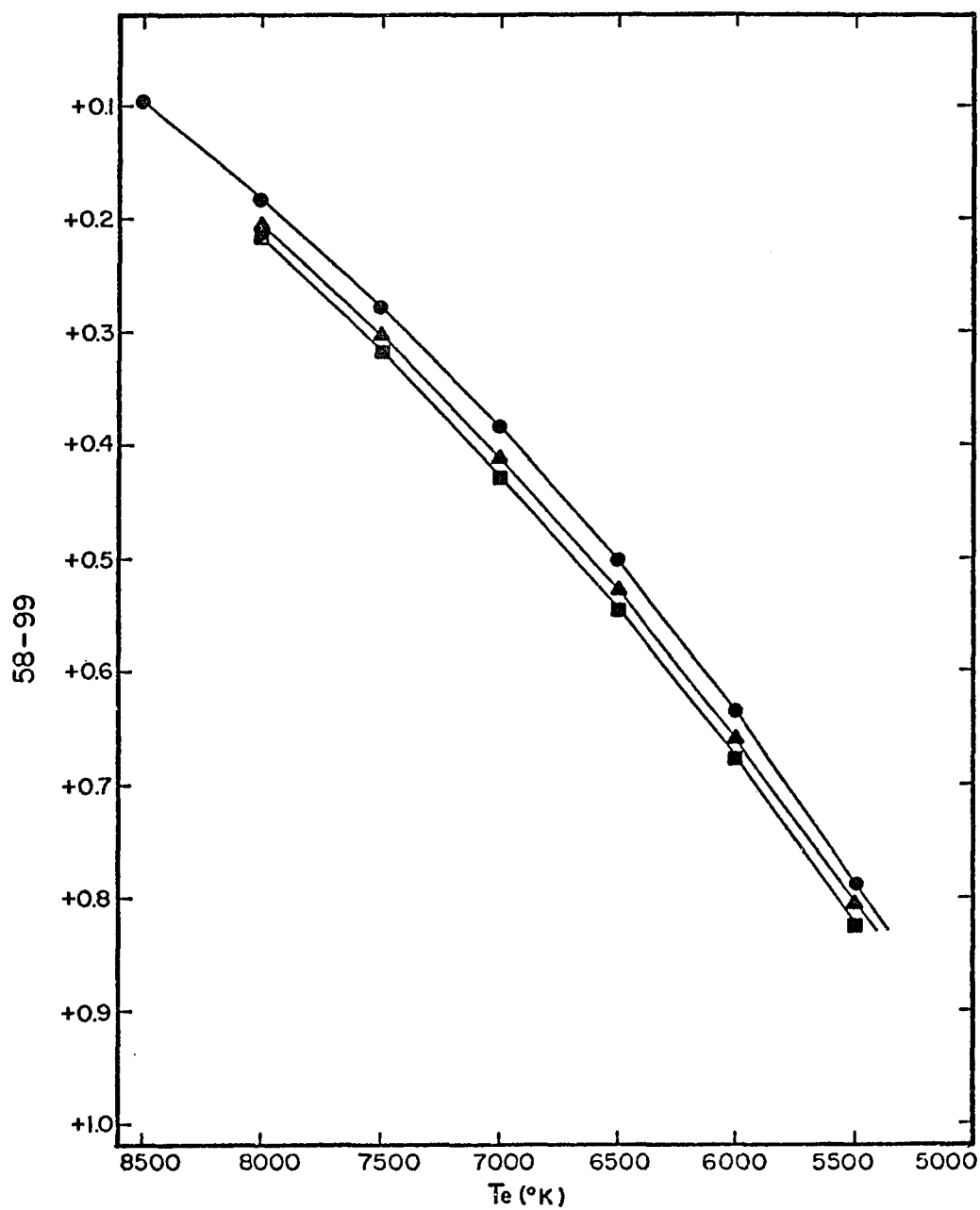
Figure 29. Theoretical 58-99 versus T_e curves. -- Filled circles are for solar abundance, triangles for 0.1 solar abundance, and squares 0.01. Log g = 4.5.

corrections for 58-99. Figure 28 shows that the corrections are small

and unchanging to at least 58-99 = 0.90 or $T_e \approx 5150°$, and so the

theoretical corrections have confidently been extrapolated to this T_e.

The corrections have also been applied to some cooler stars (with

measured values of [Fe/H]) but with considerable uncertainty involved.

It is important to inquire at this juncture whether the small

blanketing and surface-gravity corrections which the models predict for

the 45-63 and 58-99 temperature indices seem reasonable from a purely

physical point of view. If one examines the spectral regions of the

four filters, 45, 58, 63, and 99, on low-to-moderate dispersion stellar

spectra of F, G and K stars, one notices that there are no strong

spectral features falling within any of these four filters (see the

spectra of Seitter 1970 and of Abt et al. 1968). The 45 filter includes

quite a large number of lines (more than 50 are identified on the spectra

of Seitter 1970), but all of these are rather weak, and so the total

line blocking is fairly small. The other three filters contain con-

siderably fewer lines which are also fairly weak. Only the 58 filter

contains one moderately strong feature made up of two Na I lines (at

$\lambda\lambda$ 5890 and 5896). (We should also mention at this point that the

blanketing and surface-gravity changes of the 52 filter, as seen in the

bump at the 52 filter in the blanketing and luminosity-difference curves

of Chapter 5, are caused by the presence of a number of strong Mg I

lines ($\lambda\lambda$ 5167, 5173 and 5184) within this filter.) Hence, we might

expect strictly from the line-blocking argument that to correct the

45-63 and 58-99 values of a subdwarf to solar composition would require

small positive changes. We know that this is the case for 45-63 but not for 58-99. However, to understand the total blanketing problem we must also consider backwarming, which is the heating of the lower portions of a metal-rich star's atmosphere caused by the strong line opacities. That is, the atmospheres of metal-rich stars have steeper temperature gradients than the atmospheres of metal-poor stars. However, the filters 45, 58, 63 and 99 all measure primarily the continuum, and the primary continuum opacity source is H^-, for which the opacity changes very slowly with wavelength. Hence the radiation emerging from a star at the wavelengths of these four filters comes from approximately the same depths in the stellar atmosphere, and so we would expect the emergent energy of these four filters to be affected approximately equally by any temperature (backwarming) or pressure (surface gravity) changes. For the above reasons we can understand, at least qualitatively, why the blanketing and surface-gravity corrections of 45-63 and 58-99 are small.

In Table 11, columns 4 and 7, are given the observed 45-63 and 58-99 values respectively, and columns 6 and 8 give the indices corrected to solar abundance, $(45-63)_s$ and $(58-99)_s$, respectively. Only blanketing corrections have been applied using Figures 2 and 29; no gravity corrections are included. Neglecting the gravity differences should not cause errors in the derived effective temperatures of more than $50°$ for most subdwarfs. In Table 14 column 3 we give the average of the two theoretical effective-temperature determinations. In general, the 58-99 observations (plus calibration) give higher T_e's (about $130°$ higher on the

average) than the 45-63 observations (plus calibration), and so some

subdwarfs had T_e's from the 58-99 calibration but not from the 45-63

calibration due to the 5500° limit of the models. Other faint subdwarfs

were not observed with the 6RC system and so have only T_e's from 45-63.

But in general most values in column 3 Table 14 are the average of two

theoretical T_e determinations.

The observational effective temperature calibrations were

carried out using the same techniques as Johnson (1964, 1966) and

Mendoza (1969). The accuracy and usefulness of such observational cali-

brations have been clearly demonstrated in a number of previous papers

(Johnson et al. 1968, Johnson 1965, Mendoza 1969). The same 27 stars

used by Mendoza were used for the present calibrations and are listed in

Table 15. These 27 stars and their effective temperatures include the

14 stars and 12 of the temperatures used by Johnson plus remeasured

effective temperatures for two stars and new measurements of 13 other

stars from Brown et al. (1967). From this group of stars 15, of luminosity

classes V, IV-V, and IV, have been used to define the T_e calibration for

dwarfs and subdwarfs over the range $26000^o \gtrsim T_e \gtrsim 3000^o$. Unfortunately

subgiants had to be included to give a large enough number of stars,

but this is not thought to cause problems since 45-63 and 58-99 are not

sensitive to changes of surface gravity (see Figures 14 to 19 in Chapter

5). The 13-color photometry for the calibrations comes from Mitchell

and Johnson (1969), from Johnson and Mitchell (1975), from Schuster

(1976) (for the derived solar colors), and from the present thesis (for

YY Gem). In Figures 30 and 31 are plotted the observational calibrations

Table 15. Effective temperature calibration--observational.

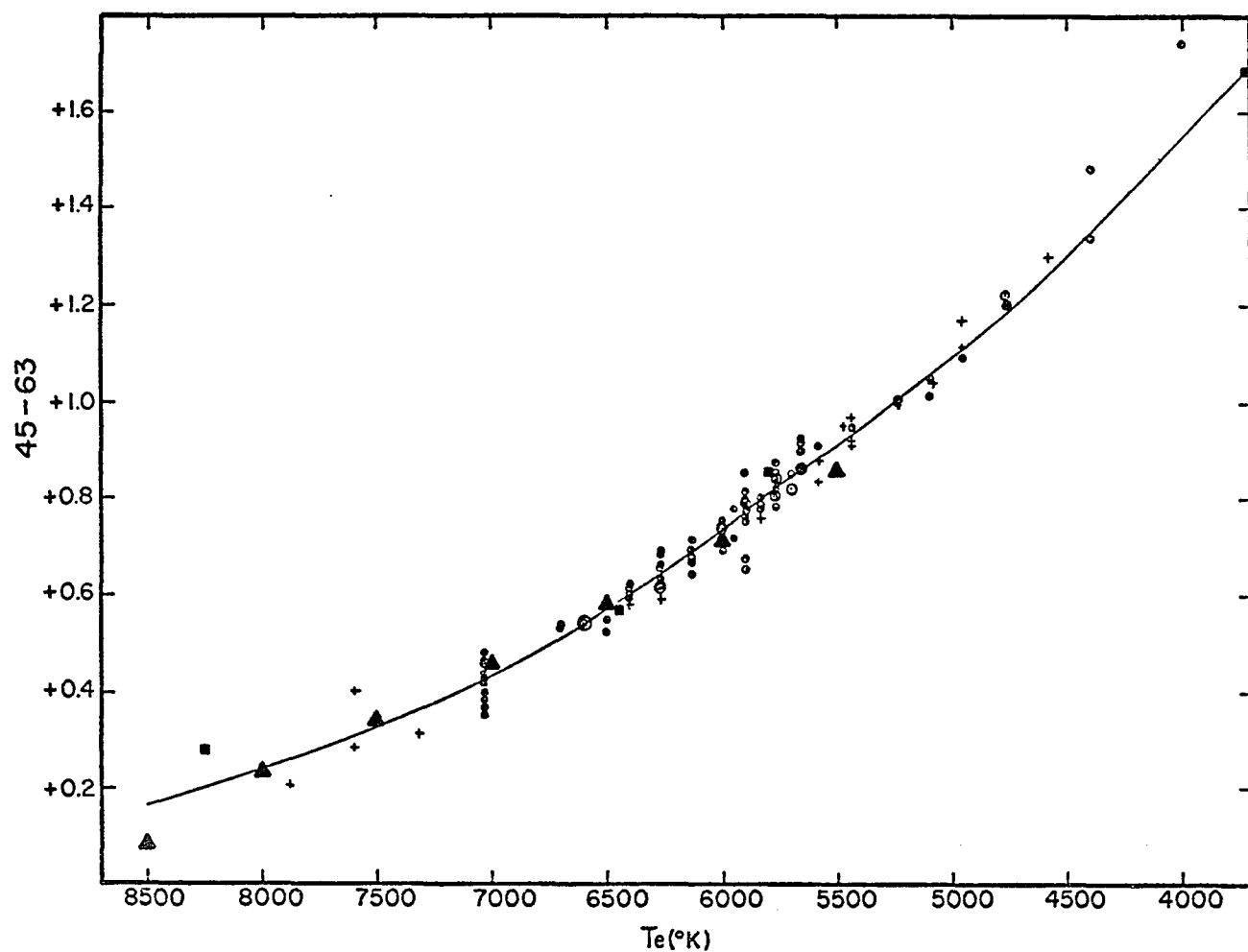| Name	T_e	Sp
Sun	5800	G2V
α Ag1	8250	A7IV-V
β Aur	10,000	A2V
α Boo	4250	K2IIIp
α CMa	10,380	A1V
ε CMa	21,000	B2II
α CMi	6450	F5IV-V
α Car	7510	F0Ib-II
o Cet:	2600	M5e
β Cru	26,600	B05IV
α Eri	14,000	B5IV
YY Gem	3720	M0.5V
α Gru	14,600	B5V
α Her:	3400	M5Ib-II
α Leo	13,000	B7V
α Lyr	9500	A0V
α Ori	3790	M2Iab
β Ori	11,200	B8Ia
γ Ori	21,000	B2III
ε Ori	21,000	B0Ia
α Pav	17,100	B3IV
β Peg	3130	M2II-III
β PerA	11,500	B8V
α PsA	9300	A3V
α Sco	3520	M2Iab
μ' Sco	19,200	B1.5V
α Tau	3860	K5III

Figure 30. The observational calibration of 45-63 versus T_e. -- Squares represent stars with measured angular diameters; circles and plus signs are for field and Hyades dwarfs, respectively, which have good spectral types. The triangles give the theoretical calibration of Figure 2, and the solid line the best fit to the observational points.
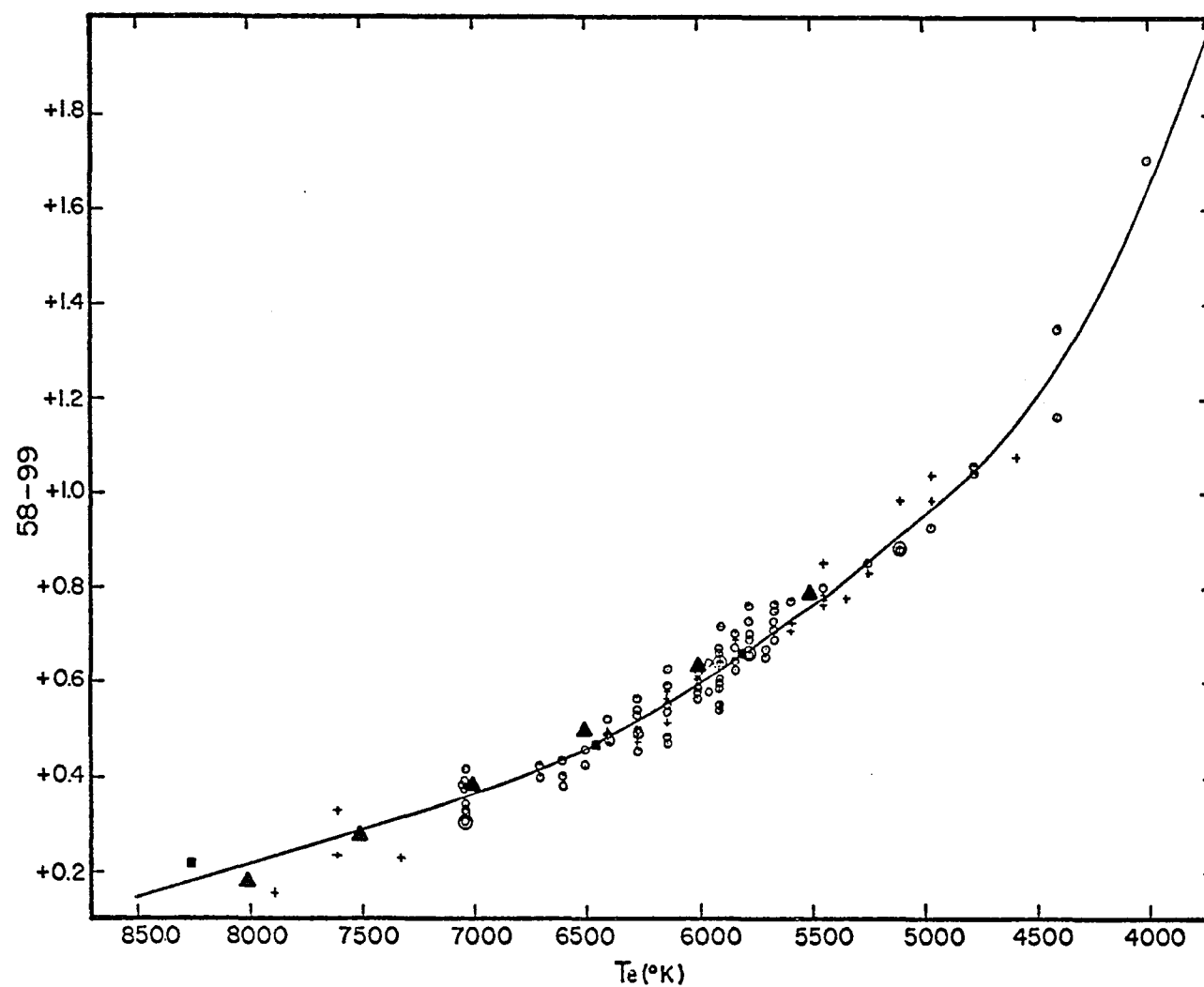
Figure 31. The observational calibration of 58-99 versus T_e. -- The symbols are the same as in Figure 30. The triangles give the theoretical calibration of Figure 29.

of T_e for 45-63 and 58-99, respectively, over the temperature range appropriate for the subdwarfs. In this range only four stars, α Aql (A7IV-V, $T_e = 8250^\circ$), α CMi (F5IV-V, 6450°), the Sun (G2V, 5800°), and YY Gem (M0.5V, 3720°) define the calibration, and so some sort of aid was needed to help in interpolating the curves, especially for T_e's between that of the Sun and that of YY Gem. For this the T_e calibration of Johnson (1966) was called upon. Johnson's calibration included fewer stars with measured angular diameters (only 14, but including the Sun and YY Gem) but used interpolations of T_e against six different color indices, including the infrared indices I-L and (R+I)-(J+K). Hence, we feel that Johnson's T_e versus spectral type relation is well interpolated, and so it has been used to derive the final curves of Figures 30 and 31. Field stars and Hyades stars with good MK spectral types (Jaschek, Conde and Sierra 1964; Morgan and Hiltner 1965) and with 13-color photometry (Mitchell and Johnson 1969, Schuster 1976, and the present thesis) have been plotted in Figures 30 and 31 using Johnson's T_e calibration. These points have been used to interpolate the final curves, especially between the Sun and YY Gem. So, in review, the absolute positions of the curves in Figures 30 and 31 depend solely upon the stars with measured angular diameters, but the shapes (the interpolations) of these curves depend somewhat upon the earlier T_e versus spectral type calibration.

In column 4 of Table 14 are given the averages of the two observational effect-temperature determinations for the subdwarfs. These were obtained using $(45-63)_s$ and $(58-99)_s$ from Table 11 plus Figures 30 and 31. Except for five subdwarfs not measured with 6RC photometry and

one very red subdwarf (G102-22), all subdwarfs have two observational determinations of T_e. In column five of Table 14 are given the final values of the effective temperatures. These values are weighted averages of the values in columns 3 and 4; the weight used was 2 if T_e (models) or T_e(obs) represents an average of two values, or the weight was 1 if they represent only a single value.

In Table 14 we see extremely good agreement between the values T_e(models) and T_e(obs). This is encouraging since we have obtained nearly the same T_e's from two completely independent means--one theoretical and the other observational. This agreement lends support for both calibrations and indicates that as long as we use both indices, 45-63 and 58-99, there are no large systematic errors. However, the agreement of Table 14 is somewhat misleading. For example, in some extreme cases a given subdwarf would have two theoretical T_e's differing by 300° or 400° and two observational T_e's differing by 200° or 300°, and yet the averages would agree to 50° or better. As mentioned earlier the (58-99)-theoretical T_e is on the average 130° higher than the (45-63)-theoretical one, and this difference is temperature dependent. And, the (45-63)-observational T_e is on the average about 50° greater than the (58-99)-observational one; this difference is independent of temperature. Also, in Figures 30 and 31 the theoretical calibrations (from Figures 2 and 29) have been plotted along with the observational calibrations. We see that (45-63)-theoretical T_e's are always less than (45-63)-observational values, and the (58-99)-theoretical curve always gives T_e's greater than the (58-99)-observational curve. Hence the good

agreement of Table 14 is dependent upon using the indices 45-63 and 58-99 together.

No attempt has been made to correct the final T_e's of Table 14 onto a completely uniform effective temperature system. Most stars with $T_e \gtrsim 5500^o$ have four T_e determinations (two theoretical and two observational) and most with $T_e \gtrsim 5500^o$ have only two observational determinations. A few stars with $T_e \approx 5500^o$ have three T_e measures (one theoretical and two observational). Hence the final values of Table 14 do not represent a completely uniform T_e system, but the agreement of T_e(models) and T_e(obs) and the above discussion indicate that the T_e's of most subdwarfs could be corrected to such a uniform system with changes of 50° or less.

In Table 16 we give a comparison between the T_e's of this paper and those of previous studies. Column one gives the star's name and column 2 gives the final T_e from Table 14. The $T_e(1)$'s come from a series of papers by the Stroms and Judith Cohen (Strom, Cohen and Strom 1967; Strom and Strom 1967; Cohen and Strom 1968; Cohen 1968). The $T_e(2)$'s come from R-I photometry (Johnson et al. 1966, Johnson et al. 1968) and the observational T_e calibration of Johnson (1966). The $T_e(3)$'s are from Travis and Matsushima (1973), and the $T_e(4)$'s from Cayrel (1968). On the average the present T_e values are higher (200° to 400° higher) than the $T_e(1)$ values. These differences can be explained, as pointed out by Strom and Strom (1967), by noting that the model atmospheres used to derive the $T_e(1)$'s were not convective nor blanketed. Neglecting blanketing for the subdwarf model atmospheres does not cause

agreement of Table 14 is dependent upon using the indices 45-63 and 58-99 together.

No attempt has been made to correct the final T_e's of Table 14 onto a completely uniform effective temperature system. Most stars with $T_e \gtrsim 5500^{\circ}$ have four T_e determinations (two theoretical and two observational) and most with $T_e \gtrsim 5500^{\circ}$ have only two observational determinations. A few stars with $T_e \approx 5500^{\circ}$ have three T_e measures (one theoretical and two observational). Hence the final values of Table 14 do not represent a completely uniform T_e system, but the agreement of T_e(models) and T_e(obs) and the above discussion indicate that the T_e's of most subdwarfs could be corrected to such a uniform system with changes of 50° or less.

In Table 16 we give a comparison between the T_e's of this paper and those of previous studies. Column one gives the star's name and column 2 gives the final T_e from Table 14. The $T_e(1)$'s come from a series of papers by the Stroms and Judith Cohen (Strom, Cohen and Strom 1967; Strom and Strom 1967; Cohen and Strom 1968; Cohen 1968). The $T_e(2)$'s come from R-I photometry (Johnson et al. 1966, Johnson et al. 1968) and the observational T_e calibration of Johnson (1966). The $T_e(3)$'s are from Travis and Matsushima (1973), and the $T_e(4)$'s from Cayrel (1968). On the average the present T_e values are higher (200° to 400° higher) than the $T_e(1)$ values. These differences can be explained, as pointed out by Strom and Strom (1967), by noting that the model atmospheres used to derive the $T_e(1)$'s were not convective nor blanketed. Neglecting blanketing for the subdwarf model atmospheres does not cause

Table 16. Comparison of effective temperatures.

Name	$(T_e)_{Ave}$	$T_e(1)$	$T_e(2)$	$T_e(3)$	$T_e(4)$
+54°223	5405	5000-5100	5200	4700	5360
-9°256	5780	5500			
+19°279	5170	5000:	5200		5100
-16°295	5350	5000	5250		5280
-26°828	5410	5130			
-13°544	5060	5000:	5100		
+25°495	6005	5620-5750	5750		5800-6200
-7°603	5635	5370	5650		
-3°592	5850		5650		
+34°796	4800	4470:		5160	4670
G175-39	5050	5000			
+45°992	5720	5370	5650		
+37°1312	5145	5000:			
+19°1185	5420	5130			
-0°1520	5760	5500			
+47°1419	5865	5370			
-33°4113	5740	6030			
+31°1684	5530	5000		5640	5360-5500
-1°1883	5240	5000		5370	
+29°1664	5360	5250	5250		
-3°2333	6205	5900			
HD74000	6090	5750			
HD84937	6270	6030			
+23°2207	6120	5900	6150		
G119-32	5845	5620			
+21°2247	5955	5620	6100		6040
G10-4	5105	4800:			
BS4550	5180	4900-5000	5100	5400	4950-5100
HD106038	5990	5620			
HD108177	6170	5750			6300
+40°2570	5835	5750	6000		5640
-9°3595	5150		5250		

Name	$(T_e)_{Ave}$	$T_e(1)$	$T_e(2)$	$T_e(3)$	$T_e(4)$
+10°2519	5580	5370			
G14-45D	4530	<4470		4700	
+34°2476	6190	6030			
+1°2920	5650	5370	5800		
+30°2536	6745	6600-6700	6850		
-21°4009	5630	5370-5620			
+25°2873	6405	6300	6650		
-15°4041	4850			5120	4650
-15°4042	5075			5300	4950
-10°4149	5725	5500	5900		5740
+42°2667	5935	5750			
+39°2947	5290	5000			
-3°3968	5110	4800			
+1°3421	5790	5370	5800		
G154-36	5470	5130			5370
+20°3926	6405	6170	6200		
+11°3833	5560	5250			
-21°5703	5720	5500			
+9°4529	6040	5750			
+17°4519	5965	5750			
G126-62	5955	5750			
-8°5980	5600	5000			
G190-15	5205	5130			
-14°6437	5920	5620	5750		
+26°4734	5350		5200		5200-5350
BS77	5700		5700		
BS219D	5770		5550		
BS1008	5510		5350		
BS6752D	5000		5050		
BS6927	5995		5900		
BS8181	6060	6100-6170	5950		

significant temperature errors since the subdwarfs are not heavily blanketed. Besides, blanketing increases the temperature gradient in a stellar atmosphere (see Strom and Kurucz 1966) and so would lead to differences between the present T_e's and the $T_e(1)$'s opposite of those observed. The main effect comes from neglecting convection. As shown by Travis and Matsushima (1973) and by Cohen and Strom (1968) convection is even more important in subdwarfs than in stars with solar compositions, and convection decreases the temperature gradient of a stellar atmosphere. Hence a convective model must be significantly hotter than a non-convective one to produce the same continuum colors. A comparison with the $T_e(2)$'s shows no systematic difference greater than about 50° and gives further proof that the T_e's of Table 14 contain no large systematic errors. The $T_e(3)$'s come from convective, unblanketed models, and the agreement with the present work is rather uneven. Cayrel derived the $T_e(4)$'s using blanketing independent indices (G-I from Stebbins and Whitford six color photometry and $(b-y)_c$), calibrations of radiative atmospheres, and differential photometric analyses. These $T_e(4)$'s agree very well with the present results.

Bolometric Magnitude Calibration

The calibration for determining bolometric corrections was motivated by the work of Eggen (1969b, 1971, 1973), who finds that M_{bol} is very nearly equal to $M(I_J)+1$ for the later-type stars (late-G, K, and M types), where I_J is the I magnitude of the Johnson (R,I) system. It was realized that a narrow-band magnitude from 13-color photometry cannot produce a relation like $M_{bol} = M(13\text{-color magnitude}) + (\text{constant})$, which

is good over a wide temperature range, as a broad-band magnitude can.
Hence, the calibration was derived in the form M_{bol} = M(13-color
magnitude) + $f(T_e)$, where $f(T_e)$ is some function of effective tempera-
ture. For convenience T_e will be represented by 45-63, and $f(T_e)$, or
rather f(45-63), will be determined empirically using the Hyades main
sequence. In deciding which 13-color magnitude to calibrate in this
form we decided to use the one which makes f(45-63) most nearly a
constant for the F, G, and early-K dwarfs. In this way any observa-
tional errors in 45-63 are inconsequential when determining the bolo-
metric corrections.

For this calibration the Hyades 13-color photometry comes from
Table 5, the Hyades V magnitudes from Johnson and Knuckles (1955) and
from Johnson, Mitchell and Iriarte (1962), and the Hyades spectral
types from Morgan and Hiltner (1965). (See Table 19.) Using the cali-
bration of Johnson (1966) the spectral types were used to derive
bolometric corrections, and these were added to the V magnitude to give
the apparent bolometric magnitudes of the Hyades main sequence stars.
These apparent bolometric magnitudes were next compared as a function of
temperature to various apparent 13-color magnitudes measured for the
same Hyades stars. It was found that the 63 magnitude produces the
most constant function, f(45-63); that is, $m_{bol} - (63)_{obs}$ is nearly con-
stant over the range of the subdwarfs. In Figure 32 we show the
calibration $m_{bol} - (63)_{obs}$ versus 45-63 as defined by 36 Hyades main
sequence stars. This calibration runs from A3 dwarfs to approximately
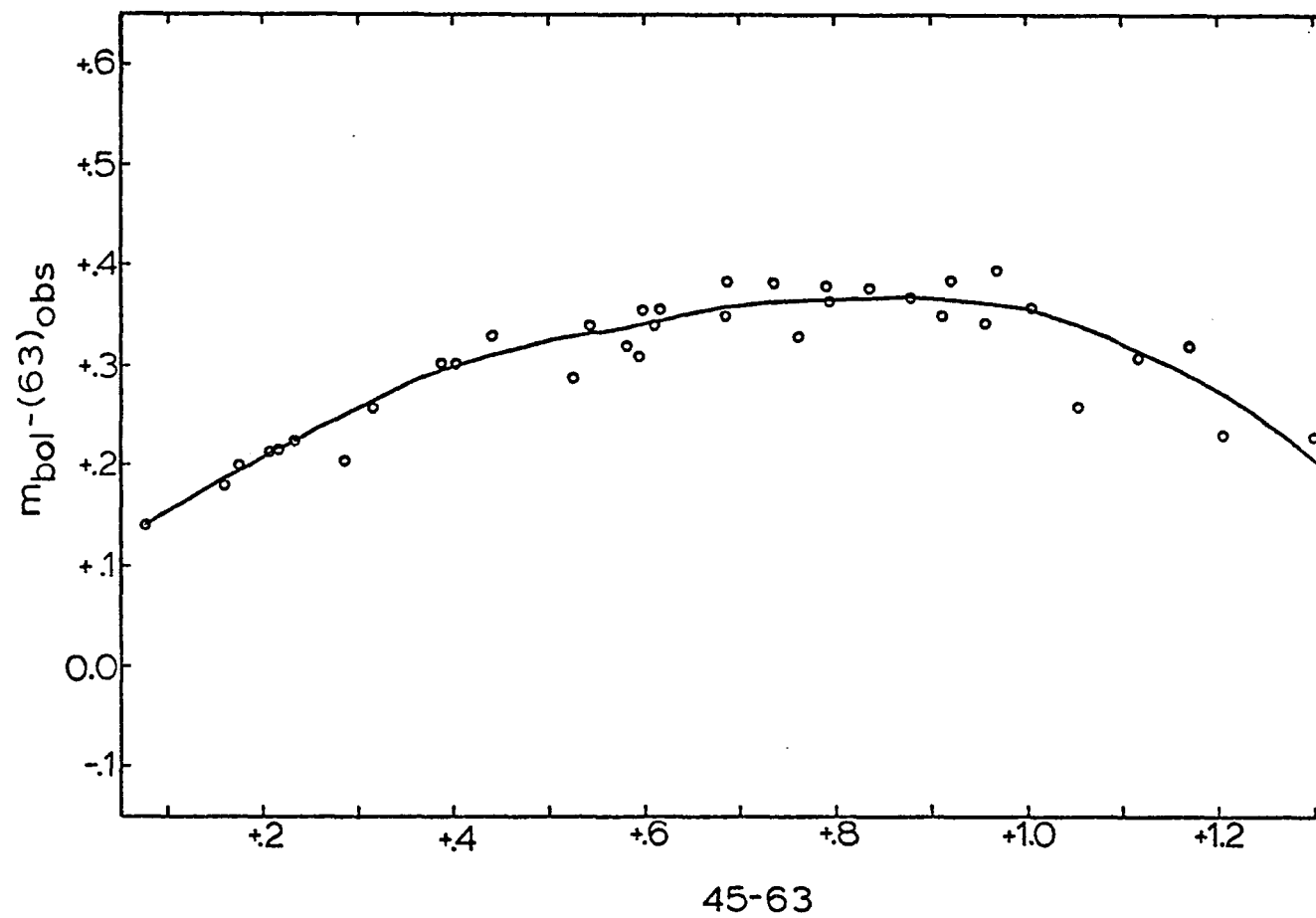K4 and seems to be defined with a probable error of ± 0.03 or less.

Figure 32. The $m_{bol}-(63)_{obs}$ versus 45-63 calibration.

We see that, indeed, $m_{bol}-(63)_{obs}$ is nearly constant for the spectral types F4 to K0 and only turns down slightly for earlier and later types. This calibration has been extended (not shown in Figure 32) to late-K and early-M stars using five field stars with good MK spectral types. This late-star calibration is good to approximately an accuracy of $\pm$ 0.1 magnitude.

Now we have nearly enough information to plot subdwarfs with parallaxes in a (M_{bol}, T_e) diagram. The only piece of information missing is the amount by which the 63 magnitudes change for constant T_e and constant bolometric magnitude but varying metallicity. That is, we need to know the absolute blanketing effects (line blocking plus backwarming) for the 63 magnitude. The blanketing curves of Chapter 5 show only the blanketing relative to filter 52; we need to know the total change of 63. Once we know this we can correct a subdwarf's 63 magnitude to Hyades composition and then from Figure 32 obtain m_{bol}. From the parallax comes M_{bol}, and T_e is derived from the calibrations of the previous sections.

The absolute blanketing for the 63 magnitude can be obtained from two sources. First, for $T_e \geq 5500^{o}$ the corrections can be found from Kurucz's models. For example, the 63 magnitude of a (5500, 4.0, 0.01X, 2) model can be subtracted from that of a (5500, 4.0, 1X, 2) model to give the 63 blanketing correction going from a subdwarf with [Fe/H] = -2.0 to solar composition. To extrapolate to Hyades composition we have assumed [Fe/H] = +0.3 is appropriate as shown in Figure 26. These extrapolations are small and are certainly defined to $\pm$0.02 magnitude

or better. Second, over the full temperature range we can estimate the

63 corrections using the observational results of Johnson et al. (1968,

p. 474) showing that at constant T_e and constant bolometric magnitude the

H, K, and L magnitudes of broad-band infrared photometry " . . . remain

practically unchanged by the removal of the metal lines from Hyades-

like stars." There is a sufficient number of K observations of sub-

dwarfs (ten such observations) to make a useful estimate of the total

blanketing corrections for the 63 magnitude. In Figure 33 we have

plotted a (63-K) versus $(45-63)_{Hyd}$ diagram, where $(45-63)_{Hyd}$ is the value

of this index for a Hyades composition; $(45-63)_{Hyd}$, which has been ob-

tained by extrapolating the blanketing corrections of the models, is

only very slightly different from $(45-63)_s$. The K observations for the

subdwarfs and Hyades stars come from Johnson et al. (1968) and Johnson

et al. (1966). In this diagram a subdwarf and a Hyades star with the

same effective temperatures have the same values of $(45-63)_{Hyd}$, and as

mentioned above the K magnitude is not affected by metallicity. Hence,

any displacement of the subdwarfs from the Hyades in Figure 33 gives a

measure of the blanketing for the 63 magnitude. The solid line of

Figure 33 represents the Hyades main sequence as defined by the observa-

tions of ten Hyades main sequence stars. The dashed line for $(45-63)_{Hyd}$

≤ 0.86 represents the change predicted by the models in going to a compo-

sition of $[Fe/H] = -2.0$. This dashed line agrees very well with the

positions of the four extreme subdwarfs which have an average $[Fe/H]$ of

-1.59. The dashed line in the region for $(45-63)_{Hyd} > 0.86$ represents

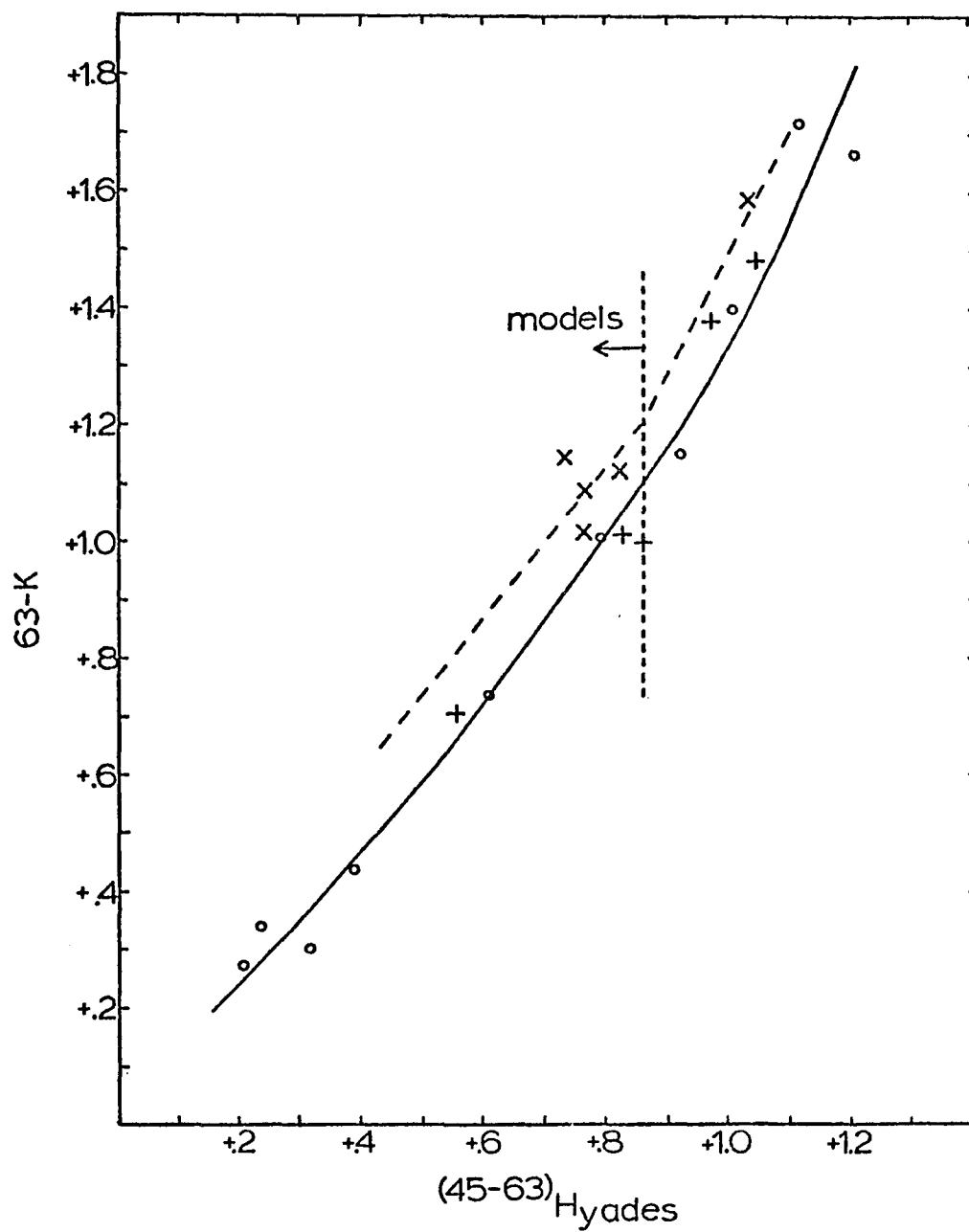an extrapolation of the theoretical results taking into account the

Figure 33. 63-K versus (45-63)$_{Hyades}$. -- The circles and solid line
represent the Hyades main sequence. The plus signs are for
mild subdwarfs and the X's for extreme subdwarfs. The
dashed lines are explained in the text.

positions and metallicities of the two mild and one extreme subdwarfs

in this part of the diagram. The above combination of theory and observa-

tion allows one to estimate the total blanketing changes of the 63 magni-

tude with a probable error of about ±0.05 magnitude. This correction

for the total blanketing is a necessary part of obtaining accurate

apparent bolometric magnitudes from Figure 32.

Surface Gravity Calibration

In Chapter 5 we introduced the luminosity sensitive diagram, G

versus 45-63, which is plotted in Figure 24. In this figure lines of

constant luminosity classification, according to the MK system, have

been sketched in. The mean Hyades main sequence colors have been used

to define the locus for luminosity class V while field giants and sub-

giants were used for luminosity classes III and IV. For the giants and

subgiants only those with "certain" luminosity classifications, as given

by Jaschek et al. (1964) and Kennedy and Buscombe (1974), were plotted

in Figure 24. By "certain" we mean that the majority of recent classi-

fications agree as to the luminosity class (but not necessarily the

spectral type). Special weight was given to classifications made by

W. W. Morgan. Also, intermediate types such as IV-V or III-IV were not

plotted. The solid lines of Figure 24 represent the average main se-

quence, the average subgiants and the average giants while the dotted

lines give the loci that separate the brightest dwarfs from the faintest

subgiants and the brightest subgiants from the faintest giants. Follow-

ing the convention suggested by Keenan (1963) the regions between the

dotted and solid lines have been designated the following: Vb, Va, IVb, IVa, IIIb, and IIIa. We see that the separation of types is fairly clear. Only three dwarfs lie in the IVb region, and two of these have at times been classified subgiants (though the majority of recent classifications have been V, Jaschek et al. 1964). Only three subgiants lie in the Va region, and one of these (the most discrepant) belongs to a multiple star system. One subgiant lies in IIIb, and four giants lie in the IV regions. The vast majority of the stars have the same photometric luminosity classification as their spectroscopic one.

Figure 24 can easily be used to assign photometric luminosity classifications to F, G, and early-K stars of normal compositions. And, since the G index measures primarily the Balmer jump which is gravity sensitive, we can use Figure 24 to get an idea of the evolutionary status of the subdwarfs as has already been done to some extent in the last section of Chapter 5. In column 6 of Table 14 are given "luminosity classes" for the subdwarfs according to their position in Figure 24. Certainly any subdwarfs with class IVa or IVb are evolved. If the conclusion of Chapter 5 that zero-age subdwarfs have greater surface gravities than Hyades stars is correct, we might expect then that the zero-age line for the subdwarfs lies below the Hyades main sequence line in Figure 24. That is, zero-age subdwarfs would have a class of Vb. Hence, many of the subdwarfs with classes Va may also be significantly evolved.

A more quantitative classification of Figure 24 has been carried out for effective temperatures greater than 5900° (45-63 $\leq$ 0.699) using

the blanketed model atmospheres to determine surface gravities of indi-
vidual stars. Cooler stars have been avoided because of the problems
with the coolest (5500°) models as mentioned earlier. In Table 17 are
listed 18 extreme subdwarfs ([Fe/H] $\leq$ -1.0), 9 Hyades stars, and 3 field
subgiants whose surface gravities have been determined. For the sub-
dwarfs the analysis was completely straightforward. Using the effective
temperature (T_e(models)) and composition ([Fe/H]) of a subdwarf,
theoretical 13-color photometry was interpolated for surface gravities
with logs of 3.5, 4.0, and 4.5. The interpolating was done in two
dimensions to match both the subdwarf's T_e and composition. Then this
theoretical photometry as well as the subdwarf's observed colors were
converted to relative energies using the revised calibration of the 13-
color system given by Johnson and Mitchell (1975), and all four energy
distributions were plotted together. Figures 34 and 35 show these plots
for $+26^{\circ}2606$ and HD84937. With these plots it is possible to interpolate
the subdwarf's surface gravity as long as its logarithm lies between
3.5 and 4.5. In general it was possible to select a surface gravity to
obtain a fairly good match of the theoretical and observational curves
except for the 37 and 40 filters. The models nearly always predicted
too little energy through these two filters as can be seen in Figures
34 and 35. For this reason there was always some uncertainty as to the
surface gravity of best fit, and so in column 4 of Table 17 we list a
range of possible surface gravities for each star. In general the upper
limit of this range comes from normalizing the energy curves above the
Balmer limit at the 52 filter as in Figures 34 and 35 and then using

Table 17. Surface gravities of stars.

| Name	[Fe/H]	T_e (Models)	log g	(log g)$_{Ave}$	δG	Luminosity Class
Subdwarfs:						
$-17^{\circ}484$	-1.82	6220	3.7-3.8	3.75	+0.085	IVb
$-13^{\circ}482$	-1.55	6250	3.7-3.8	3.75	+0.077	IVb
G4-37	-1.32	5940	4.2-4.9	4.55	-0.018	Vb
$+21^{\circ}607$	-1.19	6240	4.0-4.2	4.1	-0.018	Vb
HD74000	-1.50	6120	4.3-4.5	4.4	-0.011	Vb
$+25^{\circ}1981$	-1.37	6710	3.8-4.0	3.9	-0.040	Vb
$+9^{\circ}2190$	-1.40	6180	3.9-4.3	4.1	+0.002	Va
G48-29	-1.81	6260	3.8-4.0	3.9	+0.010	Va
HD84937	-1.38	6310	4.0-4.2	4.1	-0.003	Vb
$+44^{\circ}1910$	-1.57	6135	3.5-3.6	3.55	+0.113	IVa
$+36^{\circ}2165$	-1.11	6160	3.9-4.0	3.95	+0.034	Va
G13-9	-1.44	6285	3.8-4.0	3.9	+0.038	Va
HD108177	-1.45	6195	4.3-4.4	4.35	-0.024	Vb
$+34^{\circ}2476$	-1.41	6220	3.9-4.1	4.0	+0.027	Va
G64-37	-1.27	6370	4.0	4.0	+0.004	Va
$+26^{\circ}2606$	-1.54	6170	4.3-4.4	4.35	-0.010	Vb
G126-62	-1.10	5970	4.0-4.4	4.2	+0.016	Va
G18-39	-1.06	6035	3.8-4.1	3.95	+0.008	Va
Hyades:						
H20	+0.3	6710	3.9-4.1	4.0	-0.003	Vab
H34	+0.3	6490	4.05-4.1	4.1	+0.001	Vab
H35	+0.3	6560	4.1-4.2	4.15	+0.004	Vab
H36	+0.3	6535	4.1-4.2	4.2	+0.002	Vab
H53	+0.3	6700	3.75-3.85	3.8	+0.037	Va
H57	+0.3	6280	4.1-4.3	4.2	+0.012	Vab
H77	+0.3	6155	4.25-4.5	4.4	+0.008	Vab
H85	+0.3	6455	4.0-4.2	4.1	+0.016	Vab
H94	+0.3	6445	4.1-4.3	4.2	+0.016	Vab
Subgiants:						
BS544	+0.16	6290	3.5-3.6	3.55	+0.107	IVa
BS2484	+0.29	6435	3.6-3.75	3.7	+0.096	IVa
BS3775	-0.01	6245	3.6-3.7	3.65	+0.091	IVb
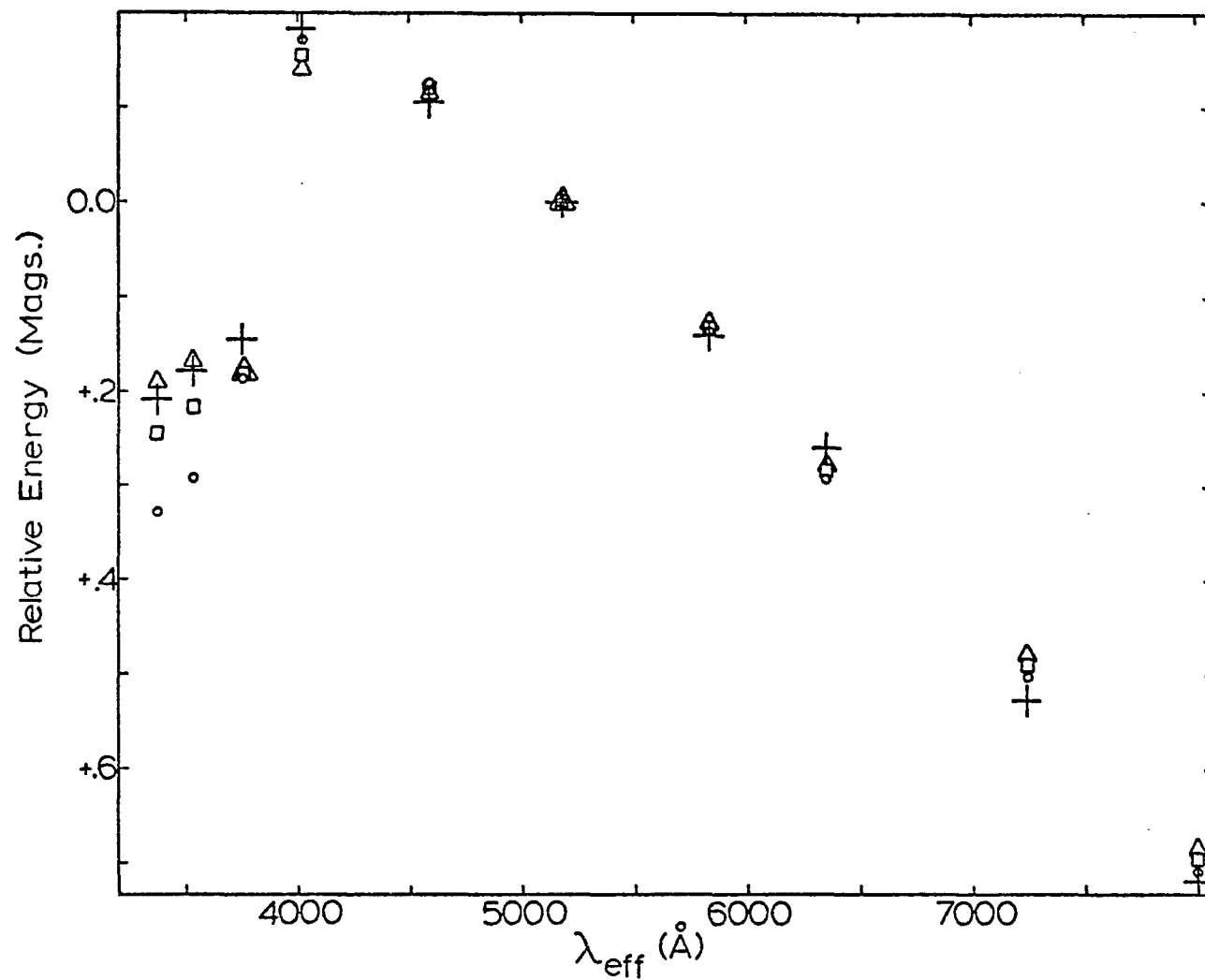
Figure 34. Theoretical and observational relative energy distributions for +26°2606.
-- Plus signs represent the observed energy distribution. Triangles,
squares, and circles give the theoretical distributions for log g =
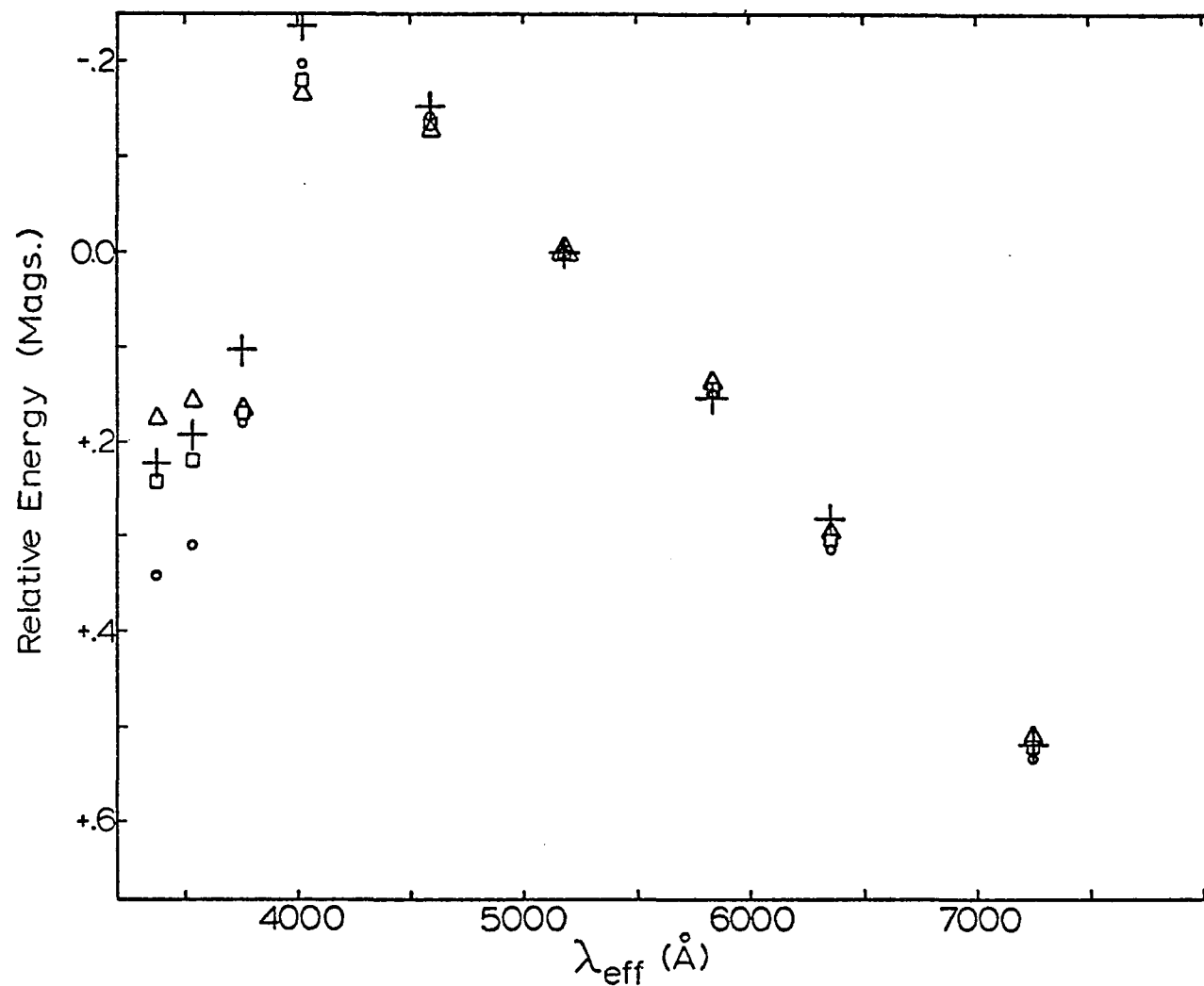4.5, 4.0 and 3.5, respectively.

Figure 35.   Theoretical and observational relative energy distributions for HD 84937. -- The symbols are the same as used in Figure 34.

the filters 33 and 35 to define the gravity. When normalized at filter 52 the curves usually match well for the longer wavelengths (filter 58, 63, 72, and 80). The lower limit of the surface gravities comes from shifting the observational curve up and down to obtain the best fit above the Balmer jump for filters 40, 45, and 52. Filter 37 was never used in determining surface gravities due to its large discrepancy. In column 5 of Table 17 is given what is thought to be the best representative value of the star's surface gravity--usually just an average of the two limits of column 4.

For the Hyades stars and for two of the subgiants the analysis was not so straightforward since the models have not been calculated for metallicities greater than the Sun's. The blanketing corrections needed to go from solar abundance to Hyades abundance were calculated in the following manner. Using a Hyades star's measured 45-63 and an expanded version of Figure 26 (scaled according to the models to be usable for a wide range of (45-63)'s), we have determined the value of $\delta(37-45)$ of a solar composition star with the appropriate 45-63. Next, by examining a 37-45 versus 45-63 diagram $\delta(37-45)$ was converted to $\Delta(37-45)$, the total blanketing of filter 37 relative to 45. Then the theoretical blanketing curves of Chapter 5 were used to obtain the ratios of the blanketing in the other colors relative to $\Delta(37-45)$, and so the blanketing corrections of all filters relative to filter 52 directly followed. These corrections were added to the theoretical colors interpolated at the Hyades star's T_e and solar composition to give the theoretical colors for the star's T_e and a Hyades composition. The analysis then proceeds

exactly as for the subdwarfs, and the surface gravity is interpolated. In Figure 36 we have plotted the relative energy curves used for determining the gravity of the Hyades star, H57. Again note the discrepancy of filters 37 and 40.

In column 7 of Table 17 are the luminosity classes of the stars according to Figure 24, and in column 6 are the values of δG, which is defined as the difference between an individual star's value of G and the value of G for the mean Hyades main sequence at constant 45-63. In Figures 37 and 38A we have plotted log g versus the luminosity class and versus δG respectively, for the subdwarfs, Hyades stars and field subgiants in the temperature range $6500^{\circ} \geq T_e \geq 6000^{\circ}$. In spite of the fact that the plotted stars represent a wide range in composition the two diagrams show surprisingly good correlations. The five Hyades stars in Figure 38A are separated by only 0.02 or 0.03 magnitude in δG from the extreme subdwarfs, and the three field subgiants are not separated at all from the three evolved subdwarfs. This gives further proof that the residual blanketing effects in the G index are very small, probably 0.02 magnitude or less, and that the position of a star in the G versus 45-63 diagram gives a good indication of the star's surface gravity independent of its metallicity. Alternatively, Figures 37 and 38A indicate that in this temperature range the behavior of the model atmospheres with regard to blanketing and surface gravity is fairly good.

It should be pointed out that the surface gravities of Table 17 may contain significant systematic errors depending in part on the models and in part on my technique of fitting the theoretical energy
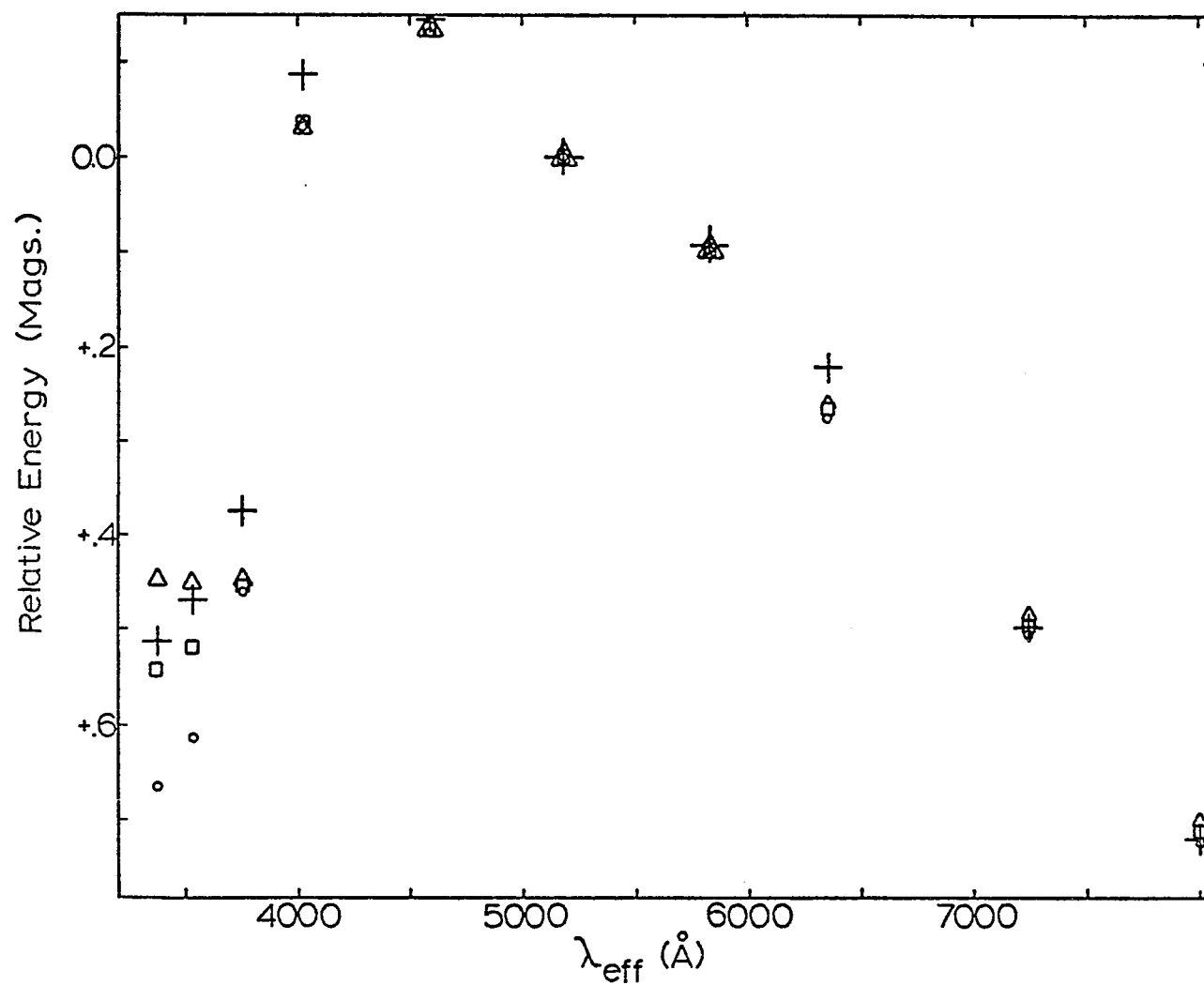
Figure 36. Theoretical and observational relative energy distributions for the Hyades dwarf, H57. -- The symbols are the same as in Figure 34.
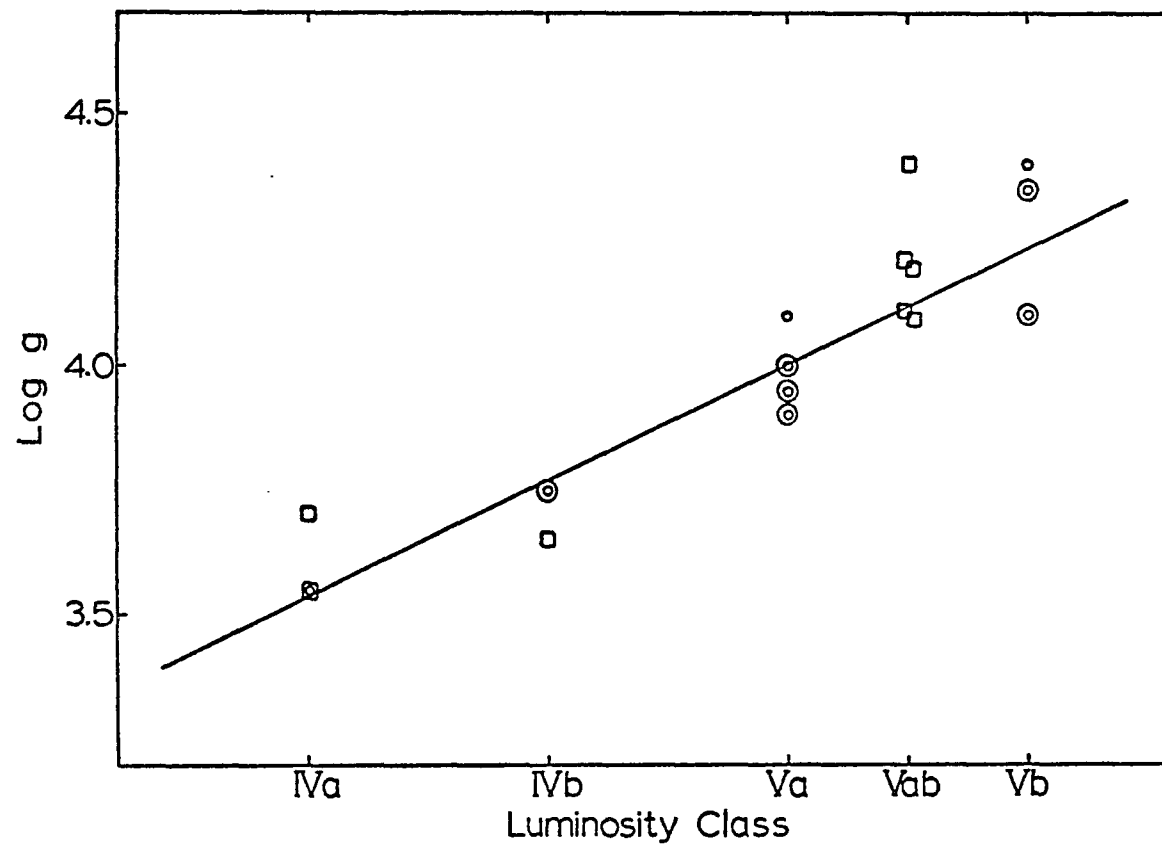
Figure 37. Log g versus "luminosity class" for stars in the range
$6500^\circ \geq T_e \geq 6000^\circ$. -- The circles and solid line represent the extreme subdwarfs while the squares are for
Hyades dwarfs and for field subgiants.

Figure 38. Log g versus δG. -- (A) For the temperature range
$6500^{\circ} \geq T_e \geq 6000^{\circ}$. The circles and solid line
represent the extreme subdwarfs while the squares
are for the Hyades dwarfs and for field subgiants.
(B) For cooler temperature ranges. The circles and
solid line represent field stars in the range
$5000^{\circ} \geq T_e \geq 4700^{\circ}$ while the triangles and dashed line
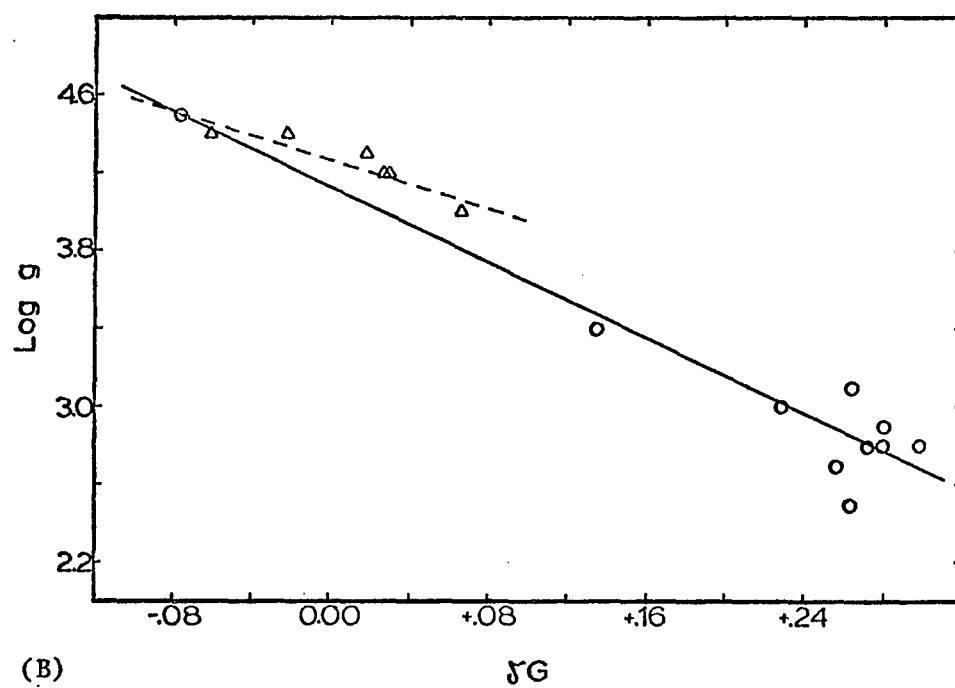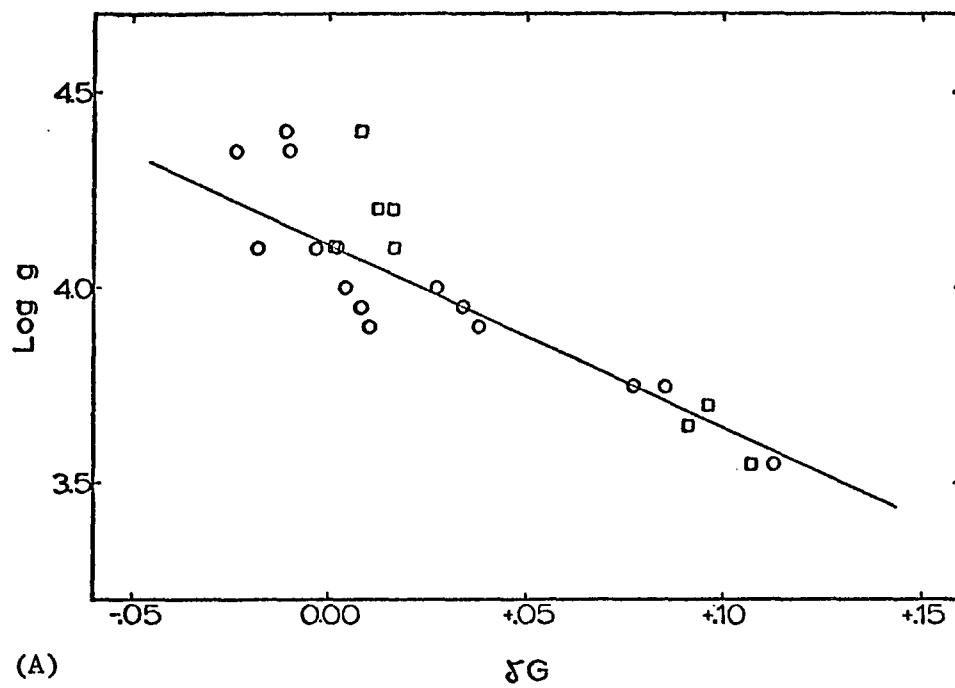are for field stars in the range $5800^{\circ} \geq T_e \geq 5200^{\circ}$.

(A)

(B)

Figure 38. Log g versus δG.

distributions to the observed ones. And, as has been shown, even for these higher temperatures ($6000°$ to $6500°$) the models still show discrepancies from the observations, especially for filters 37 and 40. Finally, it is important to note that changing the helium content in the atmospheres of F, G, and K-type stars mimicks changes in surface gravity (for example, see Strom and Strom 1967, Alexander 1967, Chaffee et al. 1971). There is reason to believe (Eggen 1963) that the Hyades stars have a helium abundance higher than the solar abundance, which is used in the model atmospheres. Also, since the subdwarfs belong to the oldest stellar population they may have helium abundances significantly smaller than the solar value. These helium differences might cause errors in the log g's as large as 0.2 but would not increase the scatter nor cause a separation of the stars in Figures 37 and 38A.

In Figure 38B is given the calibration of Log g versus δG for stars cooler than $6000°$. The stars and gravities used for this calibration came from the list of "standard stars" (Table II) of Harmer and Pagel (1973), and the 13-color photometry from Mitchell and Johnson (1969). The circles and solid line correspond to stars in the temperature range, $4700° \leq T_e \leq 5000°$, and the triangles and dashed line to $5200° \leq T_e \leq 5800°$. All of the stars plotted were carefully selected from the literature by Harmer and Pagel (1973) for having well determined values of T_e, log g, and [Fe/H].

CHAPTER 7

ANALYSIS AND DISCUSSION

In this chapter we will first compare the subdwarfs and Hyades stars in the M_{bol} versus T_e diagram. Specifically we will study the separation of these two types of stars as a function of metallicity in order to gain some ideas concerning the helium content and evolutionary status of the subdwarfs. The apparent "turnoff" of the field subdwarfs will be compared to those of a few well observed globular clusters to examine the relative ages of these different types of extreme Population II objects. Next, in the G versus 45-63 diagram a comparison between the extreme subdwarfs and known globular-cluster features will finally lead to a clear understanding of the evolutionary status of most of the subdwarfs. However, a number of severe problems of interpretation result from the apparent evolution of a number of the cool subdwarfs. A model of Population II star formation as related to the Galaxy's collapse is briefly sketched; this model explains, at least partially, the problems relating to the cool, evolving subdwarfs. Finally, the subdwarfs' positions in the (M_{bol}, T_e) and (G, 45-63) diagrams are used to estimate their masses.

M_{bol} versus T_e Diagram

In Table 18 are listed 53 stars from the subdwarf lists which have trigonometric parallaxes equal to or greater than $0\overset{''}{.}030$. These

Table 18. Subdwarfs with parallaxes $\geq 0\overset{''}{.}030$.

Name	Name	[Fe/H]	Lum. Class	63	m_{bol}	π	M_{bol}	$(T_e)_{Ave}$	$\Delta[L_H]$	Yale#
HD6582	+54°223	(-0.4)	Vb	4.756	5.06	0.129+5	5.61	5405	-0.08	219
7983	-9°256	-0.17	Va	8.577	8.91	0.033+6	6.50	5780	-0.71	274
10476	+19°279	(+0.3)	Vb	4.754	5.10	0.133+6	5.72	5170	+0.03	356
10700	-16°295	-0.26	Vb	3.060	3.35	0.275+5	5.55	5350	-0.01	365
14412	-26°828	(-0.2)	Vb	5.911	6.21	0.091+8	6.00	5410	-0.24	479
17925	-13°544	(~solar)	Va	5.511	5.77?	0.123+6	6.22?	5060	-0.12	599
25329	+34°796	-1.32	Vb	7.999	8.05?	0.054+5	6.71?	4800	-0.20	887
30649	+45°992	(-0.6)	Va	6.559	6.86	0.038+7	4.76	5720	+0.03	1076
38230	+37°1312	(+0.3)	Vb	6.827	7.17	0.067+4	6.30	5145	-0.19	1314
55575	+47°1419	-0.20	Va	5.197	5.52	0.037+6	3.36	5865	+0.48	1687
63077	-33°4113	-0.67	Va	4.961	5.25	0.057+7	4.03	5740	+0.30	1841
64090	+31°1684	(-1.6)	Vb	7.848	8.12	0.038+4	6.02	5530	-0.34	1857
64606	-1°1883	(-0.8)	Vb	6.971	7.22	0.047+11	5.58	5240	+0.04	1872
65583	+29°1664	(-0.5)	Vb	6.535	6.80	0.056+5	5.54	5360	-0.02	1889
70958	-3°2333	-0.23	Va	5.297	5.61	0.052+5	4.19	6205	-0.09	1998
89125	+23°2207	-0.10	Va	5.561	5.88	0.060+5	4.77	6120	-0.26	2413
103095	BS4550	-1.30	Vb	5.971	6.17	0.116+5	6.49	5180	-0.28	2745
106038	106038	-1.19	Va	9.830	10.09	0.038+11	7.99	5990	-1.46	2810
108177	108177	-1.45	Vb	9.374	9.61	0.031+7	7.07	6170	-1.22	2863
110897	+40°2570	-0.12	Vb	5.648	5.98	0.065+7	5.04	5835	-0.17	2935
114606	+10°2519	(-0.6)	Va	8.362	8.66	0.040+5	6.67	5580	-0.62	3010
126053	+1°2920	(-0.1)	Vb	5.878	6.21	0.059+5	5.06	5650	-0.03	3264
128167	+30°2536	-0.46	Vb	4.234	4.49	0.063+6	3.49	6745	-0.12	3300
134083	+25°2873	+0.17	Va	4.615	4.94	0.061+7	3.87	6405	-0.09	3416
140283	-10°4149	-1.99	IVb	6.844	7.09	0.031+7	4.55	5725	+0.11	3552
144579	+39°2947	(-0.7)	Vb	6.225	6.48	0.080+5	6.00	5290	-0.15	3650
157089	+1°3421	-0.52	Va	6.553	6.85	0.036+6	4.63	5790	+0.03	3943
173667	+20°3926	+0.17	Va	3.903	4.23	0.049+5	2.68	6405	+0.38	4328

Table 18. -- continued.

Name	Name	[Fe/H]	Lum. Class	63	m_{bol}	π	M_{bol}	$(T_e)_{Ave}$	$\Delta[L_H]$	Yale#
182572	+11°3833	(>+.3)	IVb	4.716	5.08?	0.059±5	3.93?	5560	+0.46	4541
193901	-21°5703	-1.48	Va	8.253	8.52	0.035±6	6.24	5720	-0.56	4852
201891	+17°4519	-0.92	Va	7.076	7.35	0.041±6	5.41	5965	-0.41	5098
203608	BS8181	-0.68	Vb	3.939	4.22	0.111±8	4.45	6060	-0.09	5152
216777	-8°5980	(-0.1)	Va	7.644	7.97	0.044±6	6.19	5600	-0.44	5561
149414	-3°3968	(-1.9)	Vb	9.125	9.31	0.046±8	7.62	5110	-0.70	3767
250792	+19°1185	(-1.0)	Vb	8.872	9.15	0.033±6	6.74	5420	-0.54	1395
+38°4955	G190-15	(<-2.0)	Vab	10.643	10.84?	0.052±13	9.42?	5205	-1.47	5617
+55°900	G175-39	(>+.3)	Vb	7.799	8.12?	0.056±7	6.86?	5050	-0.37	1002
Ross484	G14-45D	--	Vb	10.241	10.47?	0.047±8	8.83?	~4530	-0.92	3044
64379	-34°4036	-0.14	Va	4.665	4.97	0.073±7	4.29	6320	-0.20	1864
74377	+42°1922	(~solar)	Vb	7.976	8.18?	0.061±8	7.11?	4730	-0.33	2082
112758	-9°3595	(-0.45)	Vb	7.093	7.34	0.064±14	6.37	5150	-0.22	2974
144872	+39°2950	(~+.2)	Vb	8.046	8.31?	0.057±7	7.09?	4690	-0.30	3654
151877	+37°2804	(+0.2)	Vb	7.974	8.30	0.051±7	6.84	5205	-0.44	3827
224930	+26°4734	(-0.8)	Vb	5.322	5.59	0.084±4	5.21	5350	+0.13	5807
22879	-3°592	-0.79	Va	6.361	6.65	0.047±6	5.01	5850	-0.17	763
134439	-15°4042	(-1.8)	Vb	8.620	8.78?	0040±5	6.79?	5075	-0.35	3425.0A
134440	-15°4041	(-1.8)	Vb	8.912	9.01?	0.040±5	7.02?	4850	-0.34	3425.0B
--	-41°3306	(~-0.8)	Vb	8.374	8.56?	0.039±6	6.46?	5060	-0.21	4524
16623	-26°957	-0.32	IVb	8.408	8.72	0.048±12	7.13	5810	-0.99	--
--	G78-26D	--	--	9.823	9.85?	0.037±6	7.69?	~4070	-0.29?	674
--	AC+20°1463-148	--	--	9.842	9.05?	0.119±6	9.43?	~3330	--	--
--	AC+20°1463-154	--	--	9.814	8.92?	0.119±6	9.30?	~3300	--	--
--	G102-22	--	--	10.527	9.55?	0.162±4	10.60?	~3180	--	1305

stars were obtained from many different sources (Sandage and Eggen 1959, Eggen and Sandage 1962, Strom and Strom 1967, Gliese 1969, Eggen 1973), but generally the parallaxes come directly from the Yale Parallax Catalogue (Jenkins 1963). A few of the parallaxes which come from Eggen (1973), from Gliese (1969), and from van Altena and Vilkki (1975) include measurements made since the parallax catalogue was published. In order to try to use as uniform and high quality set of data as possible only stars with parallaxes greater than $0\rlap{.}''035$ and parallax errors less than or equal to $\pm\ 0\rlap{.}''008$ were used in the following analyses, with two exceptions. The two stars, HD140283 (Yale 3552, $\pi = 0\rlap{.}''031 \pm 7$) and HD250792 (Yale 1395, $\pi = 0.033 \pm 6$) were included in one (M_{bol}, T_e) diagram (Figure 39) for comparison with the results of Eggen (1973), who also uses these two stars. Six stars of Table 18 are never used in the following analyses. In Table 18 columns one and two give the star's names, column three the composition, [Fe/H], column four the luminosity class from Table 14, and column five the observed 63 magnitude. Using the 63 magnitudes plus Figure 32 to obtain bolometric corrections, and the stellar atmospheric models plus Figure 33 for blanketing corrections, the observed bolometric magnitudes (m_{bol}) have been derived (Table 18, column 6). The blanketing corrections obtained from the models and Figure 33 are always small, generally less than -0.1 magnitude and always less than -0.25 magnitude. The parallaxes, given in column seven of Table 18, are used to convert m_{bol} to M_{bol}, the absolute bolometric magnitude. The effective temperatures, $(T_e)_{ave}$, come from Table 14, and the $\Delta[L_H]$'s of Table 18 are the differences between a subdwarf's
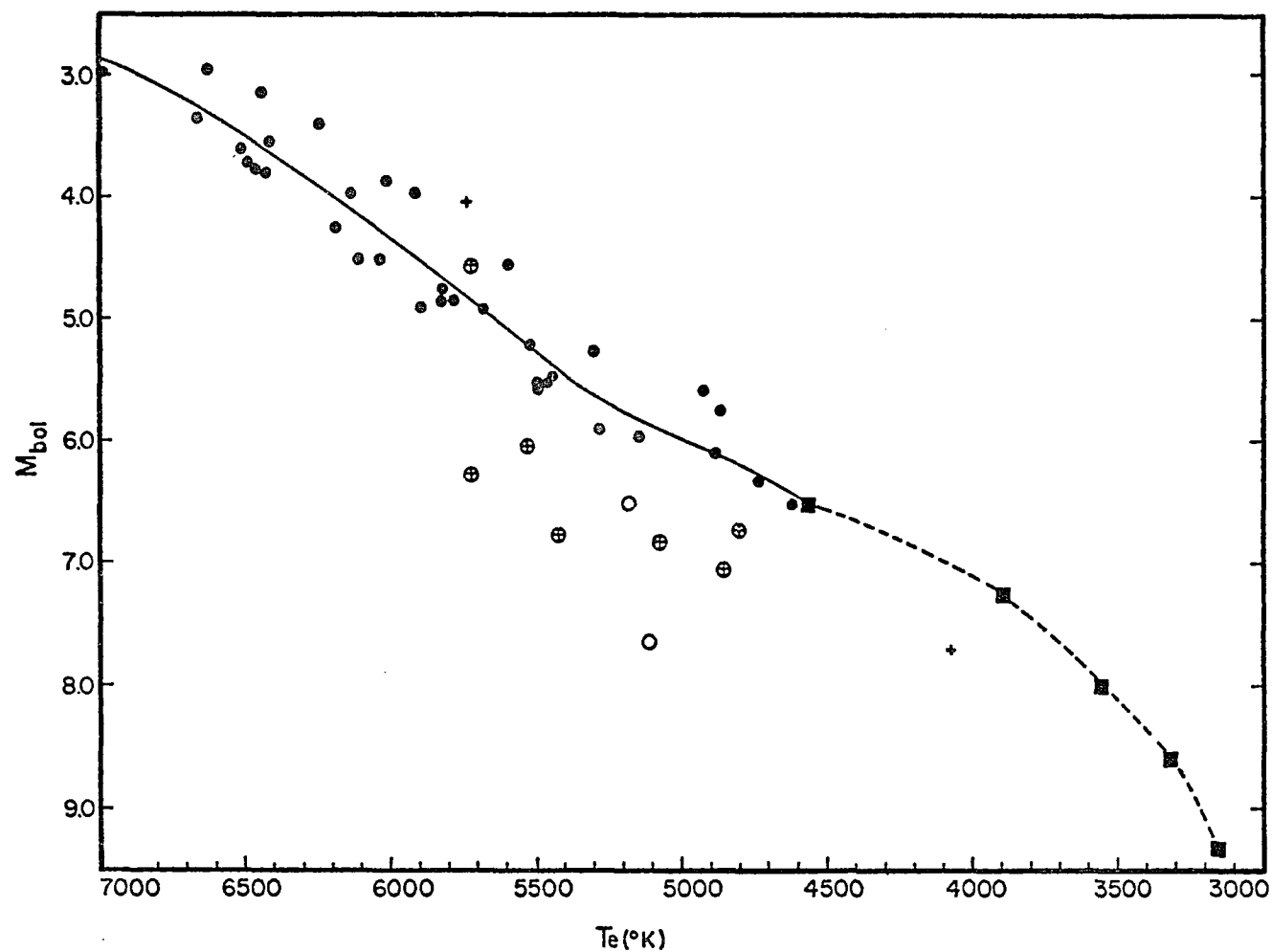
Figure 39. M_{bol} versus T_e. -- The solid line and filled circles represent the Hyades main sequence while the squares and dashed line are Eggen's (1973, 1969c) curve for the young disk main sequence. The open circles are for extreme subdwarfs, the plus signs for subdwarfs from Eggen's list of halo stars, and the crossed circles for subdwarfs which fall in both categories.

luminosity and the mean Hyades luminosity at constant T_e (calculated using Figures 39 and 40). The star's number in the Yale Parallax Catalogue is given in the last column of Table 18.

In Table 19 we give the M_{bol} and T_e values, plus other data used in deriving M_{bol}, for the individual Hyades stars. Column one gives the number of the star (van Bueren 1952), and columns 2, 3, and 4 give data already used and explained in the bolometric magnitude calibration of Chapter 6. The M_V's of column five come from Morgan and Hiltner (1965) who used the distance moduli of Heckmann and Lübeck (1956). Then M_{bol} comes from the relation $M_{bol} = M_V + B.C.$ The effective temperatures of the Hyades stars were determined in exactly the same manner as for the subdwarfs, using the indices 45-63 and 58-99, except that no blanketing corrections were applied (nor needed). For each Hyades star with $T_e \gtrsim 5500^\circ$ four independent T_e determinations were made, two from the theoretical calibrations and two from the observational ones, assuming of course that the photometry was available. For stars with $T_e \lesssim 5500^\circ$ only two determinations were made.

In Figure 39 is plotted a (M_{bol}, T_e) diagram using the data of Tables 18 and 19. The individual Hyades stars are plotted, and the solid line for temperatures $7000^\circ \geq T_e \geq 4600^\circ$ represents the mean Hyades (M_{bol}, T_e) relation. For $T_e < 4600^\circ$ the dashed line, which is Eggen's (1973, 1969c) curve for the young disk main sequence as defined by the Hyades stars and by young disk field dwarfs, will be used as the extension of our Hyades relation. Also plotted in Figure 39 are 11 subdwarfs. Nine of these subdwarfs are from the group of 27 halo stars plotted by

Table 19. Hyades stars--M_{bol} versus T_e.

Name	V	Sp	B.C.	M_v	M_{bol}	$(T_e)_{Ave}$
20	6.32	F3V	0.08	3.27	3.35	6660
22	8.34	G8V	-0.06	5.31	5.25	5300
25	9.60	K3V	-0.335	6.65	6.315	4730
26	8.63	G9V	-0.09	5.64	5.55	5490
27	8.46	G8V	-0.06	5.26	5.20	5520
29	6.88	F8V	0.03	3.84	3.87	6010
30	5.59	F0V	0.11	2.63	2.74	7320
33	5.26	A9V	0.12	2.08	2.20	7720
34	6.17	F6V	0.05	3.08	3.13	6440
35	6.80	F5V	0.06	3.54	3.60	6510
36	6.80	F6V	0.05	3.67	3.72	6485
40	6.99	G0V	0.01	3.96	3.97	5910
43	9.40	K2V	-0.23	6.31	6.08	4880
46	9.11	K1V	-0.165	6.11	5.945	5145
47	4.80	A7.5V	0.13	1.86	1.99	8010
48	7.14	F7V	0.04	4.20	4.24	6190
50	7.62	G1V	0.005	4.73	4.735	5810
51	6.97	F6V	0.05	3.72	3.77	6460
52	7.80	G1V	0.005	4.84	4.845	5815
53	5.97	F4Vn	0.07	2.90	2.97	6630
54	4.22	A7V	0.13	0.95	1.08	8230
56	4.30	A3V	0.10	1.28	1.38	8985
57	6.46	F7V	0.04	3.37	3.41	6245
58	7.53	G6V	-0.03	4.57	4.54	5590
59	7.49	F8V	0.03	4.48	4.51	6035
60	4.29	A8Vn	0.12	1.22	1.34	7220
64	8.12	G6V	-0.03	4.95	4.92	5680
65	7.42	F8V	0.03	4.46	4.49	6105
68	5.90	F0V	0.11	2.87	2.98	6990
69	8.64	G8V	-0.06	5.59	5.53	5490
73	7.85	G1V	0.005	4.82	4.825	5775
77	7.05	F7V	0.04	3.91	3.95	6130
79	8.96	K0V	-0.12	6.00	5.88	5280
82	4.78	A6Vn	0.13	1.80	1.93	8140
85	6.51	F5V	0.06	3.48	3.54	6410
87	8.58	G8V	-0.06	5.52	5.46	5440
91	8.94	K1V	-0.165	5.74	5.575	4920
92	8.66	G8V	-0.06	5.55	5.49	5460
94	6.62	F5V	0.06	3.72	3.78	6430
95	4.66	A8Vn	0.12	1.58	1.70	7770
97	7.94	G1V	0.005	4.88	4.885	5890
104	4.27	A6Vn	0.13	1.24	1.37	8420
108	4.68	A5Vn	0.13	1.31	1.44	8140
175	10.30	K4V	-0.44	6.93	6.49	4610
176	9.01	K2V	-0.23	5.96	5.73	4865

Eggen (1973, Figure 4), where halo stars are defined as having eccentricities in their galactic orbit, e, greater than 0.5. The definition of eccentricity comes from Eggen, Lynden-Bell and Sandage (1962). Seven of these nine subdwarfs are also extreme with regard to metallicity having $[Fe/H] \leq -1.0$, one (Yale 674) is too cool for an adequate composition determination, and the ninth (HD63077) has $[Fe/H] = -0.67$. In addition to Eggen's stars, two other extreme subdwarfs ($[Fe/H] \leq -1.0$), HD103095 and HD149414, which have adequate parallaxes, are also plotted. Two other stars from Eggen's group of halo objects, HD108177 and HD106038, are also found in Table 18, but were not plotted since their parallaxes are not adequate ($\pi = 0\overset{\prime\prime}{.}031 \pm 7$ and $0\overset{\prime\prime}{.}038 \pm 11$) and since Eggen plots them using distance moduli derived assuming their membership in moving groups (see Eggen 1965). The parallaxes of Table 18 give distance moduli for these two stars 2.0 to 2.5 magnitudes fainter than Eggen's moduli. Certainly the trigonometric parallaxes of HD108177 and HD106038 are not very good, but also their membership in the moving groups is anything but proven. Considering these uncertainties it was felt wiser not to plot these two subdwarfs in Figure 39.

The positions of the subdwarfs in Figure 39 confirm the previous results of Cayrel (1968), Sears and Whitford (1969) and Eggen (1973) that the cooler, extreme subdwarfs are located below the Hyades main sequence in the (M_{bol}, T_e) diagram. Sears and Whitford noted a separation between the subdwarfs and Hyades dwarfs for $G-I \gtrsim -0.05$ (Stebbins and Whitford six-color photometry) which corresponds to spectral types of G5 and later and to effective temperatures of about $5600\text{-}5700^\circ$ and less.

Cayrel showed that in the (M_{bol}, T_e) diagram the subdwarfs lie below the Hyades stars when their temperature is less than about 5600°. Eggen found that the sequences were separate for $(R-I)_K$ (Kron photometry) greater than or equal to about 0.25 which corresponds to spectral type G8 and to an effective temperature of about 5500°. Figure 39 shows that the extreme subdwarfs are distinguishable from Hyades dwarfs to an effective temperature of at least 5700°, which agrees well with the previous results. The above mentioned investigators all feel that the hotter subdwarfs do not show a separation from the Hyades in the (M_{bol}, T_e) plane due to evolution effects but that the cooler subdwarfs have not had time to evolve significantly. Unfortunately no extreme subdwarfs with adequate parallaxes and with $T_e > 5800^\circ$ are found in Table 18, and so the present data cannot provide any further comparisons between the hotter and cooler extreme subdwarfs.

However, using Figure 24 and following the discussion of the final section of Chapter 5 we can examine more closely now the temperature of the turnoff point of the subdwarfs. (In the present discussion "turnoff point" refers to the point in the (M_{bol}, T_e) diagram where the stars of a single age are the hottest and are just ready to start evolving to the right, to cooler temperatures.) Figure 24 shows the turnoff at about $(45-63)_{obs} = 0.59$ which gives $T_e \approx 6400^\circ$. Cayrel (1968, see Figure 2) suggests that the maximum temperature and turnoff of field subdwarfs occurs for $\log T_e \approx 3.8$ or $T_e \approx 6300^\circ$. However, Eggen's M_{bol} versus $(R-I)_K$ plots (1973, see Figures 4 and 5) seem to suggest that $T_e \approx 5900^\circ$ is the upper limit of the evolved halo main sequence, but

these plots are misleading in several respects. First, $T_e = 5900^o$

corresponds to $(45-63)_{obs} \approx 0.75$ or $(B-V)_{obs} \approx 0.45$ and there are many

extreme subdwarfs observed with colors bluer than these limits. (For

example, see Figures 22 and 24.) Second, the turnoff point of Eggen's

halo population is defined by five stars. Three of these have been

plotted using distance moduli assuming the star's membership in a moving

group (Eggen 1965), but the membership of these stars has never been

confirmed nor even the existence of these small Population II moving

groups proven. And, as mentioned previously two of these stars have

trigonometric parallaxes, although small and somewhat uncertain, which

give distance moduli significantly different from those used by Eggen.

Hence, the use of these three stars to define the evolving halo main

sequence is not really justifiable. Of the other two stars, one, HD63077,

does not have an extreme metal deficiency with $[Fe/H] = -0.67$ even though

the eccentricity of its galactic orbit is greater than 0.5. So perhaps

the membership of this star in the same, extreme halo population is open

to question. The fifth of Eggen's evolved halo stars is HD140283, which

is very metal poor, $[Fe/H] = -1.99$ and which does have an orbital eccen-

tricity greater than 0.5. If the subdwarf turnoff point is indeed 600 or

700° hotter than this star (T_e is about 5700° for HD140283; see Table 14),

how do we explain HD140283? Perhaps the problem is its small trigono-

metric parallax ($\pi = 0\overset{..}{.}031 \pm 7$), but there are two other possibilities.

One, as suggested by Cayrel (1968), HD140283 could be a metal-poor sub-

giant that has moved away from the turnoff at $T_e \approx 6400^o$ and is evolving

to cooler temperatures. In Figure 24 this star does appear evolved; it

has a luminosity class of IVb. However, as shown by Cayrel its trigonometric parallax does not quite fit this interpretation either. Or, two, as suggested in the final section of Chapter 5 the subdwarfs may have a range of ages, and HD140283 belongs to the turnoff of a somewhat older subdwarf population. Hence, the evolved main sequence line of Eggen's halo stars in the (M_{bol}, T_e) diagram (1973, Figure 5) may indeed represent some halo population, but it does not represent the hottest subdwarfs which are younger than the mean age corresponding to Eggen's turnoff.

At this point it would be very instructive to compare the effective temperatures of the subdwarf turnoff with the corresponding temperatures of some globular clusters. In Table 20 we give the relevant data for some well observed globular clusters. The observational data for these clusters comes from Sandage (1969a and 1969b) for M13, M15, and M92 and from Arp (1962) for M5. Sandage's observed B-V values have been corrected for reddening while Arp claims that M5 is free from reddening and so applies no corrections. In Table 20 column one gives the cluster's name, column two the observed B-V of the turnoff (corrected only for reddening), and column three the mean ultraviolet excess at some $(B-V)_{obs}$ (also given in column three) as found by Arp and Sandage. Using the values of column three plus Table 1A of Sandage (1969a) the ultraviolet excess at the turnoff is estimated; this is given in column 4 of Table 20. Then using $\delta(U-B)$ and $(B-V)_{obs}$ for the turnoff plus the blanketing corrections of Wildey et al. (1962) the correction for B-V is calculated and is listed in column 5. The B-V of the turnoff corrected

Table 20. Turnoff points of globular clusters.

Name	$(B-V)_{obs}$	$\dfrac{\delta(u-B)}{(B-V)_{obs}}$	$\delta(u-B)$ at turnoff	$\Delta(B-V)$ at turnoff	$(B-V)_{corr}$ at turnoff	T_e
M5	0.44	0.21/ 0.60	0.18	+0.13	0.57	5950°
M13	0.39	0.18/ 0.45	0.17	+0.09	0.48	6200
M15	0.36	0.22/ 0.45	0.21	+0.11	0.47	6250
M92	0.36	0.22/ 0.45	0.21	+0.11	0.47	6250

to Hyades abundance is given in column 6. Column 7 gives the effective
temperature of the globular cluster turnoffs according to the B-V cali-
bration of Johnson (1966). The temperatures of these cluster turnoffs
are in the range $6000\text{-}6250^{\circ}$ while the hottest subdwarfs have a turnoff
with $T_e \approx 6400^{\circ}$. (If any reddening corrections are needed for the sub-
dwarfs, the temperatures of their turnoff would be even higher.) Eggen's
turnoff (including HD140283) is at approximately $T_e = 5900^{\circ}$. These re-
sults present further evidence that the extreme Population II objects
represent a substantial range in ages. Or, perhaps, it could be argued
that such differences imply a range of composition (for example, see
Demarque 1967, Simoda and Iben 1968, and Iben and Rood 1970) or that the
faint-star photometry of the globular cluster turnoffs contains sig-
nificant errors (see Sandage 1964).

In Figure 40 are plotted the remainder of the stars in Table 18
which have adequate parallaxes. These stars have been divided into two
groups according to composition--mild subdwarfs with $-0.25 \geq$ [Fe/H] $>$
-1.0 and "field" stars with [Fe/H] > -0.25. Also included with the mild
subdwarfs are several stars too cool for composition determinations by
means of the calibration of Chapter 6. The division of the two groups
at [Fe/H] $= -0.25$ has been chosen since the $\delta(37\text{-}45) = +0.15$ line of
Figure 22, which seems to form a fairly good lower boundary (minimum
excess) for known subdwarfs, corresponds closely with the [Fe/H] $= -0.25$
line of Figure 27. In Figure 40 the solid line represents the Hyades
plus young disk main sequence line of Figure 39, and the dotted line
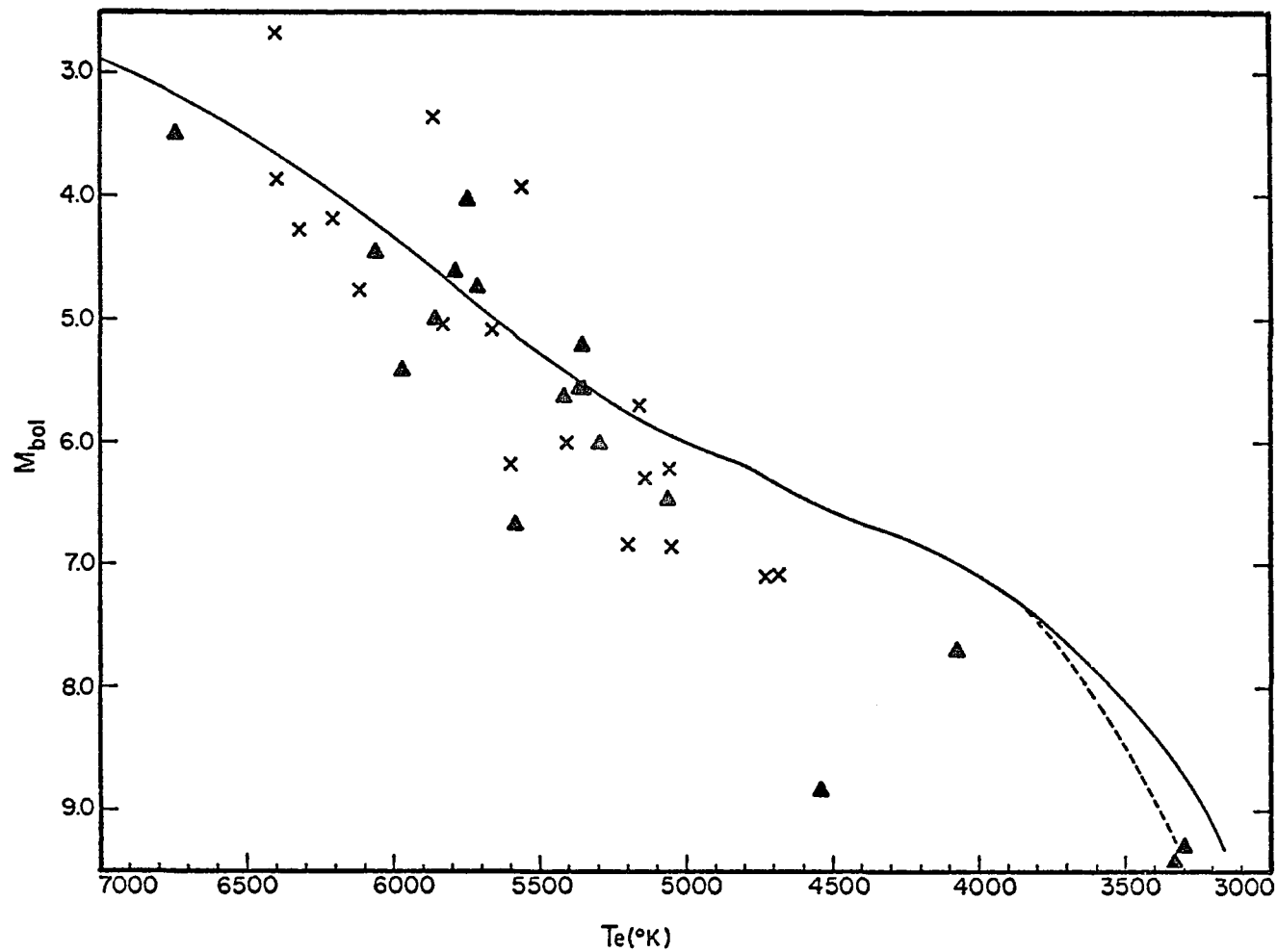(for $T_e < 3800^{\circ}$) is Eggen's (1973) old disk main sequence. As explained

Figure 40. M_{bol} versus T_e for mild subdwarfs and field stars. -- The solid line gives the locus of the Hyades-young-disk main sequence and the dashed line the old disk main sequence (Eggen 1973). The triangles are for mild subdwarfs and the X's for field stars.

earlier most of the "field" stars have been placed on our subdwarf lists

not because of their photometric or spectroscopic properties but because

their parallaxes place them 0.25 magnitudes or more below the main se-

quence in color-magnitude diagrams (Sandage and Eggen 1959). In Figure

40 the hotter "field" stars are found close below or far above the

Hyades line; the three far above the Hyades line are probably evolving--

one has class IVb and two have classes Va from Table 14. However, for

the cooler "field" stars several are noticeably below the Hyades main

sequence, especially HD74377, HD144872, HD151877, HD21677 and BD + $55^{\circ}900$.

These results do not contradict the findings of Sandage and Eggen (1959)

or Eggen and Sandage (1962), who analyzed only stars hotter than these.

However, these five stars are in disagreement somewhat with the work of

Eggen (1973), and he does not include any of these five stars in his

list of old disk stars with reliable parallaxes. Four of these five

stars (all but HD216777) come from the list of subdwarfs in Sandage and

Eggen (1959), and it is apparent in their data also (Table 1 and Figures

1, 2, and 6) that these stars are well below (~1 magnitude) the Hyades

in the (M_V, B-V) diagram but show almost no ultraviolet excess. Pagel

(1962) suggests that these K stars show almost no ultraviolet excess in

the (U-B, B-V) plane because the blanketing lines are nearly parallel to

the main sequence line for such cool stars. However, examining Figures

22 and 24 we see several cool stars, (45-63) $\gtrsim$ 1.00, which have con-

siderable 37-45 excesses and which show no evolutionary effects in the

G versus 45-63 diagram. So, it seems clear that the blanketing lines in

the 37-45 versus 45-63 diagram are not parallel to the main sequence

line. Hence, the available evidence indicates that in the temperature range of K stars there are stars which have no ultraviolet excess nor other evidence of metal deficiency and yet which are found 0.5 to 1.0 magnitude below the Hyades main sequence in the (M_{bol}, T_e) plane.

The mild subdwarfs of Figure 40 all, except for four, lie close to the Hyades main sequence (or old disk main sequence for $T_e < 3800°$) to within the errors of their trigonometric parallaxes. This peculiarity that extreme subdwarfs show a definite separation from the Hyades while mild subdwarfs (or old disk stars) with perhaps one-third the metal deficiency show no displacement has been noted previously by Cayrel (1968) and Eggen (1973, 1974). However, the four subdwarfs HD114606 ([Fe/H] = -(0.6)), HD2011891 (-0.92), Ross 484 (?), and G78-26 (?) (also in Figure 39) show significant departures below the Hyades main sequence in the (M_{bol}, T_e) plane, while other subdwarfs with similar compositions, HD6582 ([Fe/H] = -0.4), HD30649 (-0.6), and HD203608 (-0.68) for example, fall very close to the Hyades.

In Figure 41 we have plotted a $\Delta[L_H]$ versus [Fe/H] diagram, where $\Delta[L_H]$ as defined earlier is the logarithmic difference in luminosities between a subdwarf and the Hyades main sequence at constant T_e. In this diagram we have excluded all subdwarfs with small parallaxes (< 0".035), large parallax errors (> 0".008), or obvious evolutionary effects (classes IVb and IVa). For the stars with [Fe/H] $\geq$ -0.25 there are very strong selection effects involved since many of these stars have seemingly normal spectra and normal photometric qualities but have been chosen for their position below the Hyades main sequence in some HR or
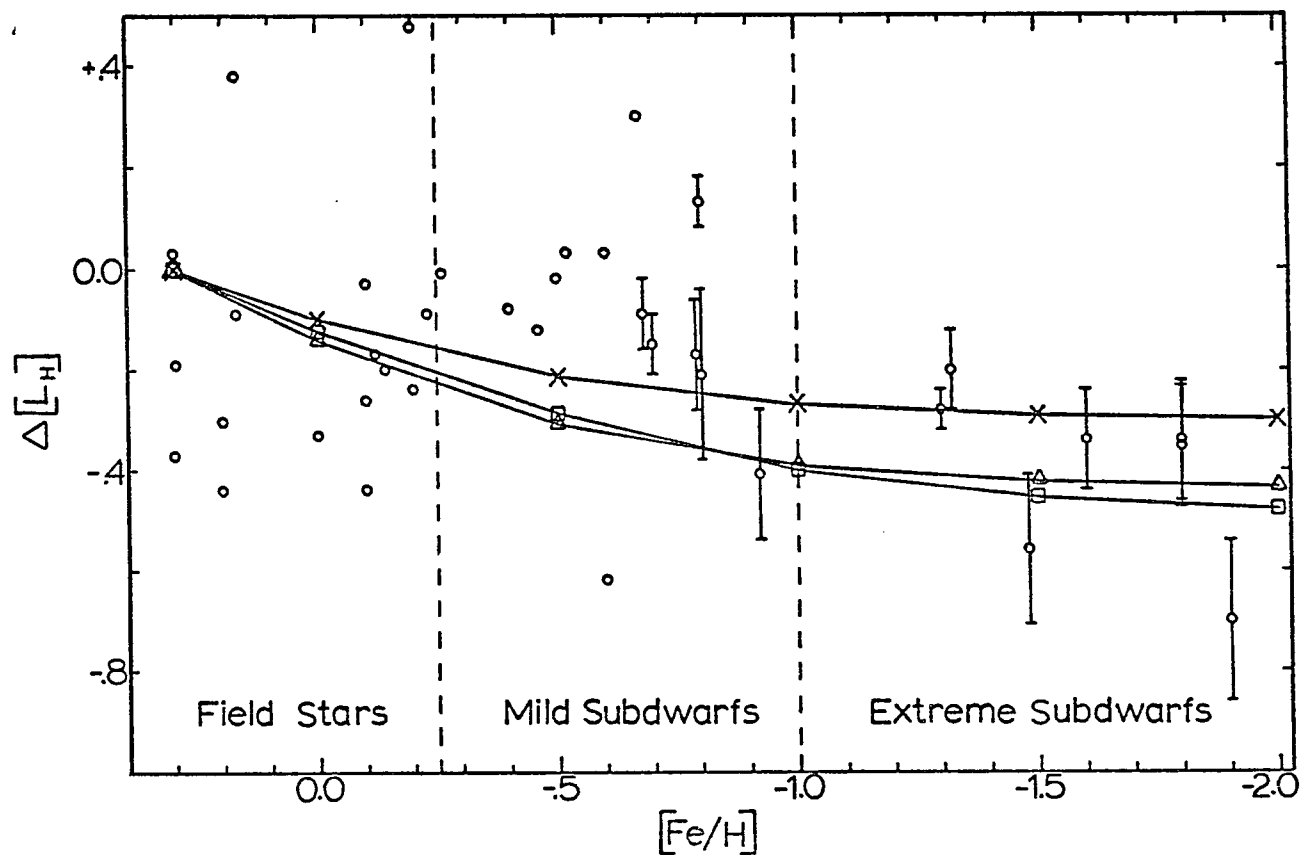
Figure 41. $\Delta[L_H]$ versus [Fe/H]. -- The circles represent the subdwarfs. Error
bars, derived from the parallax errors, have been drawn for the ex-
treme subdwarfs and for some mild ones. The X's, squares, and tri-
angles (and their corresponding curves) represent the theoretical
homology relations of Faulkner (1967), of Demarque and Schlesinger
(as quoted by Cayrel 1968), and of Copeland et al. (1970), respec-
tively.

color-magnitude diagram. Indeed, in Figure 41 nearly all of these stars with [Fe/H] $\geq$ -0.25 are fainter than Hyades stars with equal T_e. On the other hand, the mild and extreme subdwarfs should represent a more uniform group, but these stars contain sampling effects of a different sort; they have been chosen for their apparent metal deficiency in most cases and not for their parallaxes. In Figure 41 we see that in the range -0.25 $\geq$ [Fe/H] $\geq$ -0.75 the mild subdwarfs are as bright or perhaps just slightly fainter ($\sim$0.10 magnitude) than the Hyades main sequence. Somewhere in the range -0.75 $\geq$ [Fe/H] $\geq$ -1.0 the relative luminosity of the subdwarfs starts becoming sensitive to the metallicity, decreasing metallicity causing decreasing relative luminosity. At [Fe/H] = -2.0 the subdwarfs are about 1.5 magnitudes fainter than the Hyades main sequence for constant T_e. As mentioned previously these results agree in part with the observational findings of Cayrel (1968) and Eggen (1973), who found no displacements for the mild subdwarfs (metals deficient by a factor of 2 or 3 or even perhaps 10) but found a definite separation for the extreme subdwarfs. However, the observational results of Figure 41 do not agree well with homology equations derived from stellar interior models relating the stellar luminosity to the stellar hydrogen and metal abundances at constant T_e. In Figure 41 we have plotted lines corresponding to the homology relations of Faulkner (1967), of Demarque and Schlesinger (as quoted by Cayrel 1968), and of Copeland, Jensen, and Jorgensen (1970). The appropriate relation of Faulkner is log L = 2.67 log (X + 0.4) + 0.455 log (Z + 0.01) for T_e = a constant, which reduces to Δlog L = 0.455 Δlog (Z + 0.01) for constant X, where X is the mass

fraction of hydrogen and Z is the mass fraction of the metals. The relation of Demarque and Schlesinger is $\Delta \log L = 0.44 \Delta \log (Z + 0.003)$, and that of Copeland et al. is $\Delta \log L = 1.58 \Delta \log (X - 0.116) + 0.628 \Delta \log (Z + 0.009)$ at constant T_e, which reduces to $\Delta \log L = 0.628 \Delta \log (Z + 0.009)$ for constant X. In Figure 41 we have used $Z_{Hyd} = 2Z_\odot = 0.036$ for calculating the theoretical curves. We see that these curves do not follow the observations. Theory predicts the greatest changes in $\Delta[L_H]$ going from Hyades abundance to one-tenth Hyades abundance and then almost no change going to greater metal deficiencies. The observations show just the opposite behavior. Not one of the theoretical curves predict well the behavior of the mild subdwarfs, and Faulkner's models cannot even explain the extreme subdwarfs unless we assume greater helium abundances for the subdwarfs than for the Hyades stars. If we examine the complete homology relation of Faulkner, we see that increasing Y (where Y is the helium mass fraction) produces a decrease in L just like decreasing Z does. For example, taking the extreme case $X_{sbdwf} = X_{Hyd}$, $Z_{sbdwf} = 0$ and $Z_{Hyd} = 0.036$ produces $\Delta[L_H] = -0.30$, but the seven extreme subdwarfs have an average $\Delta[L_H]$ of -0.40, and so we need $X_{sbdwf} < X_{Hyd}$. However, having the helium abundances of the subdwarfs greater than that of the Hyades is completely unacceptable considering their relative ages and the enrichment sequence of the interstellar material. In Table 21 we give helium abundances derived from Faulkner's equation using various starting assumptions. (This approach is similar to that of Strom and Strom 1967.) In this table $[\overline{Fe/H}]$ and $\Delta[\overline{L_H}]$ are the average measured values of each group, Z_{sbdwf} is derived from $[\overline{Fe/H}]$ assuming

Table 21. Subdwarf helium abundances.

Group	$[\overline{Fe/H}]$	$\Delta[\overline{L_H}]$	Z_{sbdwf}	Z_{Hyd}	X_{Hyd}	Y_{Hyd}	Y_{sbdwf}
Extreme	-1.60	-0.40	0.0005	0.018	0.65	0.332	0.522
Extreme	-1.60	-0.40	0.0005	0.036	0.65	0.314	0.444
Mild	-0.65	-0.11	0.004	0.018	0.65	0.332	0.322
Mild	-0.65	-0.11	0.004	0.036	0.65	0.314	0.226
Field	0.01	-0.13	0.018	0.018	0.65	0.332	0.444
Field	0.01	-0.13	0.018	0.036	0.65	0.314	0.361
Extreme	-1.60	-0.40	0.0005	0.036	0.75	0.214	0.353
Hypothetical	$-\infty$	-0.40	0.0000	0.036	0.75	0.214	0.343

Z_o = 0.018, Z_{Hyd} and X_{Hyd} are the Hyades' values varied within acceptable limits, and Y_{sbdwf} is the derived subdwarf helium abundance. The problem with Faulkner's models is easily seen by comparing the last two columns of Table 21, Y_{Hyd} and Y_{sbdwf}, especially for the extreme subdwarfs. On the other hand the models of Demarque and Schlesinger and of Copeland et al. can explain the extreme subdwarfs by only varying Z at constant Y, but these models show an even larger discrepancy for the mild subdwarfs. The conclusion then seems to be that the comparison of models and observations indicates no helium deficiency for the subdwarfs but this conclusion is very uncertain since the models are not entirely adequate.

Figures 39, 40, and 41 do seem to disagree with the observational results of Eggen in other respects. For [Fe/H] < -1.0 the observed points of Figure 41 seem to suggest that the luminosity decreases continuously and fairly rapidly with decreasing metal content--$\Delta \log L \approx 0.4$ for Δ[Fe/H] ≈ 0.6. Also, the theoretical curves of Figure 41 indicate that there should be a continuous variation of the relative luminosity as a function of the composition, and the observational points of this figure show that indeed there are a few intermediate subdwarfs with luminosities between those of the Hyades and of the extreme subdwarfs. However, Eggen (1973, 1974) finds a separate, fairly narrow subdwarf sequence. Of course the discrepancy might be due to errors in the observed trigonometric parallaxes. In Figure 41 the vertical error bars of the seven extreme subdwarfs and for a few of the mild subdwarfs indicate only the errors arising from the parallaxes, but it appears that

the parallax errors alone are not large enough to explain the discrepancies. The relative luminosity does seem to decrease significantly with decreasing metallicity for these extreme subdwarfs, and there are a few mild subdwarfs (or old disk stars) intermediate between the extreme subdwarfs (halo stars) and the Hyades main sequence. Eggen's narrow, separate subdwarf sequence would be consistent with Figure 41 if most of his subdwarfs fell within a fairly narrow composition range. In Figure 42 is plotted a histogram showing the number of subdwarfs per 0.1 interval in [Fe/H]. The compositions have come from Table 14, and in total 85 stars are plotted. The only subdwarfs excluded are those with contaminated photometry, those with extreme evolutionary effects (luminosity classes II and III), or those with [Fe/H] outside the range $-0.2 \geq$ [Fe/H] ≥ -2.0. Indeed, in Figure 42 we see a fairly sharp peaking of composition around [Fe/H] = -1.4. In fact, nearly 50% of the extreme subdwarfs occur in the range -1.3 to -1.6, which implies in Figure 41 a range in log L of 0.15 or 0.20 and $\Delta M_{bol} \approx 0.35$ to 0.50 magnitude. This seems to fit fairly well the observed dispersion of Eggen's subdwarf sequence (1973, Figure 4), which Eggen attributes to parallax errors alone. In Figure 39 of the seven subdwarfs which are below the Hyades main sequence and which are in common with Eggen's halo stars three have [Fe/H] in the range -1.3 to -1.6 and one is too cool for a composition determination; that is, approximately half lie in the indicated composition range. And, from Figure 41 we see that [Fe/H] = -1.4 or -1.5 implies $\Delta[L_H] \approx -0.35$ or $\Delta M_{bol} \approx -0.9$ magnitude, and Eggen (1973, 1974) claims that the halo, extreme subdwarf sequence is 0.75 to 1.25 magnitudes below
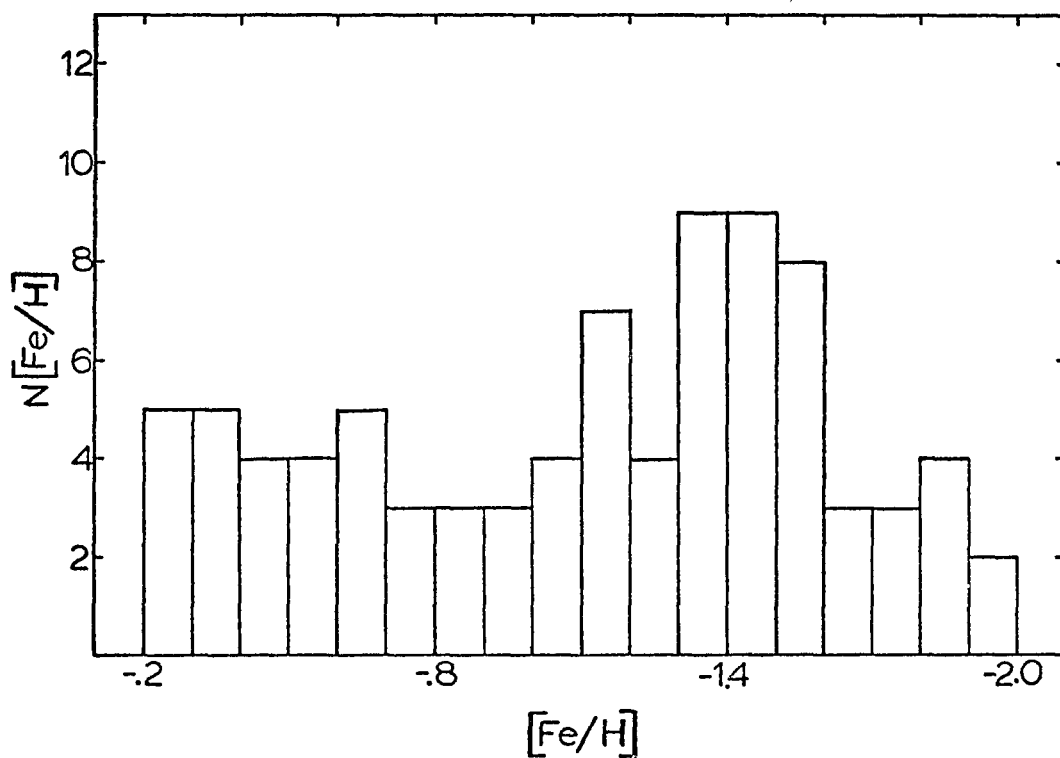
Figure 42. A histogram of N[Fe/H] versus [Fe/H]. -- The number of subdwarfs per 0.1 interval in [Fe/H] is plotted as a function of [Fe/H].

the Hyades. One should also note in Figure 41 an absence of parallax stars between [Fe/H] = -0.8 and -1.3, and in Figure 42 a minimum in the subdwarf numbers between [Fe/H] = -0.7 and -1.1. Such deficiencies at the indicated compositions could lead to the observed separation of Hyades and subdwarf sequences if indeed $\Delta[L_H]$ does depend on [Fe/H] in the manner indicated. Of course, Figure 42 probably represents a combination of real, physical effects plus selection effects. The edge of the peak at [Fe/H] = -1.3 (or possibly at -1.1) is most certainly caused by real plus selection effects since there is less and less likelihood with increasing metallicity that spectroscopists and photometrists will identify a star as a subdwarf. However, at [Fe/H] = -1.0 this will not introduce too much of a sampling effect since $\delta(U-B) \approx +0.18$ for early G stars with this abundance (Wallerstein 1962). There also exists the strong possibility that the absence of stars with [Fe/H] $\gtrsim$ -1.3 results because such mild subdwarfs have smaller space velocities and so have not received equal attention in the various proper motion surveys; many stars are selected as Population II candidates from such surveys and are later confirmed as subdwarfs spectroscopically. The drop in numbers at [Fe/H] = -1.6 in Figure 42 is probably real and tells us something about the metal content of the interstellar medium when the majority of extreme subdwarfs were forming. In any case Figure 42 represents fairly well the total sample of extreme and mild subdwarfs, which is available also to Eggen, and explains fairly well the discrepancy between Figure 41 and Eggen's separate subdwarf sequence.

The following conclusions can be drawn from the preceding discussions: (a) Our techniques of deriving effective temperatures and especially bolometric magnitudes give results in the (M_{bol}, T_e) plane which agree with previous investigations (Cayrel 1968, Sears and Whitford 1969, Eggen 1973) thereby giving confidence in these techniques. (b) Alternatively, our results confirm the previous findings that for T_e less than about 5700° the subdwarfs are separated from the Hyades main sequence in the (M_{bol}, T_e) diagram. (c) The turnoff temperature of the field subdwarfs when compared to the respective temperatures of globular clusters and to the temperatures of such evolved subdwarfs as HD140283 gives support to the idea that, if these stars are chemically similar, the extreme Population II objects did not form all at once but over a significant time interval. (d) For extreme subdwarfs their relative luminosity (compared to the Hyades main sequence) depends upon their metallicity, decreasing metallicity causing decreasing relative luminosity. For mild subdwarfs the luminosity is nearly that of the Hyades stars independent of metallicity. (e) The available stellar models do not indicate any significant helium deficiency of the extreme subdwarfs with respect to the Hyades stars. (f) In the number-of-stars versus composition histogram a fairly clear peak occurs at [Fe/H] = -1.3 to -1.6.

The Evolutionary Status of Subdwarfs

In this section we will use the G versus 45-63 color-color diagram plus a number of "blanketing" curves for individual stars to more clearly understand the evolutionary status of the subdwarfs.

In Figure 43 we have replotted the G versus 45-63 diagram of

Figure 24 but now only the extreme subdwarfs with [Fe/H] $\leq$ -1.0 are

plotted. The Hyades main sequence line and the subgiant and giant lines

have been reproduced exactly as in Figure 24. The dashed lines of

Figure 43 mark out five groups of subdwarfs, numbered one to five, plus

an outer envelope for the entire set of subdwarfs (excluding only two

"blue stragglers"). The five numbered regions include exactly the same

subdwarfs as regions one through five of Figure 22. Also plotted in

Figure 43 at 45-63 = 1.270 and G = 0.546 is the red giant HD122563 which

has an extreme metal deficiency (Wallerstein et al. 1963).

The first claim to be made from Figure 43 is that the outer

envelope, which is marked by letters a, b, c, d, e, and f, defines

roughly the locus that the stars of a globular cluster would give. Un-

fortunately no 13-color photometry of individual globular cluster

stars exists, and so this point cannot be proven explicitly. However,

by comparing the features of Figure 43 with a normal V versus B-V

diagram of a globular cluster the proof can be made by analogy. The

index 45-63 measures primarily the effective temperature and so is direct-

ly analogous to B-V. The G index measures primarily the surface gravi-

ties of stars, as shown in the preceding chapter, while V or M_V gives

an indication of the stellar luminosities. It is known that at constant

T_e (and for unique mass-luminosity relations) the surface gravity is a

monotonically decreasing function of the luminosity; for example, this

fact is used in the MK two-dimensional classification system for stellar

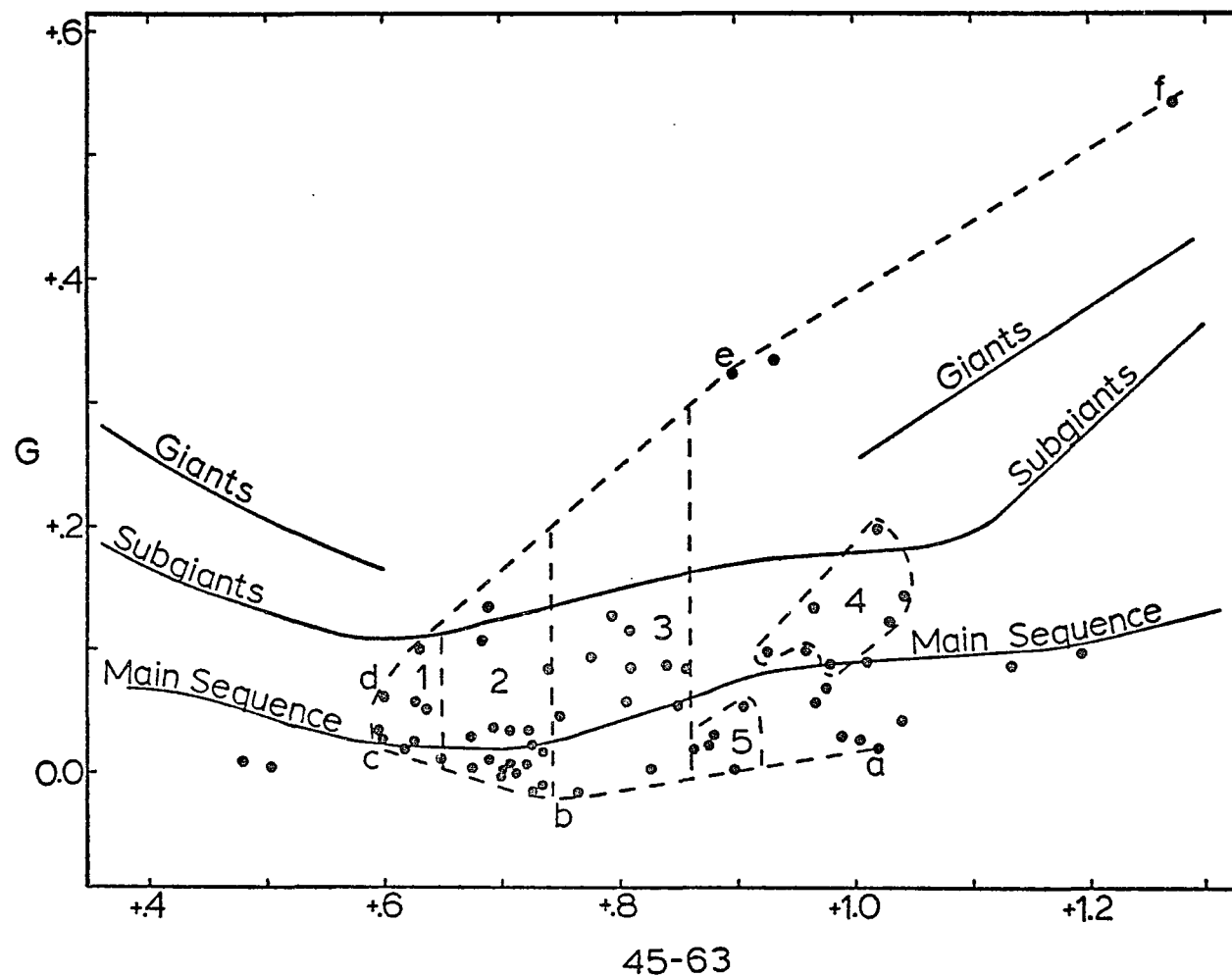spectra. Hence, there should be a one-to-one mapping of points in the

+.6

+.4

+.2

G

0.0

Giants

Subgiants

Main Sequence

Giants

Subgiants

Main Sequence

f

e

d 1
c   2   3   4
        5
b   a

+.4   +.6   +.8   +1.0   +1.2

45-63

Figure 43.   G versus 45-63 for the extreme metal-poor objects ([Fe/H] $\leq$ -1.0). -- The
filled circles are for the extreme subdwarfs plus HD122563 (at 45-63 = 1.270
and G = 0.546). Other features of this diagram are either the same as in
Figure 24 or are explained in the text.

G versus 45-63 diagram to points in the V versus B-V diagram for extreme Population II objects. We claim that in Figure 43 stars along and slightly above the dashed line segment "abc" (but beneath the main sequence line) correspond to the evolving main sequence of a globular cluster where stars between "a" and "b" are nearly unevolved and close to the "zero-age" line while stars along the segment "bc" are showing significant evolutionary effects. The stars of segment "ab" (especially for the interval $+0.8 \lesssim 45\text{-}63 \lesssim +1.0$) are in the same temperature range as the cool subdwarfs of Figure 39 which show a definite displacement below the Hyades main sequence in the (M_{bol}, T_e) diagram and which are thought (Eggen 1973, Cayrel 1968, Sears and Whitford 1969) to be unevolved. The envelope "bc" does show a significant upward deviation from the straight line of envelope "ab," and since in this G versus 45-63 diagram an upward displacement indicates evolution (or decreasing surface gravity), we conclude that indeed the hotter subdwarfs ($T_e \gtrsim 6000^{\circ}$) have evolved significantly. This agrees with the suggestion of Eggen (1973) and explains why the hotter subdwarfs move onto the Hyades main sequence in the M_V versus B-V diagram when blanketing corrections are applied (Sandage and Eggen 1959, Eggen and Sandage 1962).

The stars along and slightly to the right of the envelope segment "cd" mark the turnoff of the "globular cluster" as discussed previously. The stars close to the segment "de" are the metal deficient subgiants of our "globular cluster," where the two stars at point "e" are BD$-9^{\circ}5491$ and BD$+41^{\circ}3735$, which were mentioned in the final section of Chapter 5. Finally, the segment "ef" marks the red-giant

branch of our "cluster" where the star at point "f" is HD122563. That
the segment "ef" lies more than 0.1 magnitude above the giant line de-
fined by the field giants corresponds with the fact that Population II
red giants are 2 to 4 magnitudes brighter than Population I red giants.
(For example, see Figure 1 of Sandage 1969a.) Since Population I and II
masses are probably (?) not very different, a difference of luminosities
translates directly into a difference of surface gravities, and so the
Population II red giants show significantly smaller gravities in Figure
43 than the field giants.

However, our analogy between the envelope of Figure 43 and a
globular cluster color-magnitude diagram may be fraught with difficulties
because we know that the stars plotted represent some range in composi-
tions and because we do not know whether the stars of Figure 43 all have
the same age. In fact, we have argued in the previous section that
there is evidence for the view that the subdwarfs did not form all at
once but over a significant time interval. In Figure 43 we see further
evidence of this. Regions 1 and 2 show significantly evolved stars as
expected, but regions 3 and 4 also include subdwarfs that have evolved
from the lower envelope "abc" and could not possibly have come from the
turnoff at "cd" if they are evolving in the manner seen in the color-
magnitude diagrams of extreme globular clusters. That is, in a globular
cluster with extreme metal deficiency a star leaving the turnoff steadily
increases in luminosity as its temperature decreases (for example, see
the diagrams of Sandage 1969a or of White 1970); this implies steadily
decreasing surface gravity. But to go from the turnoff at "cd" to one

of the evolved subdwarfs of regions 3 or 4 requires a considerable drop in the temperature with almost no change in the gravity. Hence, the evolving subdwarfs of regions 3 and 4 probably represent older populations than the turnoff of region 1. So, the extremely evolved stars of the envelope segment "ef" may not belong with the same age group as the turnoff at "cd" but may belong with the evolved stars of one of the older groups. However, the observational work of Sandage (1969a, Figure 1) and various theoretical studies of globular clusters (Iben and Faulkner 1968, Rood and Iben 1968, Iben and Rood 1970, Wagner 1974) indicate that as long as the composition does not vary too widely the position of the red giant branch in the (luminosity, temperature) plane is fairly constant independent of age; the red giants of extreme Population II globular clusters probably have the same luminosities to within one magnitude at constant T_e. Hence, the line "ef" in Figure 43 represents approximately the Population II red giant branch regardless of which turnoff we consider. That is, the outer envelope "abcdef" roughly represents the locus of a globular cluster.

Figure 43 can also be used to add further evidence to our contention of Chapter 5 that the surface gravities of unevolved subdwarfs are greater than the gravities of Hyades stars with equal T_e. In the final section of the previous chapter we derived a surface gravity calibration relating δG to log g. For this calibration, which is plotted in Figure 38, only the hotter subdwarfs could be used, including the subdwarfs of region 1 (of Figure 43) and the six hottest of region 2. In Figure 38A we see that subdwarfs with surface gravities equal to the

Hyades' surface gravities are only 0.01 or 0.02 magnitude below the main sequence line of Figure 43; as we said before, the G index is nearly independent of blanketing. Also, we note in Figure 38A that of the 15 hot, extreme subdwarfs used (and certainly all of these are significantly evolved) six have surface gravities in the range of the Hyades stars, six others have surface gravities with logarithms only 0.1 or 0.2 smaller than the Hyades gravities, and only three subdwarfs have gravities significantly different from the Hyades'. Now in Figure 43 we see that the subdwarfs close to the line "ab" are 0.04 to 0.07 magnitude below the main sequence line, and since the G index has only a 0.01 to 0.02 magnitude residual blanketing effect, we are forced to conclude that the unevolved subdwarfs have higher surface gravities than the Hyades stars. (We should also point out that Figure 1 of Johnson, Mitchell and Iriarte (1962) shows that throughout this temperature range, $45\text{-}63 \gtrsim 0.6$, the Hyades stars deviate very little from the zero-age main sequence; that is, they are unevolved.)

To re-emphasize the above arguments and to make clear our understanding of the 13-color indices, the "blanketing" curves of some individual stars are given in Figures 44 to 47. In Figure 44 we give the "blanketing" curves of BD$-9°$5491 and BD$+41°$3735, which are the evolved "subdwarfs" at point "e" of Figure 43. These curves show a large depression of the 33 and 35 filters with respect to the 37 filter and also a large excess for the 37-45 index. From the diagrams and discussion of Chapter 5 it is obvious that these are metal poor and highly evolved-- Population II red giants. In Figure 45 are given the "blanketing" curves
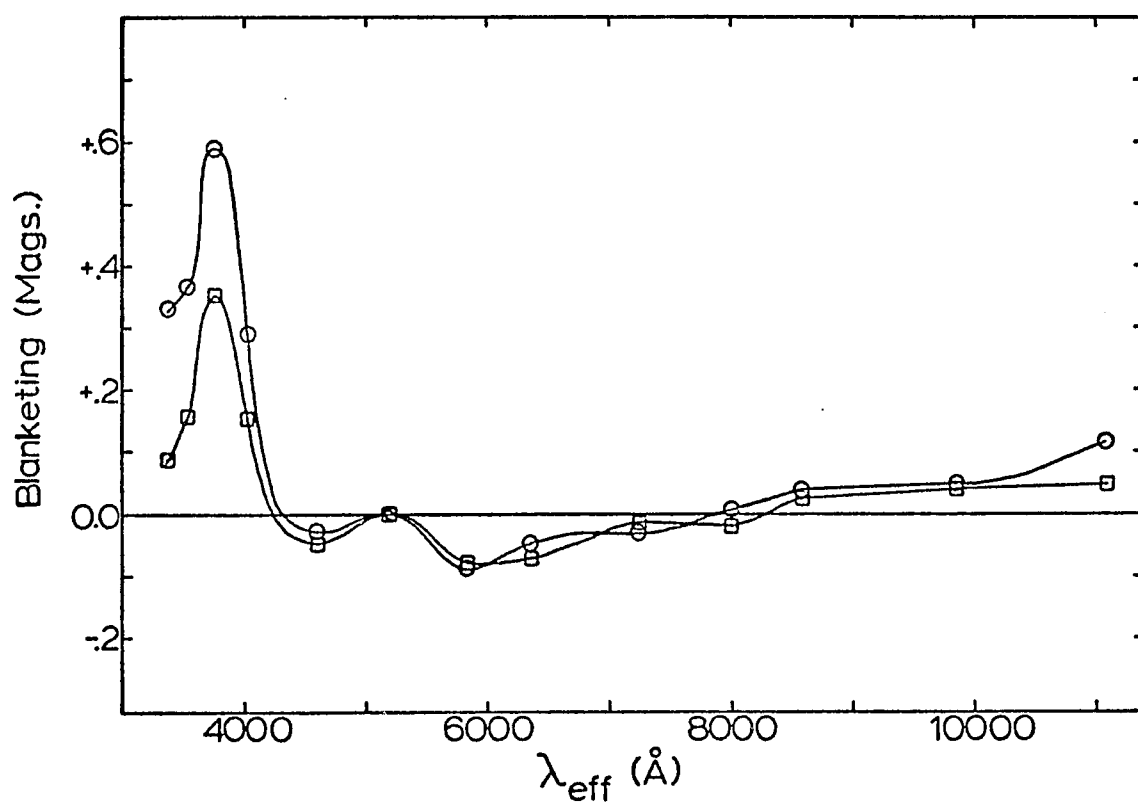
Figure 44. Observational blanketing curves for -9°5491 and for +41°3735
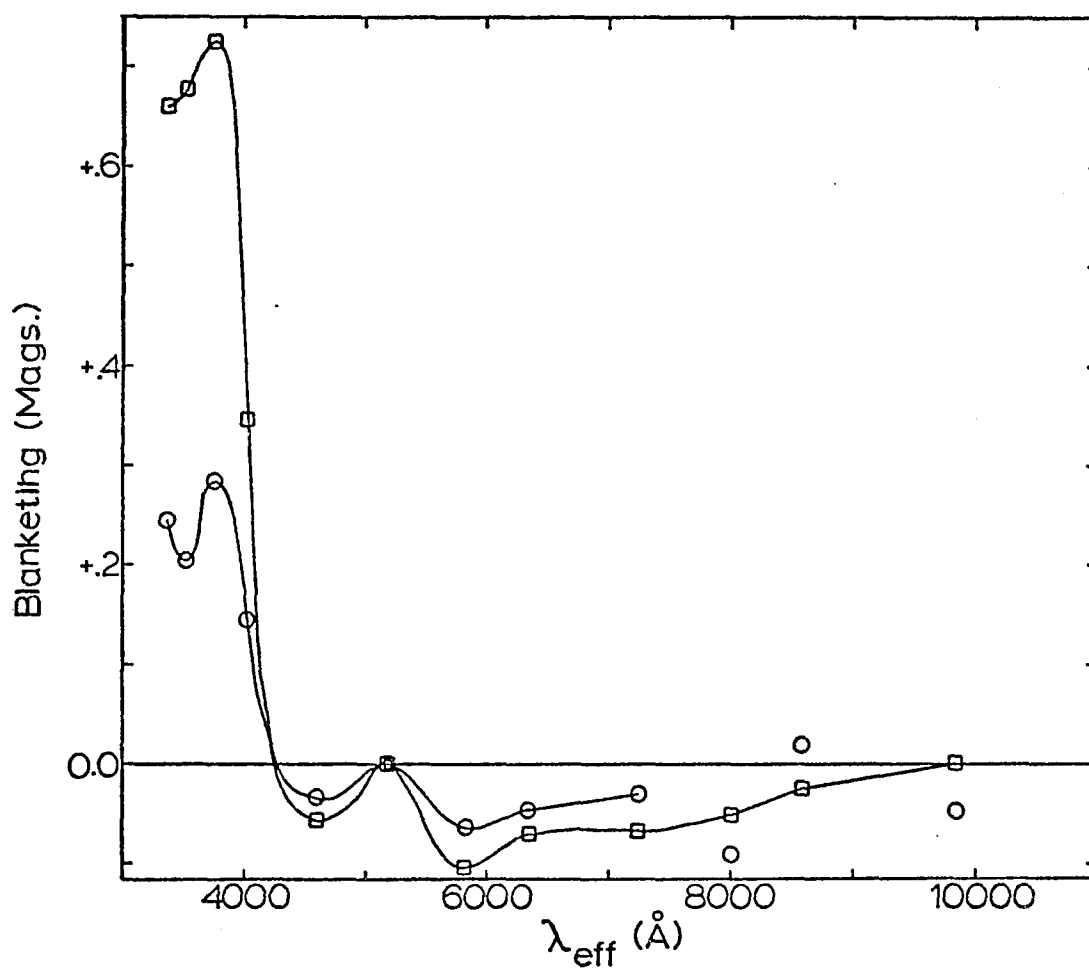-- The squares are for +41°3735 and the circles for -9°5491.

Figure 45. Observational blanketing curves for +44°1910 and for +13°3683. -- The squares represent +13°3683 and the circles +44°1910.
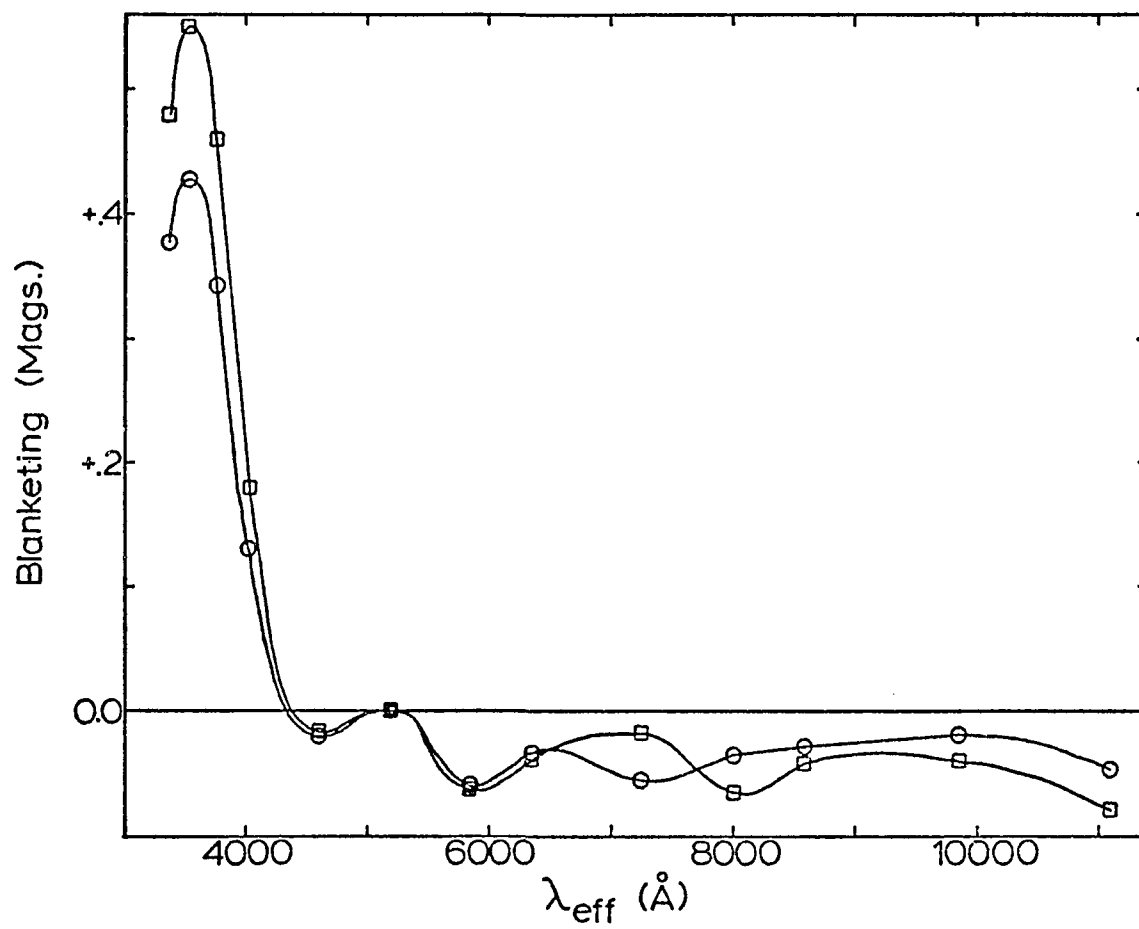
Figure 46. Observational blanketing curves for BS 4550 and for +31°1684.
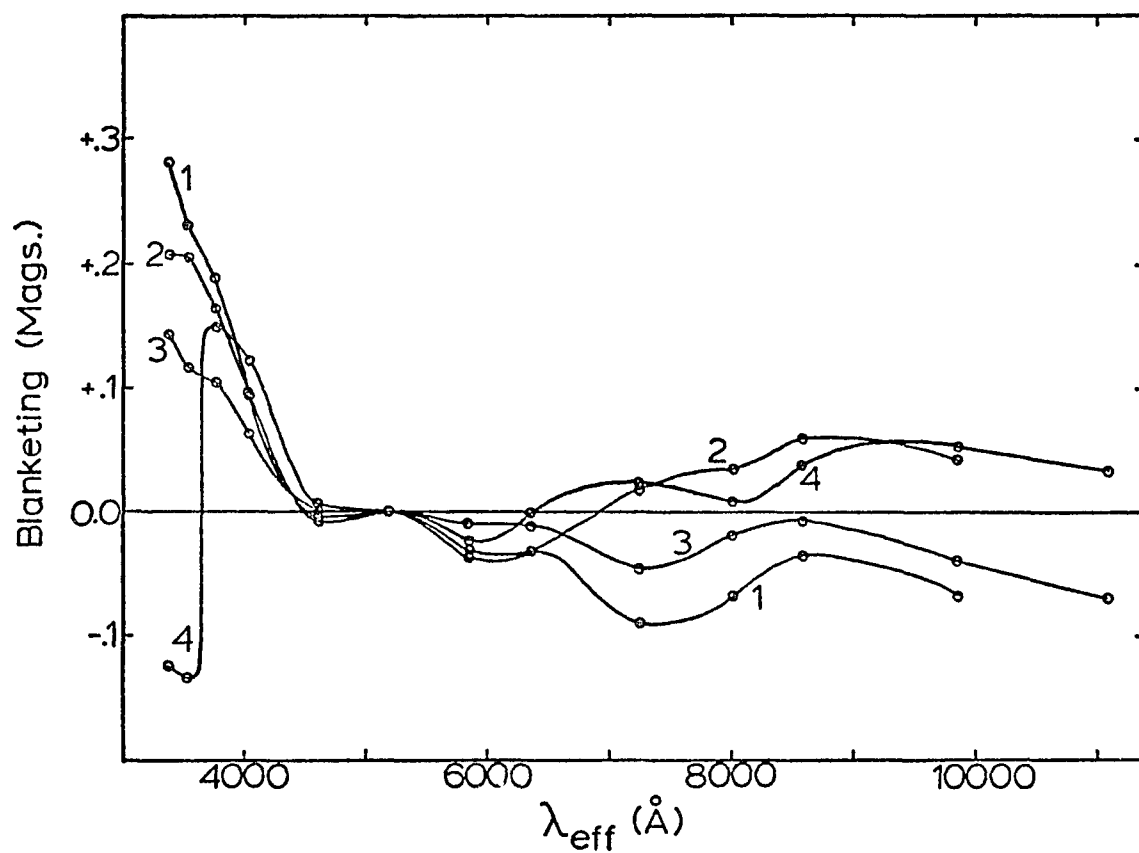   -- The squares are for +31°1684 and the circles for BS 4550.

Figure 47. Observational blanketing curves for four of the hottest metal-poor objects. -- Curve 1 represents -12°2669D, curve 2, +25°1981, curve 3, +30°2536, and curve 4, +25°3344.

for the stars BD+44°1910 and BD+13°3683. Both of these stars have
luminosity classes of IVa, lying slightly above the subgiant line of
Figure 43. BD+44°1910 has 45-63 = 0.688 and is the most evolved star of
region 2; BD+13°3683 has 45-63 = 1.018 and is the most evolved star of
region 4. Again we see a depression of the 33 and 35 filters with
respect to 37 and a large excess in the 37-45 index. The important
point to notice is the curve of BD+13°3683. This curve shows exactly
the shape we would expect (from the discussion of Chapter 5) for a metal-
poor, evolving star, and yet this subdwarf is cool (T_e = 5075°), and its
position in Figure 43 precludes the possibility that the star has evolved
from the turnoff at "cd"; in Figure 43, BD+13°3683 is nowhere near the
upper envelope "def." In fact all of the stars of region 4 present
this behavior--they are cool, evolved from the lower envelope "abc,"
and yet not near the upper envelope "def." These stars, as well as the
evolved subdwarfs of region 3, present the strongest evidence suggesting
that the subdwarfs were not all formed at once but over a significant
time interval.

In Figure 46 we give "blanketing" curves for two subdwarfs which
are along the lower envelope "abc" in Figure 43, BS4550 (HD103095 or
Grm 1830) and BD+31°1684. BS4550 has 45-63 = +1.003 and BD+31°1684,
45-63 = +0.895. These two curves show evidence of high surface gravity
and extreme metal deficiency and should be contrasted with the two curves
of Figure 45. In Figure 47 are shown the curves for all of the "sub-
dwarfs" (extreme, mild, and otherwise) which are bluer than the turnoff
at 45-63 ≈ +0.59. There are four such stars--BD+25°1981, BD-12°2669D,

BD+30°2536, and BD+25°3344. As mentioned in Chapter 5 the two stars
BD+25°1981 and BD-12°2669D can be considered "blue stragglers" for the
"globular cluster" of Figure 43 (Sandage 1964). Perhaps BD+30°2536,
which has a smaller metal deficiency ([Fe/H] = -0.46), is also in this
class. The blanketing curves of these three stars are not particularly
different nor unexpected; the curve of BD-12°2669D is somewhat unusual
but this results because its photometry has been contaminated by a near-
by star, and the curve of BD+25°1981 indicates that its surface gravity
is larger than that of Hyades stars of equal T_e. The star BD+25°3344
(HD161817) has 45-63 = 0.293 and G = +0.355, and its curve shows evi-
dence for a very small surface gravity as well as extreme metal de-
ficiency ([Fe/H] < -2.0 from Table 14). This star, which is thought to
be a Population II horizontal branch star, has been analyzed spectro-
scopically by Kodaira (1973) and by Kodaira, Greenstein and Oke (1969),
who found log g ≈ 2.9 and [Fe/H] ≈ -1.6.

Returning now to the question of the evolved subdwarfs, we
present Table 22 which gives the 14 most highly evolved stars from our
lists. Inclusion of a star in this list depends strictly on its posi-
tion in Figure 43 relative to the Hyades main sequence and subgiant
lines. The first three stars are the extreme cases already mentioned
and are easily explainable. The last three stars of this list have
Population I compositions and will be excluded from further discussions.
Of the remaining eight stars, BD-13°482, BD-17°484, and BD+44°1910 are
found in regions 1 and 2 of Figure 43 and can be easily explained as
subdwarfs which are evolving from the turnoff at "cd." But the other

Table 22. Evolved "subdwarfs."

Name	45-63	T_e	Lum. Class	[Fe/H]
$+25^o3344$	+0.293	~7595°	III?	(<-2.0)?
$+41^o3735$	+0.895	5360	II	(-1.2)
-9^o5491	+0.931	5270	II	(<-2.0)
Regions 1 and 2:				
-13^o482	+0.630	6215	IVb	-1.55
-17^o484	+0.682	6190	IVb	-1.82
$+44^o1910$	+0.688	6110	IVa	-1.57
Regions 3:				
-10^o4149	+0.793	5725	IVb	-1.99
-21^o4009	+0.809	5630	Va	-1.39
Regions 4:				
G188-30	+0.964	5270	Va	(<-2.0)
$+13^o3683$	+1.018	5075	IVa	(<-2.0)
G10-4	+1.040	5105	IVb-Va	(<-2.0)
$+20^o3926$	+0.643	6405	Va	+0.17
-26^o957	+0.774	5810	IVb	-0.32
$+11^o3833$	+0.960	5560	IVb	(>+.3)

five evolved subdwarfs lead to some interesting possibilities as suggested before. BD-10°4149 (HD140283) and BD-21°4009 are found in region 3 of Figure 43 and undoubtedly belong to the subdwarf turnoff sketched by Eggen (1973, Figures 4 and 5). As we mentioned previously Eggen's turnoff is about 500° cooler than the one of Figure 43. If we now consult globular cluster time-constant loci (isochrones) from the metal deficient stellar models of Demarque (1967), Iben and Faulkner (1968), Rood and Iben (1968), Iben and Rood (1970), and Wagner (1974), we come to some surprising conclusions. If we take the helium abundance in the range Y = 0.2 to 0.3, which seems reasonable considering the results of the first section of this chapter and the discussion of Iben (1974), then the subdwarf turnoff at 45-63 $\approx$ +0.6 ($T_e \approx 6400°$) corresponds to an age in the range (12-16)X10^9 years, which presents no problems. For the stars in region 3 of Figure 43 a turnoff at 45-63 $\approx$ +0.75 or $T_e \approx$ 5900° seems fairly reasonable and fits well the curves sketched by Eggen (1973). This turnoff temperature implies an age of 19 x 10^9 years or greater; the isochrones of Demarque give an age of (19-20) x 10^9 while the results of Iben, Faulkner, Rood and Wagner give ages in excess of 20 x 10^9 years. With these ages we are beginning to feel a bit uneasy. For the evolved stars in region 4 of Figure 43 a turnoff at 45-63 $\approx$ +0.85 or $T_e \approx$ 5700° is possible; if anything, 45-63 $\approx$ +0.85 is too blue. With this temperature an age in excess of 20 x 10^9 years is obtained for all of the models; some of the models (Iben and Rood 1970) even suggest an age greater than 25 x 10^9 years. These ages are uncomfortably large since the most recent determination of the Hubble time (Sandage and Tammann 1975) is in the range (17-20) x 10^9 years.

Hence, the subdwarf ages present us with two rather significant puzzles. First, the evolving subdwarfs of region 4 of Figure 43 require evolution times on the order of or larger than the Hubble time. To circumvent this difficulty we might claim that we really do not understand the compositions of these subdwarfs. For example, the homology relations of Faulkner (1967) and of Copeland et al. (1970) show that from a stellar interiors point of view decreasing helium content causes decreasing surface gravity (for T_e = constant), and from a stellar atmospheres point of view Strom and Strom (1967) argue that decreasing atmospheric helium content mimicks decreasing gravity. However, to use this argument to explain the large range of G values of subdwarfs with 45-63 ≈ +1.0 (as seen in Figure 43) is unsatisfactory in two respects. First, we have no reason to suspect that subdwarfs are not a fairly homogeneous class of objects; there is no reason to suspect that large differences in helium content should occur. Second, Strom and Strom (1967) argue that changing Y from 0.35 to 0.00 causes the log of the apparent surface gravity to change by about 0.2, but in Figure 43 at 45-63 ≈ +1.0 the subdwarfs seem to have a range of log g about as great as the range from the main sequence stars to giants, or at least Δlog g ≈ 1.5.

Or, perhaps we do not really know the true metal abundance of these stars in region 4. As shown in Figure 23 of Chapter 5, for stars with 45-63 ≳ +1.0 the 37-45 index starts becoming sensitive to evolutionary changes, and so for these stars which are evolving we would overestimate their metal deficiency. This would explain their unusual

positions and extreme ultraviolet excesses in Figure 22. Also, if their

metal content is not very small but more nearly that of Population I

stars then we have greatly overestimated their evolution times (for

example, see Figures 5 and 7 of Demarque 1967). However, all of the

stars of region 4 have subdwarf spectral classifications, large U-B

excesses, and/or Population II kinematic characteristics (Eggen 1964,

1969a). Perhaps then these stars of region 4 are not as metal deficient

as given in Table 14, (< -2.0), but certainly their [Fe/H] values are

not significantly different from the values -1.4 or -1.5 which are

typical of most subdwarfs. We are still faced then by the large evolu-

tion times.

The second puzzle arising from Figure 43 and from the subdwarf

evolution times is the range of ages implied. From the turnoff at "cd"

to the evolved stars of region 4 we need a range of at <u>least</u> 4×10^9

years. This conflicts strongly with the galactic collapse model of

Eggen, Lynden-Bell and Sandage (1962) that has the globular clusters and

other metal-poor objects form in a period less than one galactic rotation,

2×10^8 years. However, in agreement with our observations are the

results of Rood and Iben (1968), who find that assuming nearly uniform

helium abundances, variations in globular cluster color-magnitude

diagrams can be explained theoretically using age variations of at least

2×10^9 years. Rood and Iben also suggest a mechanism by which metal-

poor stars with highly eccentric galactic orbits could be produced over

a considerable time interval instead of during a very short collapse

phase. In their model they postulate that during the early phases of

the galaxy, equilibrium of the existing gaseous material was maintained between three sets of forces--gravitational forces, gas pressure, and "centrifugal forces." (Eggen et al. (1962) argued that the gas pressure must be negligible.) When a gas cloud condenses into a star, it is essentially released from the gas pressure and is free to plummet toward the center in a highly eccentric orbit. Such a process might continue indefinitely or at least until some process triggered the collapse which did reduce the Galaxy to its present dimensions and which produced the majority of stars in the solar neighborhood (Dixon 1965, 1966). For example, triggering of the collapse might occur if the Galaxy's rotational rate decreased due to torques produced by another closely passing galaxy. Or, perhaps during the early stages of the Galaxy star formation was a fairly improbable event, and the metal enrichment of the interstellar material occurred fairly slowly. But finally the metal content of the gas reached a level that star formation was enhanced (for example, see Talbot and Arnett 1973). More rapid star formation would lead to faster metal enrichment (as the most massive stars burned themselves out and returned their material to the interstellar medium by supernovae explosions), and so the whole process would snow-ball. As the gas went into forming more and more stars, the gas pressure supporting the gaseous part of the galaxy would diminish, and the galaxy would collapse. During this collapse the metal content of the interstellar medium would rise quickly, and so the formation of further metal-poor stars would abruptly cease. Such a scenario explains at least roughly the features observed in Figure 43. The turnoff at $T_e \approx 6400^\circ$ represents

the last metal-poor stars formed, during and slightly before the rapid collapse. The evolved subdwarfs of regions 3 and 4 were formed much earlier during the quiescent period preceding the collapse.

To investigate these ideas in greater detail we present Table 23 which gives the kinematic properties of the extreme subdwarfs in groups 1 through 5. Column one gives the group number, column two the number of stars in each group, and columns 3, 4, and 5 the average galactic velocity components, where U is directed away from the galactic center, V is toward the direction of galactic rotation, and $|W|$ is the absolute value of the component toward the north galactic pole. Columns 6, 7, and 8 give the median values and averages of the apogalactic distances, perigalactic distances, and eccentricities of the galactic orbits, and column 9 gives the average value of $\Delta(37-52)$. The values of the first five rows come from Eggen (1964), who uses the galactic model of Eggen et al. (1962) for calculating the galactic orbits. The distance moduli of most of these stars have been found by fitting their UBV photometry to the Hyades main sequence with appropriate blanketing corrections. The data of Table 23, especially that of group 4, support the idea that the cooler evolved subdwarfs have a different kinematic history than the other subdwarfs. In the fourth row we see that on the average the stars of group 4 have higher $|W|_{ave}$ values, larger perigalactic distances, and smaller eccentricities than the other subdwarf groups. The higher $|W|_{ave}$ values imply origins at larger distances from the galactic plane and probably during epochs when the distribution of the galactic material was more spherical. The larger apogalactic distances and smaller

Table 23. Kinematics of the subdwarfs.

Group	Number of Stars	U_{Ave}	V_{Ave}	$|W|_{Ave}$	Medium/Ave Apogalactic Distance	Medium/Ave Perigalactic Distance	Medium/Ave e	Average $\Delta(37-52)$
1	9	-163	-258	109	16.0/24.7	1.3/2.2	0.77/0.74	0.235
2	17	+12	-232	53	13.1/18.2	1.5/1.6	0.86/0.79	0.300
3	11	+46	-264	45	11.4/12.0	0.7/1.4	0.88/0.81	0.391
4	6	-12	-187	118	16.8/18.7	3.6/3.5	0.64/0.66	0.635
5	5	-165	-203	72	18.6/18.2	1.7/2.2	0.83/0.77	0.422
4(revised)	4	-38	-237	245	18.4/35.6	3.0/3.7	0.72/0.74	0.647

eccentricities would indicate that the formation of these stars was not associated with the rapid collapse of the galactic material. However, we have argued that the stars of group 4 are evolved and hence brighter than main sequence stars. So the distance moduli and space-motion vectors calculated by Eggen (1964) would be in error. In row six of Table 23 we give the data for four stars of group 4 assuming they are 100pcs more distant; this amounts to an approximate doubling of the distance or an increase of intrinsic brightness of about 1.5 magnitudes. Under these conditions two of the stars (G180-58 and G188-30) would no longer be bound to the galaxy and so have not been included in row 6 of Table 23. But the remaining four stars still show atypical kinematic properties. The $|W|_{ave}$ values are now extremely large, and the peri-galactic distances are still bigger than for the other subdwarf groups. The eccentricites of the galactic orbits are now larger than previously but still not quite as large as for the other subdwarf groups. These results show that the group 4 subdwarfs are also unusual kinematically and lend further support to the previous ideas relating star formation and the collapse of the galaxy.

Masses of Subdwarfs

From Figures 39 and 40 we can obtain the ratio of subdwarf and Hyades luminosities at constant T_e, L_{sbdwf}/L_{Hyd}; the logarithm of this quantity, $\Delta[L_H]$, is given in column ten of Table 18. Also, from Figure 43 (or 24) and the δG versus log g calibration of Chapter 6 (Figure 38) we can obtain the ratio of subdwarf and Hyades surface gravities at constant T_e, g_{sbdwf}/g_{Hyd}, or alternatively for the hotter subdwarfs we

can fit the theoretical 13-color photometry of Kurucz to the observed 13-color photometry to obtain the ratio of gravities. Next we have the relations $L \sim R^2 T_e^4$ and $g \sim MR^{-2}$, where M and R are the mass and radius of a star, respectively. These equations reduce to $g \sim MT_e^4 L^{-1}$, or $g \sim ML^{-1}$ at constant T_e. That is, $(M_{sbdwf}/M_{Hyd}) = (g_{sbdwf}/g_{Hyd}) \cdot (L_{sbdwf}/L_{Hyd})$ at constant T_e. So, we see that we have the necessary data to obtain the ratio of subdwarf and Hyades masses at constant T_e.

In Tables 24 and 25 are given nine stars whose masses have been found by this technique. In Table 24 are seven extreme subdwarfs whose average mass ratio, rather than individual ones, has been determined. The δG's come from Figure 43 and the $\Delta \log g$'s from the calibration of Figure 38B. The average values, $\Delta[L_H] = -0.40$ and $\Delta \log g = +0.12$ give $M_{sbdwf}/M_{Hyd} = 0.52$ at constant T_e. However, the measured $\Delta \log g$'s may be different from the true values due to differences of helium content since such differences in the atmospheres of F, G, and K stars mimic differences of surface gravity (for example, see Alexander 1967 and Strom and Strom 1967). Alexander (1967) claims that the continuous and line features of stellar spectra depend only on $g(1+4B/1+B)$, for constant T_e and for constant metallicity where B is the helium to hydrogen ratio by number of atoms. If $Y_{sbdwf} = 0$ and $Y_{Hyd} = 1.5Y_0$ (Eggen 1963), which certainly represents the extreme case, $M_{sbdwf}/M_{Hyd} = 0.87$. More reasonable helium abundances might be $Y_{sbdwf} = 0.25$ and $Y_{Hyd} = 0.35$ (Iben 1974), which give $M_{sbdwf}/M_{Hyd} = 0.58$. So, at constant T_e the best value of subdwarf-to-Hyades mass ratio falls in the range 0.50 to 0.75; this holds for the extreme subdwarfs of Table 24 which have temperatures in the range $5800^o \geq T_e \geq 4800^o$.

Table 24.   Subdwarfs for mass determinations.

Name	[Fe/H]	T_e	$\Delta[L_H]$	δG	45-63	$\Delta \log g$
$+34^{\circ}796$	-1.32	4800	-0.20	-0.007	+1.191	+0.03
$+31^{\circ}1684$	(-1.6)	5530	-0.34	-0.071	+0.895	+0.22
BS4550	-1.30	5180	-0.28	-0.063	+1.003	+0.19
$-21^{\circ}5703$	-1.48	5720	-0.56	+0.039	+0.808	-0.12
$-3^{\circ}3968$	(-1.9)	5110	-0.70	-0.071	+1.018	+0.28
$-15^{\circ}4042$	(-1.8)	5075	-0.35	-0.049	+1.037	+0.20
$-15^{\circ}4041$	(-1.8)	4850	-0.34	-0.013	+1.132	+0.06
Ave.	-1.6	5180	-0.40	-0.034	+1.012	+0.12

Table 25. Additional subdwarfs for mass determinations.

Name	[Fe/H]	T_e	$\Delta[L_H]$	log g	(log g)$_{Ave}$	Δlog g	45-63
BS8181	-0.68	6060	-0.09	3.7-4.0	3.85	-0.35	+0.721
+30°2536	-0.46	6745	-0.12	4.05-4.15	4.10	+0.10	+0.537

The gravities of the two stars of Table 25 have been found by fitting their observations to the theoretical 13-color photometry as in the final section of Chapter 6. The two stars, BS8181 and $+30^{\circ}2536$, are hot enough for this technique but unfortunately have only mild metal deficiencies. In fitting to the theoretical colors $+30^{\circ}2536$ (BS5447, HD128167) caused no problems, and a fairly unique value of log g could be derived. The Δlog g value was found for $+30^{\circ}2536$ using the four Hyades stars with $T_e > 6500^{\circ}$ from Table 17. For BS8181 (γ Pav, HD203608) the fit between the observed and theoretical colors was very poor for the 33,35, 37, and 40 filters; the fit was poorer than for any of the stars examined previously (and the blanketing curve of BS8181 is not typical). To calculate Δlog g for BS8181 the five Hyades stars of Table 17 with $6000^{\circ} \leq T_e \leq 6500^{\circ}$ were used. The derived masses, using the values of Table 25, are $M_{sbdwf}/M_{Hyd} = 0.96$ for $+30^{\circ}2536$ and 0.36 for BS8181. The mass ratio of BS8181 is suspect, but the problem is probably not the 13-color photometry. This photometry was taken during a poorer than average observing run at Cerro Tololo, but for BS8181 there are two independent 8C measures which were made nine nights apart and which agree to 0.04 magnitude or better for all of the colors (Mitchell 1975). Perhaps BS8181 has an unusual composition for which Kurucz's models are not adequate. For example, Danziger (1966) found that for BS8181 its carbon deficiency is much greater than for the other metals; the deficiency of carbon is -1.30 in the logarithm but only -0.67 for iron. For comparison Aller and Greenstein (1960) found similarly large carbon deficiencies for the subdwarfs HD140283, HD19445, and

HD219617 while Baschek (1962) in a detailed study of HD140283 determined that the carbon depletion is not much different from that of the other metals. We should note here that BS8181 is also atypical in that it has very large angular momentum about the galactic center; it leads the Sun in the Galactic rotation.

The above method of mass determination is rather crude, but since not much is known about Population II masses, we felt that the analysis is worthwhile. But it should be kept in mind that the derived masses may contain significant errors. For $+30^{\circ}2536$, which has a fairly good parallax, $\pi = 0.063 \pm 6$, and which has a fairly small uncertainty in the determination of log g, 4.05 to 4.15, the combined parallax and gravity errors would allow a mass ratio in the range 0.69 to 1.32, where the actual solution gives 0.96. And, these error estimates do not take into account systematic errors which might be present in the log g versus δG calibration (due to helium content differences and so forth).

CHAPTER 8

CONCLUSIONS

In this final chapter we will briefly summarize what we have
learned concerning the 13-color photometry and concerning the subdwarfs.
We will also outline several areas of research for which 13-color
photometry can be used in the future to expand upon the work of this
thesis.

What We Have Learned

Concerning the photometry the point to emphasize is that 13-color
indices can be used for F, G, and K-type stars to obtain good measures
of effective temperature, surface gravity, and metallicity. Indices
have been chosen which clearly separate the effects of these three
atmospheric parameters. The 45-63 and 58-99 indices are good temperature
parameters being highly sensitive to temperature changes but insensitive
to luminosity and metallicity, and the small blanketing and surface-
gravity corrections which we obtain from the model atmospheres seem
reasonable according to both our physical arguments and our observa-
tional checks. Using 45-63 and 58-99 we can obtain effective tempera-
tures with accidental errors on the order of $\pm 100^{\circ}$ and with systematic
errors less than or equal to 100°.

For determining compositions we have the 37-45 index which is
highly sensitive to metallicity and for F and early-G stars is nearly

independent of luminosity. However, this 37-45 index is also fairly sensitive to temperature and for late-G and K stars is somewhat sensitive to luminosity. The 37-45 versus 45-63 diagram allows us to measure [Fe/H] with an accuracy of about 0.1 for stars of solar temperature and hotter. For the cooler stars the accuracy of the [Fe/H] values is about 0.2.

The G index ((35-52)-(37-45)) is very important in that it is nearly free from metallicity and temperature effects for F, G, and K stars but is sensitive to surface gravity. The G versus 45-63 diagram has been calibrated to give luminosity classifications for F, G, and K stars and to give log g's accurate to 0.1 or 0.2.

We have also seen that it is possible to calibrate the 13-color photometry for two other important quantities, bolometric corrections and absolute blanketing changes. The bolometric corrections, which have been calibrated for the 63 magnitude, are nearly independent of temperature for F, G, and K stars and are defined with an accuracy of about $\pm$ 0.03 magnitude. These bolometric corrections have been calibrated using the Hyades dwarfs and so are directly applicable for determining the apparent bolometric magnitudes of stars with Hyades-like compositions. For metal-poor stars we must also include the absolute blanketing corrections to the 63 magnitude. These corrections have been estimated using far-infrared broad-band photometry of a few subdwarfs and are accurate to about $\pm$ 0.05 magnitude.

The main conclusions concerning the subdwarfs have come from studying their positions in the (M_{bol}, T_e) and (G, 45-63) diagrams. In

the (M_{bol}, T_e) diagram the extreme subdwarfs ($[Fe/H] \leq -1.0$) are indeed below the Hyades main sequence for $T_e \lesssim 5700^o$ (that is, less luminous for equal T_e), but the luminosities of the subdwarfs (both mild and extreme) as a function of metallicity do not allow a simple, unambiguous interpretation when using homology relations derived from the interior models of metal-poor stars. The mild subdwarfs with $[Fe/H] \gtrsim -0.75$ show little separation from the Hyades dwarfs while the more extreme subdwarfs have separations increasing with decreasing metallicity. Applications of the homology relations indicate that the extreme subdwarfs have helium abundances similar to Population I stars but do not give a straightforward answer for the mild subdwarfs. Either the mild subdwarfs have less helium than the extreme subdwarfs, which seems extremely unlikely, or the homology relations and interior models are incorrect, or the mild subdwarfs are in general more evolved than the extreme ones (that is, there exists some sort of correlation between metallicity and evolutionary status). This third possibility seems most acceptable.

Also, we noted in the number-of-subdwarfs versus metallicity histogram that nearly half of the extreme subdwarfs fall in the range $[Fe/H] = -1.3$ to -1.6. If indeed the separation of the extreme subdwarfs from the Hyades main sequence in the (M_{bol}, T_e) plane does increase with decreasing metallicity, such a clustering of the metallicity values would explain why some investigators (such as Eggen 1973, 1974) have spoken of a separate subdwarf sequence. In reality we should expect to find subdwarfs with metallicities of $[Fe/H] = -0.8$ to -1.2 between the Hyades main sequence and the "subdwarf sequence"; few such stars are found due to various selection effects.

In the G versus 45-63 diagram we have gleaned considerable under-
standing of the extreme subdwarfs' evolution by comparing their observed
colors with the expected colors of globular-cluster stars. Globular
clusters have not been observed with 13-color photometry, but we have
argued by analogy using the UBV color-magnitude diagrams of globular
clusters to place the cluster loci in the G versus 45-63 plane. We see
that when the extreme subdwarfs are plotted in this diagram a "zero-age"
locus is apparent for 45-63 $\gtrsim$ +0.75, evolution away from the "zero-age"
line is indicated for all extreme subdwarfs with 45-63 $\lesssim$ +0.75, and a
"turnoff" for the evolving subdwarfs occurs at 45-63 $\approx$ +0.59. Temperature-
wise these results show that unevolved subdwarfs are found for tempera-
tures less than 6000°, that all subdwarfs hotter than 6000° are evolved,
and that the subdwarfs' "turnoff" occurs at about 6400°. A number of
subdwarfs which are apparently evolving away from the turnoff toward
cooler temperatures are also noted. These highly evolved subdwarfs,
plus the two "subdwarfs" -9°5491 and +41°3735, which are in fact metal-
poor red giants, plus the extremely metal-poor red giant HD 122563 define
the locus of a subgiant-giant branch for our hypothetical globular
cluster. This Population II giant branch is parallel to the giant
branch defined by the field giants but is shifted 0.1 magnitude in the
direction of decreasing surface gravity. The "zero-age" locus of the
subdwarfs in the (G, 45-63) diagram indicates that unevolved subdwarfs
have greater surface gravities than Hyades dwarfs with equal effective
temperature. The blanketing curves of these subdwarfs support this view,
and the calibration of the G index shows that the log g's of the unevolved
subdwarfs are 0.2 to 0.3 greater than the Hyades values.

However, the interpretation of the positions of the extreme sub-dwarfs in the (G, 45-63) diagram does run into some difficulties. The subdwarf turnoff at $T_e = 6400^{\circ}$ has been compared with the turnoffs of some well observed globular clusters, M5, M13, M15 and M92. The UBV photometry of these clusters indicates turnoff temperatures in the range 6000° to 6250°. These results suggest that the globular clusters are somewhat older than the youngest field subdwarfs or that the globular clusters are slightly metal-rich or helium-deficient with respect to the subdwarfs. Also, we are confronted by difficulties when interpreting such evolved subdwarfs as HD140283. This subdwarf has a T_e of 5725°, appears considerably evolved in the (G, 45-63) diagram, but is not a part of the Population II subgiant branch which is defined by the hotter evolving subdwarfs and by $-9^{\circ}5491$ and $+41^{\circ}3735$. Probably the evolved subdwarfs like HD140283 (group 3 of Figure 43) are evolving from a turnoff with a temperature in the range of the globular cluster turnoffs. The ultimate problem of interpolation concerns the coolest subdwarfs which show evidence of evolution in the (G, 45-63) plane. Some of these (group 4 of Figure 43) have temperatures in the range 5000° to 5200° and yet appear considerably evolved from the "zero-age" line. Evolution at these temperatures for metal-poor stars indicates extreme ages (20×10^9 years or more) and points to a wide range of ages (at least 4 billion years) for the extreme Population II objects. These problems have not been resolved entirely satisfactorily.

Finally, the (M_{bol}, T_e) diagram has been used to obtain the ratios of subdwarf luminosities to Hyades-dwarf luminosities at constant T_e.

Also, the (G, 45-63) diagram and its surface-gravity calibration have
been used to obtain the ratios of subdwarf gravities to Hyades gravities
also at constant T_e. These two ratios have allowed us to estimate the
ratio of subdwarf masses to Hyades masses. For mild subdwarfs the ratio
is approximately one (from the mild subdwarf BS5447) while for extreme
subdwarfs the ratio falls in the range 0.50 to 0.75 (an average obtained
from seven extreme subdwarfs).

Prospects for Further Research

During the course of the analyses of this thesis it became
apparent that additional 13-color photometry of certain types of stars
could contribute significantly to our understanding of the subdwarfs
and Population II objects. For example, 8C observations of globular
cluster stars would show us directly whether our interpretations of the
subdwarfs in the (G, 45-63) diagram are correct. For a complete analysis
such observations should be pushed to magnitudes somewhat fainter than
the cluster turnoffs, but such observations are very difficult even
with large telescopes and broad-band photometry. The diagrams of White
(1970) show that for the brightest globular clusters we need to observe
to V magnitudes of 18 or 19 to reach the turnoffs. During the observ-
ing runs for this thesis, 8C observations to 13th or 14th magnitude were
fairly easily obtainable with the 60" of San Pedro Martir. Since that
time the 60" mirror has been realuminized, and so the telescope is now
about two magnitudes more sensitive. Magnitudes to a limit of 15 or 16
are now relatively easy to observe. If the 8C photometer were used on
the proposed new 80" of San Pedro Martir, another half magnitude of

sensitivity would be obtained, to a magnitude limit of perhaps 16.5. We would still be lacking 1 and 1/2 to 2 and 1/2 magnitudes for easing observing of a globular cluster turnoff with 8C photometry. We certainly would have to work hard to accomplish this project on the new 80"; perhaps this project is only doable with a very big telescope like the 158" of Kitt Peak or the 200" of Palomar.

A long-term project which is certainly within the capability of the existing equipment of San Pedro Martir would be the 8C observing of all unreddened A, F, G, and K-type dwarfs and subdwarfs. That is, we would observe all stars within about 100 parsecs of the Sun and with spectral types of A, F, G or K and luminosity classes of V or VI. This data could be used to repeat the analyses of Dixon (1965, 1966), who used the color-color diagram, U-B versus B-V, plus the kinematic properties of the stars to investigate past rates of star formation and the metal enrichment sequence of interstellar material. With the use of the 8C photometry we could improve upon Dixon's analyses in several respects. First, the 37-45 index is more sensitive to metallicity than is U-B, and so with 8C photometry we could discriminate between stars of differing metallicities more accurately. Second, the G versus 45-63 diagram gives us information about the surface gravities (evolutionary status), and so with 8C photometry we not only could compare the metallicities of the stars to their kinematics but also their states of evolution. And finally, perhaps with 8C photometry it is possible to identify stars with unusual ratios of the different metal abundances.

The third possibility of the preceding paragraph represents another area into which our 13-color studies of Population II objects could be extended. Can we use 8C photometry to distinguish stars for which the ratios of one metal abundance to another are anamolous? Preliminary studies suggest that this is indeed possible. For example, the subdwarf HD25329 is known to have anomalously strong CN (Harmer and Pagel 1973), and the blanketing curve for this star is certainly atypical. The ultraviolet excess in the 33 filter is about one-fifth that in the 35 and 37 filters while in other subdwarfs with similar temperatures the excesses are approximately the same in the 33, 35, and 37 filters.

It would also be profitable to extend our blanketing and composition studies to the more evolved stars of Population II. If we obtain 13-color photometry of Population II subgiants, giants and horizontal-branch stars (either in globular clusters or in the general field), we could greatly expand our investigations of blanketing, compositions, effective temperatures, and surface gravities. We have already seen in this thesis that in the (G, 45-63) diagram we can distinguish Population II red giants (such as $-9°5491$, $+41°3735$, and HD122563) and horizontal branch stars (such as $+25°3344$), but further observations of such stars would greatly improve our understanding of this diagram and provide instructive comparisons with our subdwarf results. It would also be very interesting to study the effective temperature and surface gravity changes in RR Lyrae variables of the different metallicity classes.

Finally, Hintzen and Strittmatter (1975) have argued that spectroscopically it may be possible to misclassify cool degenerate stars (cool

"white dwarfs") as subdwarfs. We might be able to avoid such difficul-
ties using 8C photometry. The degenerate stars have very high surface
gravities, and so we would expect them to lie significantly below the
subdwarfs in the (G, 45-63) diagram. Obtaining 8C photometry of a few
cool degenerate stars ($T_e \lesssim 6400^o$) would quickly show us whether our
expectations are correct. Perhaps 8C photometry will prove to be a
useful tool for studying all subluminous stars.

We have seen in this thesis that the 13-color photometric
system is very useful for studying the metallicities, effective tempera-
tures, and evolution of F, G, and K-type dwarfs and subdwarfs. Also,
we can foresee the usefulness of this photometry for investigating all
types of Population II objects, and eventually this data combined with
the kinematic properties of stars will lead to a more complete under-
standing of the evolution of stars and the evolution of the Galaxy.

REFERENCES

Abt, H. A., Meinel, A. B., Morgan, W. W., and Tapscott, J. W. 1968. An Atlas of Low-dispersion Grating Stellar Spectra (Tucson: Kitt Peak National Observatory and Steward Observatory).

Adams, W. S. 1915. Astrophys. J., 42, 187.

Adams, W. S. and Joy, A. H. 1922. Astrophys. J., 56, 262.

Adams, W. S., Joy, A. H., Humason, M. L., and Brayton, A. M. 1935. Astrophys. J., 81, 187.

Alexander, J. B. 1967. Monthly Notices Roy. Astron. Soc., 137, 41.

Allen, C. W. 1973. Astrophysical Quantities, Third Edition (London: The Athlone Press), 213.

Aller, L. H. 1963. The Atmospheres of the Sun and Stars, Second Edition (New York: The Ronald Press Company), 191.

Aller, L. H. and Greenstein, J. L. 1960. Astrophys. J. Suppl., 5, 139.

Altena, W. F. van and Vilkki, E. U. 1975. Astron. J., 80, 647.

Anderson, P. H. 1971. J. R. A. S. Canada, 65, 119.

Arp, H. 1962. Astrophys. J., 135, 311.

Baschek, B. 1962. Zs. f. Ap., 56, 207.

Bell, R. A. 1971. Monthly Notices Roy. Astron. Soc., 154, 343.

Blaauw, A. 1963. Basic Astronomical Data, ed. by K. A. Strand (Chicago: The University of Chicago Press), 383.

Borgman, J. 1961. Bull. Astr. Inst. Neth., 16, 99.

Brown, R. H., Davis, J., Allen, L. R., and Rome, J. M. 1967. Monthly Notices Roy. Astron. Soc., 137, 393.

Bueren, H. G. van. 1952. Bull. Astr. Inst. Neth., 11, 385.

Buscombe, W. 1959. J.R.A.S. Canada, 53, 7.

Catchpole, R. M., Pagel, B. E. J., and Powell, A. L. T. 1967. _Monthly Notices Roy. Astron. Soc._, 136, 403.

Cayrel, R. 1968. _Astrophys. J._, 151, 997.

Chaffee, F. H., Jr., Carbon, D. F., and Strom, S. E. 1971. _Astrophys. J._, 166, 593.

Cohen, J. G. 1968. _Astrophys. J._, 154, 179.

Cohen, J. G. and Strom, S. E. 1968. _Astrophys. J._, 151, 623.

Conti, P. S. and Deutsch, A. J. 1966. _Astrophys. J._, 145, 742.

Conti, P. S. and Deutsch, A. J. 1967. _Astrophys. J._, 147, 368.

Copeland, H., Jensen, J. O., and Jorgensen, H. E. 1970. _Astron. and Astrophys._, 5, 12.

Danziger, I. J. 1966. _Astrophys. J._, 143, 527.

Demarque, P. 1967. _Astrophys. J._, 149, 117.

Dixon, M. E. 1963. _The Observatory_, 83, 30.

Dixon, M. E. 1965. _Monthly Notices Roy. Astron. Soc._, 129, 51.

Dixon, M. E. 1966. _Monthly Notices Roy. Astron. Soc._, 131, 325.

Eggen, O. J. 1963. _Astrophys. J. Suppl._, 8, 125.

Eggen, O. J. 1964. _Royal Obs. Bull._, No. 84.

Eggen, O. J. 1965. _Galactic Structure_, ed. by A. Blaauw and M. Schmidt (Chicago: The University of Chicago Press), 111.

Eggen, O. J. 1968. _Astrophys. J._, 153, 195.

Eggen, O. J. 1969a. _Astrophys. J. Suppl._, 19, 31.

Eggen, O. J. 1969b. _Astrophys. J._, 158, 225.

Eggen, O. J. 1969c. _Astrophys. J._, 158, 1109.

Eggen, O. J. 1971. _Astrophys. J. Suppl._, 22, 389.

Eggen, O. J. 1973. _Astrophys. J._, 182, 821.

Eggen, O. J. 1974. _Pub. A.S.P._, 86, 162.

Eggen, O. J., Lynden-Bell, D., and Sandage, A. R. 1962. Astrophys. J., 136, 748.

Eggen, O. J. and Sandage, A. R. 1959. Monthly Notices Roy. Astron. Soc., 119, 255.

Eggen, O. J. and Sandage, A. R. 1962. Astrophys. J., 136, 735.

Faulkner, J. 1967. Astrophys. J., 147, 617.

Fischel, D. 1964. Astrophys. J., 140, 221.

Gliese, W. 1969. Veröffentlichungen des Astr. Rechen-Inst. Heidelb., No. 22.

Harmer, D. L. and Pagel, B. E. J. 1973. Monthly Notices Roy. Astron. Soc., 165, 91.

Harris, D. L., III, Strand, K. A., and Worley, C. E. 1963. Basic Astronomical Data, ed. by K. A. Strand (Chicago: The University of Chicago Press), 273.

Hayes, D. S. and Latham, D. W. 1975. Astrophys. J., 197, 593.

Heckmann, O. and Lübeck, K. 1956. Zs. f. Ap., 40, 53.

Heiser, A. M. 1960. Astrophys. J., 132, 506.

Helfer, H. L., Wallerstein, G., and Greenstein, J. L. 1960. Astrophys. J., 132, 553.

Helfer, H. L., Wallerstein, G., and Greenstein, J. L. 1963. Astrophys. J., 138, 97.

Herbig, G. H. 1965. Astrophys. J., 141, 588.

Hintzen, P. and Strittmatter, P. A. 1975. Astrophys. J., 201, L37.

Hoffleit, D. 1964. Catalogue of Bright Stars (New Haven, Conn.: Yale University Obs.).

Iben, I., Jr. 1974. Ann. Rev. Astron. and Astrophys., 12, 215.

Iben, I., Jr., and Faulkner, J. 1968. Astrophys. J., 153, 101.

Iben, I., Jr., and Rood, R. T. 1970. Astrophys. J., 159, 605.

Jaschek, C., Conde, H., and Sierra, A. C. 1964. Obs. Astr. Univ. Nac. La Plata Ser. Astr., 28, (2).

Jenkins, L. 1963. General Catalogue of Trigonometric Stellar Parallaxes (New Haven, Conn.: Yale University Obs.).

Johnson, H. L. 1962. Astronomical Techniques, ed. by W. A. Hiltner (Chicago: The University of Chicago Press), 157.

Johnson, H. L. 1964. Bol. Obs. Tonantzintla Tacubaya, 3, 305.

Johnson, H. L. 1965. Astrophys. J., 141, 170.

Johnson, H. L. 1966. Ann. Rev. Astron. and Astrophys., 4, 193.

Johnson, H. L. 1975. Personal discussion in Ensenada, Mexico.

Johnson, H. L. and Knuckles, C. F. 1955. Astrophys. J., 122, 209.

Johnson, H. L., MacArthur, J. W., and Mitchell, R. I. 1968. Astrophys. J., 152, 465.

Johnson, H. L. and Mitchell, R. I. 1962. Comm. Lunar and Planet. Lab., 1, 73.

Johnson, H. L. and Mitchell, R. I. 1968. Astrophys. J., 153, 213.

Johnson, H. L. and Mitchell, R. I. 1975. Revista Mexicana de Astronomía y Astrofísica, 1, 299.

Johnson, H. L., Mitchell, R. I., and Iriarte, B. 1962. Astrophys. J., 136, 75.

Johnson, H. L., Mitchell, R. I., Iriarte, B., and Wiśniewski, W. Z. 1966. Comm. Lunar and Planet. Lab., 4, 99.

Johnson, H. L., Mitchell, R. I., and Latham, A. S. 1967. Comm. Lunar and Planet. Lab., 6, 85.

Keenan, P. C. 1963. Basic Astronomical Data, ed. by K. A. Strand (Chicago: The University of Chicago Press), 78.

Kennedy, P. M. and Buscombe, W. 1974. MK Spectral Classifications Published Since Jaschek's La Plata Catalogue (Evanston, Illinois: Northwestern University Press).

Kodaira, K. 1973. Astron. and Astrophys., 22, 273.

Kodaira, K., Greenstein, J. L., and Oke, J. B. 1969. Astrophys. J., 155, 525.

Kuiper, G. P. 1938. Astrophys. J., 87, 592.

Kuiper, G. P. 1939. Astrophys. J., 89, 548.

Kuiper, G. P. and Seyfert, C. K. 1938. Astrophys. J., 87, 78.

Kurucz, R. L. 1970. S.A.O. Spec. Rpt., No. 309.

Kurucz, R. L. 1974. Center for Astrophys. Preprint Series, No. 234.

Kurucz, R. L. 1975. Personal communication by mail, Cambridge, Mass.

Labs, D. and Neckel, H. 1968. Zs. f. Ap., 69, 1.

Labs, D. and Neckel, H. 1970. Solar Phys., 15, 79.

Luyten, W. J. 1961. A Catalogue of 7127 Stars in the Northern Hemisphere with Proper Motions Exceeding 0".2 Annually (Minneapolis: The Lund Press).

Mendoza V., E. E. 1969. Publ. Depto. Astron. Univ. Chile, 1, 106.

Mitchell, R. I. 1975. Personal discussion in Ensenada, Mexico.

Mitchell, R. I. and Johnson, H. L. 1969. Comm. Lunar and Planet. Lab., 8, 1.

Morgan, W. W. and Hiltner, W. A. 1965. Astrophys. J., 141, 177.

Oke, J. B. and Schild, R. E. 1970. Astrophys. J., 161, 1015.

Ortega M, R. 1971. Unpublished Thesis. Universidad Nacional Autónoma de México, Mexico City.

Pagel, B. 1962. The Observatory, 82, 123.

Pagel, B. E. J. 1963. J. Quant. Spectrosc. Radiat. Transfer, 3, 139.

Pagel, B. E. J. and Powell, A. L. T. 1966. Royal Obs. Bull., No.124.

Parenago, P. P. 1940. Astr. J. Soviet Union, 17, No. 4, 1.

Roman, N. G. 1955. Astrophys. J. Suppl., 2, 195.

Rood, R. and Iben, I., Jr. 1968. Astrophys. J., 154, 215.

Sandage, A. 1964. Astrophys. J., 139, 442.

Sandage, A. 1969a. Astrophys. J., 158, 1115.

Sandage, A. 1969b. Astrophys. J., 157, 515.

Sandage, A. R. and Eggen, O. J. 1959. Monthly Notices Roy. Astron. Soc., 119, 278.

Sandage, A. and Smith, L. L. 1963. Astrophys. J., 137, 1057.

Sandage, A. and Tammann, G. A. 1975. Astrophys. J., 197, 265.

Schuster, W. J. 1976. Revista Mexicana de Astronomía y Astrofísica, in press.

Sears, R. L. and Whitford, A. E. 1969. Astrophys. J., 155, 899.

Seitter, W. C. 1970. Atlas for Objective Prism Spectra, Bonner Specktral Atlas 1 (Bonn: Ferd. Dümmlers Verlag).

Simoda, M. and Iben, I., Jr. 1968. Astrophys. J., 152, 509.

Strom, S. E., Cohen, J. G., and Strom, K. M. 1967. Astrophys. J., 147, 1038.

Strom, S. E. and Kurucz, R. L. 1966. J. Quant. Spectrosc. Radiat. Transfer, 6, 591.

Strom, S. E. and Strom, K. M. 1967. Astrophys. J., 150, 501.

Stromgren, B. 1966. Ann. Rev. Astron. and Astrophys., 4, 433.

Talbot, R. J. and Arnett, W. D. 1973. Astrophys. J., 186, 69.

Tomkin, J. and Bell, R. A. 1973. Monthly Notices Roy. Astron. Soc., 163, 117.

Travis, L. D. and Matsushima, S. 1973. Astrophys. J., 182, 189.

Wagner, R. L. 1974. Astrophys. J., 191, 173.

Wallerstein, G. 1962. Astrophys. J. Suppl., 6, 407.

Wallerstein, G., Greenstein, J. L., Parker, R., Helfer, H. L., and Aller, L. H. 1963. Astrophys. J., 137, 280

Wallerstein, G. and Helfer, H. L. 1959. Astrophys. J., 129, 720.

Wallerstein, G. and Helfer, H. L. 1961. Astrophys. J., 133, 562.

White, R. E. 1970. Astrophys. J. Suppl., 19, 343.

Wildey, R. L., Burbidge, E. M., Sandage, A. R., and Burbidge, G. R. 1962. Astrophys. J., 135, 94.

Wilson, R. E. 1953. <u>General Catalogue of Stellar Radial Velocities</u> (Washington, D.C.: Carnegie Institution of Washington).